



**TECHNISCHE  
UNIVERSITÄT  
WIEN**  
Vienna University of Technology

# MASTER THESIS

## DIPLOMARBEIT

### **Novel Multipolar Initiators for Two-Photon Induced Photopolymerization**

Ausgeführt am Institut für  
**Angewandte Synthesechemie**  
der **Technischen Universität Wien**

unter der Anleitung von  
**Ao.Univ.Prof. Dipl.-Ing. Dr.techn. Robert Liska**

und

**MSc. Zhiquan Li**

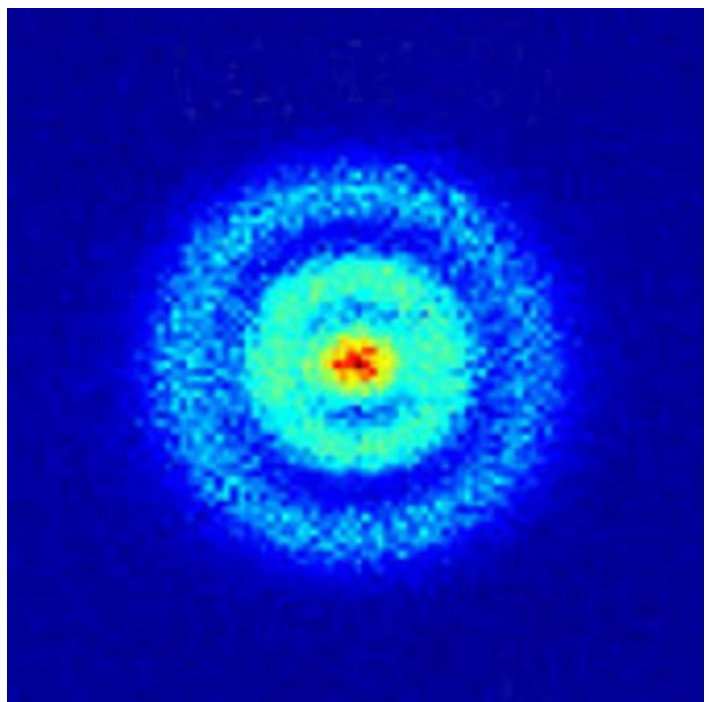
durch

**Maximilian TROMAYER, BSc.**

0525241

Hohlgasse 3, 2371, Hinterbrühl





H-atom recorded by photoionization microscopy<sup>1</sup>

"Never trust atoms... they make up everything."



## Abstract

Two-photon absorption (TPA) enables the activation of photophysical and -chemical processes at high spatial resolution (~100 nm) reaching below the diffraction limit associated with the wavelength of the absorbed light. Amongst other important technologies it is employed in, e.g. two-photon excitation microscopy (TPEM), its use is becoming increasingly popular in sub-micrometer stereolithography for microfabrication of photonic crystals, polymer-based optical waveguides on integrated circuit boards, rapid prototyping, high-density 3D optical data storage and parts for other industries requiring high precision. Furthermore the high transparency of biological tissues towards the fs-pulsed Titanium:Sapphire near infrared lasers offers the advantages of high penetration depth and little photo-damage, making TPA especially suitable for applications like bio-imaging and *in-vivo* bio-fabrication using hydrogel-based materials.

Stereolithography based on two-photon induced photopolymerization (TPIP) has employed classical one-photon initiators (OPIs) as used in radical photopolymerization. However since OPIs suffer from significant limitations regarding the quality of the attainable microstructures and especially the required fabrication parameters (high laser powers, very slow writing), the development of specialized two-photon initiators (TPIs) is of major interest.

In the present work several novel TPIs based on the lead structure of **M2CMK**, a highly efficient TPI developed by the research group in previous work, were synthesized and characterized (UV/Vis-spectra, two-photon absorption cross section  $\sigma_{\text{TPA}}$ , TPIP processing window screening & structuring tests). The first approach to improve efficiency, enhancing energy absorption via increasing the  $\sigma_{\text{TPA}}$  by introducing branched and/or planarized structural elements, yielded several initiators with features superior to the reference. **Y-B2CMK** exhibits a broad overall structuring window and especially avoids excessive damage to polymerized objects at high power densities. For high laser powers up to 110 mW, **B2Trz** shows the best performance of all tested TPIs. **B2Cbz** produces excellent results in the low to medium power range at writing speeds up to 151 mm/s. The second approach of introducing cleavable groups producing radicals while avoiding deactivation by back electron transfer (BET) was not able to enhance initiation efficiency so far because **S2CMK**, **SNB** and **PADE** all suffered from low  $\sigma_{\text{TPA}}$ . Nevertheless, successful cleavage under TPA conditions could be proved and valuable insights for future implementation of cleavable TPIs were gained.

# Kurzfassung

Zwei-Photonen-Absorption (TPA) ermöglicht die Aktivierung photophysikalischer und -chemischer Prozesse bei hoher räumlicher Auflösung (~100 nm) bis unterhalb der mit der Wellenlänge des absorbierten Lichtes assoziierten Diffraktionsgrenze. TPA kommt in wichtigen Technologien zum Einsatz z.B. der Zwei-Photonen-angeregten Mikroskopie und erfreut sich wachsender Beliebtheit in der Submikrometer-Stereolithographie. Diese dient zur Mikrofabrikation photonischer Kristalle, polymerbasierter optischer Wellenleiter in integrierten Schaltkreisen und anderer Teile für Industrien die hohe Präzision erfordern, sowie für Rapid Prototyping und optische Datenspeicherung. Weiters bietet die hohe Transparenz biologischer Gewebe gegenüber dem eingesetzten fs-gepulsten Titan:Saphir NIR Laser Vorteile wie hohe Eindringtiefe und geringe Lichtschäden, was TPA besonders für Anwendungen wie Bio-Imaging und *in-vivo* Biofabrikation von hydrogelbasierten Materialien geeignet macht.

In der auf Zwei-Photonen-induzierter Photopolymerisation (TPIP) basierten Stereolithographie wurden oft klassische Ein-Photonen-Initiatoren (OPIs) angewandt, diese leiden jedoch unter signifikanten Einschränkungen bezüglich der erzielbaren Mikrostruktur-Qualität und der benötigten Fabrikationsparameter (hohe Laserleistungen, sehr langsames Schreiben), weshalb großes Interesse an der Entwicklung spezialisierter Zwei-Photonen-Initiatoren (TPIs) besteht.

In der vorliegenden Arbeit wurden mehrere neue TPIs auf Basis von **M2CMK** (hocheffizienter TPI aus früherer Arbeit der Forschungsgruppe) als Leitstruktur und Referenz hergestellt und charakterisiert (UV/Vis-Spektren, Zwei-Photonen-Absorptionsquerschnitt  $\sigma_{\text{TPA}}$ , TPIP Prozessfensterscreenings & Strukturierungstests). Der erste Ansatz zur Effizienzsteigerung, Verbesserung der Energieabsorption durch Erhöhung der  $\sigma_{\text{TPA}}$  mittels Einführung verzweigter und/oder planarisierter Strukturelemente, brachte einige Initiatoren mit der Referenz überlegenen Eigenschaften hervor. **Y-B2CMK** weist insgesamt ein breites Prozessfenster auf und vermeidet bei hohen Leistungsdichten exzessive Schäden an polymerisierten Objekten. Bei hohen Laserleistungen bis 110 mW schneidet **B2Trz** von allen getesteten TPIs am besten ab. **B2Cbz** führt zu exzellenten Ergebnissen im mittleren Leistungsbereich bei Schreibgeschwindigkeiten bis 151 mm/s. Der zweite Ansatz, Einführung von unter Radikalbildung spaltender Gruppen zur Vermeidung der Desaktivierung aufgrund von Back-Electron-Transfer (BET), konnte die Initiierungseffizienz bislang nicht steigern, da die  $\sigma_{\text{TPA}}$  von **S2CMK**, **SNB** und **PADE** zu gering sind. Nichtsdestotrotz konnten erfolgreiche Spaltung unter TPA-Bedingungen nachgewiesen und wertvolle Erkenntnisse für die Entwicklung spaltbarer TPIs gewonnen werden.

# Acknowledgement

First of all, I would like to thank Prof. Robert Liska for being able to work in his group, contribute to research on such an interesting topic and for the freedom he gave me to be creative and propose my own ideas. Furthermore I thank my supervisor Zhiquan Li for the time and effort he spent sharing his expertise on the topic of two-photon initiators.

I would also like to thank all my colleagues and the lab staff at the Institute of Applied Synthetic Chemistry, in particular those from the Division of Macromolecular Chemistry for the pleasant and productive working environment, lively discussions on chemical problems and for the great fun had at shared leisure activities.

For the fruitful collaboration I am grateful to Prof. Jürgen Stampfl, Aleksandr Ovsianikov, Jan Torgersen and Peter Gruber from the Institute of Materials Science and Technology who helped me use the TPIP Mipro 3D-printer, to Aliasghar Ajami from the Institute of Applied Physics for performing z-scan measurements, and to Arnulf Rosspeintner from the Physical Chemistry Department of the University of Geneva for performing photo-physical measurements.

My bachelor student Zacharias Thiel deserves my gratitude for his diligence and resourcefulness in doing most of the work related to two-photon initiators based on s-triazine.

I am deeply grateful to my former chemistry teacher Wolfgang Faber for all his efforts to foster my long-standing interest in chemistry and for giving me the best possible conditions to learn.

A huge thank you goes to my dear friend Manuel, without whose kind help and support none of this would have been possible, my parents Inge and Erich who always did their best in giving me their care, emotional and also financial support, as well as my friends on whom I can rely through thick and thin.

Thank you all so very much!

# Table of Content

	EXP
<b>Introduction</b>	<b>1</b>
Radical Photopolymerization and Photoinitiators	1
Two-Photon Absorption and Two-Photon Induced Photopolymerization	6
<b>Objective</b>	<b>12</b>
<b>State of the Art Two Photon Initiators</b>	<b>14</b>
<b>Results and Discussion</b>	<b>21</b>
<b>1. Branched/multipolar triphenylamine-based analogues of M2CMK</b>	<b>21</b>
1.1. <b>Y-M2CMK</b>	22
1.1.1. Synthesis of <b>Y-M2CMK</b>	22
1.1.1.1. Synthesis of precursor (2 <i>E</i> )-2-[[4-(dimethylamino)phenyl]methylene]-4-methylcyclohexanone ( <b>1</b> )	22 85
1.1.1.2. Synthesis of precursor 4,4',4''-nitritotris(benzaldehyde) ( <b>3</b> )	23 86
1.1.1.3. Synthesis of <b>Y-M2CMK</b> - final step	24 88
1.1.2. Analysis of <b>Y-M2CMK</b> – open aperture z-scan	26
1.2. <b>Y-B2CMK</b>	26
1.2.1. Synthesis of <b>Y-B2CMK</b>	26
1.2.1.1. Synthesis of precursor (2 <i>E</i> )-2-[[4-(dibutylamino)phenyl]methylene]-4-methylcyclohexanone ( <b>4</b> )	26 90
1.2.1.2. Synthesis of <b>Y-B2CMK</b> – final step	27 91
1.2.2. Analysis of <b>Y-B2CMK</b>	28
1.2.2.1. Open aperture z-scan	28
1.2.2.2. UV/Vis - spectroscopy	28
1.2.2.3. TPIP structuring tests	29
<b>2. Planarized branched/multipolar carbazole-based analogues of M2CMK</b>	<b>34</b>
2.1. <b>B2Cbz</b>	35
2.1.1. Synthesis of <b>B2Cbz</b>	35
2.1.1.1. Synthesis of precursor 9-(phenylmethyl)-9 <i>H</i> -carbazole ( <b>5</b> )	36 93
2.1.1.2. Synthesis of precursor 9-(phenylmethyl)-9 <i>H</i> -carbazole-3,6-dicarboxaldehyde ( <b>7</b> )	36 96
2.1.1.3. Synthesis of <b>B2Cbz</b> – final step	38 97
2.1.2. Analysis of <b>B2Cbz</b>	39
2.1.2.1. UV/Vis - spectroscopy	39
2.1.2.2. Open aperture z-scan	40
2.1.2.3. TPIP structuring tests	40
2.2. <b>Cbz2CEK</b>	43
2.2.1. Synthesis of <b>Cbz2CEK</b>	43 99
2.2.2. Analysis of <b>Cbz2CEK</b>	44
2.2.2.1. UV/Vis - spectroscopy	44
2.2.2.2. Open aperture z-scan	45
2.2.2.3. TPIP structuring tests	45
<b>3. Planarized branched/multipolar triazine-based analogues of M2CMK</b>	<b>48</b>
3.1. Synthesis of <b>B2Trz</b> , <b>2B2Trz</b> and <b>3B2Trz</b>	49
3.1.1. Synthesis of precursor 2,4,6-trimethyl-1,3,5-triazine ( <b>8</b> )	49 101
3.1.2. Synthesis of <b>B2Trz</b> , <b>2B2Trz</b> and <b>3B2Trz</b> - condensation step	51 102
3.2. Analysis of <b>B2Trz</b> , <b>2B2Trz</b> and <b>3B2Trz</b>	55



3.2.1.	OPA photophysical properties	55	
3.2.2.	Open aperture z-scan	57	
3.2.3.	TPIP structuring tests	58	
<b>4.</b>	<b>Cleavable TPIs</b>	<b>64</b>	
4.1.	Cleavable Initiators based on <b>M2CMK</b> - Bifunctional C-S cleavage	64	
4.1.1.	Synthesis of <b>S2CMK</b>	65	
4.1.1.1.	Synthesis of precursor 4-(chloromethyl)benzoic acid methyl ester ( <b>9</b> )	66	107
4.1.1.2.	Synthesis of precursor 4-[(phenylthio)methyl]benzoic acid methyl ester ( <b>10</b> )	67	108
4.1.1.3.	Synthesis of precursor 4-[(phenylthio)methyl]benzaldehyde ( <b>11</b> )	67	109
4.1.1.4.	Synthesis of <b>S2CMK</b> - final step	70	111
4.1.2.	Synthesis of non-cleavable reference <b>C2CMK</b>	70	
4.1.2.1.	Synthesis of precursor (2-iodoethyl)benzene ( <b>12</b> )	70	112
4.1.2.2.	Synthesis of precursor 4-(2-phenylethyl)benzaldehyde ( <b>13</b> )	71	113
4.1.2.3.	Synthesis of <b>C2CMK</b> - final step	72	115
4.1.3.	Analysis of <b>S2CMK</b> and <b>C2CMK</b>	72	
4.1.3.1.	UV/Vis - spectroscopy	72	
4.1.3.2.	Open aperture z-scan	73	
4.1.3.3.	TPIP structuring tests	73	
4.2.	Cleavable Initiators based on <b>M2CMK</b> - C-S cleavage enhanced through strong donor group	74	
4.2.1.	Synthesis of <b>SNB</b>	74	116
4.2.2.	Analysis of <b>SNB</b>	75	
4.2.2.1.	UV/Vis - spectroscopy	75	
4.2.2.2.	Open aperture z-scan	76	
4.2.2.3.	TPIP structuring tests	76	
4.3.	Cleavable Initiator - Pentazadiene releasing gaseous nitrogen	80	
4.3.1.	Synthesis of <b>PADE</b>	81	118
4.3.2.	Analysis of <b>PADE</b>	82	
4.3.2.1.	UV/Vis - Spectroscopy	82	
4.3.2.2.	Open aperture z-scan	82	
4.3.2.3.	TPIP structuring tests	83	
	<b>Experimental Part</b>	<b>85</b>	
	<b>Conclusion</b>	<b>120</b>	
	<b>Technical Equipment &amp; Characterization Methods</b>	<b>128</b>	
	<b>Abbreviations</b>	<b>134</b>	
	<b>References</b>	<b>136</b>	



# Introduction

## Radical Photopolymerization and Photoinitiators

Radical photopolymerization is an energy efficient, environmentally friendly and very versatile technology. Its applications range from printing inks, decorative and protective coatings, dentistry, optics and electronics to stereolithography and rapid prototyping. Fast curing speeds and -depths, as well as excellent and tunable mechanical properties of the resulting polymers are further advantages.<sup>2</sup>

Suitable formulations usually are "tailor-made" systems containing multiple components for different purposes. *Reactive oligo- and polymers* (unsaturated or acryloylated polyesters, polyethers, epoxy resins and polyurethanes) are used to tune mechanical and optical properties, *reactive diluents* (mono- and multifunctional (meth-)acrylates) allow to control viscosity and degree of cross-linking. Various *additives* (stabilizers, inhibitors, fillers, plasticizers, antioxidants, surfactants, pigments,...) are used to further modify the properties. A key component are the *photoinitiators* (PIs) *and sensitizers*, which absorb energy from UV- or visible light and transform it to chemical energy, initiating radical formation and thus the polymerization and curing of the liquid formulation in a chain growth mechanism (see **Figure 1**).<sup>3</sup>

The formation of radicals occurs in three steps:<sup>4</sup>

- i) Generation of a chemically reactive excited state of the initiator molecule via direct light absorption or through energy transfer from an excited photosensitizer.<sup>5</sup>
- ii) Formation of the starter radicals from the excited state via:
  - a) photofragmentation with homolytic bond cleavage<sup>6</sup>
  - b) hydrogen abstraction from a hydrogen donor<sup>7</sup>
  - c) electron transfer<sup>8</sup>
- iii) Chain initiation via reaction of the starter radicals with reactive mono- or oligomers.<sup>9</sup>

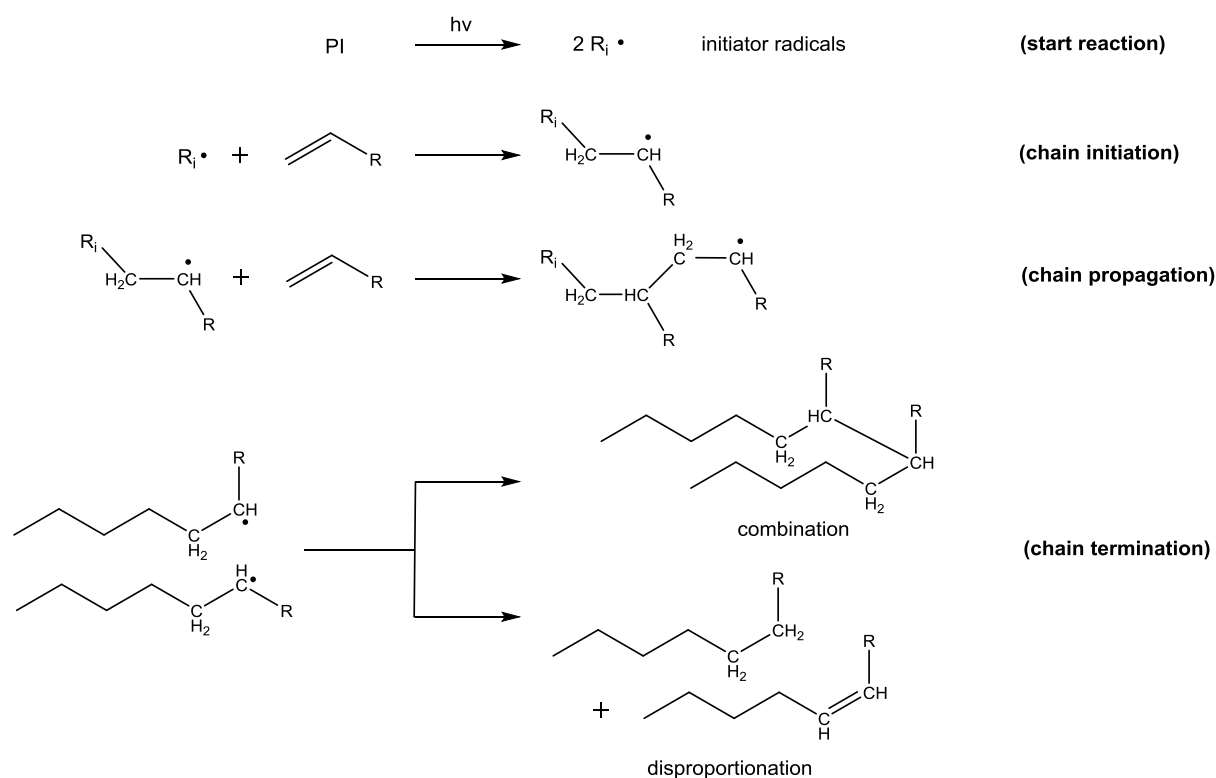


**Figure 1:** Schematic representation of the individual steps of radical photopolymerization.

In the first step a compound in the formulation absorbs UV- or visible light leading to certain excitation processes (see **Figure 2**). Either the photoinitiator directly absorbs the light energy or a photosensitizer is excited and then causes a Förster resonance energy transfer.

For the excitation process to be efficient, the absorption spectrum of the photoactive compound has to match the emission spectrum of the radiation source as closely as possible.

To absorb light the PI must contain chromophores (see **Table 1**), usually conjugated systems containing multiple bonds and in case of classical PIs most often C=O-double bonds. The responsible molecular electronic transitions can be both of  $\pi \rightarrow \pi^*$  (promotion of bonding  $\pi$ -electron to antibinding  $\pi^*$ -orbital) or  $n \rightarrow \pi^*$  (promotion of non-bonding electron  $n$  of a heteroatom to antibinding  $\pi^*$ -orbital) character, with  $\pi \rightarrow \pi^*$  transitions usually ~100 times as intense as  $n \rightarrow \pi^*$ .<sup>10,11</sup>

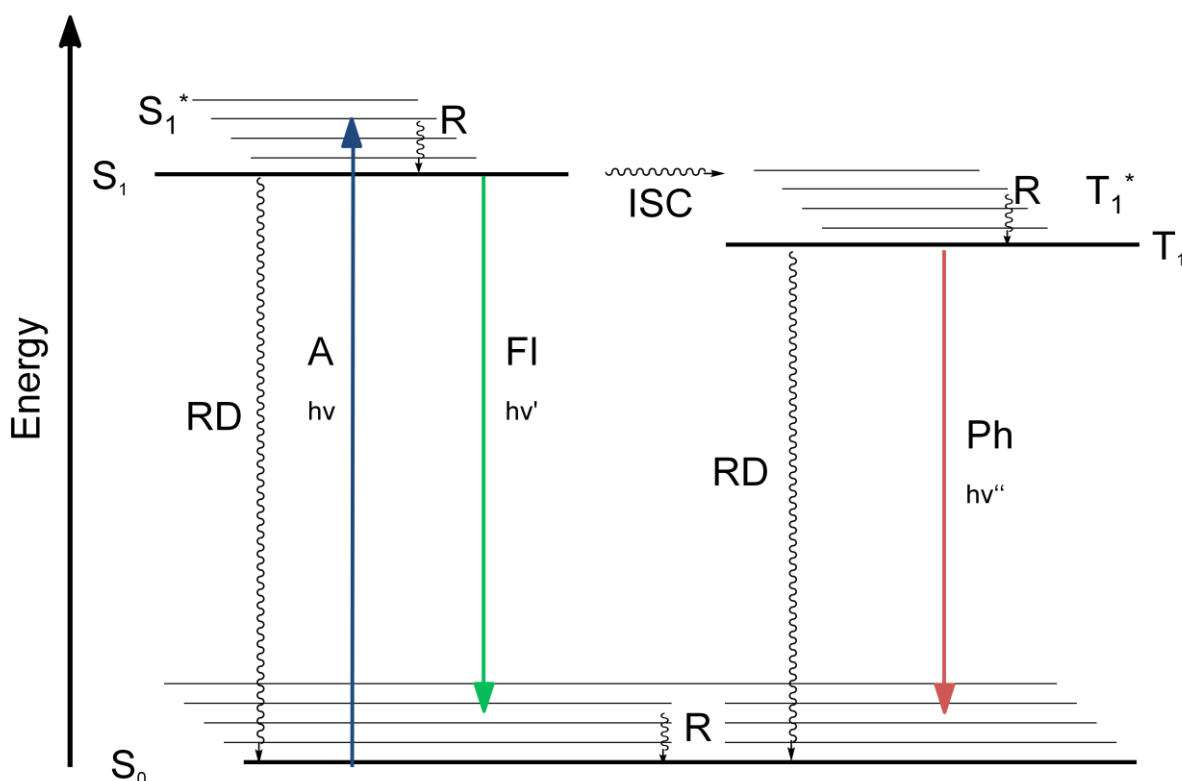


**Figure 2:** Simplified Jablonski-scheme - abbrev.: A = absorption, FI = fluorescence, RD = radiationless desactivation, Ph = phosphorescence, R = (thermal) relaxation, ISC = Intersystem Crossing. Straight arrows: radiative processes; curved arrow: radiationless processes. The various higher-energetic states close to  $S_0$  (singlet ground state),  $S_1$  (first excited singlet state), and  $T_1$  (first excited triplet state) result from excess vibration and rotation energy.

**Table 1:** Absorption of several chromophores

Chromophore	$\lambda_{\max}$ [nm] $\pi \rightarrow \pi^*$	$\lambda_{\max}$ [nm] $n \rightarrow \pi^*$
<b>C=C</b>	170	-
<b>C=O</b>	166	280
<b>C=N</b>	190	300
<b>N=N</b>	-	350
<b>C=S</b>	-	500

Many of the classical PIs for radical photopolymerization contain a carbonyl group with at least one aromatic substituent, because this ensures a sufficient absorption in the used UV-range (200-400 nm) and suitable photoreactivity. Dependent on their mechanism of radical formation, they are divided into type I (cleavable) or type II (hydrogen abstraction) PIs.

Type I PIs can be further classified according to the position of the bond that undergoes homolytic scission relative to the carbonyl group ( $\alpha$ ;  $\beta$ ;  $\beta$ -phenylogous,...), as well as the nature of the bond that is cleaved (C-C or C-X; X = heteroatom). A few examples of type I PIs, their respective classification and the bond undergoing scission are illustrated in **Figure 3**.<sup>10,12,13</sup>

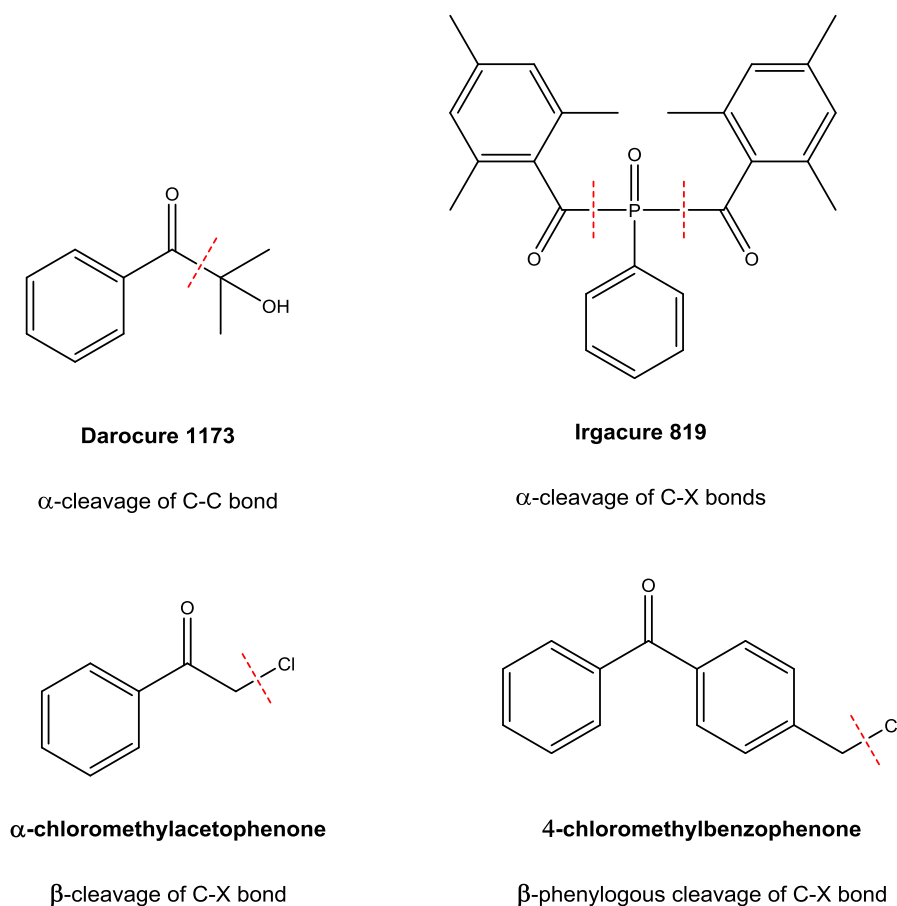


**Figure 3:** Examples for different classes of type I PIs.

Such cleaving reactions usually take place after excitation of  $n \rightarrow \pi^*$  transitions and require both a certain electronic stabilization (see **Figure 4**) of the generated radicals, as well as high reactivity of the formed radicals towards the monomers to ensure an efficient initiation of polymerization.

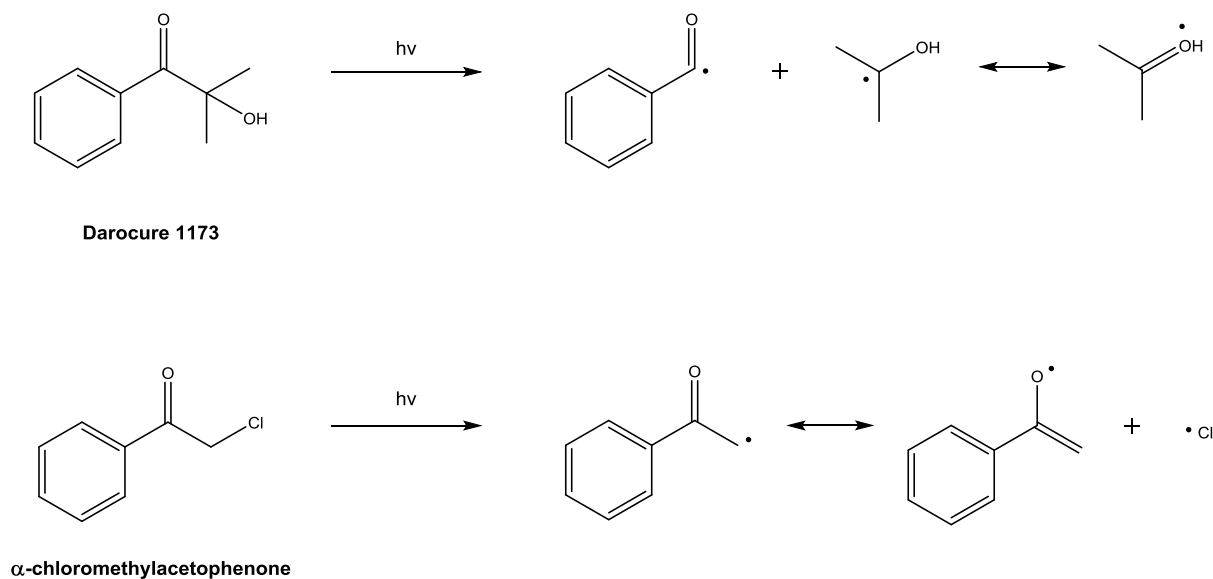


**Figure 4:** Cleavage of type I PIs and resonance structures illustrating stabilization of the formed radicals.

Type II PIs however generate radicals from suitable hydrogen donors in a bimolecular reaction. If esters or alcohols are used as hydrogen donors, the process requires the excitation of a long-lived triplet  $n \rightarrow \pi^*$  state. Tertiary amines react more efficiently via an initial electron transfer from the donor nitrogen atom and an exciplex (short-lived excited state complex of the amine and the hydrogen abstracting PI) is formed. The subsequent proton transfer from the donor's  $\alpha$ -carbon results in the net hydrogen abstraction; this process can occur both from  $\pi \rightarrow \pi^*$  and  $n \rightarrow \pi^*$  triplet states. A classical example for a type II photoinitiator system is a mixture of camphorquinone with ethyl 4-(dimethylamino)benzoate (see **Figure 5**), used in dentistry because of its ability to initiate at  $\sim 440$  nm avoiding harmful UV-light.<sup>13</sup>

A drawback that Type II PIs suffer from is the possibility of back electron transfer (BET), which simply reverses the initial electron transfer caused by the excitation. Both BET and the diffusion limitation of the bimolecular radical formation mechanism cause a reduced curing speed and efficiency of Type II PIs.

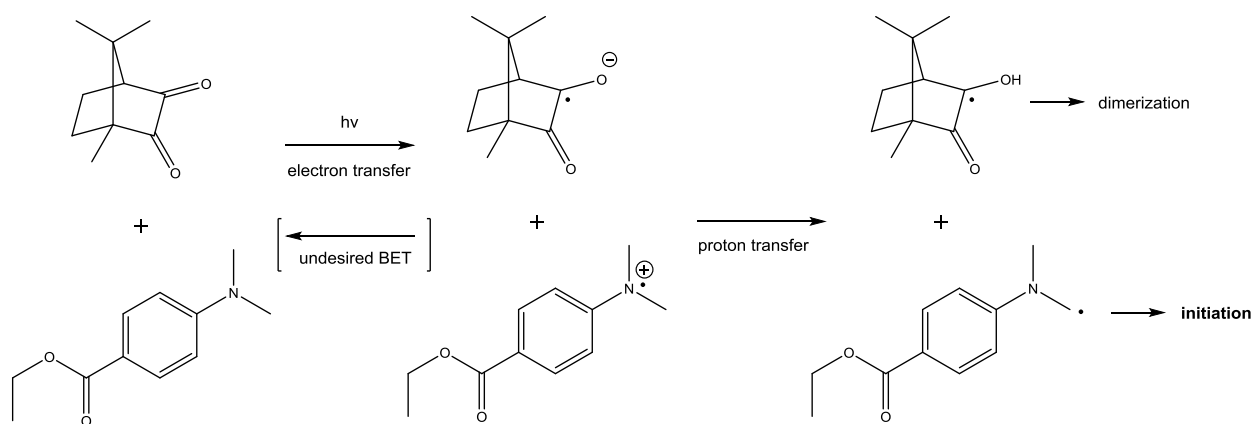


**Figure 5:** Electron and proton transfer (hydrogen abstraction) explaining the reactivity of a type II PI system. The possibility of an unwanted back electron transfer (BET) reversing the excitation is a drawback.

## Two-Photon Absorption and Two-Photon Induced Photopolymerization

The process of two-photon absorption (TPA) was first theoretically predicted by the German-American physicist Maria Göppert-Mayer (1906-1972) in her doctoral thesis at Göttingen University in 1931.<sup>14</sup> While in one-photon absorption (OPA) a molecule is excited to an electronic state of higher energy by consuming the energy of a single photon, TPA leads to an excited state of a level corresponding to the combined energy of two photons which are absorbed quasi simultaneously. This makes TPA a process with a rather low probability of occurrence, requiring extremely high light intensities to make it happen at a substantial rate, so that the phenomenon was first observed only with the advent of laser technology 30 years later.

In 1961 Kaiser and Garrett reported the first experimental confirmation of a TPA induced process, the frequency-upconversion fluorescence in a  $\text{CaF}_2:\text{Eu}^{2+}$  crystal sample irradiated by a continuous wave (CW) laser.<sup>15</sup>

Due to the high light intensities required and the low ability of most materials to undergo TPA processes, applications were limited for decades until the development of relatively simple solid-state femtosecond (fs) pulsed lasers in the late 1980ies and early 1990ies. Nowadays, titanium:sapphire (Ti:S) laser systems are state of the art to drive TPA with extremely large peak powers (up to several gigawatts) that could never be reached with CW- and nanosecond (ns) lasers. This has made TPA feasible and affordable and sparked a great deal of interest in researching TPA-related phenomena.<sup>16</sup>



TPA and OPA processes have somewhat different selection rules for respective allowed transitions. **Figure 6** shows a simplified Jablonski-scheme that illustrates the difference between an OPA fluorescence and TPA frequency-upconversion fluorescence process. The electronic transition from  $S_0$  to  $S_2$  is resonant with the combined energy of two photons with the energy  $h\nu'$  and takes place without any excited intermediate state, having only a theoretical virtual state in between.<sup>17</sup>

In centrosymmetric molecules the lowest excited state attainable via TPA usually lies at a higher energy than the one that can be reached by OPA. After rapid non-radiative decay from  $S_2$  to  $S_1$  ( $\sim 10^{-12}$ s) several other photophysical and photochemical processes can happen.<sup>18</sup> For PIs the most important of these processes is intersystem crossing (ISC) from an excited singlet state to an excited triplet state, which has a lifetime that is long enough to interact with other molecules or form radicals/ions that initiate a polymerization reaction. Other important processes than can take place include energy or electron transfer and frequency-upconversion fluorescence.<sup>19</sup>

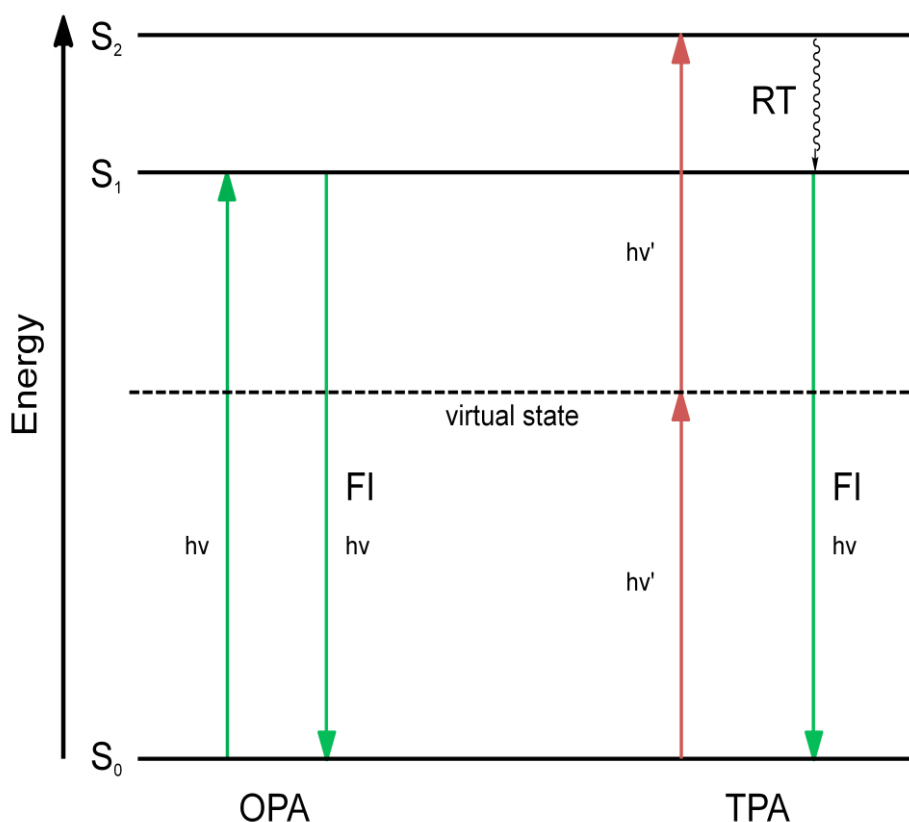


**Figure 6:** Simplified Jablonski-scheme - abbrev.: FI = fluorescence, RT = radiationless transition,  $S_0$  (singlet ground state),  $S_1/S_2$  (first/second excited singlet state), photon energy  $h\nu > h\nu'$

If the two photons absorbed in TPA have the different energies it is called a non-degenerate TPA process, if they are of the same energy, it is called degenerate. Most applications focus on the latter form.<sup>20</sup> In the case of degenerate TPA the intensity  $I(z)$  of a light beam with propagation in z-direction is described by the following differential **Equation 1**, connecting intensity  $I$  and the concentration  $c$  of the absorbing species with linear and non-linear absorption coefficients,  $\alpha$  and  $\beta$  respectively.

$$\frac{dI(z)}{dz} = -\alpha c I - \beta c I^2 \quad \text{Equation 1}$$

While in the case of OPA the solution of this equation with the boundary condition  $I(z=0) = I_0$  is simply the well-known Beer-Lambert law, in case of TPA with its extremely high light intensities the first (linear) term becomes negligible leading to the following solution (**Equation 2**):

$$I(z) = \frac{I_0}{1 + I_0 \beta c z} \quad \text{Equation 2}$$

The non-linear coefficient  $\beta$  can also be used to define an expression for the TPA cross section  $\sigma_{\text{TPA}}$  which is a measure for the efficiency of a single absorber molecule to be excited in a TPA process (**Equation 3**):

$$\sigma_{\text{TPA}} = \frac{\hbar \omega \beta}{N_A c \cdot 10^{-3}} \quad \text{Equation 3}$$

Here,  $\hbar$  is the reduced Planck constant,  $\omega$  the angular frequency of the absorbed photons,  $N_A$  Avogadro's number and  $c$  the molar concentration.<sup>19</sup> The SI unit of  $\sigma_{\text{TPA}}$  is Göppert-Mayer (GM) with  $1 \text{ GM} = 10^{-50} \text{ cm}^4 \text{ s photon}^{-1}$ . The large scaling factor of  $10^{-50}$  is introduced in order to obtain convenient values for common TPA materials.

Investigations into the relationship between molecular structure and  $\sigma_{\text{TPA}}$  found that essential factors promoting a high  $\sigma_{\text{TPA}}$  are an extended  *$\pi$ -conjugated core* ( $\pi$ ) of good *co-planarity* with various electron *donor* (D)- and/or *acceptor* (A) groups, because thus

low-energy excitations with large transition and/or mesomeric dipole moments are introduced.

Furthermore besides dipolar push-pull-systems, quadrupolar, octupolar (see **Figure 7**) and more generally multipolar TPA chromophores (even dendritic and polymeric TPA active compounds) are favorable as higher order polarity introduces a higher chromophore density compared to dipolar structures.<sup>21</sup>

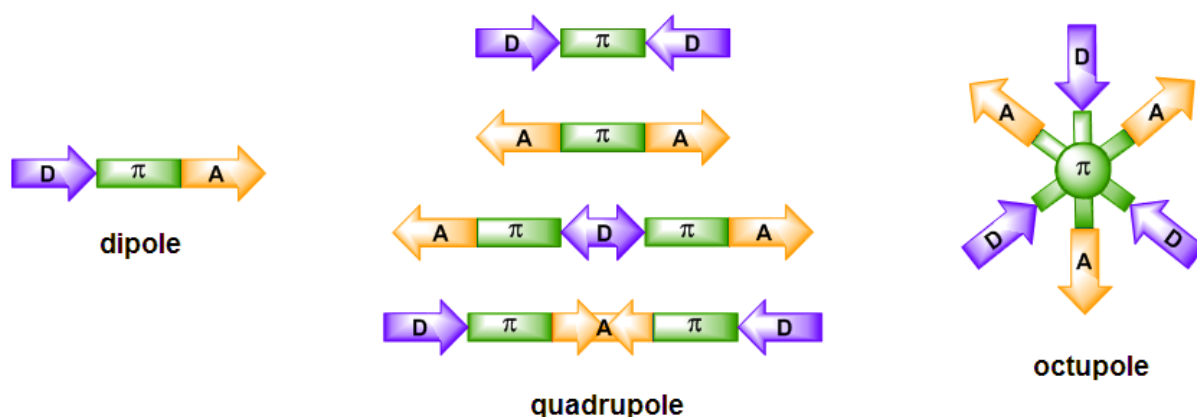


**Figure 7:**  $\pi$ -conjugated systems with polar moments of various orders, induced by donor (D) and / or acceptor (A) moieties.

The two methods currently used most often in literature to determine the  $\sigma_{TPA}$  value are two-photon excited fluorescence (TPEF) and z-scan analysis. TPEF is a highly sensitive method requiring only minute quantities of dilute TPA material solutions, however the method relies on reasonably strong fluorescence.<sup>22</sup> For two-photon photoinitiators (TPIs) it is usually desired to have as little fluorescence as possible, as emission processes only dissipate energy that could otherwise be used to induce polymerization. Thus, in the case of TPIs z-scan analysis is the preferred method as it works even for substances with extremely low fluorescence quantum yields. A drawback of the z-scan is that sensitivity of the method is low and in contrast to TPEF substantially concentrated solutions of the investigated compounds are required to obtain strong enough signals.<sup>23</sup>

Comparing measured cross sections with values from literature is usually problematic because the value is strongly dependent on the exact setup, experimental conditions and fitting calculations used, leading to different results for one and the same compound even if the same method is used.<sup>24</sup>

The fact that TPA is directly proportional to the squared light intensity has a consequence that can be taken advantage of in technology. **Figure 8** shows a dye solution exposed to two different fs-pulsed lasers focused through a microscope objective, a UV laser and an IR laser with photons of twice the wavelength and thus half the energy. Both lasers excite the dye which in turn shows fluorescence emission.<sup>25</sup> In the case of OPA a fluorescence emission is observed along the entire hour-glass shaped beam path in the cuvette, decreasing according to the Beer-Lambert law. For TPA however, the spatial distribution of the fluorescence is completely different. The combination of the tightly focused laser beam and TPA being proportional to the square of the light intensity allow only for a tiny "voxel" (volume element) of fluorescence around the very centre of the laser's focal point.

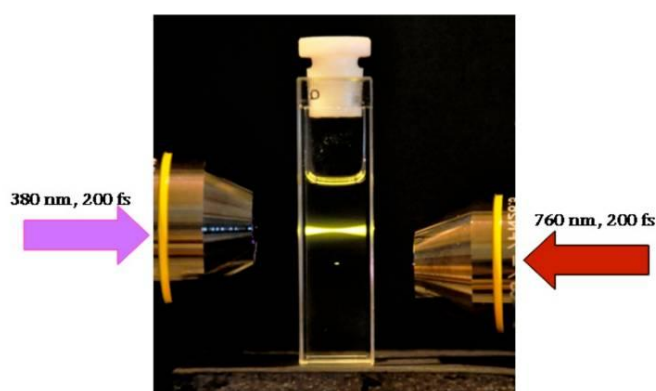


**Figure 8:** Comparison of the spatial distributions of fluorescence emission caused by OPA and TPA respectively, using tightly focused lasers beams of suitable wavelengths.

This ability to induce photophysical and -chemical process within a very small confined volume can be made use of in two-photon induced photopolymerization (TPIP). If the focal point of a fs-pulsed laser is moved within a suitable formulation of monomers and TPIs, the TPA process allows for radical formation and "writing" of dots and lines with a high resolution down to  $\sim 60$  nm, well below the diffraction limit associated with the wavelength of the laser.

Furthermore, because common organic materials are highly transparent at the wavelengths of fs-pulsed Ti:S lasers (700-1000 nm), the light can penetrate deeply into polymerizable resins. This allows for true 3D free form fabrication by TPIP, in contrast to conventional stereolithography using UV-lasers, where the OPA of organic materials

only allows shallow penetration and 3D objects have to be fabricated in a layer-by-layer process applying new resin after each finished layer (see **Figure 9**).<sup>26</sup>

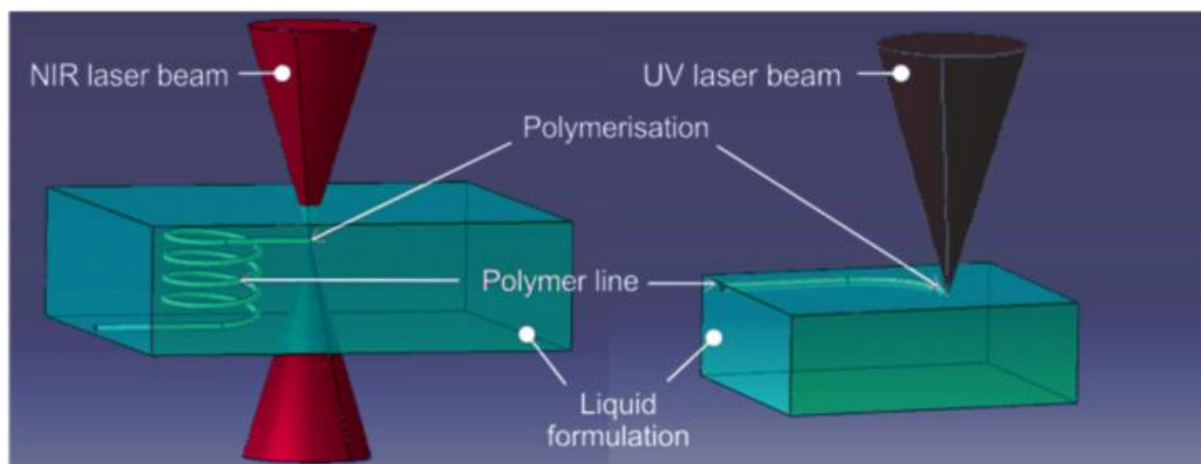


**Figure 9:** The high transparency of common organic materials in the NIR range allows for real 3D processes, whereas limited penetration of UV-light requires layer-by-layer building to obtain 3D structures.

The potential applications of TPIP are numerous. It can be used in stereolithography and rapid prototyping of structures with a feature resolution in the sub-micrometer range. Main applications include 3D printing of electronic and optical micro devices,<sup>27</sup> photonic crystals,<sup>28</sup> microfluidics channels,<sup>29</sup> optical data storage,<sup>30</sup> polymer based optical waveguides on integrated circuit boards<sup>31</sup> as well as biological applications including the fabrication of hydrogel-scaffolds for cell culturing and tissue engineering.<sup>32</sup>

However the high costs and long manufacturing times associated with such fabrication processes are hindrances to large-scale mass production. A more widespread industrial use and commercialization of TPIP will require further research and development both in the field of improving structuring devices and the printing process itself, as well as material formulations with special regard to efficient and affordable TPIs.

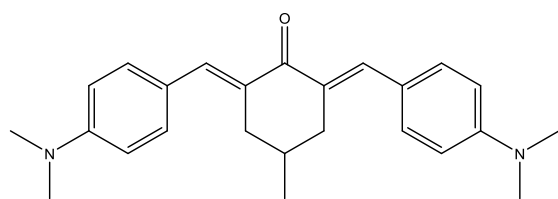
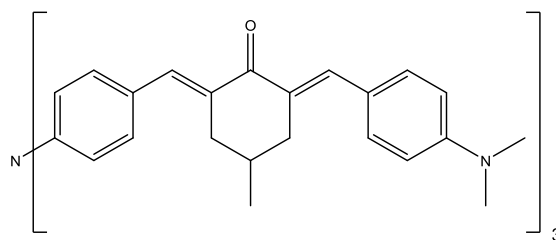
## Objective

The aim of this thesis is to synthesize and evaluate several novel two-photon initiators (TPIs) for two-photon induced photopolymerization (TPIP) structuring. The goal is to increase performance to facilitate broad processing windows, i.e. allowing the fabrication of structures with excellent quality both at high laser intensities and low writing speeds (robust polymerization tolerating high energy input without compromising structural quality) as well as low laser intensities and high writing speeds (low polymerization threshold). This is of crucial importance for applicability of such TPIs because writing speeds can vary drastically as the focal point of the laser changes its direction of movement. Furthermore splitting a single laser beam into a whole array of simultaneously moving focal points (of low intensity) would enable the mass production of microparts by TPIP.

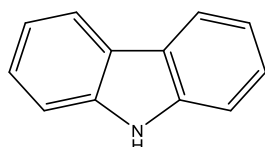
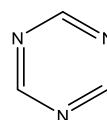
Two distinct strategies should be employed to increase the efficiency:

- enhancing the energy uptake by increasing the TPA cross section  $\sigma_{\text{TPA}}$
- enhancing the conversion of energy into polymerization by designing initiators that undergo irreversible cleavage under radical formation and thus block the deactivating mechanism of back electron transfer from formed radicals to the initiator

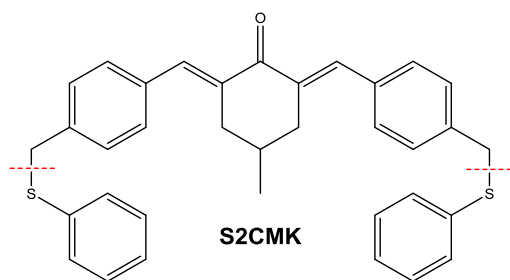
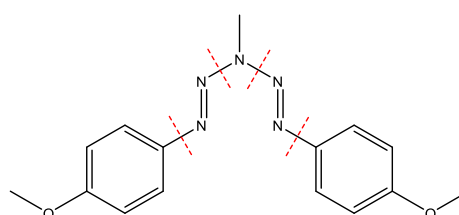
It is known from literature<sup>22</sup> that when several linear dipolar and quadrupolar chromophores are linked together via a central  $\pi$ -conjugated core to form a branched system, the  $\sigma_{\text{TPA}}$  often increases in a non-additive fashion, sometimes leading to much higher values for every added branch. Thus the first goal was to synthesize and evaluate a **Y-shaped** triphenylamine-core based branched analogue of the di-benzylidene ketone-based initiator **M2CMK** (last generation initiator from previous work of our group).

**M2CMK****Y-M2CMK**

Keeping the motif of multipolar D- $\pi$ -A structures with double bonds as  $\pi$ -bridges, the effect of using either highly planarized donor- or acceptor-groups to further increase the  $\sigma_{\text{TPA}}$  of multipolar systems should be investigated. The lead structures used here were **carbazole** and **1,3,5-triazine** respectively.

**carbazole****1,3,5-triazine**

For the second strategy of avoiding back electron transfer, an analogue of **M2CMK** capable of  $\beta$ -phenylogous cleavage, **S2CMK**, and a pentazadiene based compound **PADE** releasing gaseous nitrogen, should be prepared and evaluated.

**S2CMK****PADE**

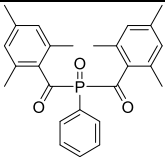
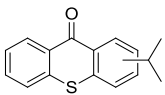
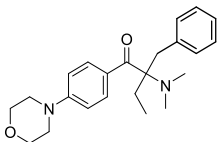
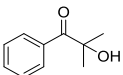
## State of the Art Two Photon Initiators

TPIP is a promising field of research because it allows 3D free form stereolithography with features and resolution in the sub-micrometer range.

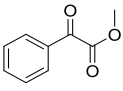
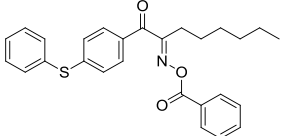
While there also have been some efforts to find efficient photo-acid generators for cationic TPIP, free radical TPIP is still a favourable method due to the large selection of suitable monomers, fast polymerization rate and ease of processing.<sup>33</sup>

Initially, classical one-photon initiators (OPIs) were used in TPIP but only with results of limited quality. They all have rather small  $\sigma_{\text{TPA}}$  and are thus not able to absorb energy efficiently from fs-pulsed lasers in a TPA process. **Table 2** shows an exemplary selection of commercial OPIs investigated regarding their  $\sigma_{\text{TPA}}$  in a study done by Schafer *et al.*<sup>34</sup> While high quantum yields of radical formation can somewhat compensate for their low absorption, they still require high excitation power and long exposure time, often resulting in damage to the polymeric structures.

**Table 2:** Several commercial OPIs, their OPA maxima  $\lambda_{\text{abs}}^{\text{OPA}}$ , wavelength  $\lambda_{\text{z-scan}}$  used for z-scan and TPA cross sections  $\sigma_{\text{TPA}}$ .

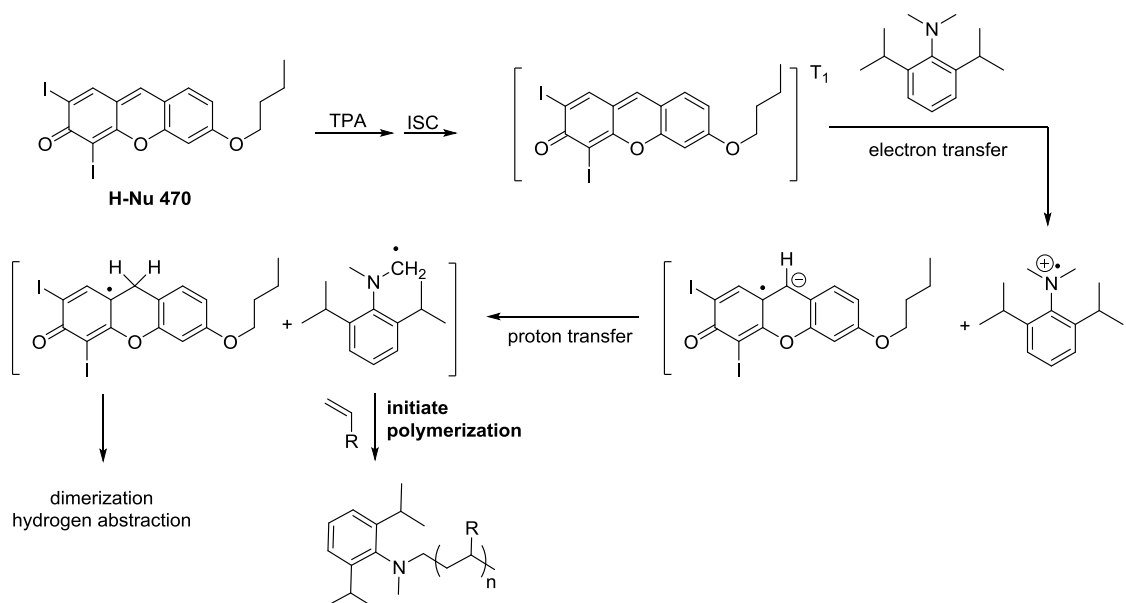
Compound		$\lambda_{\text{abs}}^{\text{OPA}}$ [nm]	$\lambda_{\text{z-scan}}$ [nm]	$\sigma_{\text{TPA}}$ (GM)
Irgacure 819		295	600	< 4
ITX		382	760	5
Irgacure 369		324	670	7
Darocure 1173		244	530	<20



Darocure MBF		255	530	27
Irgacure OXE01		328	660	31

Classical OPIs are still used in TPIP by some research groups for practical reasons. However to overcome their limitations, several different approaches to increase efficiency have been employed.

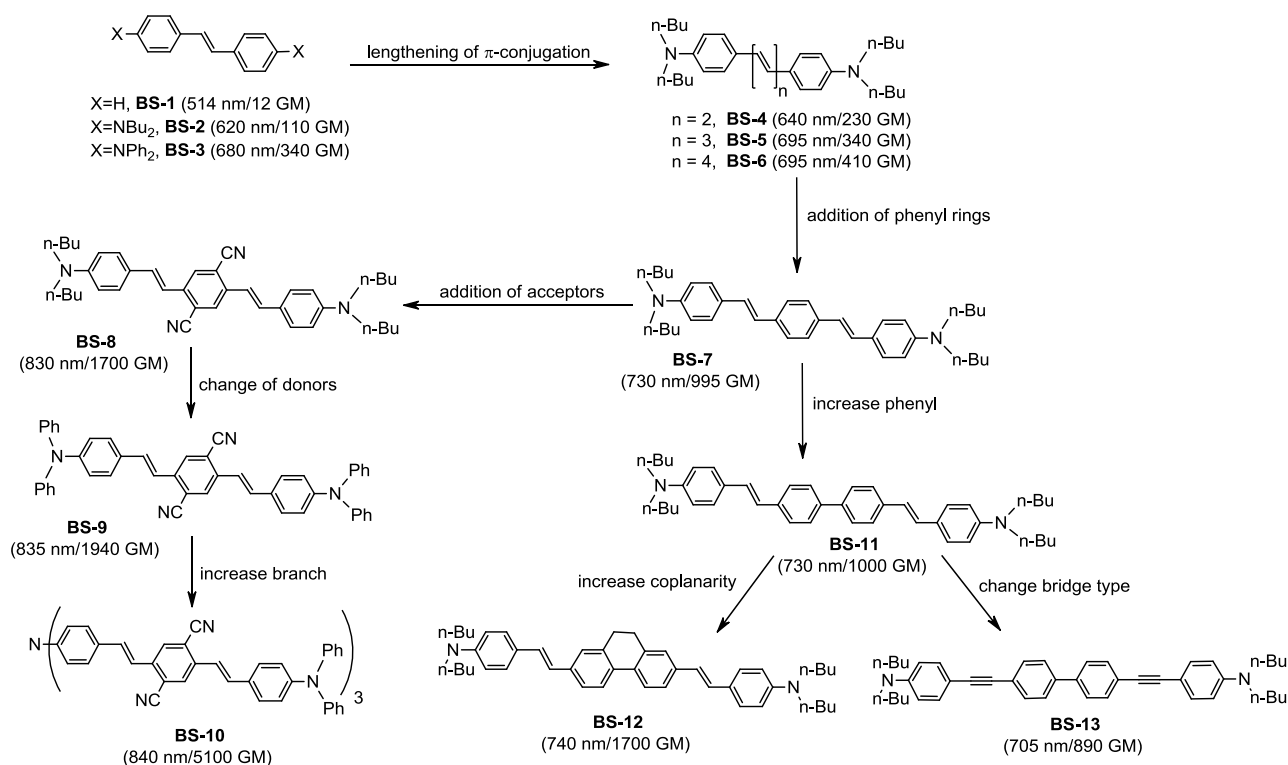
One method to increase TPA sensitivity is the combination of suitable dyes as photosensitizers together with commercial OPIs or amines as a co-initiator. A commercial TPI system combining the dye **H-Nu 470** (see **Figure 10**) and the arylamine N,N-dimethyl-2,6-diisopropylaniline was developed by Belfield *et al.*<sup>35</sup> Its mode of action is analogous to classical type II PIs that work by hydrogen abstraction. The addition of a diaryliodonium salt as co-initiator to generate active phenyl radicals can further increase the rate of polymerization.<sup>36</sup>



**Figure 10:** Initiation mechanism of dye **H-Nu 470**/amine system.

Specialized TPIs that don't resemble classical OPIs and have large  $\sigma_{\text{TPA}}$  also have been developed. The highest  $\sigma_{\text{TPA}}$  are reached with multipolar push-pull-systems where electronic donor and acceptor groups are connected via extended conjugated  $\pi$ -

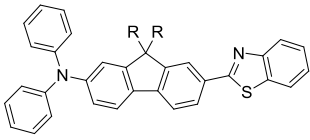
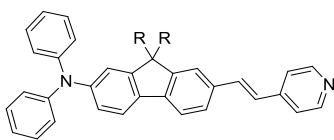
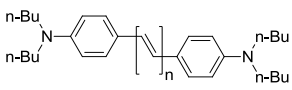
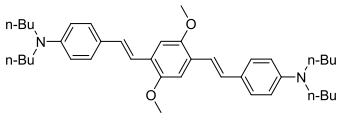
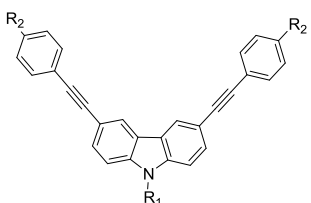
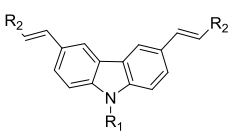
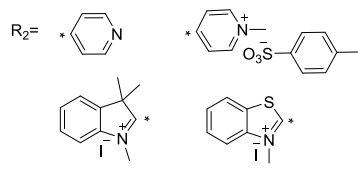
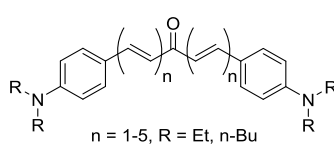
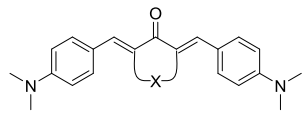
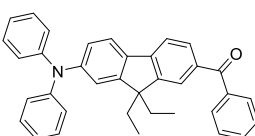
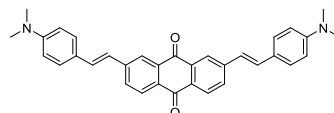
systems of high co-planarity.<sup>16</sup> But high  $\sigma_{\text{TPA}}$  alone doesn't guarantee good photoreactivity for inducing polymerization, as the energy of TPA excited states can be dissipated by various other pathways competing with radical formation, which amongst others are fluorescence and phosphorescence, thermal relaxation, various isomerisation and rearrangement processes, and in case of systems with a bimolecular mechanism also back electron transfer. Up to now, establishing reliable concepts for relationships between molecular structure and TPIP efficiency has remained a challenge. While there have been some attempts at rational design and increase of  $\sigma_{\text{TPA}}$  like the studies (see **Figure 11**) of Mongin *et al.*,<sup>37</sup> the most efficient TPIs so far have been a result of serendipitous discovery, as a multitude of factors in complex relationship with each other affect TPIP efficiency.<sup>22</sup>



**Figure 11:** Schematic overview of a rational design process to increase  $\sigma_{\text{TPA}}$  of TPA materials. The values in brackets are the TPA maxima and  $\sigma_{\text{TPA}}$  respectively.<sup>37</sup>

Some well known other examples from literature based on various core structures are listed in **Table 3**:

**Table 3:** Examples for efficient TPIs from literature.

Core Structures	TPIs	
<b>fluorene</b> <sup>35,38</sup>	 $R = C_{10}H_{21}$ <b>VS-3</b>	 $R = C_{10}H_{21}$ <b>AF-50</b>
<b>bis(styryl)benzene</b> <sup>39</sup>	 $n = 1-4$	 <b>R1</b>
<b>carbazole</b> <sup>40,41</sup>	 $R_1 = C_6H_{11}$ or $PhCH_2$ $R_2 = NO_2$ or $CHO$	 $R_1 = CH_3, C_2H_5$ or $n-C_5H_{11}$ $R_2 =$ 
<b>benzylidene ketone</b> <sup>42,43-47</sup>	 $n = 1-5, R = Et, n-Bu$	 $X = (CH_2)_2$ <b>M2CPK</b> or $CH_2(CH_2CH_3)CH_2$ <b>M2CMK</b>
<b>aromatic ketone</b> <sup>48,49</sup>		

More compounds are included in the reviews of Lee *et al.*,<sup>17</sup> Rumi *et al.*,<sup>18</sup> and Lin *et al.*<sup>50</sup>

For many of these TPIs from literature, a complex synthesis routine requiring modern coupling chemistry with expensive palladium catalysts is required. Others have their double-bonds formed in Wittig<sup>51</sup> or Horner-Wadsworth-Emmons (HWE) reactions<sup>42</sup> of non-commercial Wittig or HWE salts with corresponding aldehydes under strong alkaline conditions, which does not always lead exclusively to the desired *E*-geometry straight away, so that distinct isomerisation steps have to be performed.

Benzylidene ketones like **M2CPK**<sup>43-46</sup> (see **Table 3**) can be prepared in classical aldol condensations, often using economically favourable catalysts like alkali hydroxides or mineral acids and not having a requirement for isomerisation steps as these condensation reactions strongly favour the formation of *E*-products under the right conditions. Previous research by Z. Li from our research group resulted in the di-benzylidene ketone **M2CMK**<sup>52</sup> (see **Table 3**) which is a highly efficient TPI both compared to classical OPIs and well known TPIs from literature like **R1**.<sup>30</sup>

In this thesis, **M2CMK** should be used as a benchmark reference material and also as a starting point for improvement and the design of novel TPIs.

Because in TPIP at any one time the fs-pulsed laser generates only a minute amount of radicals in a tiny voxel, the mechanism of TPIP is inherently difficult to investigate by spectroscopic methods. Thus the exact mechanism for the formation of radicals and the initiation of polymerization is still a subject under discussion. Some compounds working well as a TPI, like **R1** (see **Table 3**), contain no molecular features like weak cleavable bonds or functionalities known for good hydrogen abstraction ability, so the classical mechanisms of type I and type II photoinitiators seem unlikely.

Lu *et al.*<sup>53</sup> proposed a mechanism that is outlined in **Figure 12**. Here, an electron rich TPI with a D- $\pi$ -D structure forms an intra-excplex via intramolecular charge transfer upon excitation by TPA. An electron is then transferred from the TPI to the monomer so that a pair of radical ions results. The radical formed from the monomer can then proceed to initiate the growth of a polymer chain.

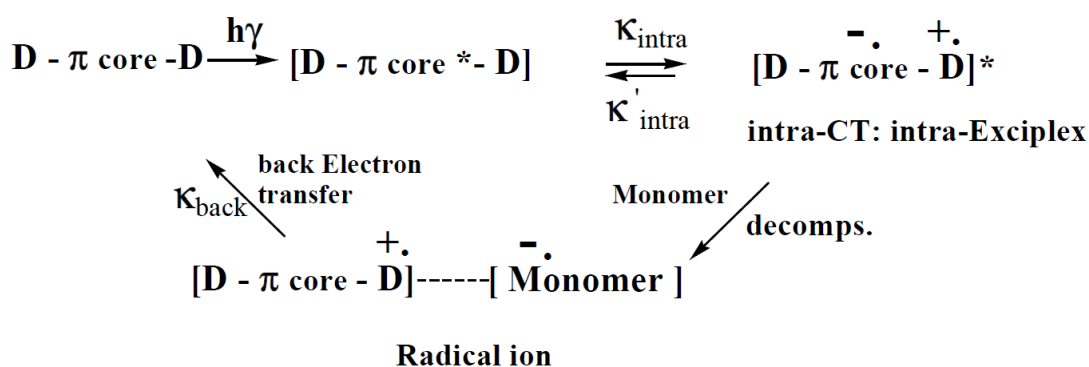


**Figure 12:** Potential initiation mechanism of TPIP proposed by Lu *et al.*<sup>53</sup>

This mechanism seems to require a good capability of the monomer to abstract electrons from the intra-exciplex, a fact that is in accordance with the particularly successful applications of acrylates in TPIP. The  $\alpha,\beta$ -unsaturated carboxyl group in acrylates is an electron acceptor and also ensures a mesomeric stabilization of the formed radical anions.

Similarly to classical type II PIs, such a mechanism could also suffer from a back electron transfer (BET) from the generated monomer radical anion to the TPI radical cation, resulting in a dissipation of the excitation energy.

Thus TPIs could also profit from a photoinduced cleavage forming radicals, since such a process is not as easily reversed. A potential problem could result from the fact that compared to classical type I OPIs, TPIs generally have rather low triplet energies of due to their extended  $\pi$ -systems with donor groups and desired main absorption band in the visible range. Furthermore, classical OPIs are known to have cleavage induced from  $n \rightarrow \pi^*$  - transitions which in case of TPIs are both too weak and at too high wavelengths to be excited efficiently by TPA.

Lalévée *et al.*<sup>54</sup> developed a branched and highly conjugated type I OPI system **Tr\_DMPA** (see **Figure 13**) with a lowest energetic transition of  $\pi \rightarrow \pi^*$  - character. This system showed increased activity compared to the commercial type I OPI parent compound **DMPA** it is based on, which cleaves from a  $n \rightarrow \pi^*$  - transition. Thus it seems plausible that an increase of activity is possible for TPIs as well by introducing cleavable groups and avoiding BET.

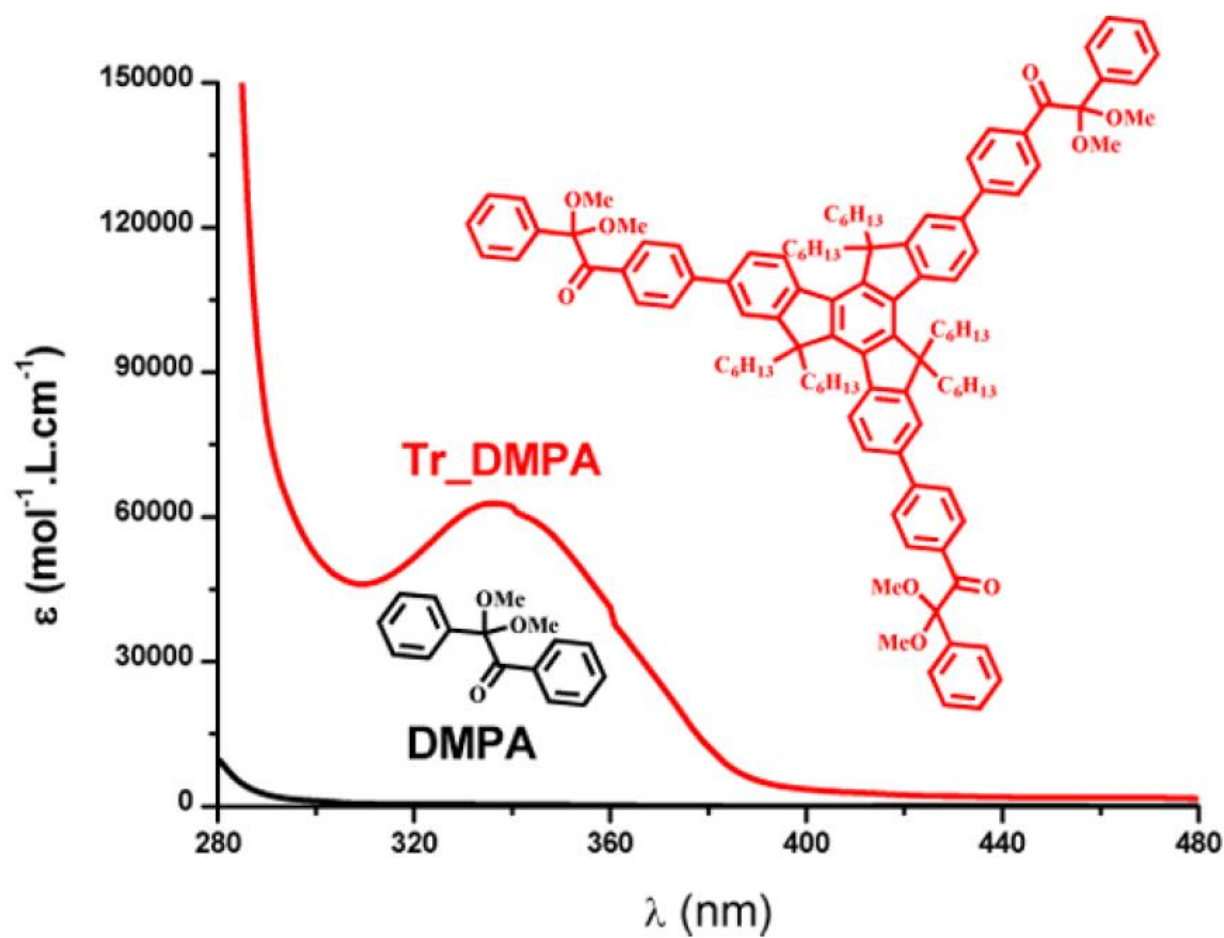


**Figure 13:** Type I OPI system **Tr\_DMPA** with increased absorption at higher wavelengths and enhanced photoreactivity compared to its parent compound **DMPA**.

## Results and Discussion

### 1. Branched/multipolar triphenylamine-based analogues of M2CMK

In a previous study<sup>55</sup> which compared the effect of the central ring size of several benzylidene ketone based TPIs, the cyclohexanone-based **M2CMK** showed a significantly increased structuring efficiency compared to the cyclopentanone-based **B2CPK** (see **Figure 14** the analogous **M2CPK** could not be tested due to low solubility). As a first strategy in attempt to further improve the efficiency of **M2CMK**, an analogous branched compound with higher  $\sigma_{\text{TPA}}$  should be synthesized.

Wu J. *et al.* showed that a tribranched benzylidene cyclopentanone dye **Y-M2CPK** (see **Figure 14**) had higher efficiency in sensitizing the commercial cationic initiator Omnicat 820 (bis(4-methylphenyl)iodonium hexafluorophosphate) than the analogous linear compound **M2CPK**, as well as a significantly increased  $\sigma_{\text{TPA}}$  for each branch in comparison to **M2CPK**.<sup>56</sup>

In the light of the superiority of cyclohexanone-based **M2CMK** over cyclopentanone-based **B2CPK** in TPIP structuring even without further added initiators like Omnicat 820, an analogous cyclohexanone-based branched compound **Y-M2CMK** should be synthesized to investigate if there is an increase in  $\sigma_{\text{TPA}}$  per branch as well as an improvement in TPIP structuring efficiency.

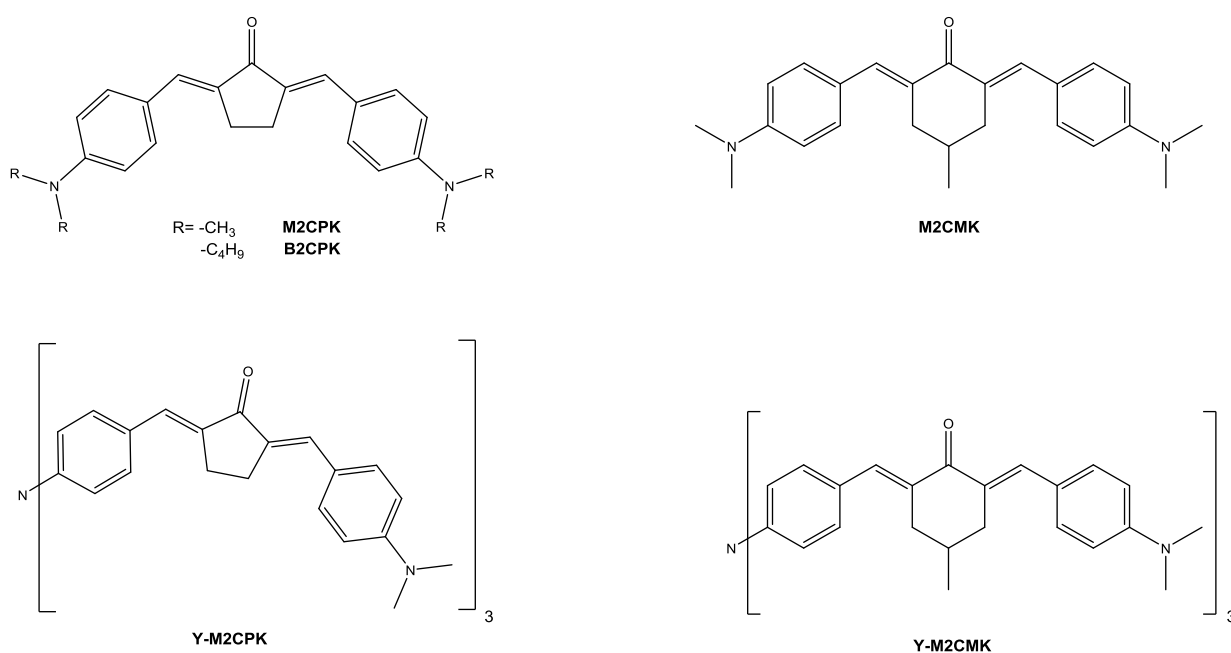


**Figure 14:** Cyclic di-benzylidene ketones and their branched analogues.

## 1.1. Y-M2CMK

### 1.1.1. Synthesis of Y-M2CMK

The chosen synthetic approach is analogous to the one used by Wu J. *et al.*<sup>56</sup> in first preparing the mono-benzylidene ketone **1** via aldol condensation of 4-(dimethylamino)-benzaldehyde and 4-methylcyclohexanone. Subsequently the remaining enolizable methylene groups of 3 equivalents of **1** are coupled to trialdehyde **3** in a further aldol condensation step (see **Figure 15**).

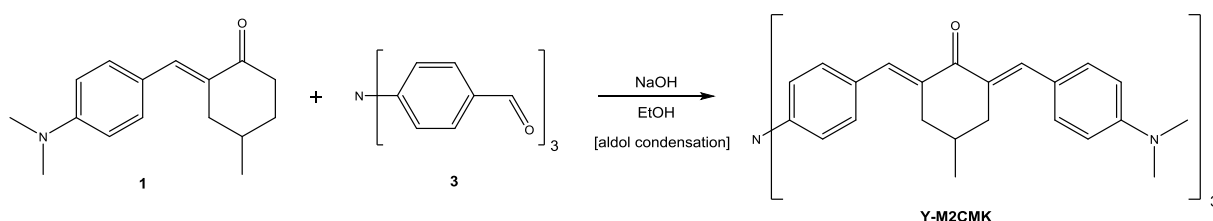


**Figure 15:** Aldol condensation route to Y-M2CMK.

#### 1.1.1.1. Synthesis of precursor (2*E*)-2-[[4-(dimethylamino)phenyl]methylene]-4-methylcyclohexanone (**1**)

For the preparation of **1** it was first attempted to follow the protocol for **M2CMK** stirring 4-(dimethylamino)benzaldehyde, 4-methylcyclohexanone and NaOH as catalyst in EtOH at room temperature, with the modification of using a 1:5 instead of 2:1 molar ratio of aldehyde to ketone to promote the formation of mono- versus di-substituted product. This approach led to several problems: Yields were low as the conversion of the aldehyde was only partial even after days of stirring. Furthermore the mono-benzylidene ketone is more reactive in aldol reactions compared to the unsubstituted ketone; substantial amounts of **M2CMK** were formed despite the large excess of ketone and the yield of **1** was decreased further to about 12%. While the bulk of **M2CMK** precipitates in EtOH as soon as formed and thus is easily removed from the reaction mixture, the separation of 4-(dimethylamino)benzaldehyde from **1** is more difficult, because both have similar solubility in various solvents and close  $R_f$ -values (less than 0.1 difference) on silica gel regardless of trying several different eluent mixtures. The residual excess 4-methylcyclohexanone further complicates the separation and attempts to remove it by vacuum distillation at elevated temperatures lead to further impurities most likely caused



by self condensation of the ketone, especially if not all traces of NaOH or acids have been removed.

To avoid these problems at least partially, **1** was also prepared according to a modified version for the preparation of mono-benzylidene cyclohexanone from literature<sup>57</sup> by refluxing a heterogeneous mixture of 1 equivalent 4-(dimethylamino)benzaldehyde, 2 equivalents 4-methylcyclohexanone and aqueous NaOH solution for 20 h (see **Figure 16**). The oily crude product was crystallized from PE while most of the excess 4-methylcyclohexanone stays dissolved in the mother liquor.

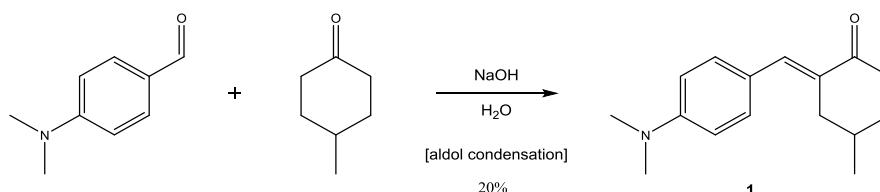


**Figure 16:** Aldol condensation route to precursor **1**.

The crystalline crude product thus obtained consist of a mixture of 4-(dimethylamino)benzaldehyde, **1** and **M2CMK**. Separation by column chromatography using a PE:EA mixture afforded pure **1** with a yield of 20%, in addition to some impure fractions containing 4-(dimethylamino)benzaldehyde.

#### 1.1.1.2. Synthesis of precursor 4,4',4''-nitrlotris(benzaldehyde) (**3**)

The efficient preparation of tri-aldehyde **3** has been subject to some research as it is an important building block in materials chemistry and known procedures resulted in poor yields. Vilsmeier-Haack reaction of triphenylamine even with optimized amounts of POCl<sub>3</sub> and DMF leads mainly to the di-aldehyde **2** as the remaining benzene ring is not activated enough for the third formylation reaction due to the strong electron withdrawing effect of the two iminium groups present in the ionic intermediate formed after the second formylation step. However if the reaction mixture is hydrolyzed to convert the iminium groups to the less deactivating formyl groups and the resulting product consisting mainly of **2** is subjected to another Vilsmeier-Haack reaction in a distinct second step, according to literature<sup>58</sup> the yield of **3** can be increased to 52% compared to 16% for direct isolation from a one-step Vilsmeier-Haack procedure (see **Figure 17**).

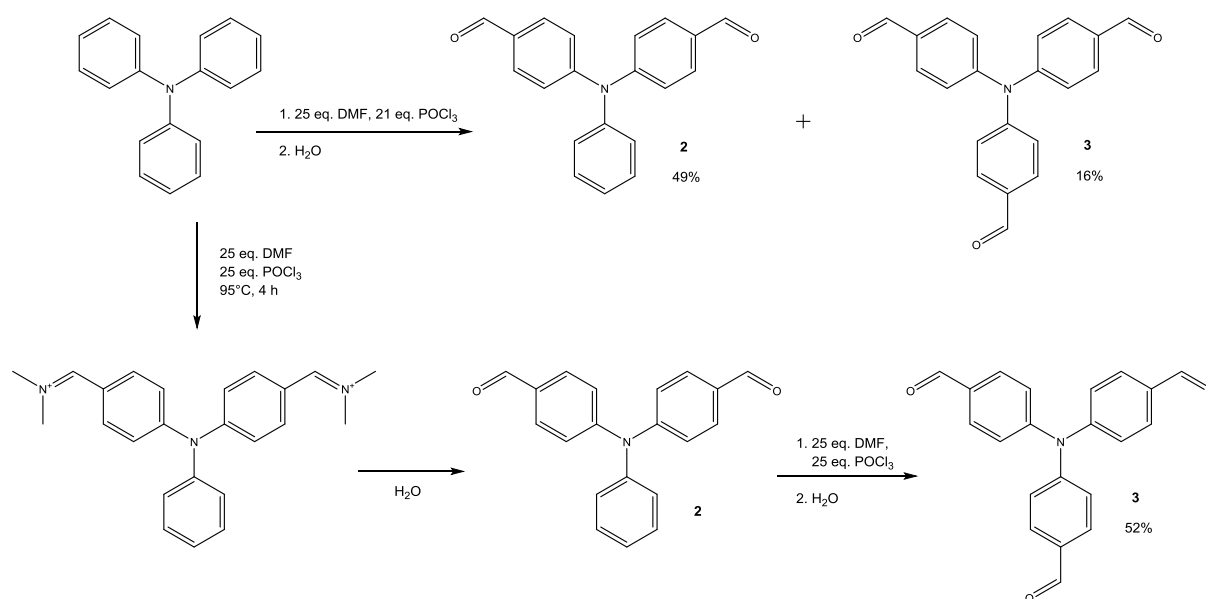


**Figure 17:** One- and two-step Vilsmeier-Haack procedure yielding precursor **3**.

Attempting to reproduce these results, the first formylation step gave a good yield of 89% (calculated for pure **2**). In the second step however, decomposition occurred and large amounts of an insoluble, foamy dark brown byproduct were formed, causing the total yield of **3** after column chromatography using silica gel 60 and DCM as eluent to drop to 16%. This problem could possibly be avoided by adding crude **2** to the reaction mixture at a lower temperature (although the Vilsmeier reagent would be solid and very difficult to stir then, leading to an inhomogeneous mixture) or diluting the starting material and/or reaction mixture with an inert solvent as it is done in a different Vilsmeier-Haack reaction employed in this work.<sup>59</sup>

#### 1.1.1.3. Synthesis of Y-M2CMK - final step

For the subsequent coupling reaction to obtain **Y-M2CMK** via aldol condensation 4.5 eq. of **1** and 1 eq. of **3** were refluxed in EtOH under alkaline catalysis with NaOH, quickly leading to the formation of an orange precipitate (see **Figure 18**).

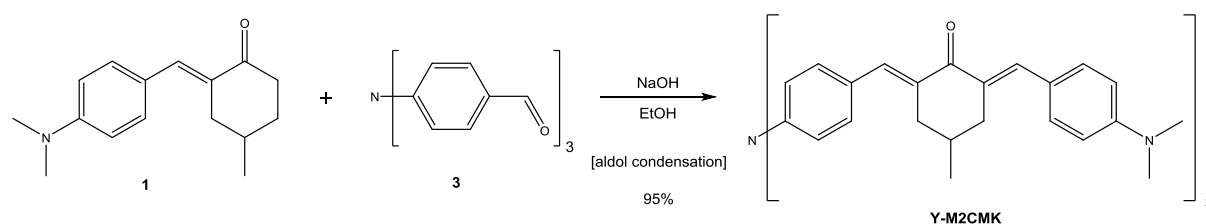


**Figure 18:** Aldol condensation of **1** and **3** to **Y-M2CMK**.

This precipitate was collected and washed with EtOH to remove residual starting materials. The crude product is acceptably soluble in  $\text{CHCl}_3$  and slightly less soluble in DCM, but the solubility in most other common organic solvents is very low, so much so that stained glassware can't be cleaned with acetone efficiently. TLC with an optimized mixture of PE:DCM:MeOH:TEA = 38:56:4:2 shows 5 orange spots: a main spot with a  $R_f = 0.47$  and 4 side products (2 below and 2 above) next to this spot within an  $R_f$ -range  $< \pm 0.1$ . At least one of the spots above the main spot must be an intermediate still containing unreacted aldehyde groups (products of only one- or twofold condensation reaction) as NMR analysis of the thoroughly washed crude product showed aldehyde signals at 9.93 and 9.88 ppm respectively, indicating a content of about 8%. Even using 4.5 eq. and several days of reflux did not lead to a complete threefold condensation - a possible explanation for this might be the extremely low solubility of **Y-M2CMK** in EtOH leading to crystal inclusions of intermediates in the precipitate and slowing down further reaction considerably.

The other spots visible are most likely stereoisomers of the main product - **1** has an asymmetric carbon atom in position 4 of the cyclohexanone ring; the racemic mixture that is used in the formation of **Y-M2CMK** leads to two diastereomeric forms of the latter, with the combinations RRR and RRS (and their enantiomeric counterparts) for the three branches of the molecule. Many *E/Z*-isomers are also possible, but the aldol condensation seems to strongly favor the *E*-products so that these are less likely impurities and would be easily discernible in NMR because of a significantly different chemical shift of the olefinic proton.

Attempts to recrystallize **Y-M2CMK** from various solvents failed, as its solubility in most solvents is very low and for solvents with reasonable solubility as DCM,  $\text{CHCl}_3$  or pyridine, the solubility difference between hot and cold solvent is too small and/or **Y-M2CMK** doesn't crystallize well but precipitates as fine powder without significant removal of impurities.

Purification via column chromatography also proved impractical both because of the complex mixture of products with similar  $R_f$ -values as well as the low solubility in the PE:DCM:MeOH:TEA-eluent system giving the best resolution of products – only about 20% of the crude product could be eluted from the silica gel column and no fractions of the main product without any side products visible by TLC could be obtained.

### 1.1.2. Analysis of Y-M2CMK – open aperture z-scan

For determination of the  $\sigma_{\text{TPA}}$   $\text{CHCl}_3$  had to be used instead of THF in which the measurements are usually performed, as the solubility of **Y-M2CMK** in THF is far too low. A 10 mM solution in  $\text{CHCl}_3$  exhibited a cross section of 570 GM which is almost exactly the threefold value of the analogous non-branched compound **M2CMK** (191 GM). The cooperative effect increasing the cross sect for branched compounds non-linearly here obviously is too weak or cancelled by other factors; the central triarylamine core is not planar but "propeller"-shaped, weakening the conjugation and thus electronic communication between the branches. Furthermore the central nitrogen is worse a donor than a dimethylamino group, as the lone pair is shared by three branches and each branch has a dominant -M-effect compared to the +I-effect of the methyl groups. The OPA spectrum of **Y-M2CMK** is compared to **M2CMK** in the next chapter (see **Figure 21**).

No polymerization tests could be performed because **Y-M2CMK** is practically insoluble in the ETA:TTA =1:1 (see chapter ) mixture used for structuring. Because of the very low solubility of **Y-M2CMK** an analogous derivative **Y-B2CMK** with n-dibutylamino- instead of dimethylamino-substituents and therefore higher solubility should be synthesized.

## 1.2. Y-B2CMK

### 1.2.1. Synthesis of Y-B2CMK

#### 1.2.1.1. Synthesis of precursor (2E)-2-[[4-(dibutylamino)phenyl]methylene]-4-methylcyclohexanone (**4**)

The same synthetic strategy used for **Y-M2CMK** was be employed, as the final coupling step worked reasonably well and the necessary tri-aldehyde **3** was already available.

For the preparation of the n-dibutylamino-group containing mono-benzylidene ketone **4** commercially available 4-(dibutylamino)benzaldehyde was condensed with 4-methylcyclohexanone in the presence of KOH as catalyst in EtOH at room temperature for 4 days (see **Figure 19**).

The isolation of **4** from the reaction mixture proved even more difficult than in case of the analogous dimethylamino-benzylidene ketone **1**. In contrast to **M2CMK**, the analogous n-dibutylamino-group containing compound **B2CMK** has high solubility in alcohols like MeOH and EtOH and thus does not precipitate from the reaction mixture.

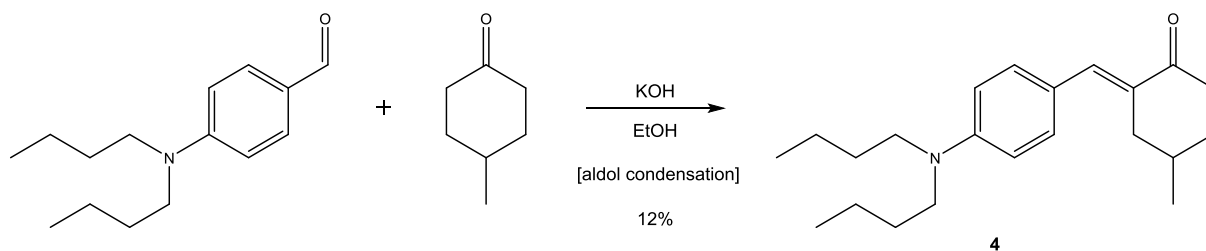


Figure 19: Aldol condensation route to **4**.

The starting material 4-(dibutylamino)benzaldehyde and **4** have identical  $R_f$ -values in various solvent mixtures preventing separation on silica gel and furthermore removing excess 4-methylcyclohexanone by recrystallization from PE is not feasible anymore as the solubility of **4** in PE is too high. Thus most of **B2CMK** and 4-methylcyclohexanone were first removed from the crude product by normal phase column chromatography using PE:EA = 10:1 as eluent. The final purification step was performed by preparative reversed phase column chromatography using MeCN:H<sub>2</sub>O = 95:5 as eluent, which effectively separated **4** from 4-(dibutylamino)benzaldehyde and the other impurities, leading to a yield of 12%.

Literature suggests there might be a much more efficient way to obtain **4** in higher yields (Kreher et. al<sup>60</sup>) using the distillable ionic liquid dimethylammonium dimethylcarbamate (DIMCARB) which acts as both solvent and catalyst, but this approach was not tested as the amount of **4** obtained by alkaline-catalyzed reaction was sufficient for the subsequent experiments of the present work.

#### 1.2.1.2. Synthesis of Y-B2CMK – final step

The subsequent coupling reaction to obtain **Y-B2CMK** via aldol condensation 4 eq. of **4** and 1 eq. of **3** were stirred in EtOH at 60°C under alkaline catalysis with KOH for 5 days (see **Figure 20**), leading to the formation of a deep red, waxy appearing precipitate.

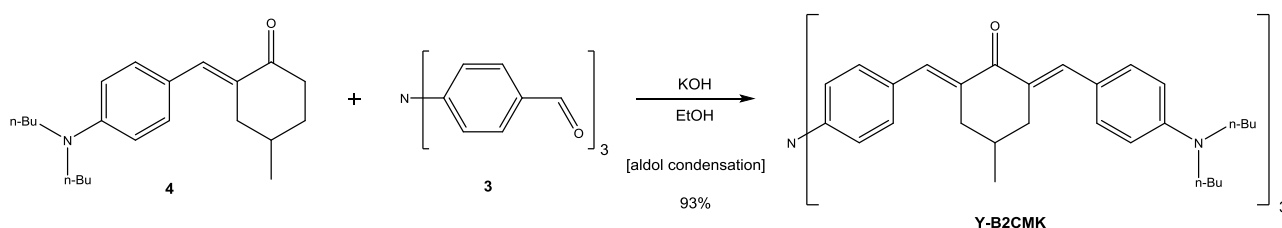


Figure 20: Aldol condensation route to **4**.

The reaction proceeded with an excellent yield of 93%. Similar to **Y-M2CMK** the crude product showed impurities visible in TLC as several faint red bands within an  $R_f$ -range  $<\pm 0.1$  next to the main spot, no solvent was found to give a resolution sufficient to reasonably perform column chromatography and attempts on recrystallisation also proved futile as **Y-B2CMK** does not crystallize well but tends to form a waxy amorphous looking solid with no sharp melting point from oversaturated solutions (six butyl groups per molecule probably hindering the formation of well-defined crystals). Thus the crude precipitate was just washed thoroughly with EtOH to remove residues of starting materials and intermediate condensation products and dried in vacuo. NMR analysis showed no traces of aldehyde groups left, so the impurities are most likely just stereoisomers and the product was used without further purification.

### 1.2.2. Analysis of Y-B2CMK

#### 1.2.2.1. Open aperture z-scan

The  $\sigma_{\text{TPA}}$  of **Y-B2CMK** was measured from a 10mM THF solution and determined to be 316 GM. Quantum chemical calculations (refer to literature<sup>55</sup>) comparing the dibenzylidene ketones obtained from condensation of cyclopentanone with 4-(dimethylamino)benzaldehyde and 4-(dibutylamino)benzaldehyde respectively show that exchanging methyl for butyl groups leads to a drop in  $\sigma_{\text{TPA}}$  from 466 GM to 327 GM because the strong pyramidity on the nitrogen atom of the  $\text{Bu}_2\text{N}$ -group leads to a twisting of the aromatic rings out of plane of about  $41^\circ$  relative to each other. A similar twisting is to be expected for **Y-B2CMK** resulting in the considerably lower value compared to **Y-M2CMK** (570 GM).

#### 1.2.2.2. UV/Vis - spectroscopy

Another possible explanation for the decrease in cross section might be that the used laser wavelength around 800 nm is not attuned to the two-photon absorption maximum of **Y-B2CMK**, which shows a red-shift as well as a strong increase of molar extinction in OPA spectra ( $\lambda_{\text{abs}}^{\text{OPA}} = 444 \text{ nm}$ ,  $\epsilon = 1.2 \cdot 10^5 \text{ M}^{-1} \text{ cm}^{-1}$ , see **Figure 21**) compared to **M2CMK** ( $\lambda_{\text{abs}}^{\text{OPA}} = 430 \text{ nm}$ ,  $\epsilon = 4.7 \cdot 10^4 \text{ M}^{-1} \text{ cm}^{-1}$ ), and a slight blueshift compared to **Y-M2CMK** ( $\lambda_{\text{abs}}^{\text{OPA}} = 451 \text{ nm}$ ,  $\epsilon = 8.5 \cdot 10^4 \text{ M}^{-1} \text{ cm}^{-1}$ ,  $\text{CHCl}_3$ ).

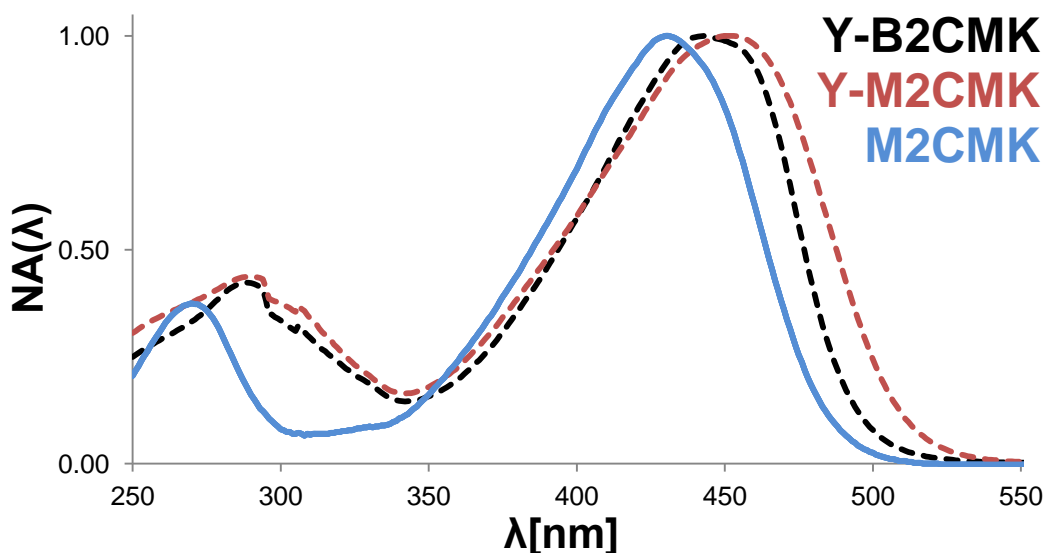


**Figure 21:** Normalized OPA spectra of **Y-B2CMK** (black dotted line, measured in THF), **Y-M2CMK** (red dotted line, measured in  $\text{CHCl}_3$ ) and reference compound **M2CMK** (blue line, measured in MeCN) all measured at a concentration of  $10^{-5} \text{ mol L}^{-1}$

### 1.2.2.3. TPIP structuring tests

For the evaluation of TPI performance the following procedure was used in this work: The TPI was dissolved in a mixture of acrylate resins (1:1 mixture of trimethylolpropane triacrylate **TTA** and ethoxylated-(20/3)-trimethylolpropane triacrylate **ETA**) and woodpile-structures were written at different laser intensities and writing speeds. Scanning electron microscopy (SEM) images of the polymerized structures were judged visually and divided in four different quality classes (see **Figure 22**) to estimate a processing window for the TPI, i.e. how well it works depending on laser intensity and writing speed.

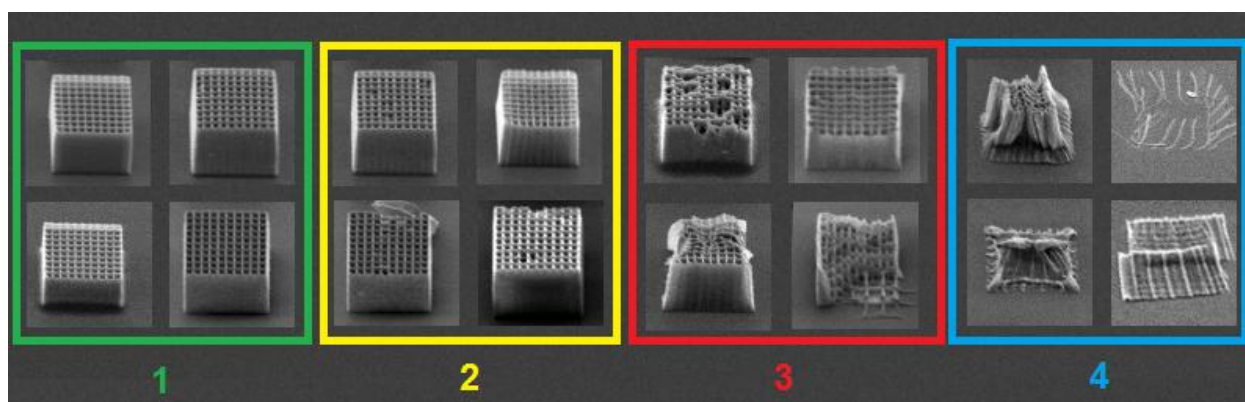


**Figure 22:** Examples for the different structure quality classes and their color codes as used in this work.

While as discussed in **Chapter 1.1.2** no processing window for **Y-M2CMK** could be determined because of low solubility, the introduction of the dibutylamino-groups fulfilled its purpose. Pre-dissolving **Y-B2CMK** in acetone (removed again in vacuo after mixing with ETA/TTA) was still necessary, but the compound formed a stable solution with ETA/TTA = 1:1 at a concentration of 6.3  $\mu\text{mol PI/g resin}$ . It would be more accurate to account for the larger  $\pi$ -system by choosing a lower concentration for **Y-B2CMK** than for the reference **M2CMK**, but it is hard to decide on meaningful alternative values as the ratio and relative strength of donor to acceptor groups change as well.

Performance tests with woodpile structures written at different laser intensities and writing speeds show a significant improvement for **Y-B2CMK** (6.3  $\mu\text{mol PI/g resin}$ , see **Figure 25 & Figure 26**) compared to **M2CMK** (6.3  $\mu\text{mol PI/g resin}$ , see **Figure 23 & Figure 24**) especially for higher energies (class 1 structures up to 90 mW at 1 mm/s for **Y-B2CMK** versus only 60-70 mW for **M2CMK**), and it also seems to be slightly more sensitive at lower energies.

<b>M2CMK</b>							
mW	1	26	51	76	101	126	151 mm/s
130	3	1	1	1	1	1	1
120	3	1	1	1	1	1	1
110	3	1	1	1	1	1	1
100	3	1	1	1	1	1	1
90	3	1	1	1	1	1	1
80	3	1	1	1	1	1	1
70	2	1	1	1	1	1	1
60	1	1	1	1	1	1	1
50	1	1	1	1	1	1	1
40	1	1	1	2	3	3	4
30	1	2	4	4	4	4	4
20	1	4	-	-	-	-	-
10	-	-	-	-	-	-	-

**Figure 23:** Processing window of reference **M2CMK** (6.3  $\mu\text{mol PI/g}$  ETA:TTA =1:1).



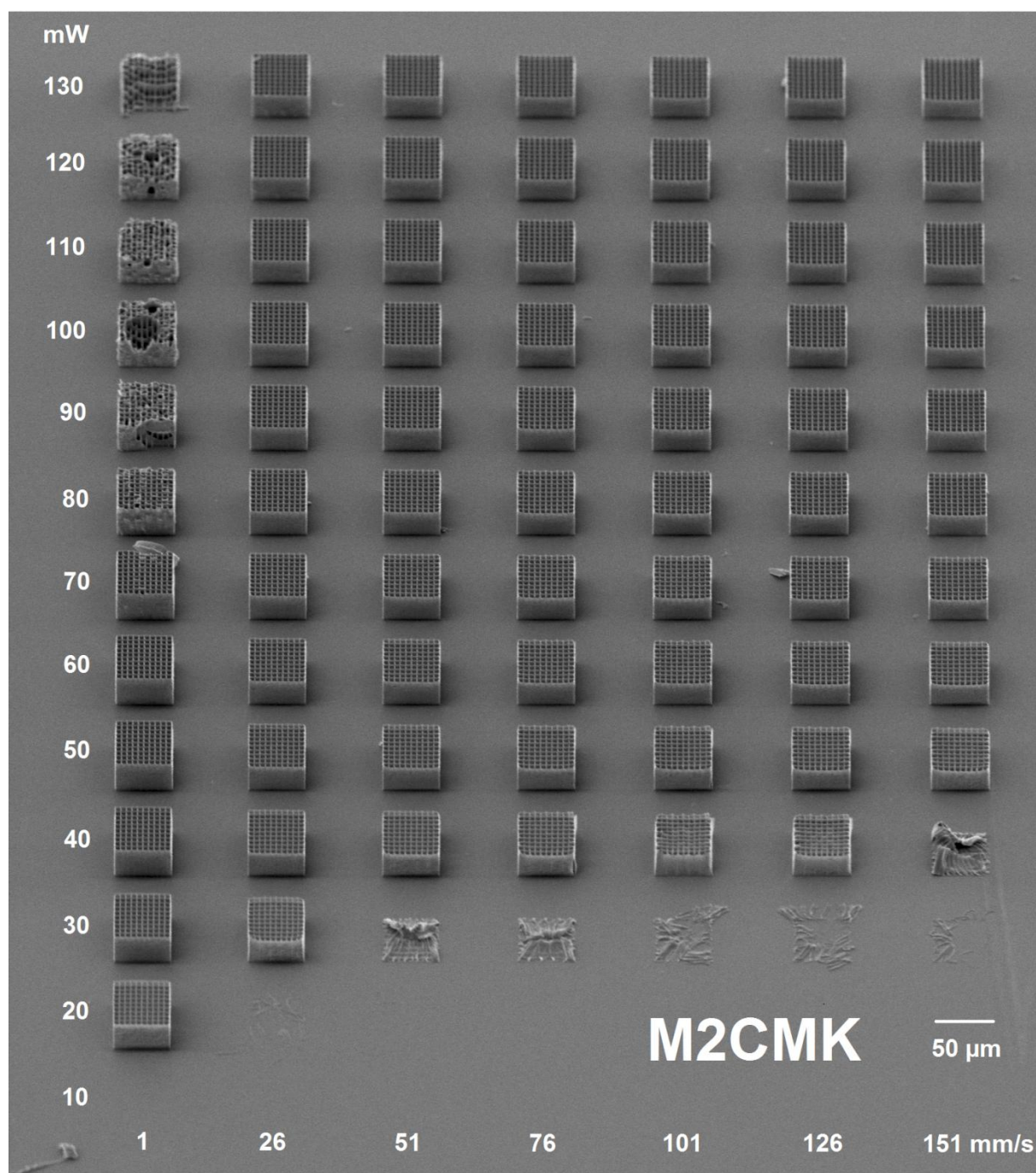


**Figure 24:** SEM-image of woodpile structures built with reference **M2CMK** (6.3  $\mu\text{mol PI/g ETA:TTA} = 1:1$ ).

Y-B2CMK								
mW	1	26	51	76	101	126	151	mm/s
130	3	1	1	1	1	1	1	
120	3	1	1	1	1	1	1	
110	3	1	1	1	1	1	1	
100	3	1	1	1	1	1	1	
90	1	1	1	1	1	1	1	
80	2	1	1	1	1	1	1	
70	1	1	1	1	1	1	1	
60	1	1	1	1	1	1	1	
50	1	1	1	1	1	1	1	
40	1	1	1	2	3	3	2	
30	1	1	4	4	4	4	4	
20	1	4	4	4	-	-	4	
10	4	-	-	-	-	-	-	

**Figure 25:** Processing window of Y-B2CMK (6.3  $\mu\text{mol PI/g}$  ETA:TTA =1:1).

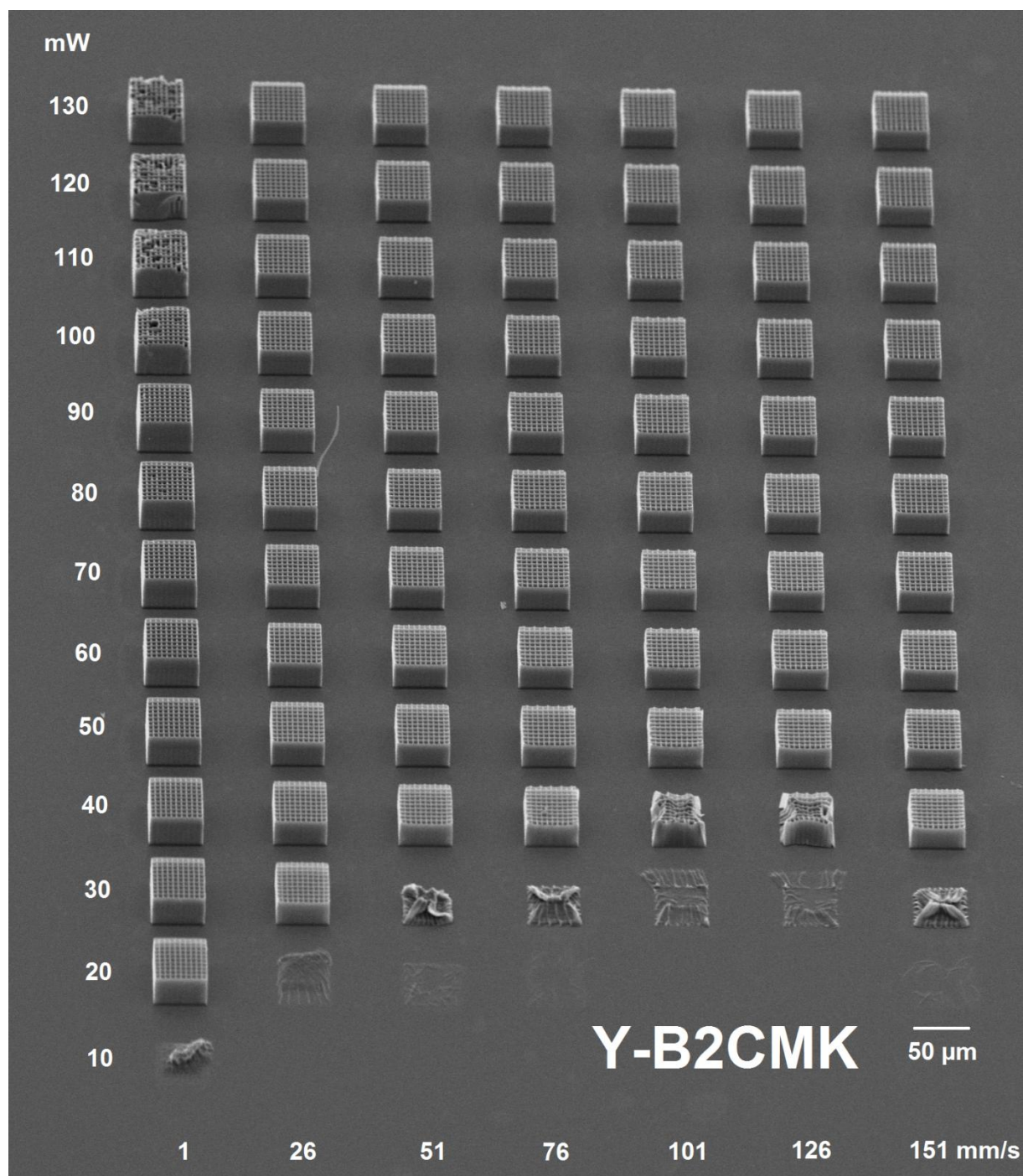


**Figure 26:** SEM-image of woodpile structures built with **Y-B2CMK** ( $6.3 \mu\text{mol PI/g ETA:TTA} = 1:1$ ).

## 2. Planarized branched/multipolar carbazole-based analogues of M2CMK

As discussed in the last chapter, branched systems based on triphenylamine as a core element did not exhibit a significant improvement in  $\sigma_{\text{TPA}}$  compared to the singular branch. One of the possible reasons for this is the geometry of triphenylamine, which is not planar but "propeller"-shaped, thus having low conjugation between its three rings. Branches attached to them are twisted and bent out of co-planarity, leading to a weakened electronic coupling.

Thus the effect of a planarized core element should be investigated. A 2007 article by Xing *et al.*<sup>61</sup> explores A- $\pi$ -D- $\pi$ -A structures based on carbazole as a donor and central element. They compared n-pentyl- and benzyl-groups as substituents for the carbazole nitrogen, and got lower polymerization threshold intensities for the benzyl-substituents. This fact they ascribe to an intermediate radical that is not only in alpha-position to nitrogen but also in benzylic position and thus has a better mesomeric stabilization.

The  $\sigma_{\text{TPA}}$  of the compounds investigated in the article<sup>61</sup> were determined by TPEF and ranged from 308 GM for the weakest absorber **AP3CB** to 916 GM for the strongest absorber **NP3CB** (depicted in **Figure 27**). **NP3CB** also happened to exhibit the lowest polymerization threshold and thus highest initiation efficiency of the four compounds, despite the fact that nitro-groups are known to act as inhibitor by radical scavenging.

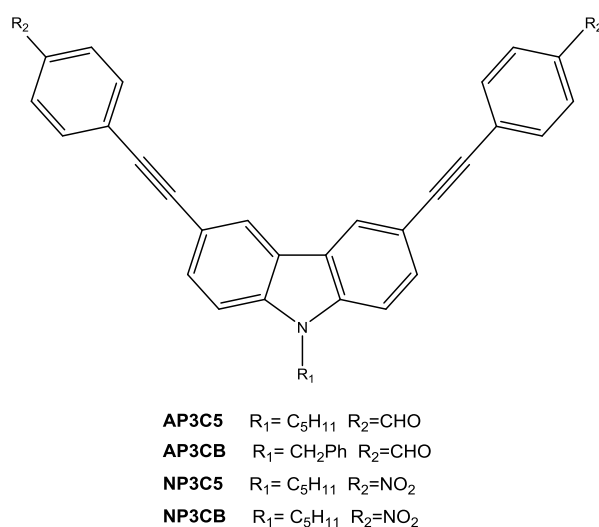


**Figure 27:** Several carbazole based TPAs from literature.<sup>61</sup>

The promising characteristics of the compound **NP3CB** from literature led to the choice of incorporating N-benzyl carbazole as a core element and donor group for a benzylidene ketone-based di-branched TPI.

## 2.1. B2Cbz

### 2.1.1. Synthesis of B2Cbz

To build this TPI **B2Cbz**, an analogous synthetic strategy to the triphenylamine-based compounds from **Chapter 1** should be employed. From the syntheses of the latter, the necessary mono-benzylidene ketones were already available.

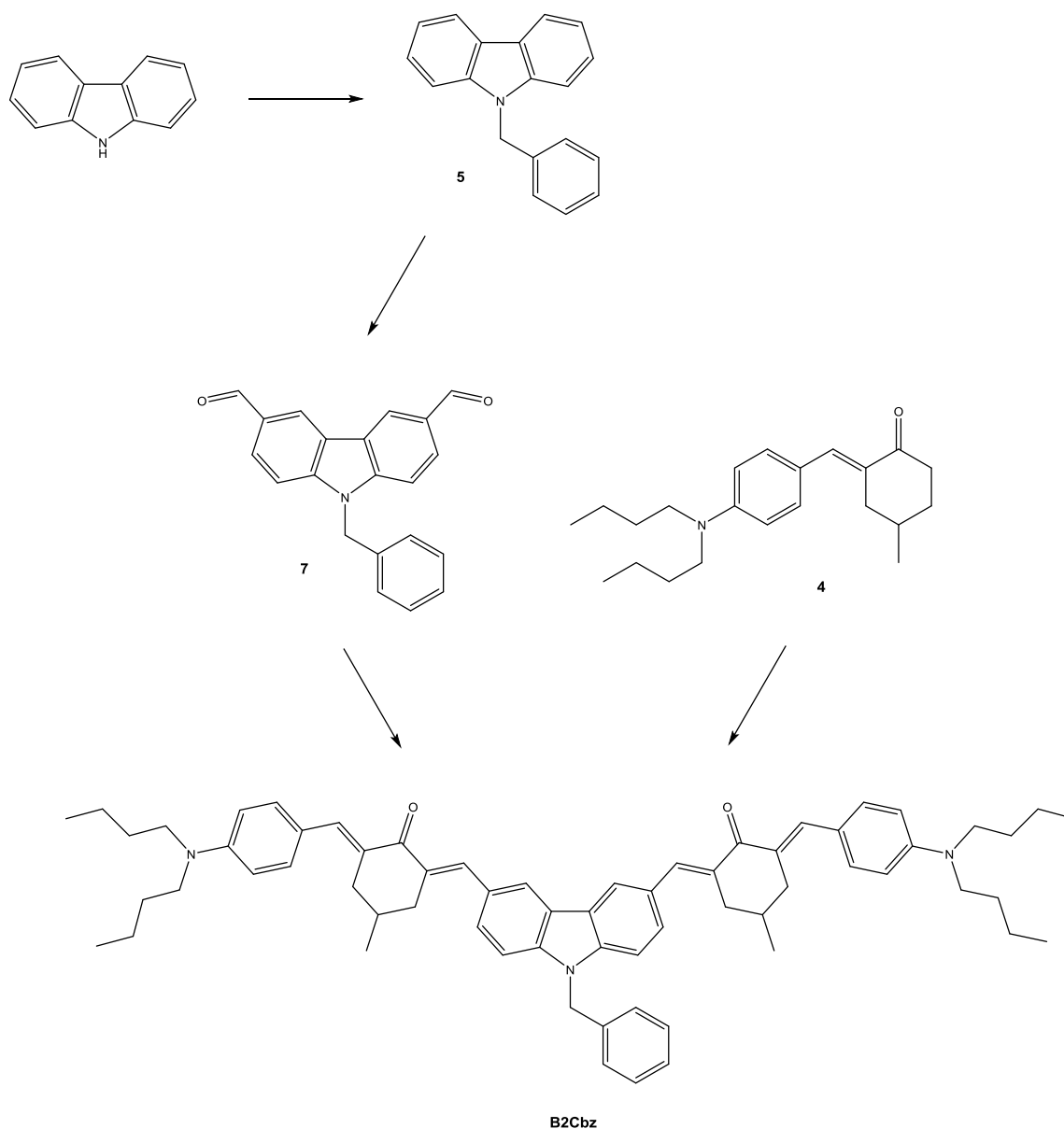


**Figure 28:** Overview of the synthesis of **B2Cbz**.

#### 2.1.1.1. Synthesis of precursor 9-(phenylmethyl)-9H-carbazole (5)

The di-aldehyde **7** was required for the final aldol condensation step and was to be prepared starting from carbazole. The first step was to N-alkylate 9H-carbazole according to literature<sup>59</sup> (see **Figure 29**) using benzyl bromide and NaOH in DMSO as an alkaline catalyst to partially deprotonate the secondary amine in carbazole and neutralize hydrogen bromide formed in the alkylation reaction. After diluting the reaction mixture with water, the crude product precipitated and was purified by double recrystallization from EtOH (product of first recrystallization still had a brownish tinge and unsubstituted carbazole was still visible in TLC) to yield benzylated carbazole **5** in a good yield of 72%.

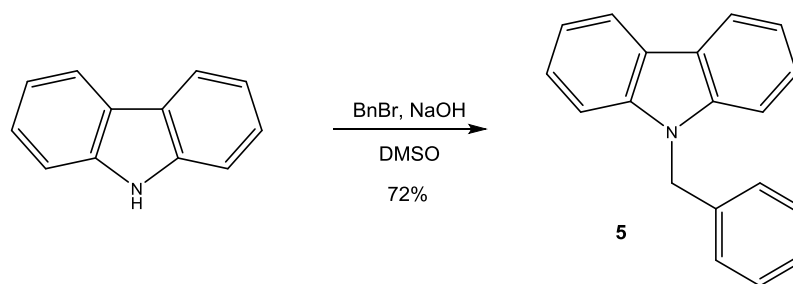


**Figure 29:** N-alkylation of carbazole to obtain precursor **5**.

#### 2.1.1.2. Synthesis of precursor 9-(phenylmethyl)-9H-carbazole-3,6-dicarboxaldehyde (7)

For the next step, a Vilsmeier-Haack reaction was employed to introduce the aldehyde functionalities in position 3 and 6 of benzylated carbazole **5**. In the course of the reaction two iminium groups are introduced successively, with the introduction of the first group being significantly easier than the second. This is because the electronic coupling between the two six-membered rings in carbazole is strong and the -M-effect of the first iminium group hinders the introduction of the second one. The effect is even more prominent than with triphenylamine and thus after hydrolysis a mixture of the mono-aldehyde **6** and the di-aldehyde **7** is to be expected (see **Figure 30**).

Two experimental procedures were considered for the formylation. Both employ a halogenated co-solvent to add the substrate as a solution, possibly to avoid problems like they were encountered in this thesis in the preparation of tri-aldehyde **3** were

considerable amounts of the starting material were lost to side reactions forming a black insoluble mass.

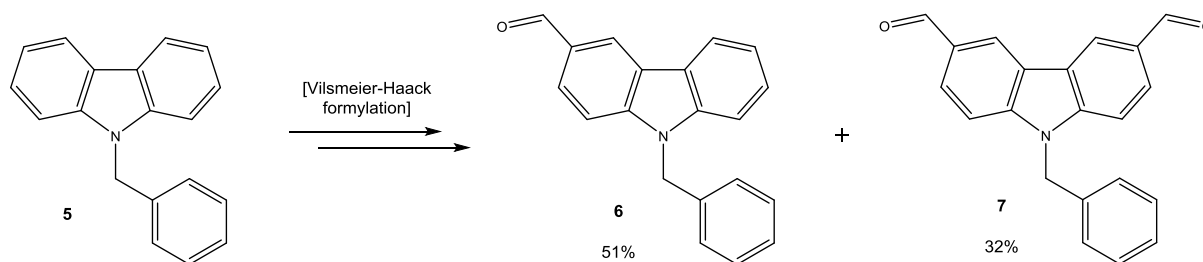


**Figure 30:** Vilsmeier-Haack formylation to obtain precursor aldehydes **6** and **7** from **5**.

The literature<sup>59</sup> where the procedure for benzylated carbazole **5** was taken from also contained instructions for the preparation of di-aldehyde **7**, however it claims a low yield of 21% and uses 1,2-dichloroethane which would require special drying and has a relatively high toxicity. Another procedure from literature<sup>62</sup> for a similar compound (n-hexyl instead of the benzyl group) uses DCM which was available pre-dried and claims a much higher yield of 72%. Thus the latter strategy was chosen.

The low boiling point of DCM made it difficult to reach the reaction temperature. To get close to 90°C internal temperature, the oil bath had to be heated to about 125°C so that DCM evaporated at a high rate and mostly stayed in the reflux condenser. So the use of the higher boiling 1,2-dichloroethane (84°C) versus DCM (40°C) would likely have been advantageous for the reaction.

After 48 h TLC of a small hydrolyzed sample showed full conversion of the starting material **5** and as expected two intense product spots. The reaction mixture was hydrolyzed, alkalized and the product mixture was extracted and stripped of solvents. Separation by column chromatography using a PE:EA gradient provided a reasonable amount of the mono-aldehyde **6** (51% of theory) but the mainly desired product **7** had too low solubility in PE:EA = 3:1 which would provide a reasonable  $R_f$  of about 0.3 so that only minimal amounts eluted from the column at the right polarity.

Thus the precipitated solids at the start of the column were washed out with pure EE. After removal of solvents the residue consisting mostly of di-aldehyde **7** was separated further by Kugelrohr distillation into a yellow oily more volatile fraction (mostly mono-aldehyde **6**), pure di-aldehyde **7** (32% of theory) crystallizing as dense white flakes and a dark brown higher boiling residue.

It should be noted that DCM dissolves **6** considerably better than **7**. Thus the separation could be improved by first removing all DMF from the crude product in vacuo, and then repeatedly macerating it with small amounts of DCM to gain a solution rich in **6** (purified further by column chromatography) and a solid residue rich in **7** (purified further by Kugelrohr distillation).

### 2.1.1.3. Synthesis of B2Cbz – final step

The final step towards the TPI again was an alkali catalyzed aldol condensation reaction with an excess of a mono-benzylidene ketone.

Preliminary experiments showed that the solubility of the dimethylamino-substituted compound obtained by condensation with mono-benzylidene ketone **1** was very low, so that product was not even purified further.

Thus to obtain a better soluble TPI substituted with dibutylamino-groups, di-aldehyde **7** was reacted with 3 eq. of mono-benzylidene ketone **4** by stirring for 5 days at 60°C using KOH as a catalyst and EtOH as solvent (see **Figure 31**).

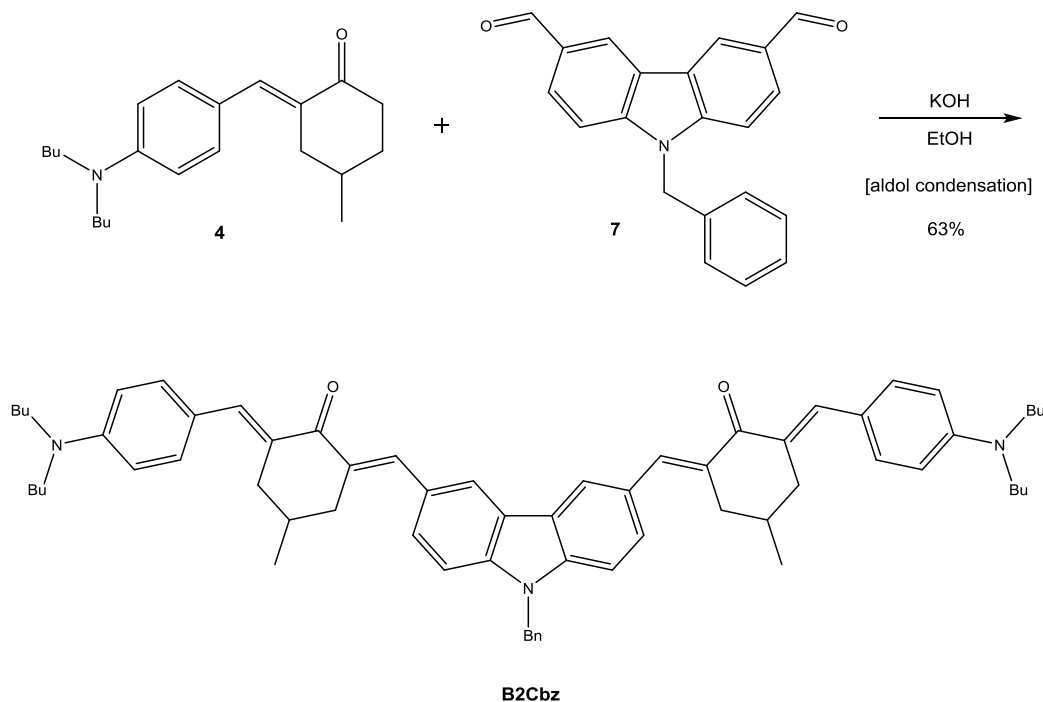


**Figure 31:** Aldol condensation route to **B2Cbz**.

The product **B2Cbz** precipitated as a deep orange waxy solid that was washed with EtOH and dried in vacuo, leading to an acceptable yield of 63% of theory. TLC analysis showed two faint orange bands (isomers) with  $R_f$ -difference of less than 0.1 to the main



spot, and trace amounts of aldehyde-groups with a shift of 10.13 ppm were visible in NMR. Attempts of purification by recrystallization from various solvents were not successful, as **B2Cbz** similarly to **Y-B2CMK** doesn't crystallize well but tends to precipitate as waxy, gelatinous flakes rather than crystals. As in  $^1\text{H}$ -NMR only trace amounts of aldehyde (signal at 10.14 ppm barely above baseline noise) were visible, the product was used without further purification.

## 2.1.2. Analysis of B2Cbz

### 2.1.2.1. UV/Vis - spectroscopy

**Figure 32** shows the normalized OPA spectra of **B2Cbz** as well as the reference compound **M2CMK**. The absorption bands of **B2Cbz** ( $\lambda_{\text{abs}}^{\text{OPA}} = 429 \text{ nm}$ ,  $\epsilon = 7.7 \cdot 10^4 \text{ M}^{-1} \text{ cm}^{-1}$ ) and **M2CMK** ( $\lambda_{\text{abs}}^{\text{OPA}} = 430 \text{ nm}$ ,  $\epsilon = 4.7 \cdot 10^4 \text{ M}^{-1} \text{ cm}^{-1}$ ) in the visible range are well aligned.

The length increase of the conjugated  $\pi$ -system and the increased donor strength of dibutylamino- versus dimethylamino-groups (both causing a red-shift and an increase in the molar extinction) seem to be attenuated and even compensated by the weaker donor strength of N-benzyl carbazole.

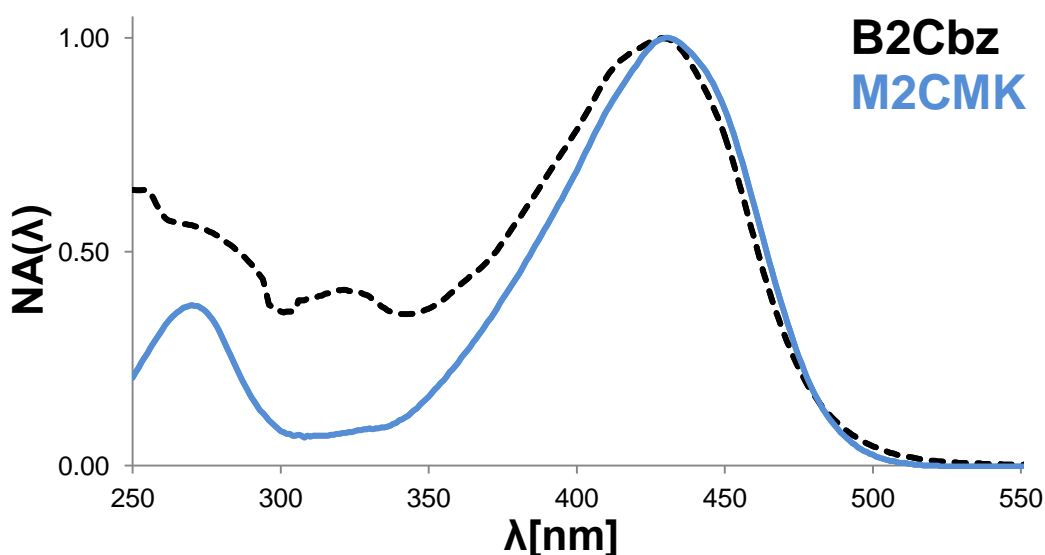


**Figure 32:** Normalized OPA spectra of **B2Cbz** (black dotted line, measured in THF) and reference compound **M2CMK** (blue line, measured in MeCN), both measured at a concentration of  $10^{-5} \text{ mol L}^{-1}$

### 2.1.2.2. Open aperture z-scan

The  $\sigma_{\text{TPA}}$  of **B2Cbz** was measured from a 10mM THF solution and determined to be 109 GM. This value is rather low compared to **M2CMK** (191 GM). One reason for this fact might be that the butyl groups lead to a drop in  $\sigma_{\text{TPA}}$  because of the pyramidalicity on the nitrogen atom of the  $\text{Bu}_2\text{N}$ -group leading to a twisting of the aromatic rings out of plane (like shown in literature<sup>55</sup> for the condensation product of cyclopentanone with 4-(dibutylamino)benzaldehyde, and also when comparing **Y-M2CMK** and **Y-B2CMK**).

Another possible reason for the low cross section is that the used laser wavelength around 800 nm is not attuned to the two-photon absorption maximum of **B2Cbz**. Yet another reason could be that N-benzyl carbazole is a significantly worse electron donor than a (dimethylamino)phenyl-group.

### 2.1.2.3. TPIP structuring tests

The dibutylamino-group bearing **B2Cbz** had sufficient solubility in acetone in which it was pre-dissolved and mixed with ETA/TTA = 1:1. After removal of the acetone, a solution of **B2Cbz** in ETA/TTA = 1:1 with a concentration of 6.3  $\mu\text{mol PI/g}$  resin was obtained. It would be more accurate to account for the larger  $\pi$ -system by choosing a lower concentration for **B2Cbz** than for the reference **M2CMK**, but it is hard to decide on meaningful alternative values as the ratio and relative strength of donor to acceptor groups change significantly as well. Performance tests with woodpile structures written at different laser intensities and writing speeds show a result very similar to **M2CMK** (see **Figure 23** & **Figure 24**), with **B2Cbz** (see **Figure 33** & **Figure 34**) providing a slight improvement especially at lower energies (only class 1 and 2 structures at 30 mW versus some class 3 and 4 structures for **M2CMK** at 30 mW and high writing speeds). However the improvement seems not significant enough to justify the considerably more complex synthesis of **B2Cbz** compared to **M2CMK**.

<b>B2Cbz</b>							
mW	1	26	51	76	101	126	151 mm/s
130	3	1	1	1	1	1	1
120	3	1	1	1	1	1	1
110	3	1	1	1	1	1	1
100	3	1	1	1	1	1	1
90	3	1	1	1	1	1	1
80	3	1	1	1	1	1	1
70	1	1	1	1	1	1	1
60	1	1	1	1	1	1	1
50	1	1	1	1	1	1	1
40	1	1	1	1	2	2	2
30	1	1	4	4	4	4	4
20	1	4	4	4	-	-	-
10	4	-	-	-	-	-	-

**Figure 33:** Processing window of **B2Cbz** (6.3  $\mu\text{mol}$  PI/g ETA:TTA =1:1).

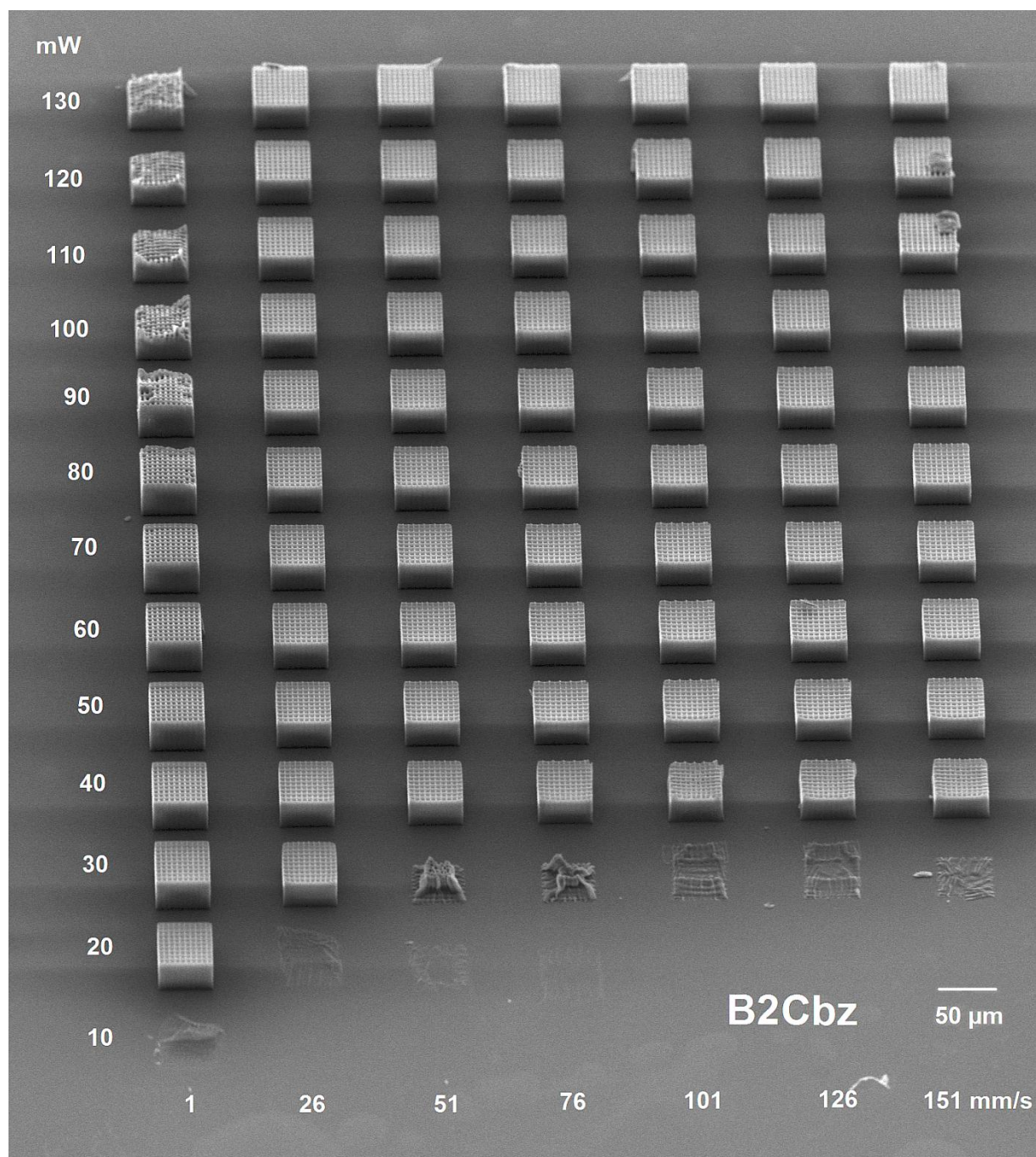


**Figure 34:** SEM-image of woodpile structures built with **B2Cbz** (6.3 μmol PI/g ETA:TTA = 1:1).

## 2.2. Cbz2CEK

### 2.2.1. Synthesis of Cbz2CEK

As the mono-aldehyde **6** was available as a byproduct from the synthesis of di-aldehyde **7**, an aldol condensation with 4-methylcyclohexanone should be attempted and the properties of the resulting TPI tested. However, preliminary experiments showed that the solubilities of the condensation products with both 4-methylcyclohexanone and 4-tert-butylcyclohexanone would be too low for processing.

Thus condensation of **7** with ethyl 4-oxocyclohexanecarboxylate, another cyclohexanone derivative available at the institute, was tried successfully to yield the TPI **Cbz2CEK**.

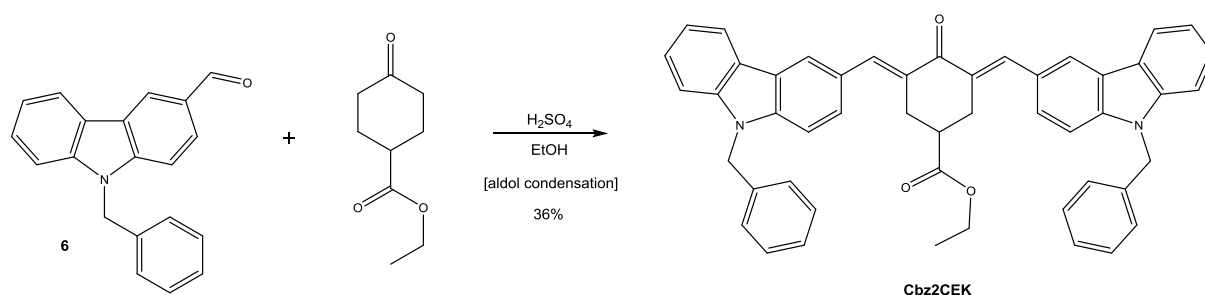


**Figure 35:** Acid catalyzed aldol condensation route to **Cbz2CEK**.

The aldol condensation method used for all other compounds so far, involving alkali hydroxide, could not be employed here as the ester group essential for solubility would be destroyed by that method.

Thus the reaction was performed in dry EtOH in the presence of H<sub>2</sub>SO<sub>4</sub> as a Brønsted acidic catalyst, so that any carboxylic acid formed through hydrolysis by traces of water (also formed in the aldol condensation reaction) would be immediately converted back to the ethyl ester by the large excess of EtOH.

For the synthesis, 1 eq. ethyl 4-oxocyclohexanecarboxylate was stirred with 2.1 eq. mono-aldehyde **6** and 0.75 eq. H<sub>2</sub>SO<sub>4</sub> in dry EtOH at 60°C for two days (see **Figure 35**). In the course of the reaction, the solution turned olive green as a result of the dark yellow color of the target compound in combination with an intense blue coloration probably caused by protonated intermediates/higher condensation products (blueish very polar byproduct which has R<sub>f</sub> ~ 0 in TLC and mostly disappears after shaking with base).

Because starting material mono-aldehyde **6** and the product **Cbz2CEK** had too similar  $R_f$ -values to be separated efficiently in normal phase chromatography and the crude product was not crystalline, reversed phase column chromatography was employed. Thus the crude product was first pre-purified by normal phase chromatography using PE:EA = 4:1 as an eluent to remove all impurities with different  $R_f$  than mono-aldehyde **6** and **Cbz2CEK**. The final purification step was performed by preparative reversed phase column chromatography using pure MeCN as eluent, which successfully separated **Cbz2CEK** from mono-aldehyde **6** leading to a yield of 36%.

## 2.2.2. Analysis of Cbz2CEK

### 2.2.2.1. UV/Vis - spectroscopy

**Figure 36** compares the normalized OPA spectra of **Cbz2CEK** and the reference compound **M2CMK**. The visible-range absorption band of **Cbz2CEK** ( $\lambda_{\text{abs}}^{\text{OPA}} = 392 \text{ nm}$ ,  $\epsilon = 3.7 \cdot 10^4 \text{ M}^{-1} \text{ cm}^{-1}$ ) is significantly blue-shifted relative to **M2CMK** ( $\lambda_{\text{abs}}^{\text{OPA}} = 430 \text{ nm}$ ,  $\epsilon = 4.7 \cdot 10^4 \text{ M}^{-1} \text{ cm}^{-1}$ ). The weaker electron donor strength of N-benzyl carbazole and different  $\pi$ -system compared to the (dimethylamino)phenyl-group lead to the blue-shift and a reduced absorption in the visible range as well as a more dominant absorption in the UV-range for **Cbz2CEK**.

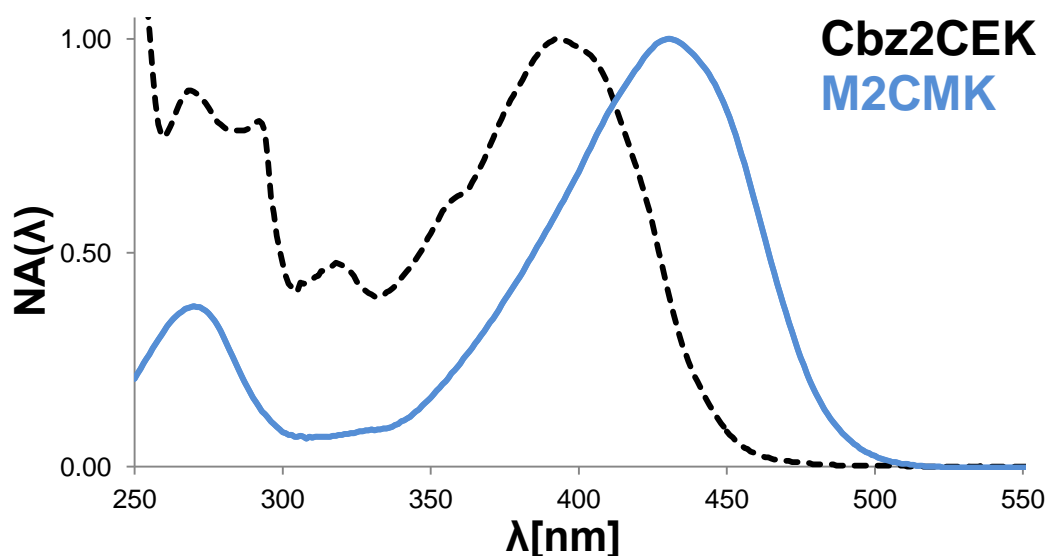


**Figure 36:** Normalized OPA spectra of **Cbz2CEK** (black dotted line, measured in THF) and reference compound **M2CMK** (blue line, measured in MeCN), both measured at a concentration of  $10^{-5} \text{ mol L}^{-1}$

### 2.2.2.2. Open aperture z-scan

Determination of the  $\sigma_{\text{TPA}}$  of **Cbz2CEK** from a 10mM THF solution resulted in a value of 83 GM. This value is less than half of the  $\sigma_{\text{TPA}}$  of **M2CMK** (191 GM). The first major reason for this is likely that N-benzyl carbazole is a significantly worse electron donor than a (dimethylamino)phenyl-group, which leads to a lower two-photon absorption. Furthermore, it causes a blue-shift in one-photon absorption spectra compared to **M2CMK** (see **Figure 36**) and thus the TPA maximum is likely also further away from the used laser wavelength around 800 nm.

Another possible explanation could be the steric effect of the ethoxycarbonyl-group that was used to assure sufficient solubility of **Cbz2CEK**. Literature<sup>55</sup> compares the  $\sigma_{\text{TPA}}$  of **M2CMK** (the methyl group in 4-position was also introduced to increase solubility) and the analogous cyclohexanone based compound without the methyl group in 4-position. For these two compounds, even though one-photon absorption spectra were identical, there is a distinct difference in the  $\sigma_{\text{TPA}}$ : 191 GM for **M2CMK** versus 352 GM for the compound without the methyl group in 4-position.

### 2.2.2.3. TPIP structuring tests

The TPI **Cbz2CEK** has sufficient solubility to be dissolved at a concentration of 6.3  $\mu\text{mol}$  PI/g resin directly in ETA/TTA = 1:1, without requiring any co-solvents. The processing window (determined by performance tests with woodpile structures written at different laser intensities and writing speeds) is significantly worse for **Cbz2CEK** (see **Figure 37** & **Figure 38**) compared to **M2CMK** (see **Figure 23** & **Figure 24**). At 1 mm/s writing speed, class 1 structures were obtained from 20-60 mW for **M2CMK** versus only 20-40 mW for **Cbz2CEK**. At 40 mW laser power **Cbz2CEK** gave recognizable woodpile structures only up to 26 mm/s, whereas **M2CMK** was able to produce flawed but recognizable structures at up to 126 mm/s writing speed. At 40 mW laser power **M2CMK** gave flawless results even at the highest tested speed of 151 mm/s, in contrast to **Cbz2CEK** which produced acceptable results only up to 76 mm/s.

Furthermore, the woodpile structures built with **Cbz2CEK** showed massive damage in the high energy section (1 mm/s, high laser powers).

Cbz2CEK							
mW	1	26	51	76	101	126	151 mm/s
100	3	1	1	1	1	1	1
90	3	1	1	1	1	1	1
80	3	1	1	1	1	1	1
70	3	1	1	1	1	1	1
60	3	1	1	1	1	1	1
50	2	1	1	1	3	3	4
40	1	1	4	4	4	4	4
30	1	4	4	4	4	4	4
20	1	4	-	-	-	-	-
10	4	-	-	-	-	-	-

**Figure 37:** Processing window of **Cbz2CEK** (6.3  $\mu$ mol PI/g ETA:TTA =1:1).



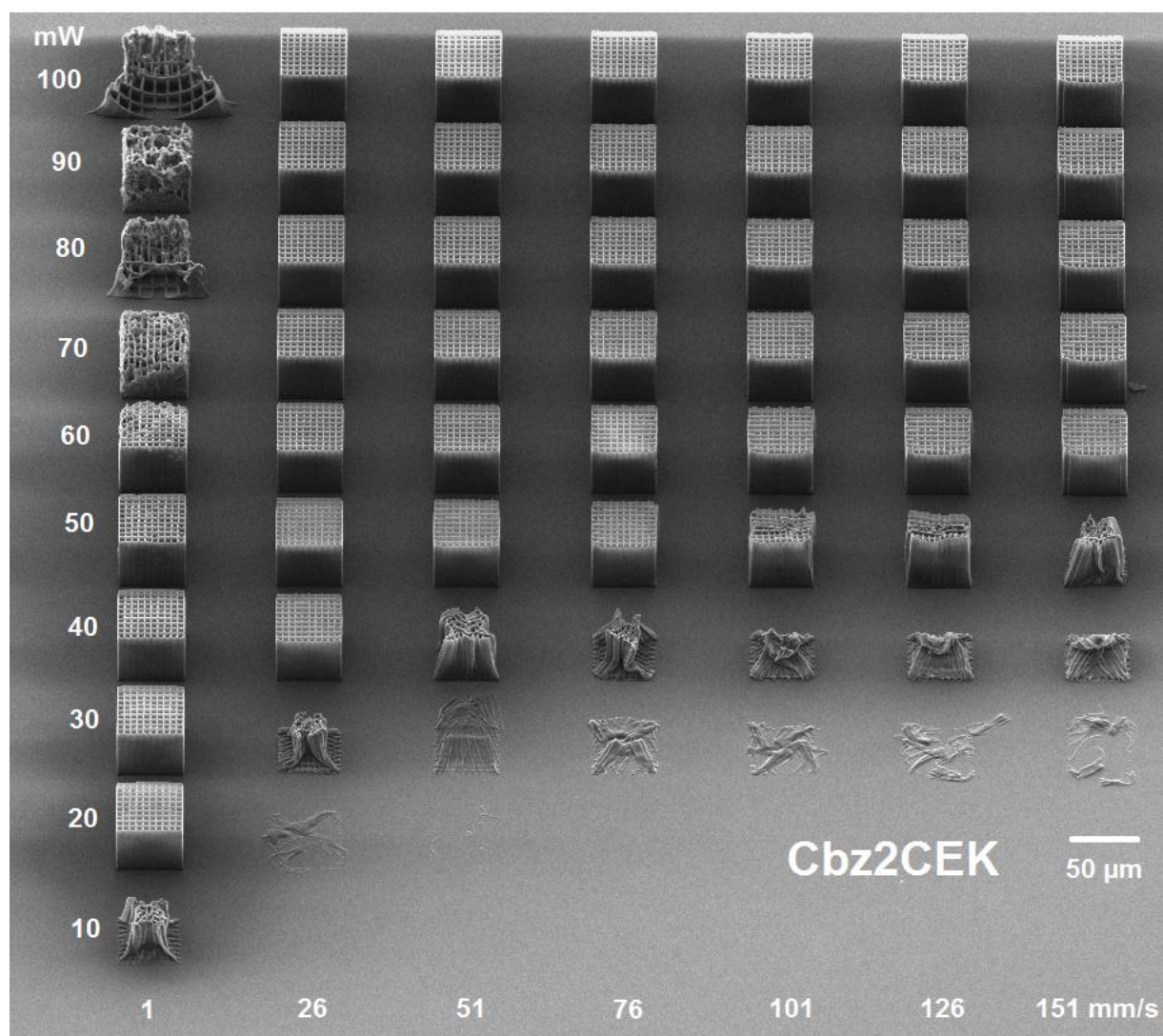


**Figure 38:** SEM-image of woodpile structures built with **Cbz2CEK** (6.3  $\mu\text{mol PI/g}$  ETA:TTA =1:1).

### 3. Planarized branched/multipolar triazine-based analogues of M2CMK

All of the TPIs prepared so far in the course of this thesis contain carbonyl moieties as electronic acceptor groups.

One of the main reasons for this is that it is desirable for TPIs to have low fluorescence quantum yields, as two-photon induced fluorescence dissipates energy that could be used to induce polymerization. Carbonyl groups are known to introduce low-lying  $n \rightarrow \pi^*$  - transitions which have far longer lifetimes than  $\pi \rightarrow \pi^*$  - transitions (e.g.  $10^{-6}$  s for  $n \rightarrow \pi^*$  vs.  $10^{-8}$  s for  $\pi \rightarrow \pi^*$ ).<sup>11</sup> Thus the time-frame for non-radiative processes to occur is much larger and the fluorescence quantum yield decreased.

Heterocycles that contain pyridine-type nitrogen atoms (i.e. one single and one double bond to nitrogen) also show this effect which is desirable for TPIs.

Thus the heterocyclic system 1,3,5-triazine was chosen as a core element for a series of multipolar TPIs. It is a strongly electron deficient heterocycle and thus an excellent electronic acceptor group. Furthermore it supports highly planar molecular geometries and has three carbon atoms for branches to be attached.

Detailed structure analyses of star shaped 1,3,5-triazine-based compounds were carried out by Cui *et al.*<sup>63</sup> to investigate the planarity of the system. X-ray structure analyses of the one- and two-branched counterparts and a computer model of the three-branched compound revealed a highly planar conformation of the  $\pi$ -systems. Previous studies by Meier *et al.*<sup>64</sup> and Cui *et al.*<sup>63,65</sup> show that 1,3,5-triazine derivatives bearing 1,4-phenylenevinylene arms with terminal dialkylamino-groups exhibit relatively high TPA that strongly increases in a non-linear fashion with the number of branches. Fluorescence quantum yields were also determined by Cui *et al.*<sup>63</sup> and resulted in relatively low values from 0.0013 to 0.109 strongly depending on the solvent and the number of branches.

All these factors indicate that branched 1,3,5-triazine-based compounds bearing 1,4-phenylenevinylene arms with terminal dialkylamino groups could also show interesting properties as TPIs, which have not been investigated before for this type of molecules.

Thus a series of three TPIs **B2Trz**, **2B2Trz** and **3B2Trz** (see **Figure 39**) based on 1,3,5-triazine should be synthesized, forming a series of di-, quadru- and octupolar molecules respectively.

Meier *et al.*<sup>64</sup> and Cui *et al.*<sup>63,65</sup> investigated similar series but employed methyl- and ethyl-groups as substituents on the terminal amino-groups. To ensure high solubility in acrylate resin mixtures, dibutylamino-groups should be employed as they have already proven their value in the course of this thesis.

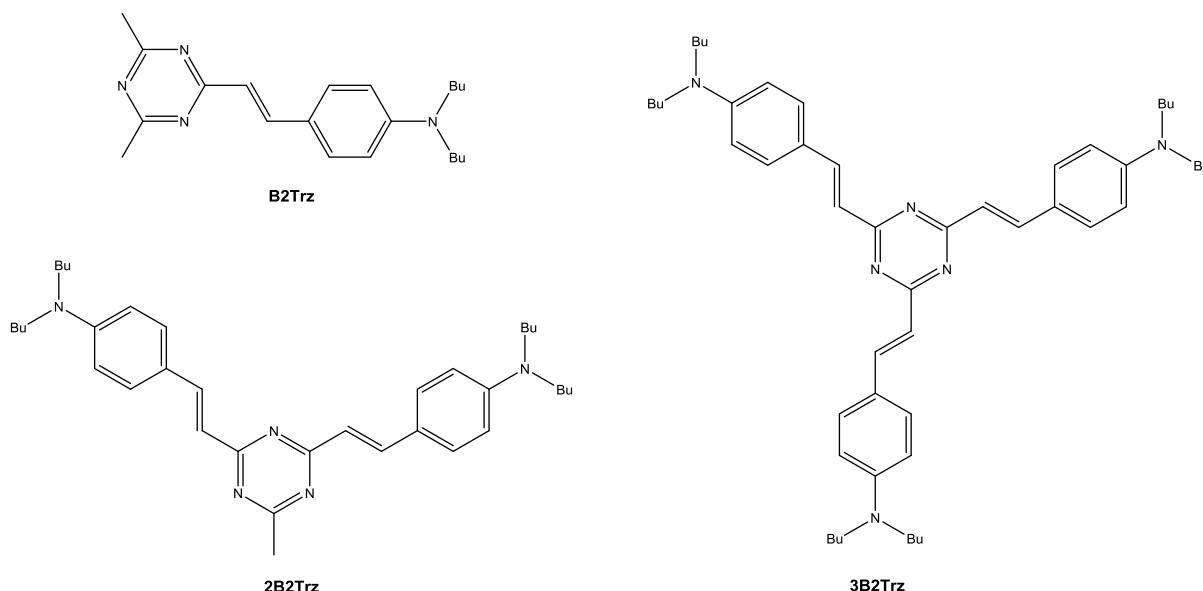


**Figure 39:** Structures of three 1,3,5-triazine-based di-, quadru- and octupolar TPIs respectively.

### 3.1. Synthesis of B2Trz, 2B2Trz and 3B2Trz

The synthetic strategy was straightforward and analogous to the ones used by Meier *et al.*<sup>64</sup> and Cui *et al.*<sup>63,65</sup>, except for the used aldehyde. All three compounds should be obtained from an aldol condensation between 4-(dibutylamino)benzaldehyde and 2,4,6-trimethyl-1,3,5-triazine (**8**), preferably from one reaction if the separation of the three condensation products is feasible from the mixture.

Although this would certainly not be the most efficient way if a specific one of the three compounds be desired (different aldehyde/triazine ratios required to maximize the yield of each compound), it is the fastest way to obtain small samples of all three for first experiments to investigate the properties.

#### 3.1.1. Synthesis of precursor 2,4,6-trimethyl-1,3,5-triazine (**8**)

Despite the simple molecular structure of the required triazine **8** and a broad variety of other derivatives of 1,3,5-triazine being commercially available, no commercial source

could be found for the compound. Thus it had to be prepared from the commercially available ethyl acetimidate hydrochloride according to a 1961 procedure<sup>66</sup> by Schaefer and Peters.

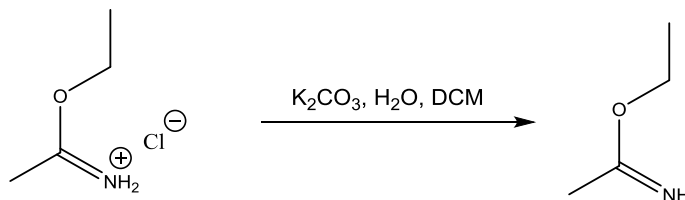


**Figure 40:** Preparation of ethyl acetimidate freebase.

First, ethyl acetimidate freebase was prepared (see **Figure 40**) by dissolving the hydrochloride in an aqueous solution of  $K_2CO_3$  and extracting twice with DCM. This extract was then dried and concentrated by rapid distillative removal of DCM using a Vigreux column, until the bottom product had about 83% freebase content (determined by titration against aqueous HCl). The trimerization of ethyl acetimidate freebase was carried out by reaction with catalytic amounts of AcOH. This is at first a slightly exothermic process and kept at 25-30°C by water cooling, then proceeds at room temperature over night. Pure triazine **8** is then obtained in a yield of 50% by removal of formed EtOH and residual AcOH, followed by fractioned distillation using a Vigreux column. It is curious to note that the compound has an intense characteristic smell, which at lower concentrations is reminiscent of (burnt) popcorn.

There would be an alternative and more convenient route<sup>67</sup> (see **Figure 41**) to **8** claiming a yield of 89% by trimerization of MeCN in the presence of triflic anhydride. However triflic anhydride is needed in an amount equimolar to the product and rather expensive compared to the reagents used in the procedure<sup>66</sup> by Schaefer and Peters. Such a route might be advantageous in the preparation of more complex triazines.

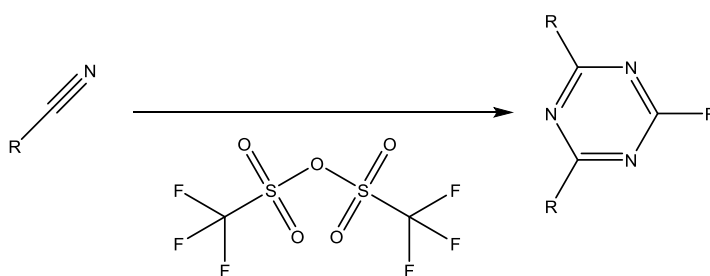


**Figure 41:** Trimerization of nitriles mediated by triflic anhydride.

### 3.1.2. Synthesis of B2Trz, 2B2Trz and 3B2Trz - condensation step

To obtain the series of 1,3,5-triazine-based TPIs, triazine **8** was condensed with 4-(dibutylamino)benzaldehyde in MeOH under alkaline conditions (see **Figure 42**), analogous to the procedure used by Meier *et al.*<sup>64</sup>

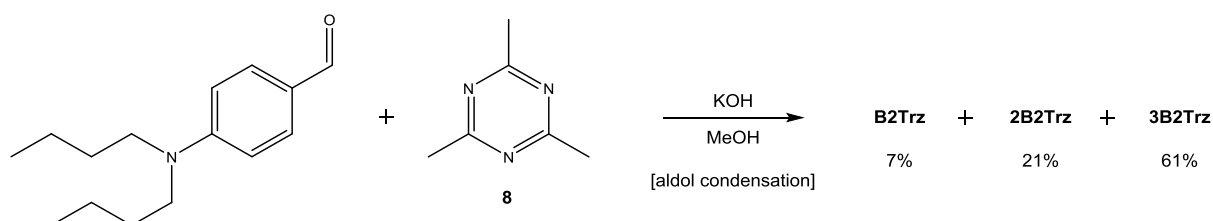


**Figure 42:** Aldol condensation step to obtain a mixture of **B2Trz**, **2B2Trz** and **3B2Trz**.

For this aldol condensation reaction 1.0 eq. of triazine **8** was dissolved in a solution of 20% KOH in MeOH and 2.7 eq. of the aldehyde were added as a solution in MeOH. The amount of aldehyde was chosen to promote the formation of the higher condensation products **2B2Trz** and **3B2Trz** (expected to be more potent TPIs) while still keeping some **B2Trz** in the reaction mixture. The reaction mixture was stirred at 60°C for 5 days, until all **8** and most of the aldehyde had been consumed and the reaction mixture had turned deep orange. After diluting the mixture with water, neutralizing the base with saturated NH<sub>4</sub>Cl and extracting the products with DCM, they were separated by column chromatography. Compared to PE, toluene as apolar component for the eluent gave significantly better resolution between the different products as well as the aldehyde (eluting between **2B2Trz** and **3B2Trz**). A longer detection wavelength of 295 nm instead of the usual 254 nm had to be used for reliable peak detection in the presence of toluene. An eluent system of toluene with 5-30% Et<sub>2</sub>O was employed successfully to separate all three condensation products using silica gel 60 as stationary phase.

The overall yield of isolated condensation products relative to the starting material **8** was 89%. Only **3B2Trz** (21% yield) could be obtained in crystalline form, both **2B2Trz** (61% yield) and **B2Trz** (7% yield) didn't crystallize well and were isolated as sticky or waxy resins respectively.

To develop a faster synthesis routine as well as a method to monitor the progress of the reaction and roughly estimate the conversion to the different products **B2Trz**, **2B2Trz** and **3B2Trz**, another synthetic method should be investigated.

In 1976 Bonham *et al.* filed a patent<sup>68</sup> where they performed similar aldol coupling reactions on halomethyl-substituted 1,3,5-triazines using piperidinium acetate as a catalyst. The reaction can be carried out in solvents like toluene using a dean-stark trap to remove water formed in the reaction, or even by heating aldehyde together with triazine without any solvent in the presence of molten piperidinium acetate at 140°C. The latter method claims to lead to full conversion after just 60 min reaction time.

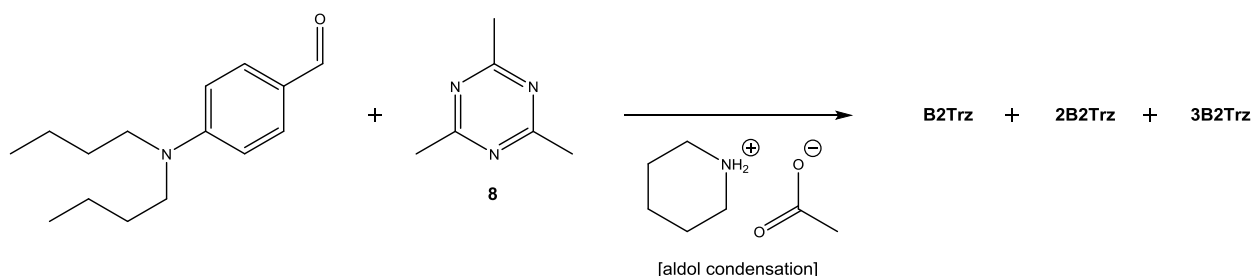


**Figure 43:** Faster aldol condensation catalyzed by piperidinium acetate to obtain a mixture of **B2Trz**, **2B2Trz** and **3B2Trz**.

Thus an experiment was carried out melting 3.5 eq. 4-(dibutylamino)benzaldehyde, 1 eq. 2,4,6-trimethyl-1,3,5-triazine and 3 eq. piperidinium acetate at 140°C oil bath temperature (see **Figure 43**), drawing samples for <sup>1</sup>H-NMR spectroscopy after 1 and 6.5 h respectively. Before measuring the samples were treated by dissolving in DCM, extracting piperidinium acetate by washing with 1 N HCl, sat. NaHCO<sub>3</sub> and deionized water, then removing the solvents in vacuo.

**Figure 44** shows <sup>1</sup>H-NMR spectra of the samples taken after 1 h and 6.5 h respectively. The <sup>1</sup>H-NMR peaks characterising the condensation products as well as starting material 4-(dibutylamino)benzaldehyde are presented in **Table 4**.

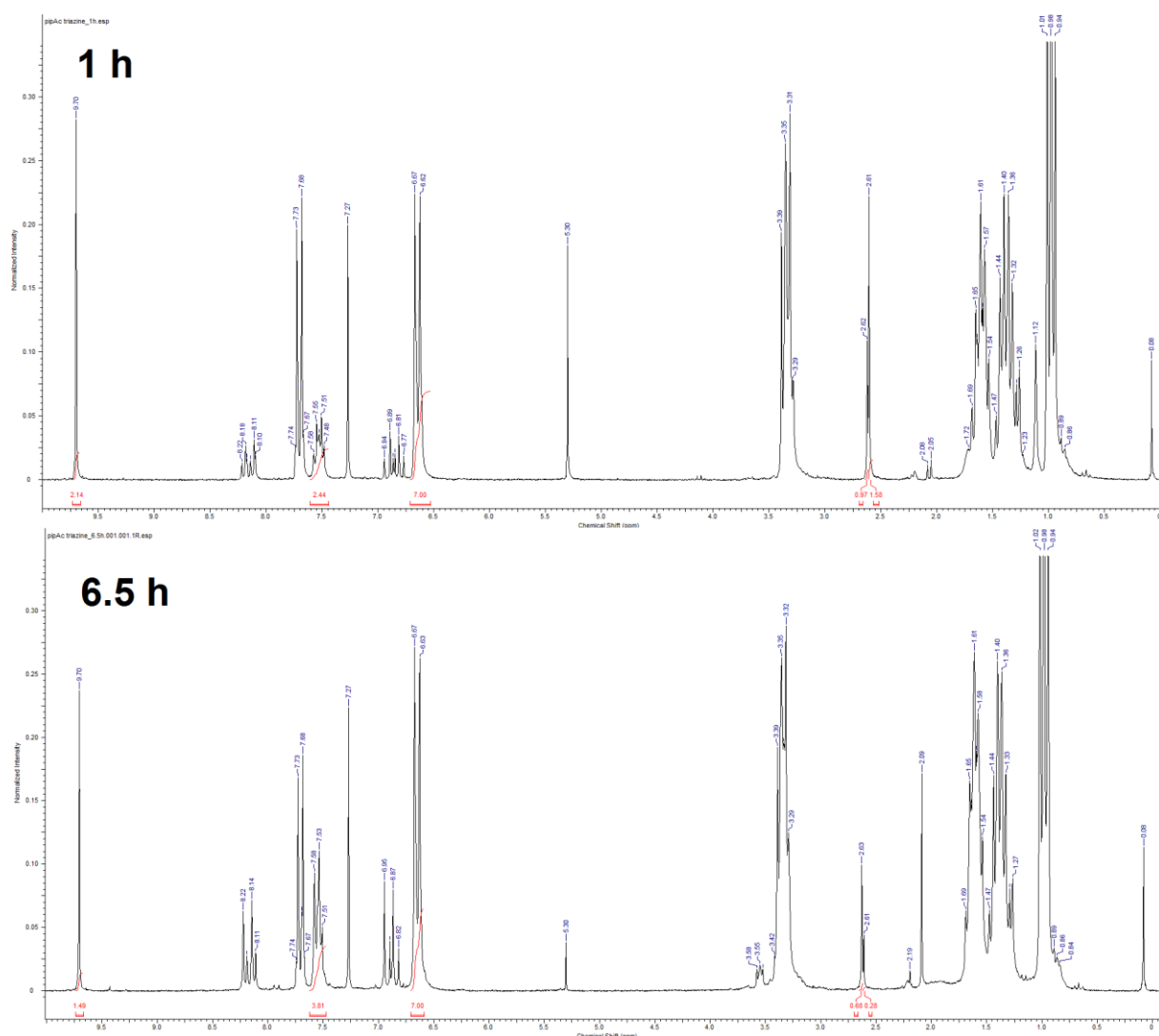


**Figure 44:**  $^1\text{H}$ -NMR spectra of samples taken from a piperidinium acetate catalyzed condensation reaction between 4-(dibutylamino)benzaldehyde and triazine **8** at  $140^\circ\text{C}$ , after 1 h and 6.5 h respectively. The integrals of the relevant groups are shown in red.

**Table 4:** Peaks and moieties used for the calculation of the ratio of the condensation products, as well as their respective integrals after 1 and 6.5 h.

Peak ( $\delta$ ppm)	Moiety	I after 1 h	I after 6.5 h
2.61	Trz-CH <sub>3</sub> ( <b>B2Trz</b> )	1.58	0.28
2.62	Trz-(CH <sub>3</sub> ) <sub>2</sub> ( <b>2B2Trz</b> )	0.97	0.68
6.65	Bu <sub>2</sub> -N-Ar-H <sup>3,5</sup> (aldehyde, <b>B2Trz</b> , <b>2B2Trz</b> , <b>3B2Trz</b> )	7.00	7.00
7.53	Bu <sub>2</sub> -N-Ar-H <sup>2,6</sup> ( <b>B2Trz</b> , <b>2B2Trz</b> , <b>3B2Trz</b> )	2.44	3.81
9.70	Bu <sub>2</sub> -N-Ar-CHO	2.14	1.49

Using the respective integrals, the relative amounts of 4-(dibutylamino)benzaldehyde (a), **B2Trz** (b), **2B2Trz** (c) and **3B2Trz** (d) in the reaction mixture were calculated according to **Equations 4-7**:

$$a = I_{9.70} - a_{\text{excess}} = I_{9.70} - \frac{I_{6.65}}{2} \cdot \frac{0.5}{3.5} \quad \text{Equation 4}$$

$$b = \frac{I_{2.61}}{2 \cdot 3} \quad \text{Equation 5}$$

$$c = \frac{I_{2.62}}{3} \quad \text{Equation 6}$$

$$d = \frac{1}{6} (I_{7.53} - 2 \cdot b - 4 \cdot c) \quad \text{Equation 7}$$

The conversion of the aldehyde  $X_a$  was calculated using **Equations 8 & 9**, with  $a$  representing the amount of 4-(dibutylamino)benzaldehyde present in the reaction mixture at the moment of drawing the sample,  $a_{\text{excess}}$  taking into account the over-stoichiometric use of aldehyde and  $a_0$  representing the starting amount of the aldehyde.

$$X_a = \frac{a_0 - a}{a_0} \quad \text{with} \quad a_0 = \frac{I_{6.65}}{2} \cdot \frac{3}{3.5} \quad \text{Equations 8 \& 9}$$

For convenience sake, the integrals of  $I_{6.65}$  (representing the aromatic protons that have practically the same chemical shift in the aldehyde and all three condensation products) were always set to 7.00, so that  $a_0 = 3$  and  $a_{\text{excess}} = 0.5$ , corresponding to the used 3.5 eq. 4-(dibutylamino)benzaldehyde.

**Table 5** presents the calculated ratios of the three different condensation products **B2Trz**, **2B2Trz** and **3B2Trz** after 1 and 6.5 hours, as well as the calculated conversion respective to the aldehyde in comparison to the total isolated yield of all three different condensation products obtained from the KOH catalyzed reaction.



**Table 5:** Molar ratios and obtained yields (calculated from aldehyde conversion) of the piperidinium acetate catalyzed reaction after 1 and 6.5 h compared to the KOH catalyzed reaction after 120 h.

reaction time	B2Trz	2B2Trz	3B2Trz	conversion [%]
1 h	2.5	3.1	1.0	45
6.5 h	1.0	4.9	10.0	67
KOH catalyzed 120 h (2.7 eq. aldehyde)	1.0	8.7	3.0	89 (isolated yield)

In the KOH catalyzed reaction less 4-(dibutylamino)benzaldehyde (only 2.7 eq.) was used to ensure that sufficient amounts of **B2Trz** and **2B2Trz** could be obtained, which makes a direct comparison difficult.

The results still clearly show that using piperidinium acetate as a catalyst leads to high yields of **2B2Trz** and **3B2Trz** in a comparatively very short time. <sup>1</sup>H-NMR spectroscopy allows for monitoring of the reaction to provide a rough estimate of both the conversion and the ratio of the three condensation products relative to each other.

After isolating samples of all three potential TPIs, the photophysical properties and initiation capabilities should be investigated.

## 3.2. Analysis of B2Trz, 2B2Trz and 3B2Trz

### 3.2.1. OPA photophysical properties

UV/Vis-measurements for **B2Trz**, **2B2Trz** and **3B2Trz** were carried out to obtain information on the behavior of the synthesized compounds under one-photon conditions.

MeCN and n-pentane were chosen as solvents. **Table 6** presents the most common photophysical properties for OPA processes, including the absorption- and emission maximum wavelength ( $\lambda_{\text{abs}}^{\text{OPA}}$  and  $\lambda_{\text{em}}^{\text{OPA}}$ ), the decadic molar extinction coefficient ( $\epsilon$ ), and the emission quantum yield ( $\Phi_{\text{em}}^{\text{OPA}}$ ). As reference for  $\Phi_{\text{em}}^{\text{OPA}}$  coumarin 30 in MeCN was used. The obtained spectra are presented in **Figure 45**.

**Table 6:** Photophysical properties for OPA processes of **B2Trz**, **2B2Trz**, and **3B2Trz**.  $\lambda^{\text{OPA}}_{\text{abs}}$ ,  $\lambda^{\text{OPA}}_{\text{em}}$  and  $\Phi^{\text{OPA}}_{\text{em}}$  in MeCN (left value) and n-pentane (right value).  $\epsilon$  was measured in DCM, values refer to the respective wavelength maximum in DCM (418nm, 436nm, and 441nm).

TPI	$\lambda^{\text{OPA}}_{\text{abs}}$ [nm]		$\lambda^{\text{OPA}}_{\text{em}}$ [nm]		$\Phi^{\text{OPA}}_{\text{em}}$		$\epsilon$ ( $\lambda^{\text{OPA}}_{\text{abs}}$ ) [Lmol <sup>-1</sup> cm <sup>-1</sup> ]
<b>B2Trz</b>	412	387	518	444	0.11	0.013	$4.3 \cdot 10^4$
<b>2B2Trz</b>	433	415	~580	427	$3.6 \cdot 10^{-3}$	0.04	$8.0 \cdot 10^4$
<b>3B2Trz</b>	439	416	~580	427	$4.3 \cdot 10^{-3}$	0.051	$1.2 \cdot 10^5$

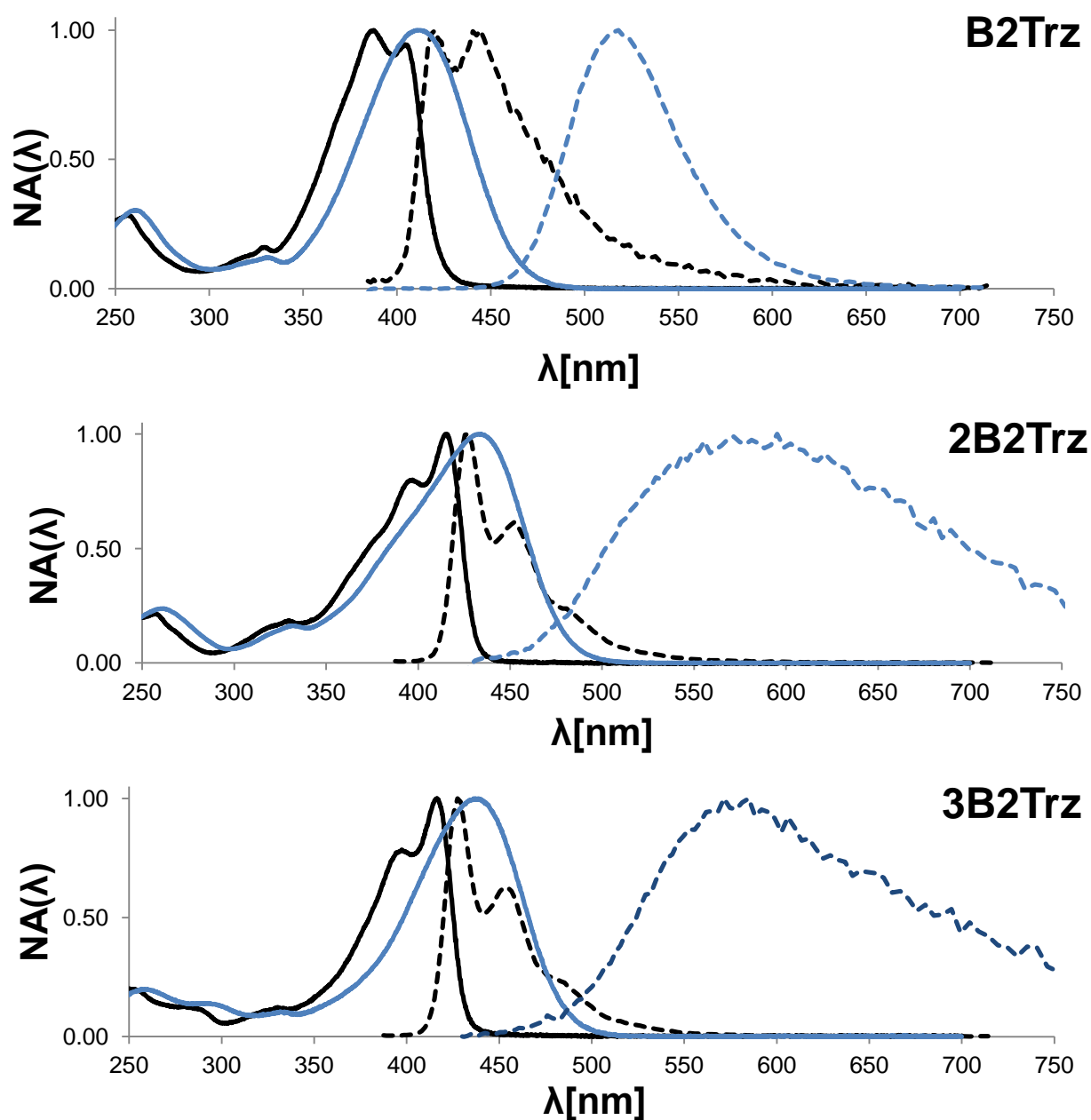


**Figure 45:** Normalized absorption (full line) and emission (scattered line) spectra of **B2Trz**, **2B2Trz** and **3B2Trz** in acetonitrile (blue) and pentane (black).

Regarding the absorption behavior, the higher solvent polarity of MeCN compared to n-pentane leads to a red shift of about 18 - 25 nm for  $\lambda_{\text{abs}}^{\text{OPA}}$  of each of the compounds. A similar red-shift of  $\lambda_{\text{abs}}^{\text{OPA}}$  of about 21 - 28 nm is observed when increasing the number of branches from **B2Trz** to **2B2Trz**, while going from **2B2Trz** to **3B2Trz** hardly causes any red-shift. The molar extinction coefficient  $\epsilon$  rises in an almost exactly linear fashion for the one-photon absorption (branches 1:2:3  $\rightarrow$  extinction coefficient 1:1.9:2.8), in contrast to the behavior of the  $\sigma_{\text{TPA}}$ .

Comparing the fluorescence behavior of the three compounds, **B2Trz** in MeCN showed the strongest fluorescence with a quantum yield of 11%, while **2B2Trz** and **3B2Trz** both had extremely low quantum yields in MeCN. In pentane, all the quantum yields of the three compounds were in a range between 1 - 5%.

### 3.2.2. Open aperture z-scan

The  $\sigma_{\text{TPA}}$  of **B2Trz**, **2B2Trz** and **3B2Trz** were measured in THF solution at the same molar concentration of 10mM for all three compounds.

A strong non-linear dependence of the  $\sigma_{\text{TPA}}$  on the number of branches could be observed. Doubling the number of branches from one branch in **B2Trz** (60 GM) to two branches in **2B2Trz** (244 GM) lead to a more than fourfold cross section for the latter compound. However, adding a third branch in **3B2Trz** (275 GM) only led to a slight increase (4.6-fold the value of **B2Trz**) of the cross section compared to **2B2Trz** (see **Figure 46**).

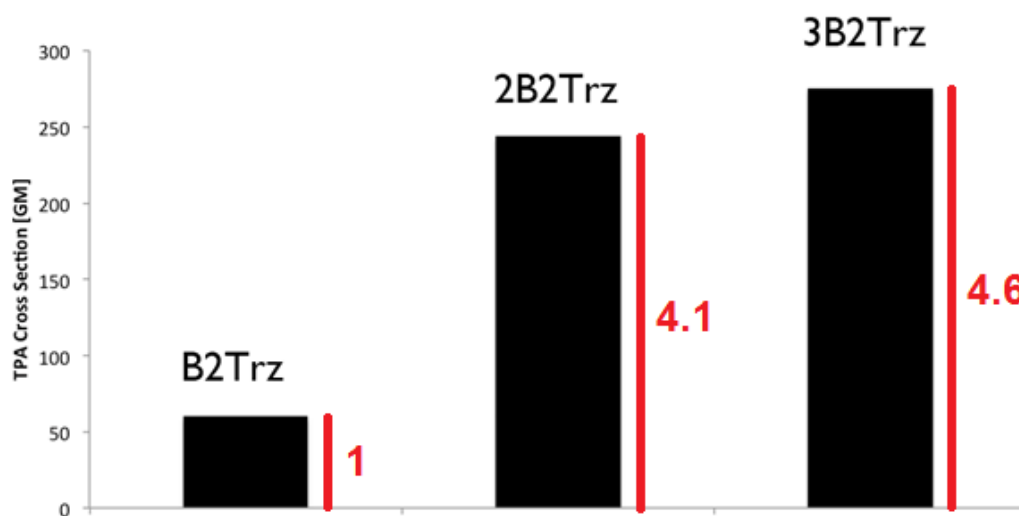


**Figure 46:** TPA cross sections  $\sigma_{\text{TPA}}$  of **B2Trz**, **2B2Trz** and **3B2Trz** and their ratios.

Cui *et al.*<sup>63,65</sup> determined the  $\sigma_{\text{TPA}}$  of the (dimethylamino)- and (diethylamino)-analogues of the (dibutylamino)-substituted series investigated in this thesis. Their results (obtained from TPEF comparison with coumarine 307 as a reference) ranged from 343 - 2405 GM (branches 1:2:3  $\rightarrow \sigma_{\text{TPA}}$  1:3.3:7.0) for the (dimethylamino)-series measured in THF, and 240 - 671 GM (branches 1:2:3  $\rightarrow \sigma_{\text{TPA}}$  1:2.2:2.8) for the (diethylamino)-series measured in  $\text{CHCl}_3$ .

This shows a familiar drop of the  $\sigma_{\text{TPA}}$  when going from methyl-groups to higher alkyl chains on the nitrogen substituents, possibly caused by the stronger pyramidity of the nitrogen atoms. Furthermore, the weakening of the cooperative effect when going from two to three branches with increasing length of the alkyl chains is consistent within the series. It is not clear why the cooperative effect for going from one to two branches first drops when the chain length is increased from methyl- to ethyl-groups, then for butyl-groups even rises above the value for methyl-groups.

### 3.2.3. TPIP structuring tests

Preparing samples for the structuring tests, no solubility problems were encountered. In fact **2B2Trz** showed excellent solubility in  $\text{ETA/TTA} = 1:1$ , being dissolved far easier than the reference **M2CMK** and any other TPI investigated in this thesis - without the need for addition of any co-solvent, **2B2Trz** dissolved rather quickly in  $\text{ETA/TTA}$  on shaking. **B2Trz** also was well soluble; only **3B2Trz** required the addition of acetone (removed again after obtaining a clear solution) for dissolution, most likely because in contrast to the other two compounds it is crystalline. All of the compounds were dissolved at  $6.3 \mu\text{mol PI/g resin}$  to maintain comparability to the reference **M2CMK**. While it would be more accurate to account for the different size of the  $\pi$ -system by choosing different concentrations within the series, it is hard to decide on meaningful alternative values as the ratio and relative strength of donor to acceptor groups change as well.

Performance tests with woodpile structures written at different laser intensities and writing speeds showed some interesting results. In comparison to **M2CMK** (see **Figure 23** & **Figure 24**), **2B2Trz** (see **Figure 49** & **Figure 50**) and **3B2Trz** (see **Figure 51** & **Figure 52**) have very similar processing windows, with slight improvements enabling the use of higher writing speeds at lower laser intensities. The fast and easy dissolution of **2B2Trz** in  $\text{ETA/TTA}$  might be the most significant advantage compared to **M2CMK**.

**B2Trz** (see **Figure 47** & **Figure 48**) has quite a small processing window with significantly worse performance than **M2CMK** at higher writing speeds and lower laser intensities. However, at 1 mm/s and high laser powers, it was the only initiator investigated in this thesis which could provide satisfying results, with class 1 structures being obtained even at 110 mW (during these measurements the laser was unable to reach 120 - 130 mW as in the previous measurements, see **Chapter 1**).

<b>B2Trz</b>							
mW	1	26	51	76	101	126	151 mm/s
110	1	1	1	1	1	1	1
100	1	1	1	1	1	1	1
90	1	1	1	1	1	1	1
80	1	1	1	2	3	3	4
70	1	2	4	4	4	4	4
60	1	4	4	4	4	4	4
50	3	4	4	4	4	4	4
40	-	-	-	-	-	-	-
30	-	-	-	-	-	-	-
20	-	-	-	-	-	-	-
10	-	-	-	-	-	-	-

**Figure 47:** Processing window of **B2Trz** (6.3  $\mu\text{mol PI/g}$  ETA:TTA =1:1).

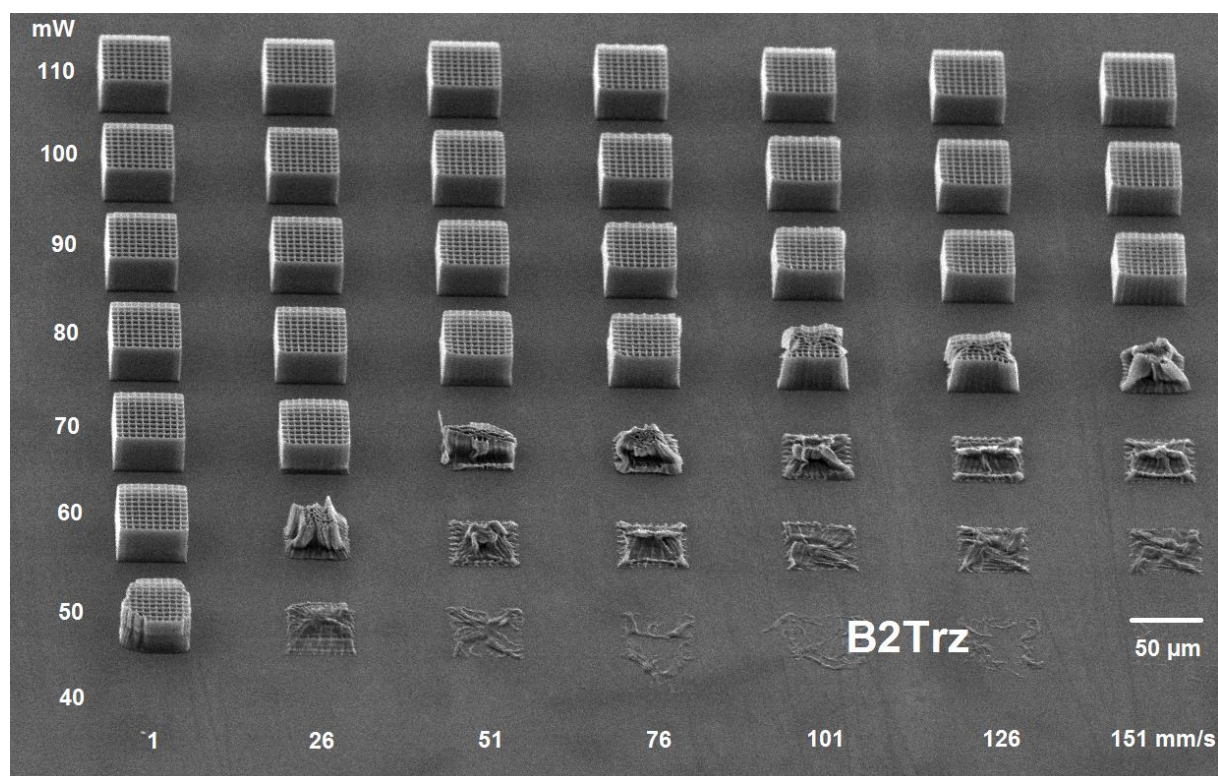


**Figure 48:** SEM-image of woodpile structures built with **B2Trz** (6.3  $\mu\text{mol PI/g ETA:TTA} =1:1$ ).

<b>2B2Trz</b>							
mW	1	26	51	76	101	126	151 mm/s
110	3	1	1	1	1	1	1
100	3	1	1	1	1	1	1
90	3	1	1	1	1	1	1
80	3	1	1	1	1	1	1
70	2	1	1	1	1	1	1
60	1	1	1	1	1	1	1
50	1	1	1	1	1	1	1
40	1	1	1	1	2	2	3
30	1	2	4	4	4	4	4
20	1	4	4	-	-	-	-
10	-	-	-	-	-	-	-

**Figure 49:** Processing window of **2B2Trz** (6.3  $\mu\text{mol PI/g ETA:TTA} =1:1$ ).

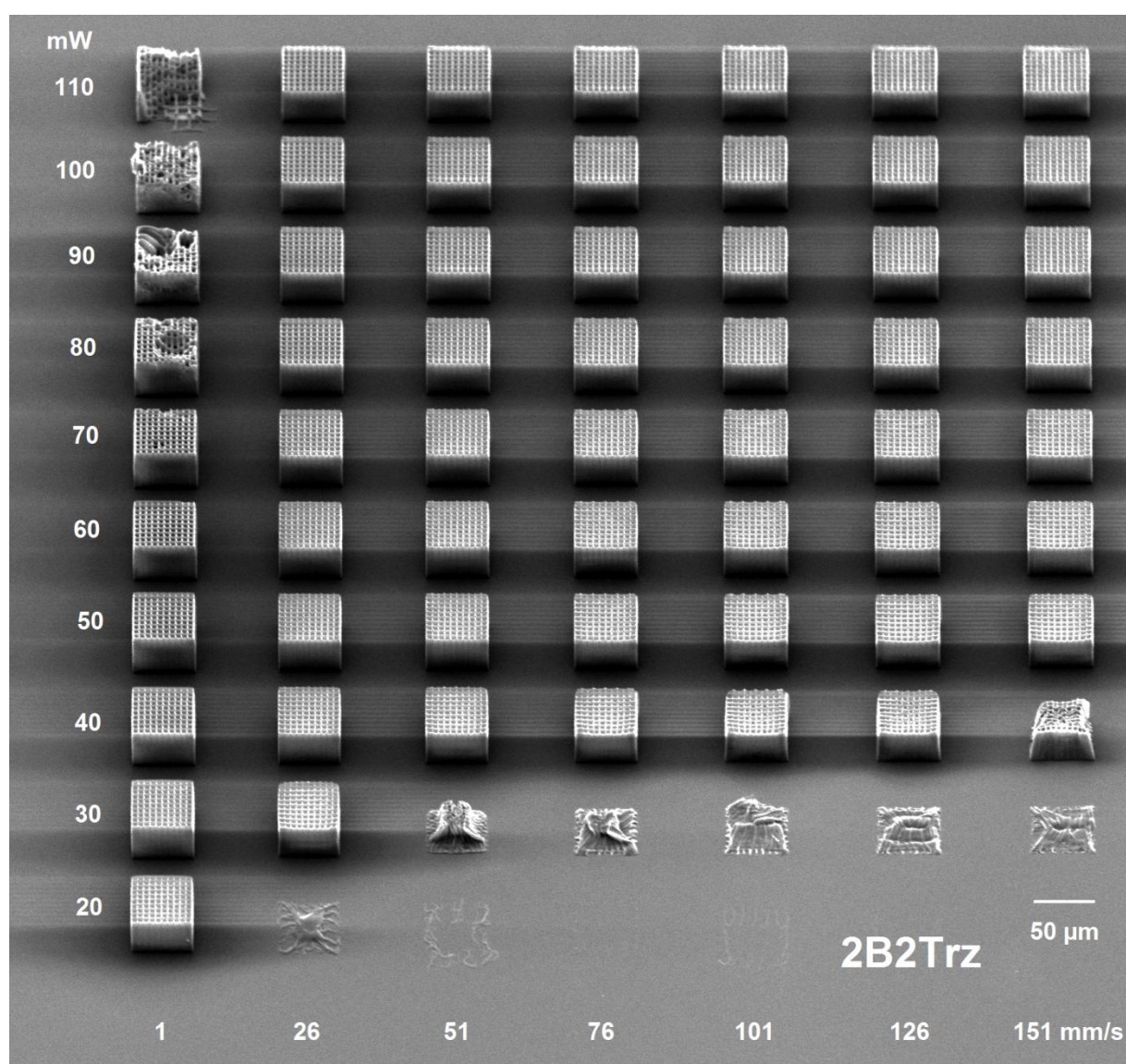


**Figure 50:** SEM-image of woodpile structures built with **2B2Trz** (6.3  $\mu\text{mol}$  PI/g ETA:TTA = 1:1).



3B2Trz								
mW	1	26	51	76	101	126	151	mm/s
110	3	1	1	1	1	1	1	
100	3	1	1	1	1	1	1	
90	3	1	1	1	1	1	1	
80	3	1	1	1	1	1	1	
70	2	1	1	1	1	1	1	
60	1	1	1	1	1	1	1	
50	1	1	1	1	1	1	1	
40	1	1	1	1	2	2	3	
30	1	1	2	3	4	4	4	
20	1	4	4	4	4	4	4	
10	4	-	-	-	-	-	-	

**Figure 51:** Processing window of **3B2Trz** (6.3  $\mu\text{mol}$  PI/g ETA:TTA =1:1).



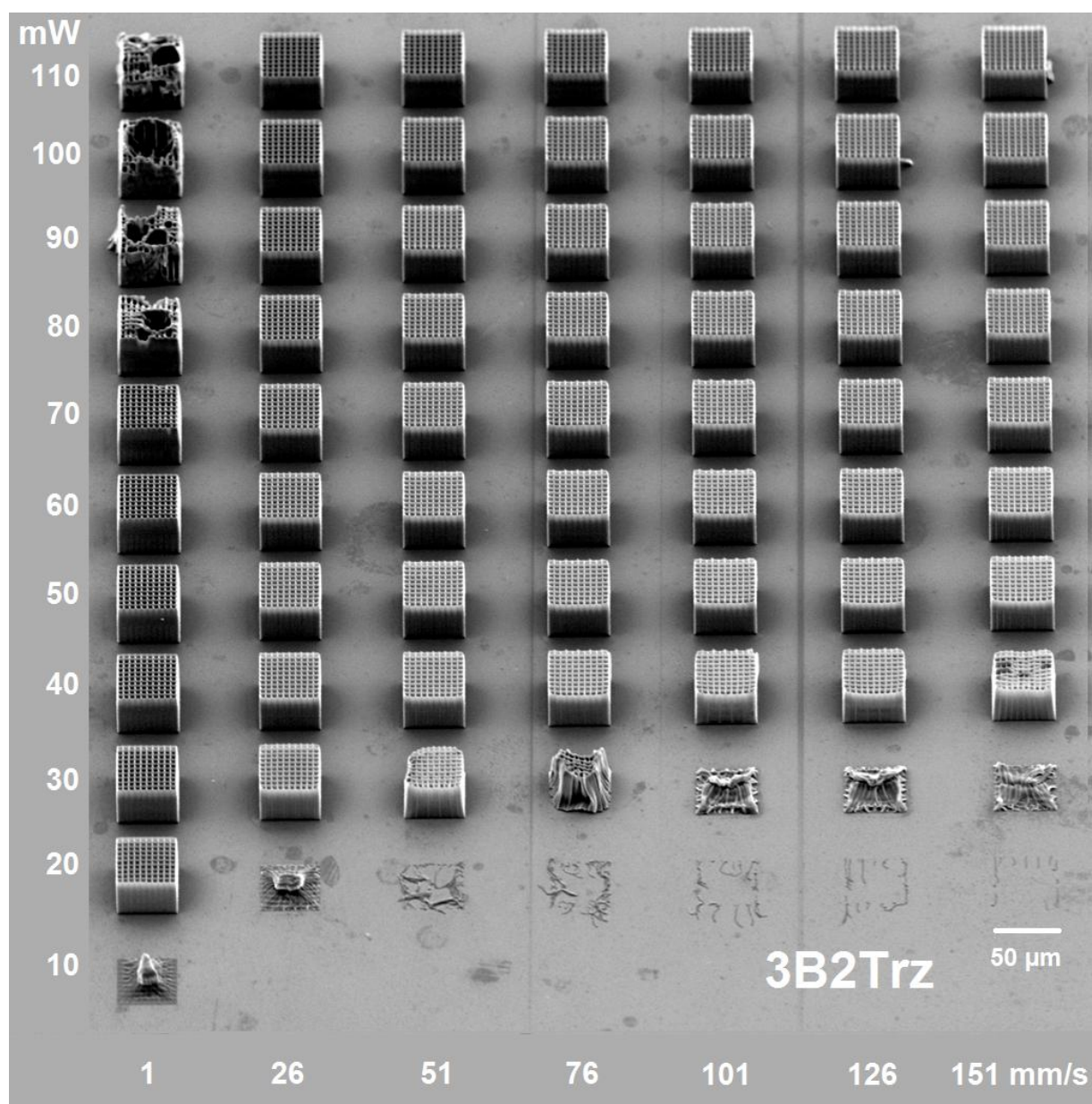


**Figure 52:** SEM-image of woodpile structures built with **3B2Trz** (6.3  $\mu\text{mol}$  PI/g ETA:TTA = 1:1).

## 4. Cleavable TPIs

As already discussed in the introduction and the state of the art-chapter, it is well known that Type I PIs allow for high efficiency and fast curing speeds in photopolymerization because they form radicals in a unimolecular reaction. Type II PIs suffer from a bimolecular mechanism and the diffusion limitations that go along with it, as well as back electron transfer between formed radical ions quenching the initiation reaction and posing another significant drawback.

The mechanism that most TPIs are postulated to follow doesn't require a bimolecular reaction with a separate co-initiator to form radicals; they are formed in a bimolecular process, but directly from the monomer material which is abundant. However radical ion pairs are formed from the TPI and the monomer molecules in a reversible process, so back electron transfer can still occur and reduces the initiation efficiency.

This leads us to the second approach employed in this thesis to attempt increasing the efficiency of TPIs. By creating a cleavable TPI, radicals would be formed in a unimolecular reaction and the possibility of back electron transfer would be avoided.

### 4.1. Cleavable Initiators based on M2CMK - Bifunctional C-S cleavage

In the introduction chapter it was discussed that type I PIs usually are aryl alkyl ketones that cleave the alkyl side in  $\alpha$ - or  $\beta$ -position to the carbonyl group. However there are also other examples known, like  $\beta$ -phenylogous cleavage of p-benzoylbenzyl phenyl sulfide (**BBPS**) investigated in a publication<sup>69</sup> by Yamaji *et al.* with a quantum yield of the cleavage up to 1.0.

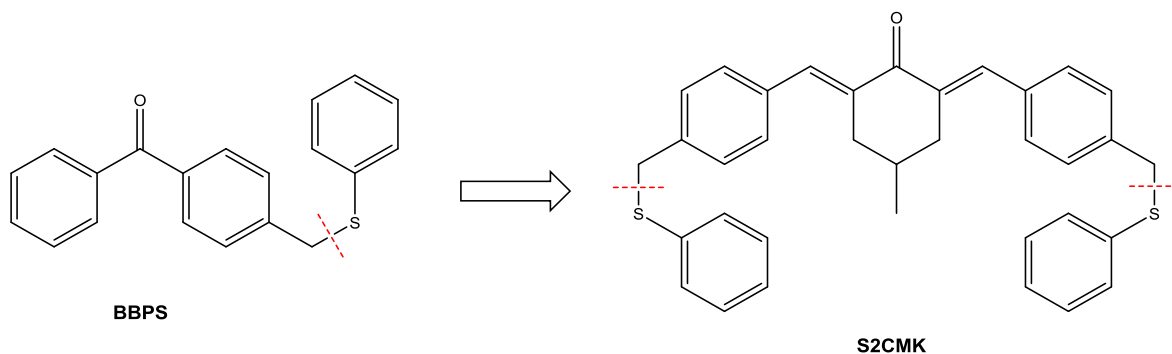


**Figure 53:** Transfer of the concept of  $\beta$ -phenylogous cleavage of **BBPS** to an extended  $\pi$ -system similar to **M2CMK**.

Such a successful cleavage of the C-S bond far from the carbonyl group makes this a promising starting point for the development of novel TPIs, which require an extended  $\pi$ -system to provide sufficiently high  $\sigma_{\text{TPA}}$ . Thus the compound **S2CMK** (see **Figure 53**) should be synthesized, which is analogous to **BBPS** but with a longer  $\pi$ -system and a symmetrical structure with two (phenylthio)methyl-groups.

Because of the familiar aldol-condensation strategy using 2 eq. of aldehyde and 1 eq. of symmetrical ketone, **S2CMK** is an easily accessible compound with two cleavable moieties, in contrast to **BBPS** which is obtained from commercially available 4-(bromomethyl)benzophenone. Furthermore, the bifunctionality of **S2CMK** allows for additional cross-linking through the initiator and thus more efficient curing.

To prove the mechanism of  $\beta$ -phenylogous cleavage, an analogous but non-cleavable compound **C2CMK** (see **Figure 54**), with methylene-groups instead of the two sulfur atoms, should also be synthesized and tested.

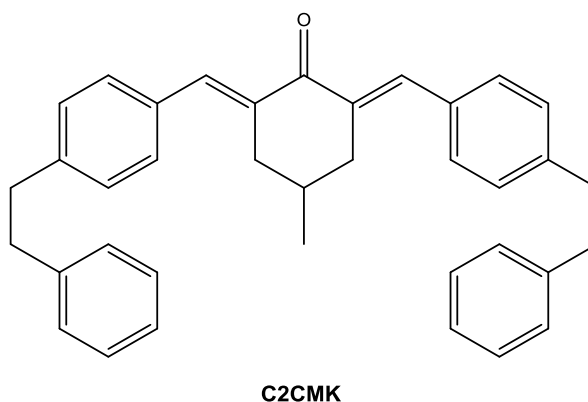


**Figure 54:** Non-cleavable reference compound **C2CMK**.

#### 4.1.1. Synthesis of **S2CMK**

The synthetic strategies to obtain **S2CMK** and **C2CMK** were analogous to **M2CMK**, by classical aldol condensation of 1 eq. of 4-methylcyclohexanone with 2 eq. of the corresponding aldehyde under alkaline conditions. However the aldehydes were not commercially available and had to be prepared.

In the retrosynthesis of the aldehyde **11** (see **Figure 55**) required for **S2CMK**, the most practical disconnection taking into account natural polarity and reactivity would be

cleavage of the C-S-bond as to obtain a benzylium and a thiolate synthon, favoring a nucleophilic substitution.

Because no commercial source could be found for a suitable aldehyde as synthetic equivalent to the benzylium synthon, as well as the rather high reactivity of unprotected aldehydes towards thiolates (eventually forming dithioacetals), a different oxidation state than the carbonyl group would be sensible i.e. alcohol or carboxylic acid. The carboxylic acid level was chosen because 4-(chloromethyl)benzoic acid was readily available at the institute (and also would be cheaper commercially than the alcohol).

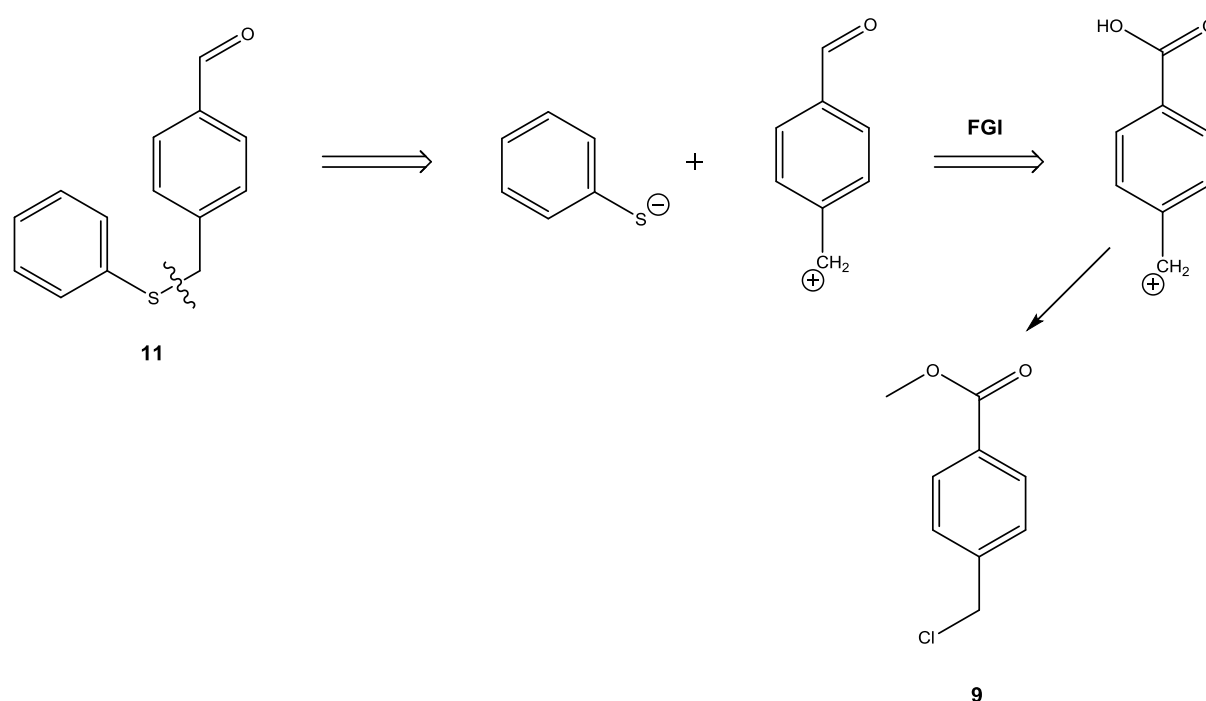


**Figure 55:** Retrosynthetic disconnection of aldehyde **11** and corresponding synthons/synthetic equivalents.

#### 4.1.1.1. Synthesis of precursor 4-(chloromethyl)benzoic acid methyl ester (**9**)

As carboxylic acids consume an additional equivalent of expensive hydride reduction reagents just for salt formation under release of hydrogen gas (let alone solubility problems of such salts in solvents suitable for the reduction reaction), the methyl ester **9** of 4-(chloromethyl)benzoic acid was selected (see **Figure 55**) as a more convenient substrate for the nucleophilic substitution and successive reduction to the aldehyde.

The ester **9** was easily obtained in a yield of 81% by refluxing 4-(chloromethyl)benzoic acid in MeOH with a catalytic amount of concentrated H<sub>2</sub>SO<sub>4</sub> and subsequent recrystallization of the extracted crude product from PE.

#### 4.1.1.2. Synthesis of precursor 4-[(phenylthio)methyl]benzoic acid methyl ester (**10**)

In the next step, the phenylthio-group should be introduced via nucleophilic substitution. Here the ester **9** is expected to react well in both competing S<sub>N</sub>1 and S<sub>N</sub>2 reactions, as the carbon atom which is attacked can form a resonance stabilized benzylium cation in suitable solvents and is also a primary haloalkane which should be highly reactive towards the good nucleophile phenylthiolate.

The protocol that was selected for this reaction was based on the procedure<sup>70</sup> for a similar reaction performed by Greeves and Torode, who used methyl 4-chloroacetoacetate as a substrate. Thiophenol was converted to the salt by reaction with sodium methanolate which was generated in situ from sodium metal scrapings in dry MeOH. The ester **9** was added at 0°C and the reaction continued at room temperature for 18 h. It was probably completed after a much shorter time, but product and starting material have almost identical R<sub>f</sub>-values in TLC, so that the formation of the product was not apparent in the beginning and was only confirmed by a <sup>1</sup>H-NMR of the crude product. Part of the solvent was removed in vacuo, the precipitated product was filtered off, washed with MeOH and then purified by Kugelrohr distillation to obtain substituted ester **10** with a yield of 85%.

#### 4.1.1.3. Synthesis of precursor 4-[(phenylthio)methyl]benzaldehyde (**11**)

The ester **10** was then to be reduced to the aldehyde **11**. There are several specialized hydride reagents that are able to reduce esters directly to aldehydes (rather than proceeding to the alcohol level), the most popular and easily available of them being diisobutyl aluminium hydride (DIBAH). In the 1960ies Zakharkin *et al.* investigated the reduction of esters<sup>71</sup> using DIBAH, finding that aromatic and α,β-unsaturated esters generally give lower yields than aliphatic esters, and that ether solvents also lead to reduced yields (more alcohol byproduct) compared to aromatic and aliphatic hydrocarbon solvents. The reason for this lies in the different kinetics of aldehyde

elimination from the formed aluminium complex depending on solvent coordination. In non-coordinating solvents the primary aluminium complex tends to accumulate and thus the aldehyde is obtained on hydrolysis (see **Figure 56**).<sup>72</sup>

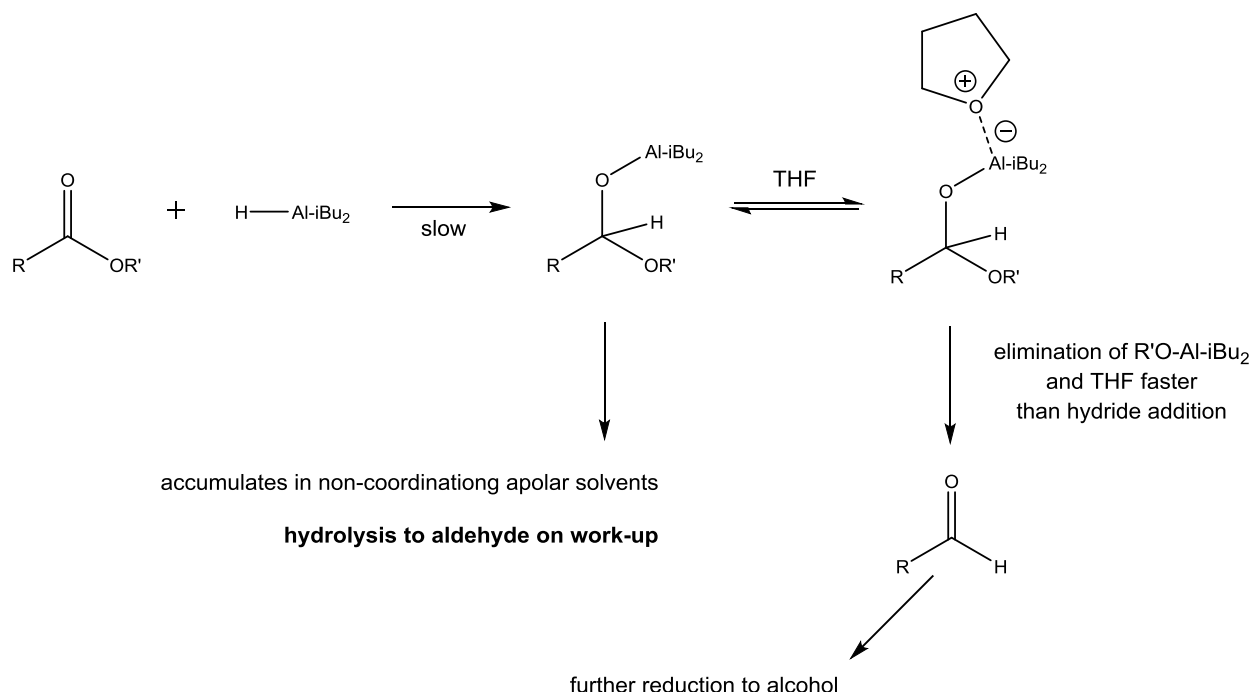


**Figure 56:** Mechanism of the DIBAH-reduction in different solvents.

In 1989 researchers around Kim *et al.* developed an improved synthesis routine<sup>73</sup> claiming higher aldehyde yields by using 3 eq. of DIBAH along with 2 eq. of *o*-anisidine per eq. of ester starting material.

The latter approach should be tested in the synthesis of the aldehyde **11**. Thus 1 eq. of ester **10** and 2 eq. of *o*-anisidine were dissolved in toluene and reacted with 3 eq. DIBAH (solution in heptane) at  $-78^\circ\text{C}$ .

It is crucial that the temperature of the reaction mixture does not rise too much throughout the whole reaction, as this leads to faster elimination of the aldehyde from the primary aluminium complex and increases the chances of over-reduction to the alcohol level (see **Figure 56**). This is achieved by carefully monitoring temperature with an internal thermometer, mechanical stirring, using enough toluene so that the mixture remains well stirrable below  $-78^\circ\text{C}$  and adding DIBAH-solution in small portions. The quenching with 4 N HCl was also done in a fashion so that the solution does not warm up too quickly. The crude product was obtained by drying the organic layer after

quenching and removing the solvent in vacuo; pure aldehyde **11** was isolated in a yield of 25% by column chromatography using silica gel 60 and PE with 6% EA.

**Figure 57** is briefly summing up the synthesis of aldehyde **11**:

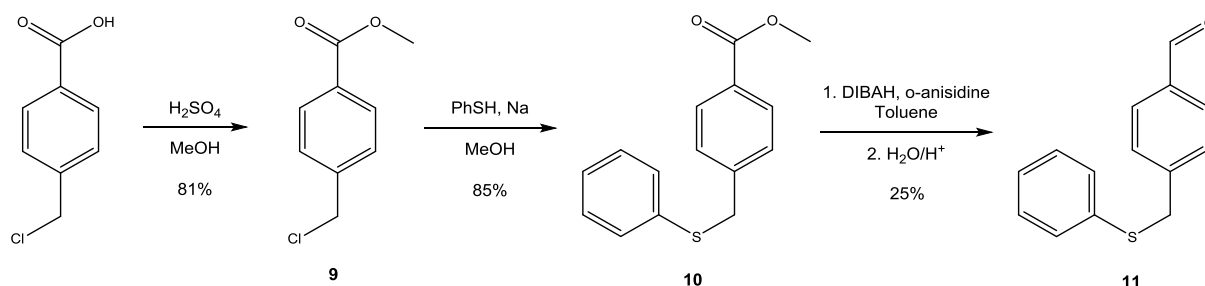


**Figure 57:** Overview of the synthesis of aldehyde **11** starting from 4-(chloromethyl)benzoic acid.

A yield of 25% for the reduction step is acceptable but still rather low. There are various possible reasons for this, the first one being that in column chromatography there was an overlap between the peaks of starting material ester **10** and the desired product ( $R_f$ -difference only slightly above 0.1), so not all of the aldehyde that was formed could be isolated by one chromatography run. The ester **10** was still present in the crude product in large amounts - besides the intrinsic lower reactivity of aromatic esters (especially electron-rich ones) towards DIBAH, too low solubility of ester **10** in toluene at  $-78^\circ\text{C}$  could be a reason, as the cooled reaction mixture was a milky white slurry even before the addition of DIBAH.

Alternative approaches to bypass this low yielding reaction would be to use a nitrile instead of an ester for the reduction step (aromatic nitriles are known to lead to higher aldehyde yields in DIBAH-reductions), but this would require the whole sequence to use a different starting material. Another way would be to cleanly reduce ester **10** to the corresponding benzyl alcohol and then use a method like Swern- or Dess-Martin-oxidation to obtain the aldehyde - requiring an additional step to the whole reaction sequence.

#### 4.1.1.4. Synthesis of S2CMK - final step

The final step towards **S2CMK** (see **Figure 58**) was analogous to the synthesis of the other di-benzylidene ketones: 1 eq. of 4-methylcyclohexanone was condensed with 2 eq. of aldehyde **11** in EtOH under alkaline catalysis with KOH at 60°C.

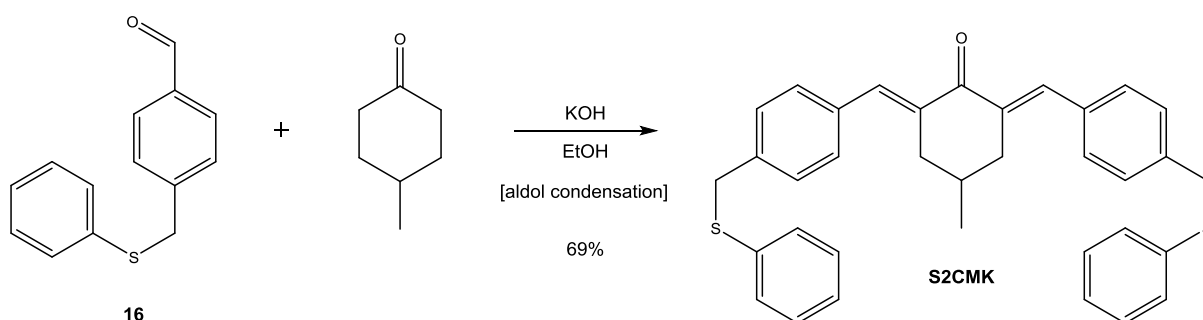


**Figure 58:** Aldol condensation step to **S2CMK**.

After stirring for 18 h the precipitated crude product was filtered off, washed with EtOH and purified by column chromatography using PE:DCM = 1:2 and silica gel 60 to afford **S2CMK** in a yield of 69%.

#### 4.1.2. Synthesis of non-cleavable reference C2CMK

To obtain the reference compound **C2CMK** containing a C-C- instead of a C-S-bond, the corresponding aldehyde **13** had to be synthesized. This compound had recently been prepared by Shen *et al.* in a screening of suitable substrates for their method<sup>74</sup> of employing water-tolerant indium alkyl reagents in coupling reactions with aryl halides using palladium based catalysts.

##### 4.1.2.1. Synthesis of precursor (2-iodoethyl)benzene (**12**)

To prepare the required starting material (2-iodoethyl)benzene (**12**) for the sequence to aldehyde **13** (overview is given in **Figure 59**), 2-phenylethanol was converted to the iodoalkane in an Appel reaction according to literature<sup>75</sup> in a yield of 74%.



#### 4.1.2.2. Synthesis of precursor 4-(2-phenylethyl)benzaldehyde (**13**)

Iodoalkane **12** was then converted to a monoalkyl indium halide reagent by stirring with metallic indium powder and CuCl in THF at room temperature, filtering off the solids and concentrating the filtrate in vacuo. It is crucial that not all THF is removed, as it seems to play an important role in stabilizing the alkyl indium - Shen *et al.* reported the complete decomposition of the reagent when the solvent is evaporated to dryness or purification on silica gel is attempted. Other than that, alkyl indium reagents are versatile and easily handled synthetic tools - they tolerate a wide variety of functional groups and even water or air.

The concentrated residue containing the alkyl indium reagent was thus used for the next step without further purification. For the coupling reaction to 4-bromobenzaldehyde, 0.7 eq. of the latter were dissolved in DMA together with the alkyl indium compound (1 eq., calculation based on the initially employed iodoalkane **12**) and 5 mol%  $[\text{PdCl}_2(\text{PPh}_3)_2]$  as well as 2 eq. LiCl as catalysts. After stirring the mixture for 24 h at 100°C, the crude product was extracted with  $\text{Et}_2\text{O}$  (removing DMA by washing with saturated  $\text{NH}_4\text{Cl}$ -solution and water) and purified by Kugelrohr distillation in vacuo (bp ~ 130-135°C at 0.2 mbar) to afford aldehyde **13** as a clear oil in a yield of 82% (calculation based on 4-bromobenzaldehyde).

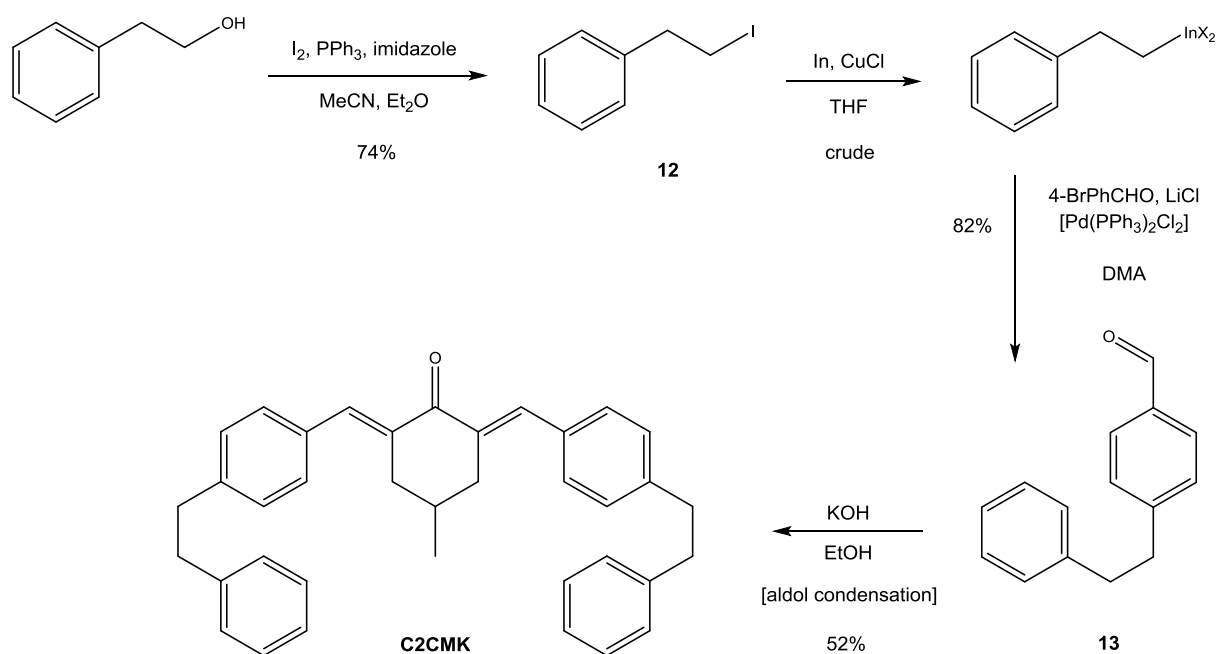


Figure 59: Overview of the synthesis of C2CMK.

#### 4.1.2.3. Synthesis of C2CMK - final step

**Figure 59** gives an overview of all steps towards **C2CMK**; the final condensation step again was following the proven aldol condensation routine for di-benzylidene ketones. A solution 1 eq. of 4-methylcyclohexanone and 2 eq. of aldehyde **13** in EtOH was stirred with KOH at 60°C. After 24 h the precipitated crude product was filtered off, washed with EtOH and purified by column chromatography (gradient elution PE with 30-40% DCM on silica gel 60) to afford **C2CMK** in a yield of 52%.

#### 4.1.3. Analysis of S2CMK and C2CMK

##### 4.1.3.1. UV/Vis - spectroscopy

**Figure 60** shows the normalized OPA spectra of **S2CMK** and **C2CMK** as well as the reference compound **M2CMK**. The strong blue-shift of about 90 nm for both **S2CMK** and **C2CMK** ( $\lambda_{\text{abs}}^{\text{OPA}} = 340 \text{ nm}$ ,  $\epsilon = 3.7 \cdot 10^4 \text{ M}^{-1} \text{ cm}^{-1}$ ) as well as a reduced extinction coefficient in comparison to the reference **M2CMK** ( $\lambda_{\text{abs}}^{\text{OPA}} = 430 \text{ nm}$ ,  $\epsilon = 4.7 \cdot 10^4 \text{ M}^{-1} \text{ cm}^{-1}$ ) both result from the lack of a good electron donor group in conjugation with the  $\pi$ -system.

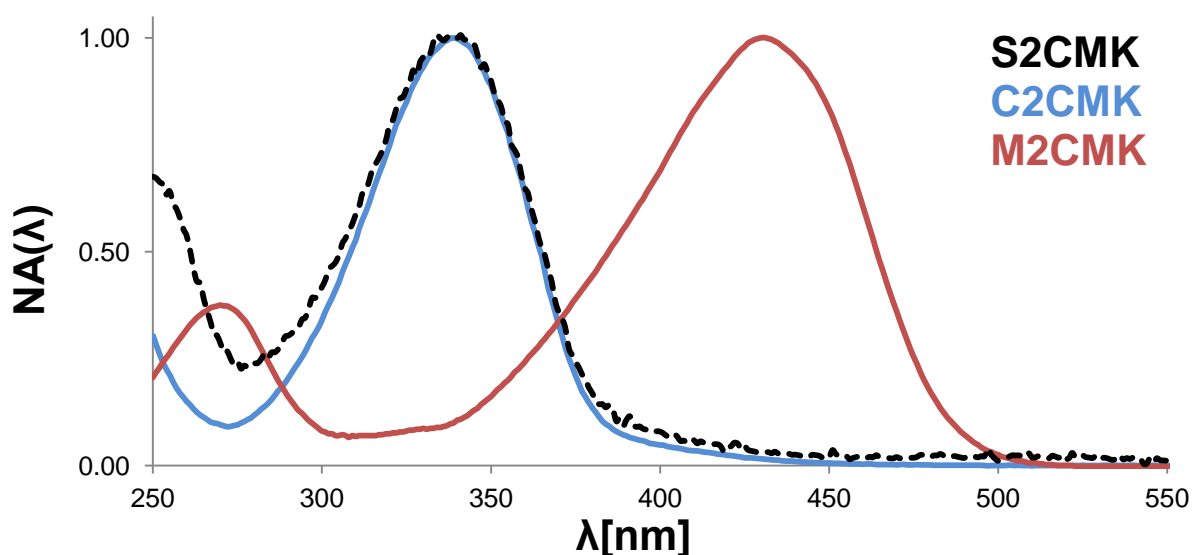


**Figure 60:** Normalized OPA spectra of **S2CMK** (black dotted line), **C2CMK** (blue line) and reference compound **M2CMK** (red line) all measured at a concentration of  $10^{-5} \text{ mol L}^{-1}$  in MeCN

#### 4.1.3.2. Open aperture z-scan

The open aperture z-scan for **S2CMK** and **C2CMK** (10 mM in THF) resulted in no detectable signal, indicating that their  $\sigma_{\text{TPA}}$  at 800 nm must lie well below the detection limit of about 20 GM. This is in accordance with the extremely weak absorption of **S2CMK** and **C2CMK** around 400 nm, caused by the lack of suitable good electron donor groups.

#### 4.1.3.3. TPIP structuring tests

Finally **S2CMK** and **C2CMK** were each dissolved at a concentration of 6.3  $\mu\text{mol PI/g}$  resin in ETA/TTA = 1:1. Both dissolved at an acceptable rate only after addition of acetone as a co-solvent (removed in vacuo before the polymerization).

In performance tests with woodpile structures no acceptable structures could be obtained at any of the different laser intensities and writing speeds, as was expected from the very low  $\sigma_{\text{TPA}}$ . Compared to each other **S2CMK** performed significantly better than **C2CMK** (see **Figure 61**), with the former being able to generate polymer networks at least resembling the shape of a woodpile, while all structures written with the latter simply collapsed. This is some evidence there might be an  $\beta$ -phenylogous cleavage causing the better performance of **S2CMK**. As other effects like the structure of the solvation shell have a large influence on the  $\sigma_{\text{TPA}}$  (which couldn't be determined), detection of the formed radicals would be a more reliable proof, but such experiments are not easily performed and beyond the scope of this work due to the tiny reaction volumes involved in TPA processes.

It should be noted that **S2CMK** showed a rather unique behavior when the power density was so low that the woodpile structures totally collapsed: As visible in **Figure 62** well defined thin polymer lines remained, which seem to have formed mainly at the outermost meeting points of the grid lines. This is precisely where the laser remains longest as it turns around to write the next line, possibly indicating that a low polymerization rate might be the limiting factor that leads to low double-bond conversion when a (phenylthio)methyl-group is involved.

S2CMK					C2CMK			
mW	1	26	51	76	mW	1	26	mm/s
110	3	4	4	4	110	4	-	
100	3	4	4	4	100	4	-	
90	3	4	4	4	90	4	-	
80	3	4	4	4	80	4	-	
70	3	4	4	4	70	-	-	

**Figure 61:** Processing windows of **S2CMK** and **C2CMK** (6.3  $\mu\text{mol PI/g ETA:TTA} = 1:1$ ).

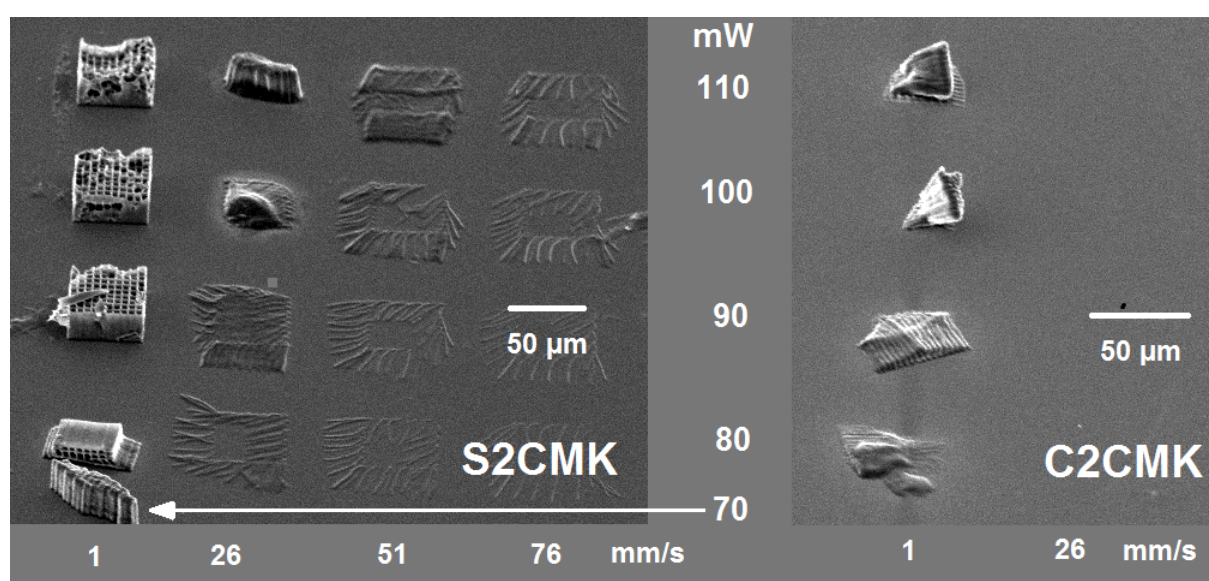


**Figure 62:** SEM-image of structures built with **S2CMK** and **C2CMK** (6.3  $\mu\text{mol PI/g ETA:TTA} = 1:1$ ).

## 4.2. Cleavable Initiators based on M2CMK - C-S cleavage enhanced through strong donor group

### 4.2.1. Synthesis of SNB

The main reason for the extremely small processing window and inability of **S2CMK** to produce any ideal structures at reasonable writing speeds is most likely the lack of a strong electron donor group, which is required for efficient TPA. Thus a system **SNB** (see **Figure 63**) containing a dimethylamino-group as a donor as well as the (phenylthio)methyl-group capable of C-S-bond cleavage should be prepared and investigated. To better understand the effects of such a combined system, the

properties of the half containing the donor group alone (the benzylidene ketone **1** already prepared earlier in this thesis) should be examined as well.

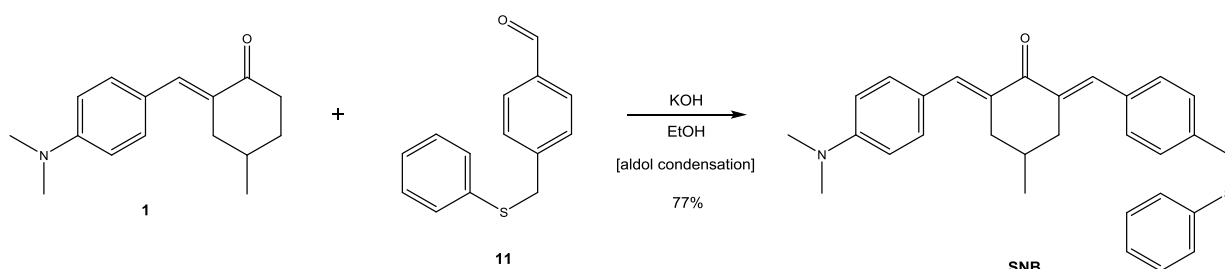


**Figure 63:** Aldol condensation route to **SNB**.

Both the required benzylidene ketone **1** and aldehyde **11** were already available from the syntheses of other TPIs, so just the aldol condensation step needed to be performed. This was following the usual protocol, 1.1 eq. of aldehyde **11** (slight excess) and 1 eq. of benzylidene ketone **1** were dissolved in EtOH and stirred with KOH at 60°C for 24 h. The crude precipitate was filtered off, washed with EtOH and purified by column chromatography (DCM, silica gel 60) to afford **SNB** in a yield of 77%.

#### 4.2.2. Analysis of **SNB**

##### 4.2.2.1. UV/Vis - spectroscopy

A comparison of the normalized OPA spectra (see **Figure 64**) of **SNB** as well as benzylidene ketone **1** and the reference compound **M2CMK** already revealed some interesting properties of **SNB**. While the spectrum of ketone **1** ( $\lambda_{\text{abs}}^{\text{OPA}} = 372 \text{ nm}$ ,  $\epsilon = 3.2 \cdot 10^4 \text{ M}^{-1} \text{ cm}^{-1}$ ) is considerably blue-shifted compared to **M2CMK** ( $\lambda_{\text{abs}}^{\text{OPA}} = 430 \text{ nm}$ ,  $\epsilon = 4.7 \cdot 10^4 \text{ M}^{-1} \text{ cm}^{-1}$ ), **SNB** ( $\lambda_{\text{abs}}^{\text{OPA}} = 420 \text{ nm}$ ,  $\epsilon = 3.5 \cdot 10^4 \text{ M}^{-1} \text{ cm}^{-1}$ ) has its absorption maximum much closer to **M2CMK** than ketone **1**. This suggests that the mere extension of the  $\pi$ -system without any additional donor group causes a significant red-shift. Furthermore the benzylidene group without a strong donor substituent has its own distinct absorption band (maximum  $\sim 322 \text{ nm}$ ,  $\epsilon = 2.0 \cdot 10^4 \text{ M}^{-1} \text{ cm}^{-1}$ ) which is lacking in both **M2CMK** and ketone **1**, but close to the strongest absorption of **S2CMK** ( $\lambda_{\text{abs}}^{\text{OPA}} = 340 \text{ nm}$ ). This indicates that for such non-symmetric systems there is some electronic communication between both sides of the carbonyl group (strong red-shift of one

maximum, slight blue-shift of the other), but they still retain an independent character as well.

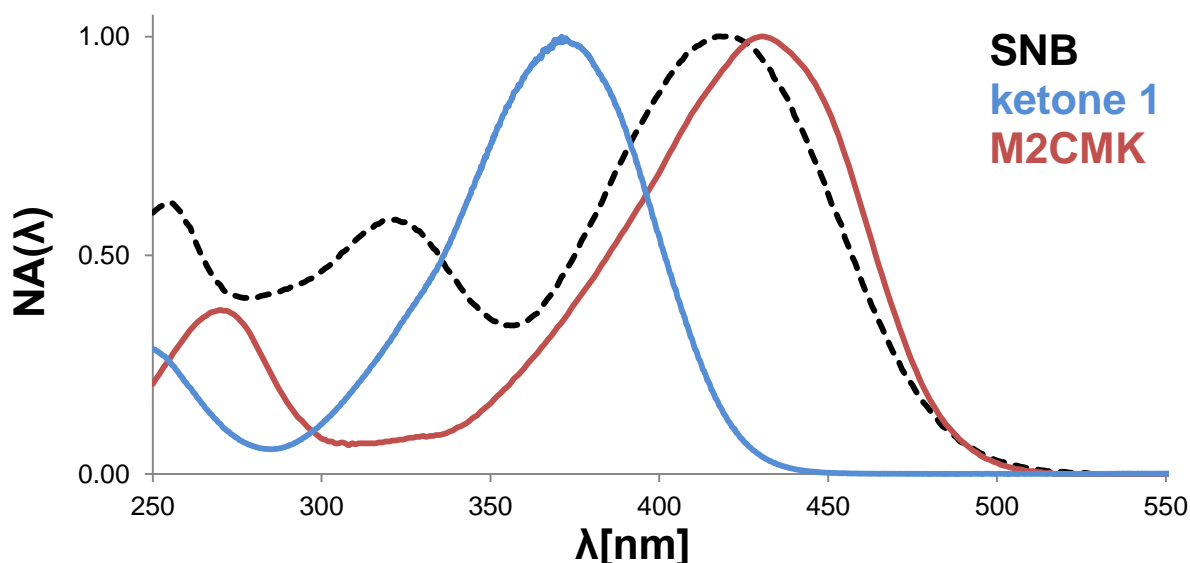


**Figure 64:** Normalized OPA spectra of **SNB** (black dotted line), ketone **1** (blue line) and reference compound **M2CMK** (red line) all measured at a concentration of  $10^{-5}$  mol L<sup>-1</sup> in MeCN

#### 4.2.2.2. Open aperture z-scan

The  $\sigma_{\text{TPA}}$  of **SNB** was measured from a 10 mM solution in THF and determined to be 99 GM, which is a bit more than half the value of the reference **M2CMK** (191 GM) and in accordance with the findings from OPA spectroscopy.

#### 4.2.2.3. TPIP structuring tests

For TPIP structuring tests, **SNB** was dissolved in ETA/TTA = 1:1 at a concentration of 6.3  $\mu\text{mol}$  PI/g resin. No addition of co-solvents was necessary, likely due to the low symmetry of the molecule **SNB** dissolved quickly without any problems. Performance tests with woodpile structures written at different laser intensities and writing speeds shows a significantly smaller processing window for **SNB** (see **Figure 66** & **Figure 67**) compared to **M2CMK** (see **Figure 23** & **Figure 24**) at lower energies (class 4 instead of class 1 structures between 30 - 60 mW at higher writing speeds). While at higher energies (80 - 110 mW, 1 mm/s) with **SNB** still only class 3 structures were obtained, they seem less extensively damaged than those written with **M2CMK**. Furthermore, at

high speeds where the structures totally collapsed, the remnants again show characteristic polymer threads which were so far only encountered with **S2CMK**. This suggests either a formation of thiyl-radicals or at least some other modifying involvement of the (phenylthio)methyl-group in the polymerization process.

Ketone **1** was also tested as a reference, dissolved in ETA/TTA = 1:1 at 6.3  $\mu\text{mol PI/g}$  resin. Its behavior drastically differs from **SNB**, ketone **1** (see **Figure 68** & **Figure 69**) clearly was not able to generate any satisfying woodpile structures under the tested conditions. The reason for this most likely is that the conjugated system is too short for efficient TPA (see **Figure 65**).

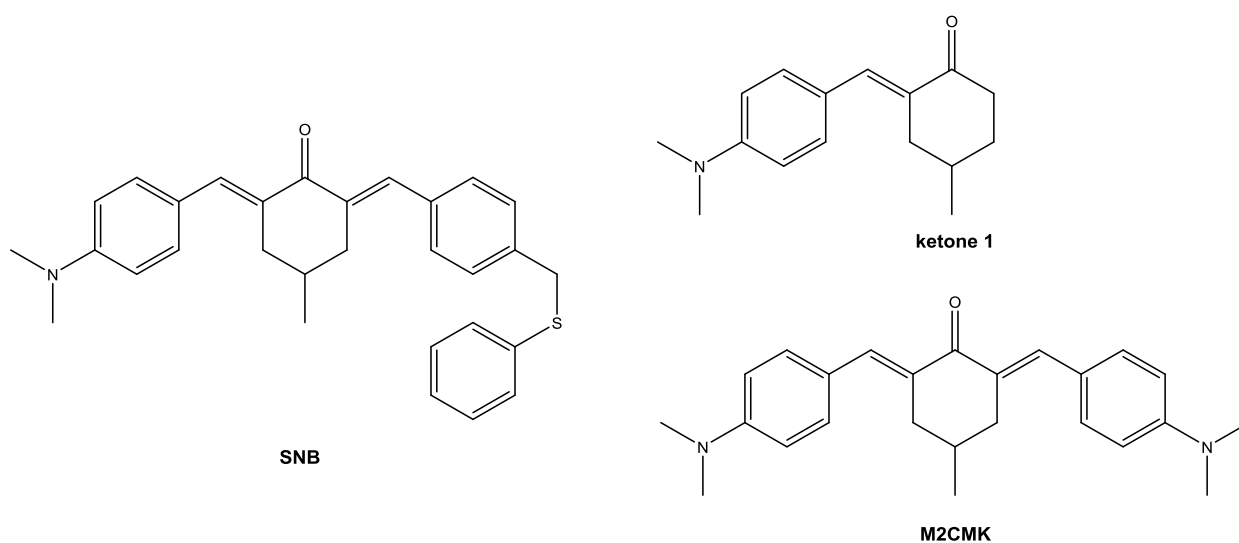


**Figure 65:** Comparison of the structures of **SNB**, ketone **1** and reference compound **M2CMK** indicating the  $\pi$ -systems of different length and donor strength substitution.



<b>SNB</b>							
mW	1	26	51	76	101	126	151 mm/s
110	3	1	1	1	1	1	1
100	3	1	1	1	1	1	1
90	3	1	1	1	1	1	1
80	3	1	1	1	1	1	1
70	2	1	1	1	1	1	1
60	1	1	1	1	4	4	4
50	1	1	4	4	4	4	4
40	1	4	4	4	4	4	4
30	1	4	4	4	4	4	4
20	1	4	-	-	-	-	-

**Figure 66:** Processing window of **SNB** (6.3  $\mu$ mol PI/g ETA:TTA =1:1).

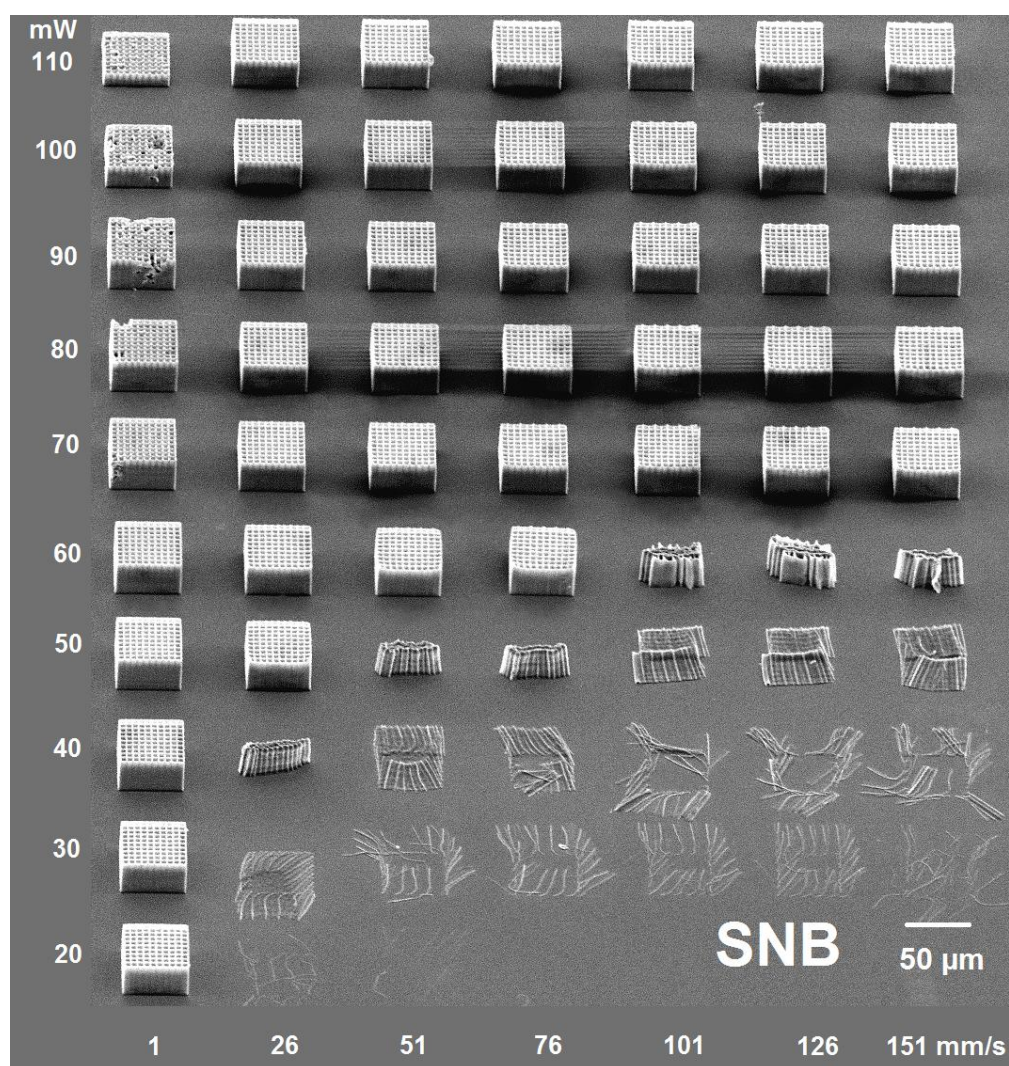


**Figure 67:** SEM-image of woodpile structures built with **SNB** (6.3  $\mu$ mol PI/g ETA:TTA =1:1).



**ketone 1**

mW	1	26	51	76	101	126	151	mm/s
110	3	4	4	4	4	4	4	
100	3	4	4	-	-	-	-	
90	3	4	-	-	-	-	-	
80	3	-	-	-	-	-	-	
70	3	-	-	-	-	-	-	
60	2	-	-	-	-	-	-	
50	4	-	-	-	-	-	-	

**Figure 68:** Processing windows of ketone **1** (6.3  $\mu\text{mol PI/g}$  ETA:TTA =1:1).

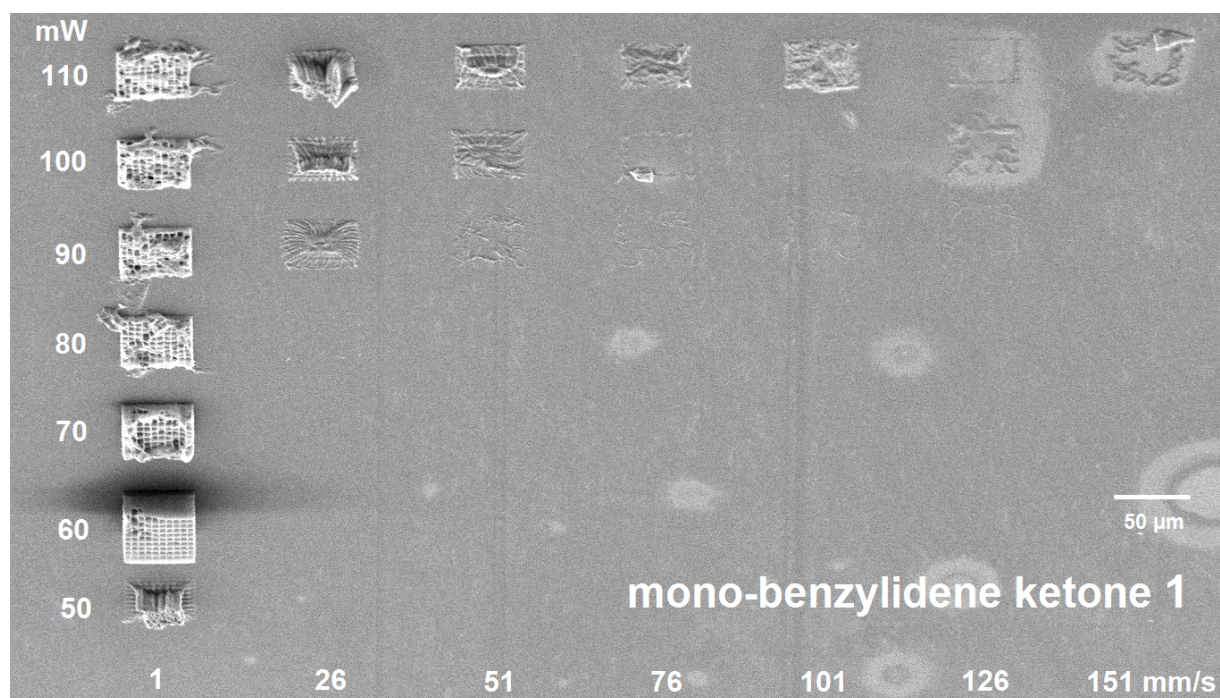


**Figure 69:** SEM-image of structures built with ketone **1** (6.3  $\mu\text{mol PI/g}$  ETA:TTA =1:1).

### 4.3. Cleavable Initiator - Pentazadiene releasing gaseous nitrogen

Another way to ensure efficient and irreversible cleavage of radical initiators is the release of a gaseous compound. Due to the related entropy increase, such reactions are often thermodynamically favored, as is the case with the radical initiator azobisisobutyronitrile (**AIBN**) which releases elementary nitrogen and two radicals upon thermal decomposition (see **Figure 70**).

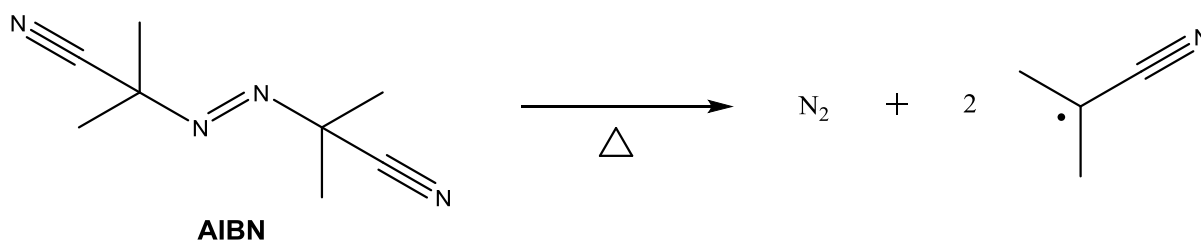


**Figure 70:** Thermal decomposition of **AIBN**.

While **AIBN** is able to cleave photolytically, it does not absorb significantly in the visible range and the conjugated system is far too small to for efficient TPA.

There is another class of compounds capable of photolytic cleavage and generating radicals while releasing nitrogen, the 1,4-pentazadienes. They have a more extensive  $\pi$ -system and a strong absorption band close to 400 nm, making them promising candidates to be efficient TPIs.

The compound that should be investigated in preliminary tests is 1,5-bis(4-methoxyphenyl)-3-methyl-1,4-pentazadiene (**PADE**). **PADE** was first described by Goldschmidt and Badl<sup>76</sup> in 1889 and successfully used for the polymerization of acrylates under one-photon conditions e.g. by Novikova *et al.*<sup>77</sup>

#### 4.3.1. Synthesis of PADE

The synthetic approach chosen here was a slightly modified one-step procedure (see **Figure 71**) described by Baidl.<sup>78</sup> First 2 eq. of p-anisidine were diazotized with  $\text{NaNO}_2$  and  $\text{HCl}$  in aqueous solution slightly below  $0^\circ\text{C}$ , then the diazonium salt was coupled with 1 eq. of aqueous methylamine and an excess of  $\text{Na}_2\text{CO}_3$  at temperatures rising up to  $5^\circ\text{C}$  towards the end of the reaction.

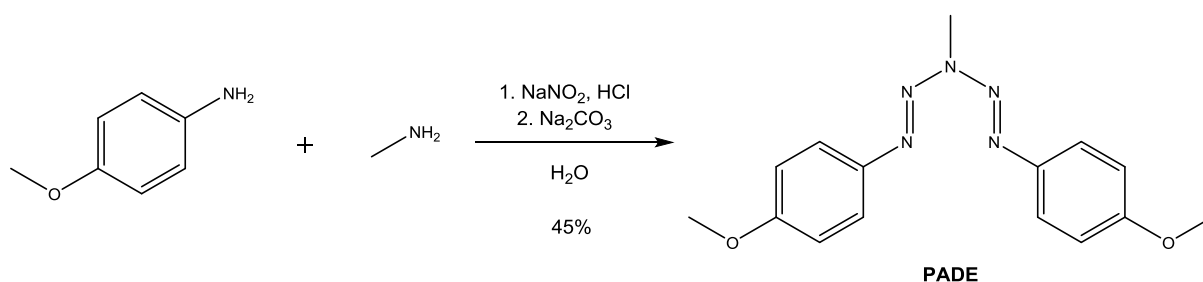


**Figure 71:** Synthesis of **PADE**.

A sample of the crude product that had precipitated was filtered off and washed with water; attempts to recrystallize from acetone at  $-78^\circ\text{C}$  as described by Baidl<sup>78</sup> were unsuccessful. Thus the reaction mixture (aqueous phase and crude precipitate) was extracted with DCM and the extract subjected to flash chromatography over silica gel 60 using DCM as eluent. Substantial amounts of a deep crimson red, very polar compound were retained at the start of the flash column. The product **PADE** was obtained as fluffy yellow needles in a yield of 45% by careful evaporation (heating and/or white light lead to decomposition) of the solvent in vacuo.

### 4.3.2. Analysis of PADE

#### 4.3.2.1. UV/Vis - Spectroscopy

The normalized OPA spectrum of **PADE** ( $\lambda_{\text{abs}}^{\text{OPA}} = 386 \text{ nm}$ ,  $\epsilon = 4.4 \cdot 10^4 \text{ M}^{-1} \text{ cm}^{-1}$ ) in **Figure 72** shows that while its absorption is strong, the maximum of the band in the visible range is considerably blue-shifted compared to **M2CMK** ( $\lambda_{\text{abs}}^{\text{OPA}} = 430 \text{ nm}$ ,  $\epsilon = 4.7 \cdot 10^4 \text{ M}^{-1} \text{ cm}^{-1}$ ).

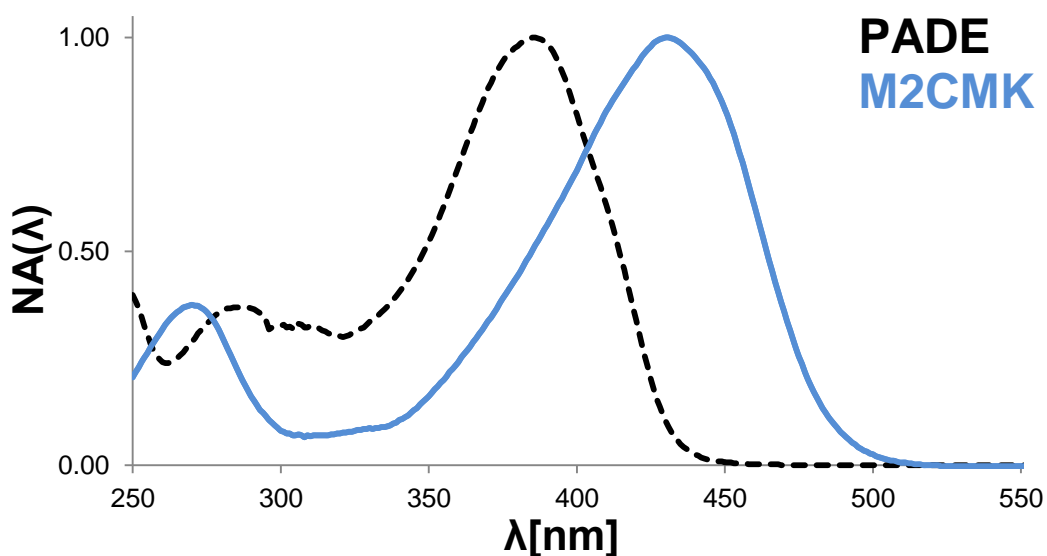


**Figure 72:** Normalized OPA spectra of **PADE** (black dotted line,  $10^{-5} \text{ mol L}^{-1}$  in THF) and reference compound **M2CMK** (blue line  $c = 10^{-5} \text{ mol L}^{-1}$  in MeCN)

#### 4.3.2.2. Open aperture z-scan

The shape of the z-scan fitting curve (see **Figure 73**, comparison with **Y-B2CMK**) of the measurement of **PADE** in 10 mM THF solution indicated that the underlying multi-photon absorption process might in fact be three-photon absorption. This is surprising as the OPA at 400 nm ( $\sim \frac{1}{2}$  of the fs-pulsed laser wavelength) is much stronger than at 266 nm ( $\sim \frac{1}{3}$  of the fs-pulsed laser wavelength). The  $\sigma_{\text{TPA}}$  was calculated according to appropriate fitting curve to be 85 GM; for the three-photon fitting curve, the resulting value would be  $57 \cdot 10^{-80} \text{ cm}^6 \text{ s}^2 \text{ photon}^{-2}$ .

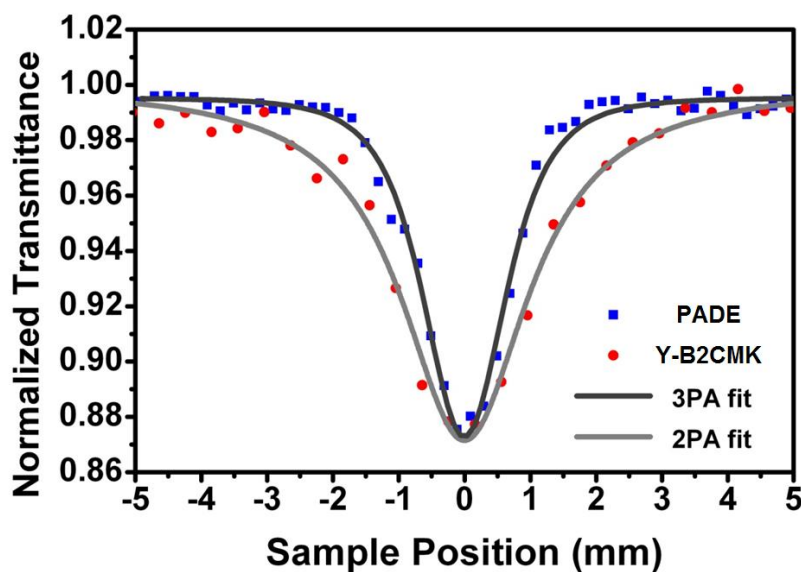


**Figure 73:** Z-scan fitting curve of **PADE** showing better fit with 3-photon-absorption (3PA).

#### 4.3.2.3. TPIP structuring tests

In TPIP structuring tests performed with **PADE** dissolved at a concentration of  $6.3 \mu\text{mol PI/g}$  resin in  $\text{ETA/TTA} = 1:1$ , no acceptable woodpile structures could be obtained (see **Figure 74** & **Figure 75**). However the photolysis of **PADE** was still evident, as pictures (see **Figure 75**) of the camera used to monitor the TPIP process clearly show the formation of nitrogen gas bubbles during the writing process. It is not clear whether the bubble formation leads to an additional deformation of the woodpile structures, but the main reason for them collapsing seems to be too little cross linking caused either by low concentration of radicals or radicals that don't initiate polymer chains efficiently.

<b>PADE</b>			
mW	1	26	mm/s
110	3	4	
100	3	4	
90	3	-	
80	3	-	
70	4	-	

**Figure 74:** Processing windows of **PADE** ( $6.3 \mu\text{mol PI/g}$  ETA:TTA =1:1).

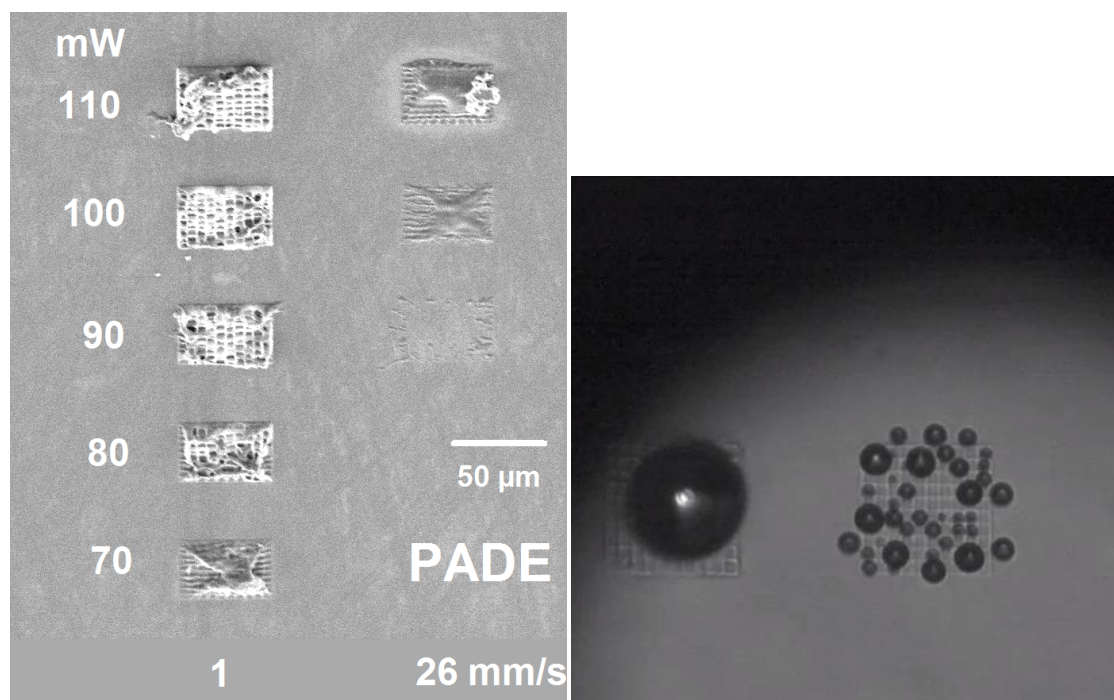
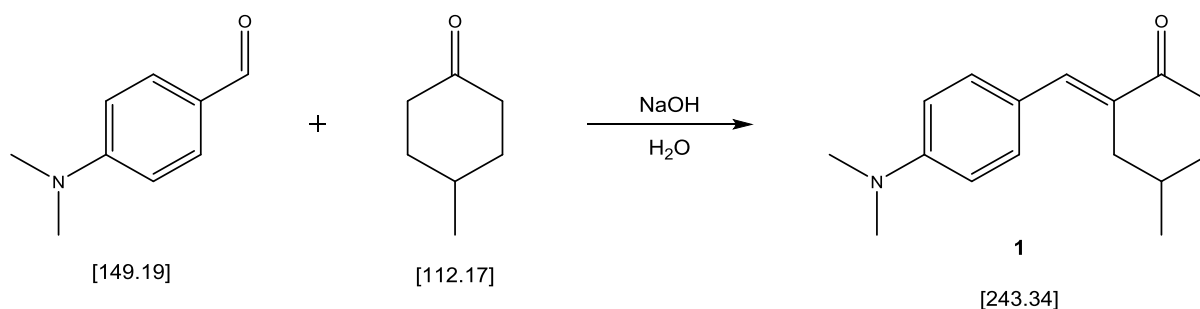


**Figure 75:** SEM-image of structures built with **PADE** (6.3 μmol PI/g ETA:TTA =1:1) and CMOS camera image of N<sub>2</sub>-bubble formation/evidence of cleavage during the writing process.

A possibility for future studies to enhance the initiation efficiency would be to use stronger electron donors like dimethylamino-groups instead of methoxy-groups, or also change the central substituent on the nitrogen chain to increase stability. Such a compound hasn't been described in literature so far. Increasing donor strength on the terminal aryl substituent is known to destabilize the system both towards thermo- and photolysis, while exchanging the central methyl-group e.g. for a hydroxyethyl-group increases the thermal stability while photosensitivity remains intact.<sup>78</sup>

## Experimental Part

### 1.1.1.1. (2*E*)-2-[[4-(Dimethylamino)phenyl]methylene]-4-methylcyclohexanone (**1**)<sup>57</sup>



Reagents	MW [g/mol]	[g]	[mL]	[mmol]	[eq.]
4-(dimethylamino)benzaldehyde	149.19	2.98		20.0	1.0
4-methylcyclohexanone	112.17	4.49		40.0	2.0
NaOH	40.0	0.80		20.0	1.0
deionized water			20		

### Procedure

All steps were performed in an orange light room. To a solution of NaOH (0.80 g, 20.0 mmol, 1.0 eq.) in deionized water (20 mL) 4-(dimethylamino)benzaldehyde (2.98 g, 20.0 mmol, 1.0 eq.) and 4-methylcyclohexanone (4.49 g, 40.0 mmol, 2.0 eq.) were added and the resulting emulsion was held at reflux for 20 h under argon atmosphere and with magnetic stirring.

After cooling to room temperature the reaction mixture was diluted with deionized water (150 mL) and extracted with DCM (3 x 100 mL). The combined organic layers were subsequently washed with saturated NH<sub>4</sub>Cl-solution (50 mL) and deionized water (50 mL) and finally dried with anhydrous NaSO<sub>4</sub>.

Removal of the solvent in vacuo yielded an orange oil (7.2 g) which was recrystallized from PE to obtain the crude product as a light orange crystal mass (4.4 g), then further purified by column chromatography (PE:EA = 83:17, 477 g silica gel 60).

**Yield**

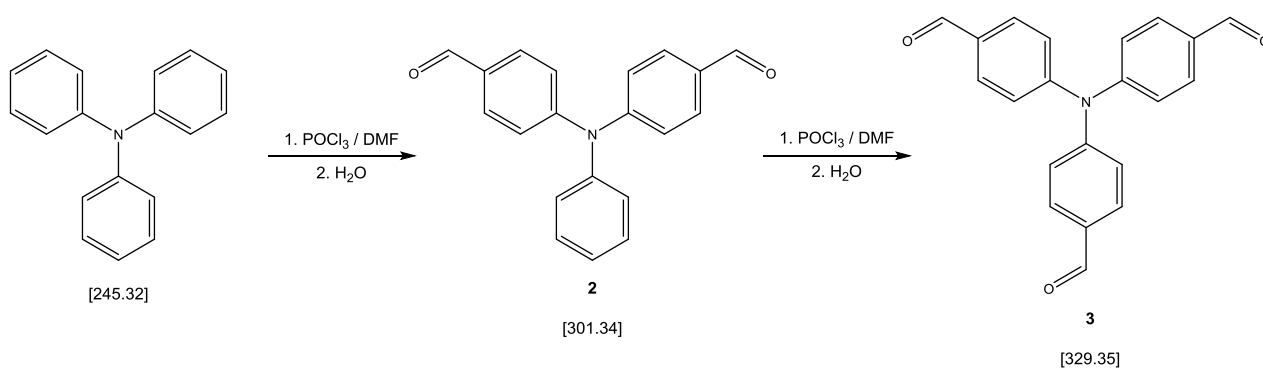
0.98 g of yellow crystals (20 % of theory)

**Analysis**TLC:  $R_f = 0.55$  (PE:EA = 3:1)

mp: 119 - 122°C

$^1\text{H}$  NMR (200 MHz,  $\text{CDCl}_3$ )  $\delta$  (ppm) = 7.53 (1H, s,  $-\text{C}=\text{CH}$ ), 7.40 (2H, d,  $J = 8.8$  Hz ar-H2,6), 6.70 (2H, d,  $J = 8.8$  Hz, -N-ar-H3,5), 2.91 - 3.15 (7H, m,  $-\text{N}(\text{CH}_3)_2$ ;  $-\text{CH}_2-\text{C}=\text{CH}$ ), 2.25 - 2.70 (3H, m,  $-\text{CH}_2-\text{C}=\text{CH}$ ;  $-\text{CH}_2-\text{C}=\text{O}$ ), 1.46 - 2.01 (3H, m,  $-\text{CH}_2-\text{CH}$ ;  $-\text{CH}-\text{CH}_3$ ), 1.09 (3H, d,  $J = 6.3$  Hz,  $-\text{CH}-\text{CH}_3$ )

$^{13}\text{C}$ -NMR (50 MHz,  $\text{CDCl}_3$ )  $\delta$  (ppm) = 201.0 (1C,  $-\text{C}=\text{O}$ ), 150.5 (1C, N-ar-C4), 137.2 (1C,  $-\text{C}=\text{CH}$ ), 132.6 (2C, -ar-C2,6), 131.0 (1C,  $-\text{C}=\text{CH}$ ), 123.5 (1C, -ar-C1), 111.6 (2C, -N-ar-C3,5), 40.1 (2C,  $-\text{N}(\text{CH}_3)_2$ ), 39.0 + 37.6 + 31.1 (3C,  $-\text{C}=\text{O}-\text{CH}_2-\text{CH}_2-\text{CH}-\text{CH}_2-\text{C}=\text{CH}$ ), 30.2 (1C,  $-\text{CH}-\text{CH}_3$ ) 22.0 (1C,  $-\text{CH}-\text{CH}_3$ )

**1.1.1.2.****4,4',4''-Nitrilotris(benzaldehyde) (3)<sup>58</sup>**

Reagents	MW [g/mol]	[g]	[mL]	[mmol]	[eq.]
triphenylamine	245.32	7.36		30.0	1.0
step 1:					
DMF	73.09	50.4		690	23.0



POCl <sub>3</sub>	153.33	115	750	25.0
step 2:				
DMF	73.09	40.4	552	18.4
POCl <sub>3</sub>	153.33	92.0	600	20.0

## Procedure

A 250 mL three-neck round-bottom flask equipped with reflux condenser, mechanical stirrer and dropping funnel was charged with dry DMF (50.4 g, 690.0 mmol, 23.0 eq.), purged with argon and cooled to -5° – 0°C. Freshly distilled POCl<sub>3</sub> (115 g, 750.0 mmol, 25.0 eq.) was added dropwise over a period of 30 min under stirring and cooling, leading to the formation of a yellowish-white crystalline paste. Stirring was continued for another 30 min at room temperature. The mass was then melted at 40°C and after addition of triphenylamine (7.36 g, 30.0 mmol, 1.0 eq.) heated to 95°C, leading to a color change from intense yellow to orange to reddish brown. After stirring for 4 h at 95°C the reaction mixture was cooled to room temperature and poured into 1500 mL of ice/water mixture and stirred overnight at room temperature. The solution was alkalized to pH 9 with NaOH-solution (800 mL, 4 mol/L), extracted with DCM (4 x 400 mL), the combined organic layers washed with deionized water (4 x 250 mL), dried with anhydrous Na<sub>2</sub>SO<sub>4</sub>, and filtered over silica gel 60 (50 g), causing the solution to change color from dark brown to deep yellow. Removal of the solvent in vacuo yielded crude di-aldehyde **2** (8.04 g) as a light brown oil. The aforementioned procedure for preparation of the Vilsmeier reagent was repeated using dry DMF (40.4 g, 552.0 mmol, 18.4 eq.) and freshly distilled POCl<sub>3</sub> (92.0 g, 600.0 mmol, 20.0 eq.), the di-aldehyde **2** was added to the molten Vilsmeier salt at 40°C, heated to 95°C and stirred at that temperature for 1.5 h leading to a dark brown viscous mixture. After cooling to room temperature the reaction mixture was poured into 1500 mL of ice/water mixture, alkalized to pH 8 with NaOH-solution (840 mL, 4 mol/L) and extracted with DCM (4 x 400 mL). The combined organic layers were washed with deionized water (3 x 400 mL), dried with anhydrous Na<sub>2</sub>SO<sub>4</sub> and the solvent was removed in vacuo (finally using a fine vacuum of 3·10<sup>-2</sup> mbar to remove DMF at 45°C) leaving a yellow oil. Pure tri-aldehyde **3** was isolated from this crude product by column chromatography (DCM, 477 g silica gel 60).

**Yield**

1.41 g of pale yellow crystals (16 % of theory)

**Analysis**

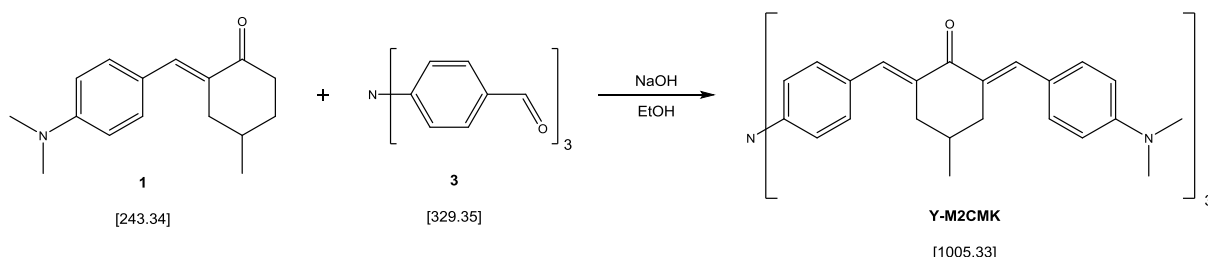
TLC:  $R_f = 0.20$  (DCM)

mp: 231- 232°C

$^1\text{H}$  NMR (200 MHz,  $\text{CDCl}_3$ )  $\delta$  (ppm) = 9.87 (3H, s,  $\text{H}-\text{C}=\text{O}$ ), 7.77 (6H, d,  $J = 8.6$  Hz, - ar- $\text{H}^{2,6}$ ), 7.18 (6H, d,  $J = 8.6$  Hz, -ar- $\text{H}^{3,5}$ )

$^{13}\text{C}$ -NMR (50 MHz,  $\text{CDCl}_3$ )  $\delta$  (ppm) = 190.4 (3C,  $-\text{C}=\text{O}$ ), 151.1 (3C, -ar- $\text{C}^4$ ), 132.5 (3C, -ar- $\text{C}^1$ ), 131.4 (6C, -ar- $\text{C}^{2,6}$ ), 124.5 (6C, -ar- $\text{C}^{3,5}$ )

**1.1.1.3. 2,2',2''-[Nitrilotris(4,1-phenylenemethyldiylne)]tris[6-[4-(dimethylamino)phenyl]methylene]-4-methylcyclohexanone (Y-M2CMK)<sup>56</sup>**



Reagents	MW [g/mol]	[mg]	[mL]	[mmol]	[eq.]
(2E)-2-[[4-(dimethylamino)-phenyl]methylene]-4-methylcyclohexanone ( <b>1</b> )	243.34	390		1.62	4.5
4,4',4''-nitrilotris(benzaldehyde) ( <b>3</b> )	329.35	118		0.36	1.0
NaOH	40.0	30		0.75	2.1
EtOH			22		

**Procedure**

All steps were performed in an orange light room. Ketone **1** (390 mg, 1.62 mmol, 4.5 eq.) and tri-aldehyde **3** (118 mg, 0.36 mmol, 1.0 eq.) were dissolved in hot EtOH (20 mL) and a solution of NaOH (30 mg, 0.75 mmol, 2.1 eq.) in EtOH (2 mL) was added. The mixture was held at reflux under magnetic stirring for 5 days, which lead to

precipitation of a dark orange solid. After cooling to room temperature this solid was filtered off, washed with EtOH and dried to yield 343 mg (95%) crude **Y-M2CMK**.

200 mg of the crude sample were purified by column chromatography (PE:DCM:MeOH:TEA = 50:46:3:1, 113 g silica gel 60) to yield a 51 mg (14%) sample with reasonable purity for analysis.

### Yield

343 mg of orange powder (95 % of theory, mixture of diastereomers of **Y-M2CMK** + CHO-containing impurity)

51 mg (14%) analytical sample (aldehyde content about 2%)

### Analysis

TLC:  $R_f = 0.35$  (PE:DCM:MeOH:TEA = 50:46:3:1)

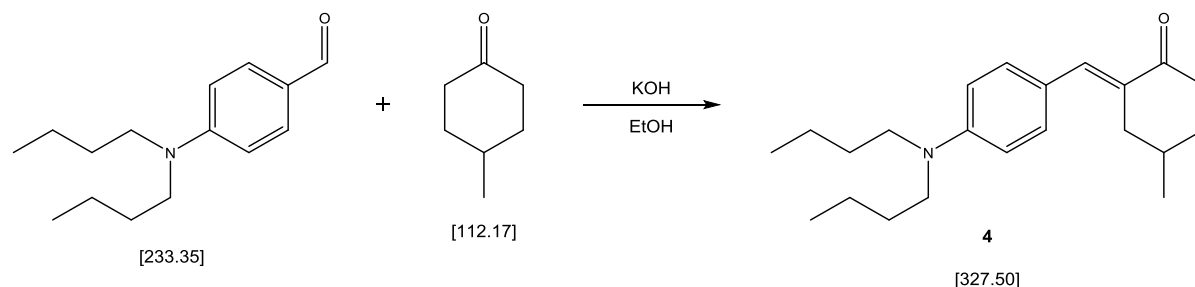
$R_f = 0.47$  (PE:DCM:MeOH:TEA = 38:56:4:2)

mp: still solid at 300°C, turns dark

$^1\text{H}$  NMR (200 MHz,  $\text{CDCl}_3$ )  $\delta$  (ppm) = 7.68 - 7.84 (6H, *m*, -C=CH), 7.31 - 7.55 (12H, *m*, -ar<sub>2</sub>-N-ar-H<sup>3,5</sup>; (CH<sub>3</sub>)<sub>2</sub>-N-ar-H<sup>3,5</sup>), 7.12 - 7.23 (6H, *m*), 6.74 (6H, *d*, *J* = 8.8 Hz, (CH<sub>3</sub>)<sub>2</sub>-N-ar-H<sup>2,6</sup>), 2.96 - 3.22 (24H, *m*, -CH<sub>2</sub>-C=CH; (CH<sub>3</sub>)<sub>2</sub>-N-ar-), 2.37 - 2.65 (6H, *m*, -CH<sub>2</sub>-C=CH), 1.91 (3H, *d*, *J* = 3.3 Hz, -CH-CH<sub>3</sub>), 1.13 (9H, *d*, *J* = 6.5 Hz, -CH-CH<sub>3</sub>)

$^{13}\text{C}$ -NMR (50 MHz,  $\text{CDCl}_3$ )  $\delta$  (ppm) = 189.7 (3C, -C=O), 150.3 (3C, (CH<sub>3</sub>)<sub>2</sub>-N-ar-C<sup>1</sup>), 146.8 (3C, ar<sub>2</sub>-N-ar-C<sup>1</sup>), 138.2 + 135.4, + 134.7 + 132.6 (12C, ar<sub>2</sub>-N-ar-CH=C-; (CH<sub>3</sub>)<sub>2</sub>-N-ar-CH=C-), 131.9 + 131.5 (12C, ar<sub>2</sub>-N-ar-C<sup>3,5</sup>; (CH<sub>3</sub>)<sub>2</sub>-N-ar-C<sup>3,5</sup>), 130.5 (3C, ar<sub>2</sub>-N-ar-C<sup>4</sup>), 125.2 + 123.9 (9C, ar<sub>2</sub>-N-ar-C<sup>2,6</sup>; (CH<sub>3</sub>)<sub>2</sub>-N-ar-C<sup>4</sup>), 111.6 (6C, (CH<sub>3</sub>)<sub>2</sub>-N-ar-C<sup>2,6</sup>), 40.1 (6C, (CH<sub>3</sub>)<sub>2</sub>-N-ar-), 36.9 + 36.7 (6C, -C=O-C-CH<sub>2</sub>-CH-CH<sub>2</sub>-C-), 29.4 (3C, -CH-CH<sub>3</sub>), 21.8 (3C, -CH-CH<sub>3</sub>)

### 1.2.1.1. (2E)-2-[[4-(Dibutylamino)phenyl]methylene]-4-methylcyclohexanone (**4**)



Reagents	MW [g/mol]	[g]	[mL]	[mmol]	[eq.]
4-(dibutylamino)benzaldehyde	233.35	2.79		12.0	1.0
4-methylcyclohexanone	112.17	2.68		23.9	2.0
KOH	56.11	0.335		0.60	0.5
EtOH			20		

#### Procedure

All steps were performed in an orange light room. To a solution of 4-(dibutylamino)benzaldehyde (2.79 g, 12.0 mmol, 1.0 eq.) and 4-methylcyclohexanone (2.68 g, 23.9 mmol, 2.0 eq.) in EtOH (20 mL) finely powdered KOH (335 mg, 0.60 mmol, 0.50 eq.) was added and the resulting solution was magnetically stirred at room temperature for 4 days.

The reaction mixture was diluted with deionized water (80 mL) and extracted with DCM (3 x 100 mL). The combined organic layers were subsequently washed with saturated NH<sub>4</sub>Cl-solution (50 mL) and deionized water (50 mL) and finally dried with anhydrous NaSO<sub>4</sub>.

Removal of the solvent and parts of 4-methylcyclohexanone in vacuo yielded an red oil which was first subjected to column chromatography (PE:EA = 10:1, 235 g silica gel 60) and the fractions containing the majority of mono-substituted product were stripped of solvent to yield an orange oil (1.6 g). This oil was subsequently separated by reversed phase column chromatography (MeCN:H<sub>2</sub>O = 95:5, Buechi Sepacore RP C18 Flash Cartridges 80 g + 4 g precolumn) and pure **4** was thus obtained.

#### Yield

471 mg of yellow crystals (12 % of theory)

**Analysis**

TLC:

$R_f = 0.35$  (PE:EA = 10:1),  
0.26 (RP18, MeCN:H<sub>2</sub>O = 95:5)

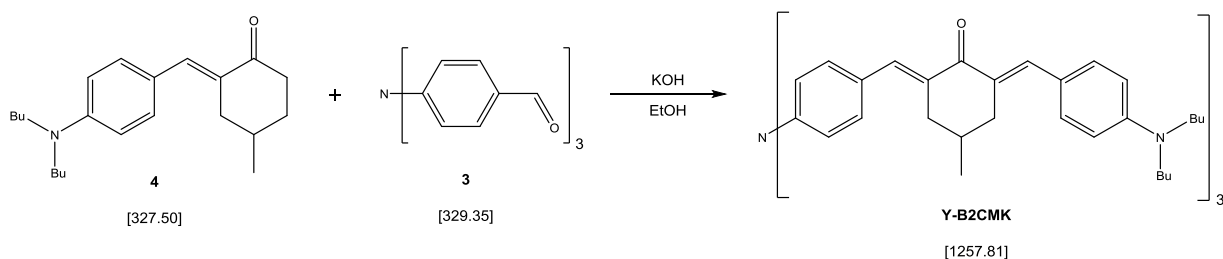
mp:

58 - 59 °C (DCM)

<sup>1</sup>H NMR (200 MHz, CDCl<sub>3</sub>)  $\delta$  (ppm) = 7.52 (1H, s, -C=CH), 7.39 (2H, d,  $J = 8.8$  Hz, -N-ar-H<sup>3,5</sup>), 6.64 (2H, d,  $J = 8.8$  Hz, -N-ar-H<sup>2,6</sup>), 3.31 (4H, t,  $J = 7.5$  Hz, -N(CH<sub>2</sub>-CH<sub>2</sub>-CH<sub>2</sub>-CH<sub>3</sub>)<sub>2</sub>), 3.08 (1H, m, -CH<sub>2</sub>-C=CH), 2.24 - 2.71 (3H, m, -CH<sub>2</sub>-C=CH; -CH<sub>2</sub>-C=O), 1.73 - 2.00 (2H, m, -CH<sub>2</sub>-CH; -CH-CH<sub>3</sub>), 1.48 - 1.73 (5H, m, -CH<sub>2</sub>-CH; -N(CH<sub>2</sub>-CH<sub>2</sub>-CH<sub>2</sub>-CH<sub>3</sub>)<sub>2</sub>), 1.37 (4H, m, -N(CH<sub>2</sub>-CH<sub>2</sub>-CH<sub>2</sub>-CH<sub>3</sub>)<sub>2</sub>), 1.10 (3H, d,  $J = 6.3$  Hz, -CH-CH<sub>3</sub>), 0.85 - 1.04 (6H, m, -N(CH<sub>2</sub>-CH<sub>2</sub>-CH<sub>2</sub>-CH<sub>3</sub>)<sub>2</sub>)

<sup>13</sup>C-NMR (50 MHz, CDCl<sub>3</sub>)  $\delta$  (ppm) = 200.9 (1C, -C=O), 148.4 (1C, -N-ar-C<sup>1</sup>), 137.4 (1C, -C=CH), 132.9 (2C, -N-ar-C<sup>3,5</sup>), 130.1 (1C, -C=CH), 122.4 (1C, -N-ar-C<sup>4</sup>), 110.9 (2C, -N-ar-C<sup>2,6</sup>), 50.6 (2C, -N(CH<sub>2</sub>-CH<sub>2</sub>-CH<sub>2</sub>-CH<sub>3</sub>)<sub>2</sub>), 38.9 + 37.6 + 31.1 (3C, -C=O-CH<sub>2</sub>-CH<sub>2</sub>-CH-CH<sub>2</sub>-C=CH), 30.1 (2C, -N(CH<sub>2</sub>-CH<sub>2</sub>-CH<sub>2</sub>-CH<sub>3</sub>)<sub>2</sub>), 29.3 (1C, -CH-CH<sub>3</sub>), 21.9 (1C, -CH-CH<sub>3</sub>), 20.2 (2C, -N(CH<sub>2</sub>-CH<sub>2</sub>-CH<sub>2</sub>-CH<sub>3</sub>)<sub>2</sub>), 13.9 (2C, -N(CH<sub>2</sub>-CH<sub>2</sub>-CH<sub>2</sub>-CH<sub>3</sub>)<sub>2</sub>)

**1.2.1.2. 2,2',2''-[Nitrilotris(4,1-phenylenemethylidene)]tris[6-[4-(dibutylamino)-phenyl]methylene]-4-methylcyclohexanone (Y-B2CMK)**



Reagents	MW [g/mol]	[mg]	[mL]	[μmol]	[eq.]
4,4',4''-nitrilotris(benzaldehyde) ( <b>3</b> )	329.35	50.3		153	1

(2 <i>E</i> )-2-[[4-(dibutylamino)phenyl]- methylene]-4- methylcyclohexanone ( <b>4</b> )	327.50	200	611	4
KOH	56.11	11.2	200	1.3
EtOH			10	

### Procedure

All steps were performed in an orange light room. Ketone **4** (200 mg, 611  $\mu$ mol, 4 eq.), tri-aldehyde **3** (50.3 mg, 153  $\mu$ mol, 1 eq.) and KOH (11.2 mg, 200  $\mu$ mol, 1.3 eq.) were dissolved in EtOH (10 mL). The mixture was magnetically stirred at 60°C for 120 h, which lead to precipitation of a red solid. After cooling to room temperature this solid was filtered off, washed with EtOH and dried to afford **Y-B2CMK** as a red solid.

### Yield

178 mg of amorphous red solid (93 % of theory)

### Analysis

TLC:  $R_f = 0.43$  (PE:EA = 4:1)

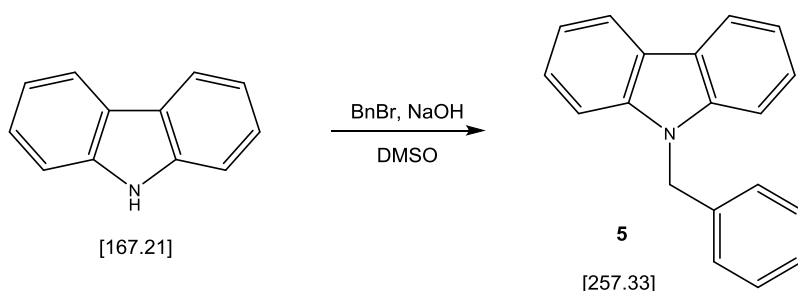
mp: amorphous, no sharp melting point

$^1\text{H}$  NMR (200 MHz,  $\text{CDCl}_3$ )  $\delta$  (ppm) = 7.79 (6H, *br. s.*, -C=CH), 7.33 - 7.55 (12H, *m*, -ar<sub>2</sub>-N-ar-H<sup>3,5</sup>; Bu<sub>2</sub>-N-ar-H<sup>3,5</sup>), 7.18 (6H, *d*,  $J = 8.4$  Hz, -ar<sub>2</sub>-N-ar-H<sup>2,6</sup>), 6.67 (6H, *d*,  $J = 8.8$  Hz, Bu<sub>2</sub>-N-ar-H<sup>2,6</sup>), 3.33 (12H, *t*,  $J = 7.3$  Hz, -N(CH<sub>2</sub>-CH<sub>2</sub>-CH<sub>2</sub>-CH<sub>3</sub>)<sub>2</sub>), 3.03 - 3.20 (6H, *m*, -CH<sub>2</sub>-C=CH), 2.42 - 2.65 (6H, *m*, -CH<sub>2</sub>-C=CH), 1.75 - 2.05 (3H, *m*, -CH-CH<sub>3</sub>), 1.50 - 1.75 (12H, *m*, -N(CH<sub>2</sub>-CH<sub>2</sub>-CH<sub>2</sub>-CH<sub>3</sub>)<sub>2</sub>), 1.22 - 1.50 (12H, *m*, -N(CH<sub>2</sub>-CH<sub>2</sub>-CH<sub>2</sub>-CH<sub>3</sub>)<sub>2</sub>), 1.14 (9H, *d*,  $J = 6.5$  Hz, -CH-CH<sub>3</sub>), 0.92 - 1.06 (18H, *m*, -N(CH<sub>2</sub>-CH<sub>2</sub>-CH<sub>2</sub>-CH<sub>3</sub>)<sub>2</sub>)

$^{13}\text{C}$ -NMR (50 MHz,  $\text{CDCl}_3$ )  $\delta$  (ppm) = 189.6 (3C, -C=O), 148.5 (3C, Bu<sub>2</sub>-N-ar-C<sup>1</sup>), 146.8 (3C, ar<sub>2</sub>-N-ar-C<sup>1</sup>), 138.4 + 135.3 + 134.8 + 133.0 (12C, ar<sub>2</sub>-N-ar-CH=C-; Bu<sub>2</sub>-N-ar-CH=C-), 131.8 + 131.5 (12C, ar<sub>2</sub>-N-ar-C<sup>3,5</sup>; Bu<sub>2</sub>-N-ar-C<sup>3,5</sup>), 130.4 (3C, ar<sub>2</sub>-N-ar-C<sup>4</sup>), 123.9 (3C, Bu<sub>2</sub>-N-ar-C<sup>4</sup>), 123.0 (6C, ar<sub>2</sub>-N-ar-C<sup>2,6</sup>), 111.1 (6C, Bu<sub>2</sub>-N-ar-C<sup>2,6</sup>), 50.7 (6C, -N(CH<sub>2</sub>-CH<sub>2</sub>-CH<sub>2</sub>-CH<sub>3</sub>)<sub>2</sub>),

37.0 + 36.7 (6C, -C=O-C-CH<sub>2</sub>-CH-CH<sub>2</sub>-C-), 29.5 (9C, -N(CH<sub>2</sub>-CH<sub>2</sub>-CH<sub>2</sub>-CH<sub>3</sub>)<sub>2</sub>; -CH-CH<sub>3</sub>), 21.9 (3C, -CH-CH<sub>3</sub>), 20.3 (6C, -N(CH<sub>2</sub>-CH<sub>2</sub>-CH<sub>2</sub>-CH<sub>3</sub>)<sub>2</sub>), 14.0 (6C, -N(CH<sub>2</sub>-CH<sub>2</sub>-CH<sub>2</sub>-CH<sub>3</sub>)<sub>2</sub>)

## 2.1.1.1.

9-(Phenylmethyl)-9*H*-carbazole (**5**)<sup>59</sup>

Reagents	MW [g/mol]	[g]	[mL]	[mmol]	[eq.]
9 <i>H</i> -carbazole	167.21	10.0		59.8	1.0
benzyl bromide	171.03	10.7		62.6	1.05
NaOH	40.00	2.6		65.0	1.09
DMSO			50		

## Procedure

A 100 mL three-neck round-bottom flask equipped with reflux condenser and dropping funnel was charged with 9*H*-carbazole (10.0 g, 59.8 mmol, 1.0 eq.), NaOH (2.6 g, 65 mmol, 1.09 eq.) and DMSO (50 mL), purged with argon and heated to 60°C under magnetic stirring for 1 h, leading to dissolution of most of the NaOH and a color change to dark brown. Benzyl bromide (10.7 g, 62.6 mmol, 1.05 eq.) was added dropwise via the dropping funnel during 1 h and then the reaction mixture was stirred at 60°C for 20 h. Hydrolysis with deionized water (300 mL) led to formation of a brownish precipitate, which was recrystallized twice from EtOH to yield **5**.

## Yield

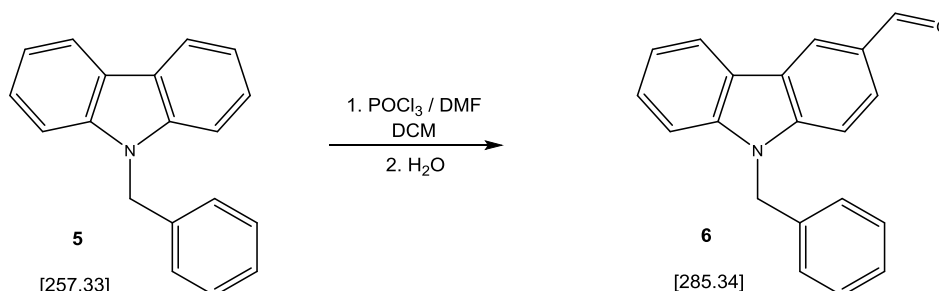
11.1 g of off-white fluffy needles (72% of theory)

**Analysis**TLC:  $R_f = 0.65$  (PE:EA = 15:1)

mp: 121 - 122°C

$^1\text{H}$  NMR (200 MHz,  $\text{CDCl}_3$ )  $\delta$  (ppm) = 8.16 (2H, *d*,  $J = 7.6$  Hz, -cbz-H<sub>4,5</sub>), 7.02 - 7.54 (11H, *m*, -cbz-H<sub>1,2,3,6,7,8</sub>; -ph-H<sub>2-6</sub>), 5.52 (2H, *s*, -N-CH<sub>2</sub>-ph)

$^{13}\text{C}$ -NMR (50 MHz,  $\text{CDCl}_3$ )  $\delta$  (ppm) = 140.7 (2C, cbz-C<sup>8a,9a</sup>), 137.3 (1C, -N-CH<sub>2</sub>-ph-C<sup>1</sup>), 128.8 (2C, -N-CH<sub>2</sub>-ph-C<sup>3,5</sup>), 127.5 (1C, -N-CH<sub>2</sub>-ph-C<sup>4</sup>), 126.5 (2C, -N-CH<sub>2</sub>-ph-C<sup>2,6</sup>), 125.9 + 120.5 (4C, cbz-C<sup>2,4,5,7</sup>), 123.1 (2C, cbz-C<sup>4a,4b</sup>), 119.3 (2C, cbz-C<sup>3,6</sup>), 109.0 (2C, cbz-C<sup>1,8</sup>), 46.6 (1C, -N-CH<sub>2</sub>-ph)

**2.1.1.2. 9-(Phenylmethyl)-9*H*-carbazole-3-carboxaldehyde (6)<sup>62</sup>**

Reagents	MW [g/mol]	[g]	[mL]	[mmol]	[eq.]
9-(phenylmethyl)-9 <i>H</i> -carbazole ( <b>5</b> )	257.33	8.23		32	1
DMF	73.09		70	900	28.0
$\text{POCl}_3$	153.33		50	520	16.3
DCM			30		

**Procedure**

Dry DMF (70 mL, 900 mmol, 28.0 eq.) was filled into 500 mL three-neck round-bottom flask equipped with reflux condenser, mechanical stirrer and dropping funnel. The apparatus was purged with argon and  $\text{POCl}_3$  (50 mL, 520 mmol, 16.3 eq.) was added dropwise over a period of 1 h under stirring and cooling to -5°C with an NaCl/ice bath, leading to formation of a white, thick crystal mass. After stirring the mixture for 30 min at



room temperature, 9-(phenylmethyl)-9*H*-carbazole (**5**) (8.23 g, 32 mmol, 1.0 eq.) dissolved in dry DCM (30 mL) was added dropwise during 1 h, leading to a brown suspension which was then heated to 90°C and held at this temperature for 48 h.

For the workup the reaction mixture was poured onto ice/deionized water-mixture (700 mL). After stirring for 30 min a solution of NaOH (80 g) in deionized water (300 mL) was added dropwise. The alkalized solution was extracted with DCM (3 x 500 mL), the combined organic layers were subsequently washed with saturated NH<sub>4</sub>Cl-solution (300 mL) and deionized water (500 mL) and finally dried over anhydrous NaSO<sub>4</sub>. The solvents were removed in vacuo (finally using a fine vacuum of  $\sim 2 \cdot 10^{-2}$  mbar to remove most of the residual DMF at 45°C), the brownish residue thus obtained was separated by column chromatography (PE:EA, 18-100% EA gradient, 477 g silica gel 60). Elution at about 25% EA provided reasonably pure mono-aldehyde **6** and then pure EA was used to wash out the residual product consisting mainly of di-aldehyde **7**.

### Yield

4.76 g of white crystal needles (51% of theory)

### Analysis

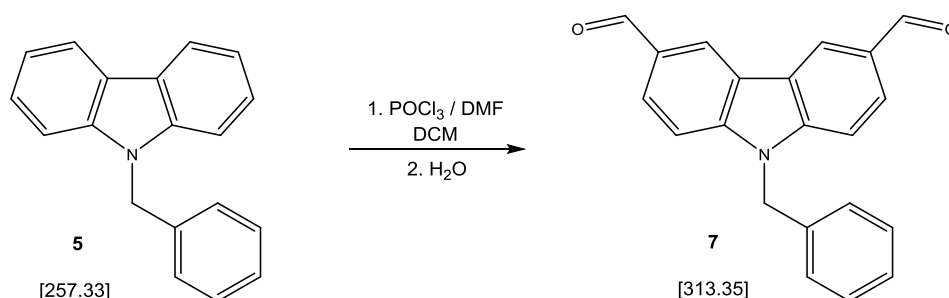
TLC:  $R_f = 0.56$  (PE:EA = 3:1)

mp: 136 - 138°C

<sup>1</sup>H NMR (200 MHz, CDCl<sub>3</sub>)  $\delta$  (ppm) = 10.11 (1H, s, H-C=O), 8.65 (1H, d,  $J = 1.0$  Hz, -cbz-H<sup>4</sup>), 8.20 (1H, d,  $J = 8.0$  Hz, -cbz-H<sup>1</sup>), 7.98 (1H, dd,  $J = 1.0$  and  $8.0$  Hz, -cbz-H<sup>2</sup>), 6.99 - 7.57 (9H, m, -cbz-H<sup>5-8</sup>; -ph-H<sup>2-6</sup>), 5.55 (2H, s, -N-CH<sub>2</sub>-ph)

<sup>13</sup>C-NMR (50 MHz, CDCl<sub>3</sub>)  $\delta$  (ppm) = 191.7 (1C, -C=O), 144.2 (1C, cbz-C<sup>3</sup>), 141.4 (1C, cbz-C<sup>8a</sup>), 136.2 (1C, -N-CH<sub>2</sub>-ph-C<sup>1</sup>), 129.0 (2C, -N-CH<sub>2</sub>-ph-C<sup>3,5</sup>), 128.9 (1C, cbz-C<sup>9a</sup>), 126.4 (2C, -N-CH<sub>2</sub>-ph-C<sup>2,6</sup>), 127.8 + 127.5 + 127.0 + 123.8 + 123.3 + 123.1 + 120.8 + 120.7 (8C, cbz-C<sup>1,4,4a,4b,5,6,7</sup>; -N-CH<sub>2</sub>-ph-C<sup>4</sup>), 109.7 + 109.2 (2C, cbz-C<sup>2,8</sup>), 46.8 (1C, -N-CH<sub>2</sub>-ph)

### 2.1.1.2. 9-(Phenylmethyl)-9*H*-carbazole-3,6-dicarboxaldehyde (**7**)<sup>62</sup>



Reagents	MW [g/mol]	[g]	[mL]	[mmol]	[eq.]
9-(phenylmethyl)-9 <i>H</i> -carbazole ( <b>5</b> )	257.33	8.23		32	1
DMF	73.09		70	900	28.0
POCl <sub>3</sub>	153.33		50	520	16.3
DCM		30			

#### Procedure

The residual crude product (3.83 g) used to isolate di-aldehyde **7** was obtained by final elution with pure EA in the column chromatography of the same reaction mixture used to produce mono-aldehyde **6**. The brown residue was therefore subjected to Kugelrohr distillation using a fine vacuum of  $3 \cdot 10^{-2}$  to  $1 \cdot 10^{-1}$  mbar and an oven temperature of 225-245°C. Pure dialdehyde **7** crystallized as dense white flakes.

#### Yield

3.20 g of white crystalline flakes (32% of theory)

#### Analysis

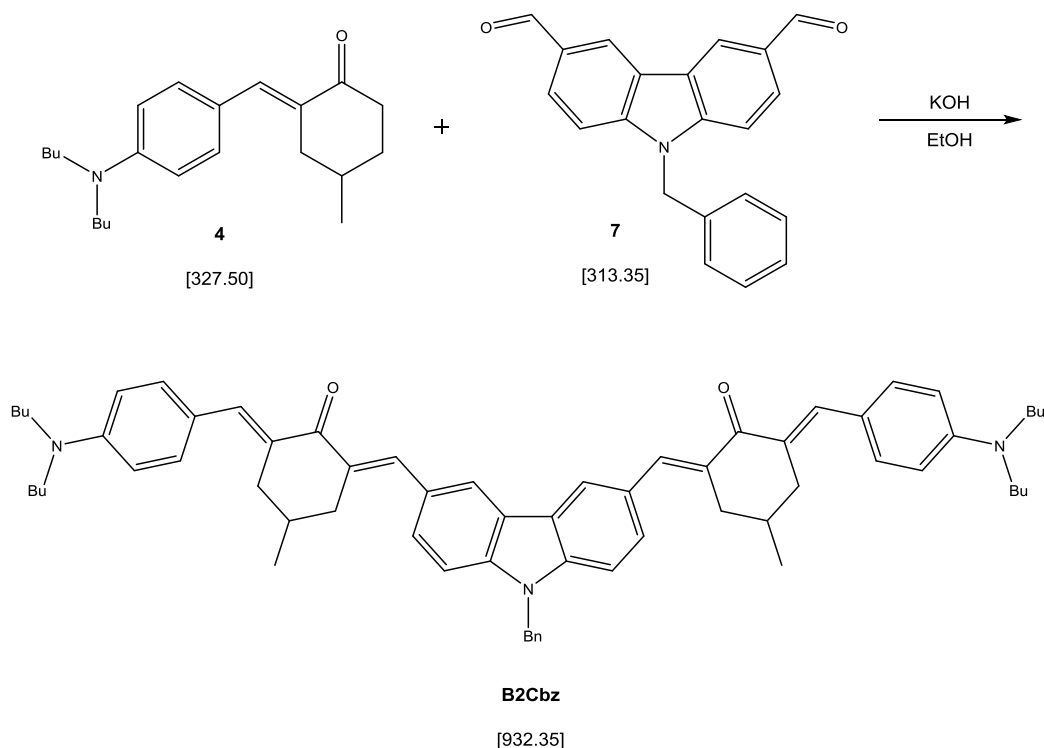
TLC:  $R_f = 0.29$  (PE:EA = 3:1)

mp: 230 - 231°C

<sup>1</sup>H NMR (200 MHz, DMSO-*d*<sub>6</sub>)  $\delta$  (ppm) = 10.15 (2H, s, H-C=O), 8.71 (2H, *d*,  $J = 1.6$  Hz, -cbz-H<sup>4,5</sup>), 8.06 (2H, *dd*,  $J = 1.5$  and 8.5 Hz, -cbz-H<sup>2,7</sup>), 7.54 (2H, *d*,  $J = 8.6$  Hz, -cbz-H<sup>1,8</sup>), 7.05 - 7.41 (5H, *m*, -ph-H<sup>2-6</sup>), 5.62 (2H, s, -N-CH<sub>2</sub>-ph)

$^{13}\text{C}$ -NMR (50 MHz, DMSO- $d_6$ )  $\delta$  (ppm) = 191.9 (2C, -C=O), 144.5 (2C, cbz-C $^{3,6}$ ), 136.6 (1C, -N-CH $_2$ -ph-C $^1$ ), 129.5 + 128.7 + 127.6 + 126.7 + 122.6 (12C, cbz-C $^{1,4,4a,4b,5,8,8a,9a}$ , -N-CH $_2$ -ph-C $^{2,6}$ , -N-CH $_2$ -ph-C $^{3,5}$ ), 124.4 (1C, -N-CH $_2$ -ph-C $^4$ ), 110.9 (2C, cbz-C $^{2,7}$ ), 46.1 (1C, -N-CH $_2$ -ph)

**2.1.1.3. (2*E*,6*E*,6'*E*)-6,6'-[[9-(Phenylmethyl)-9*H*-carbazole-3,6-diyl]dimethylidyne]bis[2-[[4-(dibutylamino)phenyl]methylene]]-4-methylcyclohexanone (B2Cbz)**



Reagents	MW [g/mol]	[mg]	[mL]	[ $\mu\text{mol}$ ]	[eq.]
9-(phenylmethyl)-9 <i>H</i> -carbazole-3,6-dicarboxaldehyde ( <b>7</b> )	313.35	55.8		178	1
(2 <i>E</i> )-2-[[4-(dibutylamino)phenyl]methylene]-4-methylcyclohexanone ( <b>4</b> )	327.50	175		534	3
KOH	56.11	12.0		214	1.2

EtOH

10

### Procedure

All steps were performed in an orange light room. Ketone **4** (200 mg, 611  $\mu$ mol, 4 eq.), di-aldehyde **7** (50.3 mg, 153  $\mu$ mol, 1 eq.) and KOH (11.2 mg, 200  $\mu$ mol, 1.3 eq.) were dissolved in EtOH (10 mL). The mixture was magnetically stirred at 60°C for 120 h, which lead to precipitation of a dark orange solid. After cooling to room temperature this solid was filtered off, washed with EtOH and dried to afford **B2Cbz** as an orange solid.

### Yield

105 mg of orange solid **B2Cbz** (63 % of theory)

### Analysis

TLC:  $R_f = 0.32$  (PE:EA = 4:1)

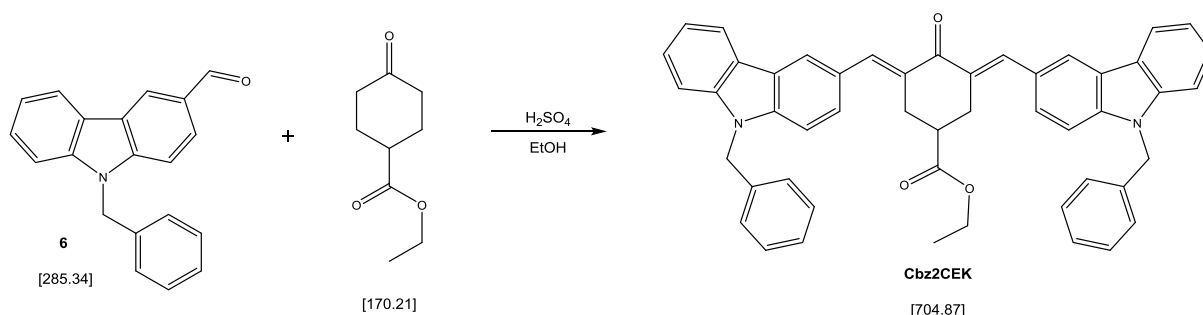
mp: decomposition (turns dark) ~ 200 °C before melting

$^1\text{H}$  NMR (200 MHz,  $\text{CDCl}_3$ )  $\delta$  (ppm) = 8.29 (2H, s, -cbz- $\text{H}^{4,5}$ ), 8.04 (2H, s, -C=CH-cbz), 7.81 (2H, s, -C=CH-ar-N-Bu<sub>2</sub>), 7.61 (2H, d,  $J = 8.6$  Hz, -cbz- $\text{H}^{1,8}$ ), 7.47 (4H, d,  $J = 8.8$  Hz, Bu<sub>2</sub>-N-ar- $\text{H}^{3,5}$ ), 7.40 (2H, d,  $J = 8.6$  Hz, -cbz- $\text{H}^{2,7}$ ), 7.14 - 7.33 (5H, m, -ph- $\text{H}^{2,6}$ ), 6.67 (4H, d,  $J = 8.8$  Hz, Bu<sub>2</sub>-N-ar- $\text{H}^{2,6}$ ), 5.55 (2H, s, -N-CH<sub>2</sub>-ph), 3.08 - 3.40 (12H, m, -N(CH<sub>2</sub>-CH<sub>2</sub>-CH<sub>2</sub>-CH<sub>3</sub>)<sub>2</sub>; -CH<sub>2</sub>-C=CH), 2.47 - 2.73 (4H, m, -CH<sub>2</sub>-C=CH), 1.81 - 2.06 (2H, m, -CH-CH<sub>3</sub>), 1.49 - 1.71 (8H, m, -N(CH<sub>2</sub>-CH<sub>2</sub>-CH<sub>2</sub>-CH<sub>3</sub>)<sub>2</sub>), 1.39 (8H, dd,  $J = 7.2$  and  $14.9$  Hz, -N(CH<sub>2</sub>-CH<sub>2</sub>-CH<sub>2</sub>-CH<sub>3</sub>)<sub>2</sub>), 1.15 (6H, d,  $J = 6.5$  Hz, -CH-CH<sub>3</sub>), 0.89 - 1.06 (12H, t,  $J = 7.2$  Hz, -N(CH<sub>2</sub>-CH<sub>2</sub>-CH<sub>2</sub>-CH<sub>3</sub>)<sub>2</sub>)

$^{13}\text{C}$ -NMR (50 MHz,  $\text{CDCl}_3$ )  $\delta$  (ppm) = 189.7 (2C, -C=O), 148.5 (2C, Bu<sub>2</sub>-N-ar-C<sup>1</sup>), 136.6 (1C, -N-CH<sub>2</sub>-ph-C<sup>1</sup>), 140.9 + 138.2 + 137.0 + 134.0 + 133.9 + 133.0 + 130.6 (14C, cbz-CH=C-; Bu<sub>2</sub>-N-ar-CH=C-; cbz-C<sup>3,4a,4b,6,8a,9a</sup>), 129.2 + 128.9 + 128.2 (8C, Bu<sub>2</sub>-N-ar-C<sup>3,5</sup>; -N-CH<sub>2</sub>-ph-C<sup>2,3,5,6</sup>), 127.7 + 126.5 + 123.1 + 122.9 (7C, cbz-C<sup>1,2,7,8</sup>; -N-CH<sub>2</sub>-ph-C<sup>4</sup>; Bu<sub>2</sub>-N-ar-C<sup>4</sup>), 111.1 (4C, Bu<sub>2</sub>-N-ar-C<sup>2,6</sup>), 109.1 (2C, cbz-C<sup>4,5</sup>), 50.7 (4C, -N(CH<sub>2</sub>-CH<sub>2</sub>-CH<sub>2</sub>-CH<sub>3</sub>)<sub>2</sub>), 46.8 (1C, -N-CH<sub>2</sub>-ph), 37.1 + 36.8 (4C, -

C=O-C-CH<sub>2</sub>-CH-CH<sub>2</sub>-C-), 29.7 (2C, -CH-CH<sub>3</sub>), 29.5 (4C, -N(CH<sub>2</sub>-CH<sub>2</sub>-CH<sub>2</sub>-CH<sub>3</sub>)<sub>2</sub>), 21.9 (2C, -CH-CH<sub>3</sub>), 20.4 (4C, -N(CH<sub>2</sub>-CH<sub>2</sub>-CH<sub>2</sub>-CH<sub>3</sub>)<sub>2</sub>), 14.0 (4C, -N(CH<sub>2</sub>-CH<sub>2</sub>-CH<sub>2</sub>-CH<sub>3</sub>)<sub>2</sub>)

### 2.2.1. (3*E*,5*E*)-4-Oxo-3,5-bis[[9-(phenylmethyl)-9*H*-carbazol-3-yl]methylene]-cyclohexanecarboxylic acid ethyl ester (Cbz2CEK)



Reagents	MW [g/mol]	[mg]	[mL]	[μmol]	[eq.]
9-(phenylmethyl)-9 <i>H</i> -carbazole-3-carboxaldehyde ( <b>6</b> )	285.34	285		1000	2.1
ethyl 4-oxocyclohexanecarboxylate	170.21	81		476	1
H <sub>2</sub> SO <sub>4</sub>		35		357	0.75
dry EtOH			15		

### Procedure

All steps were performed in an orange light room. Ethyl 4-oxocyclohexanecarboxylate (81 mg, 476 μmol, 1 eq.), mono-aldehyde **6** (285 mg, 1000 μmol, 2.1 eq.) and H<sub>2</sub>SO<sub>4</sub> (35 mg, 357 μmol, 0.75 eq.) were dissolved in dry EtOH (15 mL). The mixture was magnetically stirred at 60°C for 48 h which lead to a color change of the solution to olive green. After cooling down to room temperature, the reaction mixture was diluted with deionized water (85 mL) and extracted with DCM (3 x 75 mL). The combined organic layers were subsequently washed with 1N NaOH-solution (50 ml) and deionized water (100 mL) and finally dried with anhydrous NaSO<sub>4</sub>. The solvent was evaporated in vacuo, leaving an orange residue which was first subjected to column chromatography (PE:EA = 4:1, 113 g silica gel 60). The fractions containing the majority of the desired product were stripped of solvent to yield an orange residue (320 mg). This residue was

subsequently separated by reversed phase column chromatography (MeCN, Buechi Sepacore RP C18 Flash Cartridges 80 g + 4 g precolumn) and pure **Cbz2CEK** was thus obtained.

### Yield

121 mg of deep yellow solid (36 % of theory)

### Analysis

TLC:  $R_f = 0.13$  (PE:EA = 4:1)

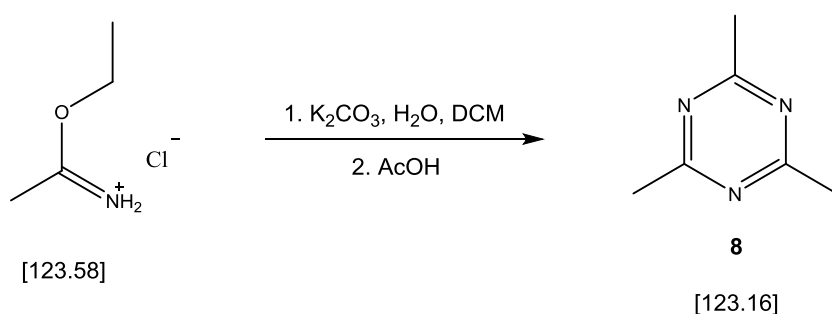
0.37 (RP18, MeCN)

mp: decomposition (turns dark) ~ 160 °C before melting

$^1\text{H}$  NMR (200 MHz,  $\text{CDCl}_3$ )  $\delta$  (ppm) = 8.38 (2H, s, -cbz-H<sup>4</sup>), 8.23 - 8.34 (4H, m, -cbz-H<sup>5</sup>; -C=CH-cbz), 7.71 (2H, d,  $J = 8.2$  Hz, -cbz-H<sup>8</sup>), 7.17 - 7.65 (18H, m, -cbz-H<sup>1,2,6,7</sup>, -ph-H<sup>2-6</sup>), 5.56 (4H, s, -N-CH<sub>2</sub>-ph), 4.28 (2H, q,  $J = 7.2$  Hz, O=C-O-CH<sub>2</sub>-CH<sub>3</sub>), 3.48 - 3.68 (2H, m, -CH<sub>2</sub>-C=CH), 3.16 - 3.43 (2H, m, -CH<sub>2</sub>-C=CH), 2.78 - 3.02 (1H, m, -CH-COO-), 1.33 (3H, t,  $J = 7.2$  Hz, O=C-O-CH<sub>2</sub>-CH<sub>3</sub>)

$^{13}\text{C}$ -NMR (50 MHz,  $\text{CDCl}_3$ )  $\delta$  (ppm) = 188.5 (1C, -C=O), 174.5 (1C, O=C-O-), 141.1 + 140.8 + 139.5 + 136.8 + 131.2 + 129.1 (12C, cbz-CH=C; cbz-C<sup>3,8a,9a</sup>; -N-CH<sub>2</sub>-ph-C<sup>1</sup>), 128.9 + 127.7 + 127.1 (12C, cbz-C<sup>1,4a</sup>; -N-CH<sub>2</sub>-ph-C<sup>2,3,5,6</sup>), 126.5 + 123.3 + 123.2 + 123.0 (8C, cbz-C<sup>4b,5,7</sup>; -N-CH<sub>2</sub>-ph-C<sup>4</sup>), 120.6 + 119.9 (4C, cbz-C<sup>2,6</sup>), 109.3 + 109.0 (4C, cbz-C<sup>4,8</sup>), 60.8 (1C, O=C-O-CH<sub>2</sub>-CH<sub>3</sub>), 46.7 (2C, -N-CH<sub>2</sub>-ph), 40.2 (1C, -CH<sub>2</sub>-CH-CH<sub>2</sub>-), 31.1 (2C, -CH<sub>2</sub>-CH-CH<sub>2</sub>-), 14.2 (1C, O=C-O-CH<sub>2</sub>-CH<sub>3</sub>)

## 3.1.1.

2,4,6-Trimethyl-1,3,5-triazine (8)<sup>66</sup>

Reagents	MW [g/mol]	[g]	[mL]	[mmol]	[eq.]
ethyl acetimidate, hydrochloride	123.58	44.5		360	1
K <sub>2</sub> CO <sub>3</sub>	138.21	52.2		378	1.05
DCM			115		
deionized water			180		
AcOH	60.05	1.14		19	see text

**Procedure**

Ethyl acetimidate hydrochloride (44.5 g, 360 mmol, 1 eq.) was added to a vigorously stirred emulsion of DCM (65 mL) and a solution of K<sub>2</sub>CO<sub>3</sub> (52.2 g, 378 mmol, 1.05 eq.) in deionized water (180 mL). The organic phase was collected after 10 min of stirring, and the aqueous phase was re-extracted by stirring with DCM (50 mL) for 30 min. The combined organic layers were dried over anhydrous K<sub>2</sub>CO<sub>3</sub> overnight at 4°C under argon atmosphere. The dry solution was then concentrated by rapid distillation using a Vigreux column until the boiling point could no longer be held below 60°C at a useful distillation rate. The concentration of the residue (27.9 g) was determined to be 83% ethyl acetimidate freebase by titration against 1 N HCl using methyl orange as indicator, resulting in a yield of 74% pure freebase.

The rest of the ethyl acetimidate freebase solution (25 g, 83% in DCM, 238 mmol, 1 eq.) was mixed with 8 mol % AcOH (1.14 g, 19 mmol, 0.08 eq.) by adding AcOH dropwise over a period of 30 min. The solution was stirred in a water bath so that the temperature was kept at 25-30°C for the whole time of the addition plus 1 h of additional reaction time. The mixture was then allowed to stand for 16 h at room temperature. The majority of the formed EtOH was carefully removed using a rotary evaporator, the residue diluted

with DCM (30 mL), solid precipitate filtered off and discarded and the organic phase shaken with solid  $K_2CO_3$  and a minimal amount of deionized water. The organic phase was separated and dried with anhydrous  $CaCl_2$ . The product was obtained by distillation over a Vigreux column at atmospheric pressure, keeping the water in the Liebig condenser at about 50-70°C using a hot air gun, so that the product didn't solidify prematurely.

### Yield

7.35 g of colorless crystals (50 % of theory, relative to ethyl acetimidate hydrochloride)

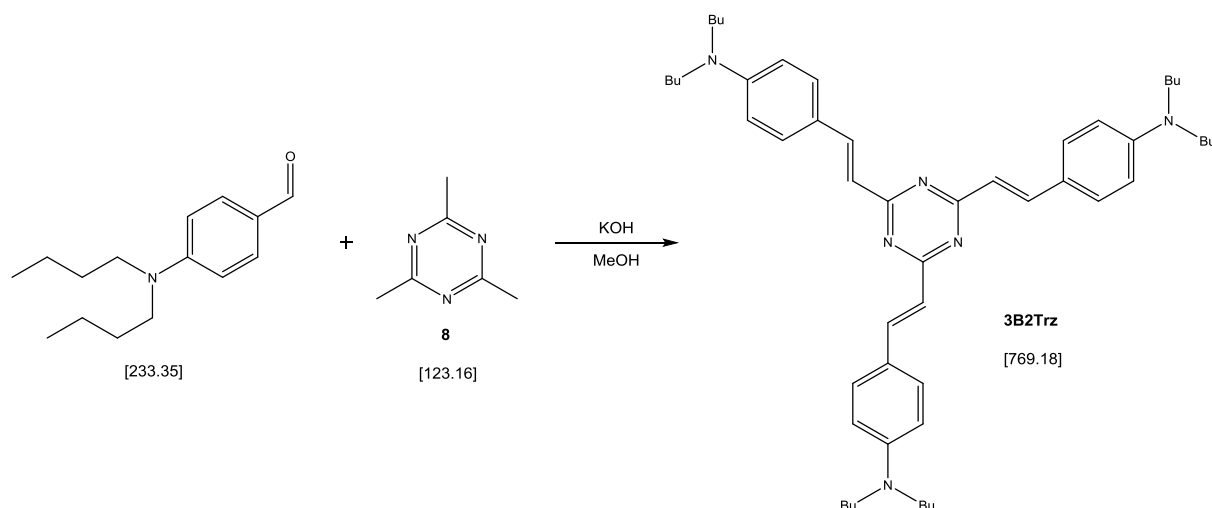
### Analysis

mp: 54 - 56°C

$^1H$  NMR (200 MHz,  $CDCl_3$ )  $\delta$  (ppm) = 2.46 (9H, s,  $CH_3$ -trz)

$^{13}C$ -NMR (50 MHz,  $CDCl_3$ )  $\delta$  (ppm) = 175.8 (3C, trz- $C^{1,3,5}$ ), 25.3 (3C,  $CH_3$ -trz)

### 3.1.2. 4,4',4''-[1,3,5-Triazine-2,4,6-triyltri-(1E)-2,1-ethenediyl]tris[N,N-dibutylbenzenamine] (3B2Trz)



Reagents	MW [g/mol]	[mg]	[mL]	[mmol]	[eq.]
4-(dibutylamino)benzaldehyde	233.35	855		3.66	2.7
2,4,6-trimethyl-1,3,5-triazine ( <b>8</b> )	123.16	168		1.36	1.0
KOH 20% in MeOH			9		



MeOH

9

### Procedure

All steps were performed in an orange light room. To 2,4,6-trimethyl-1,3,5-triazine (**8**) (168 mg, 1.36 mmol, 1.0 eq.) dissolved in a 20% w/w solution of KOH in MeOH (9 mL), a solution of 4-(dibutylamino)benzaldehyde (855 mg, 3.66 mmol, 2.7 eq.) in MeOH (9 mL) was added. The flask was purged with argon and the reaction mixture magnetically stirred for 120 h at 60°C. In the course of the reaction, the whole mixture turned dark red and an oily second phase separated at the bottom.

After cooling to room temperature, the reaction mixture was dissolved in DCM (150 mL), washed with saturated NH<sub>4</sub>Cl-solution (3 x 50 mL) and deionized water (100 mL). The organic phase was dried with Na<sub>2</sub>SO<sub>4</sub> and the solvent removed in vacuo to yield ~820 mg of a brownish residue. The mixture was separated via column chromatography (Toluene with 5-30% Et<sub>2</sub>O, 235 g silica gel 60, detection  $\lambda$  = 295 nm). **3B2Trz** eluted as first major peak from the column using 5% Et<sub>2</sub>O. The pure product was obtained by removal of the solvents and drying in vacuo at 40°C.

### Yield

223 mg of dark red solid **3B2Trz** (21% of theory)

### Analysis

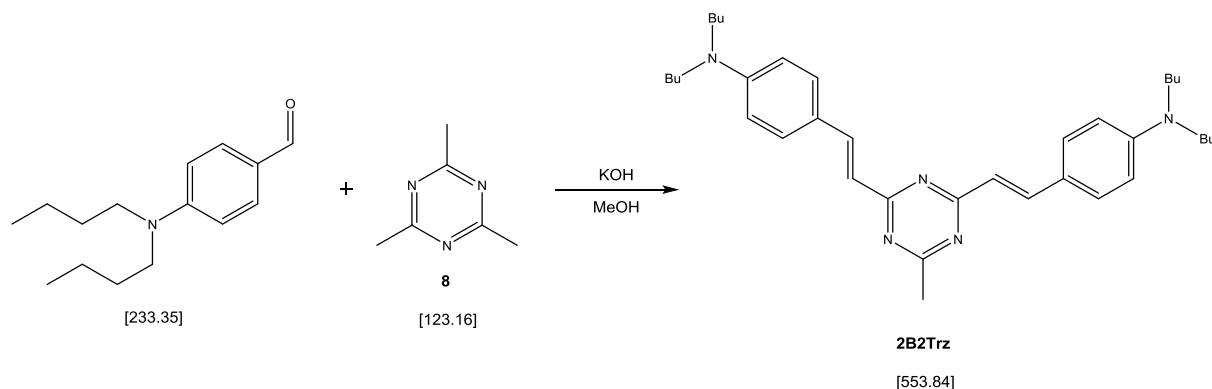
TLC:  $R_f$  = 0.56 (Tol/Et<sub>2</sub>O 20:1); 0.95 (Tol/Et<sub>2</sub>O 5:1)

mp: 88 - 90°C (DCM)

<sup>1</sup>H NMR (200 MHz, CDCl<sub>3</sub>)  $\delta$  (ppm) = 8.20 (3H, *d*, *J*=15.65 Hz, -CH=CH-*ar*), 7.57 (6H, *d*, *J*=8.80 Hz, Bu<sub>2</sub>-N-*ar*-H<sup>2,6</sup>), 6.93 (3H, *d*, *J*=15.65 Hz, -CH=CH-*ar*), 6.66 (6H, *d*, *J*=8.80 Hz, Bu<sub>2</sub>-N-*ar*-H<sup>3,5</sup>), 3.34 (12H, *t*, *J*=7.34 Hz, -N(CH<sub>2</sub>-CH<sub>2</sub>-CH<sub>2</sub>-CH<sub>3</sub>)<sub>2</sub>), 1.54 - 1.68 (12H, *m*, -N(CH<sub>2</sub>-CH<sub>2</sub>-CH<sub>2</sub>-CH<sub>3</sub>)<sub>2</sub>), 1.17 - 1.39 (12H, *m*, -N(CH<sub>2</sub>-CH<sub>2</sub>-CH<sub>2</sub>-CH<sub>3</sub>)<sub>2</sub>), 0.99 (18H, *t*, -N(CH<sub>2</sub>-CH<sub>2</sub>-CH<sub>2</sub>-CH<sub>3</sub>)<sub>2</sub>)

<sup>13</sup>C-NMR (50 MHz, CDCl<sub>3</sub>)  $\delta$  (ppm) = 171.12 (3C, trz-C<sup>2,4,6</sup>), 149.31 (3C, Bu<sub>2</sub>-N-*ar*-C<sup>4</sup>), 141.52 (3C, -CH=CH-*ar*), 129.96 (3C, Bu<sub>2</sub>-N-*ar*-C<sup>1</sup>), 122.69 (6C, Bu<sub>2</sub>-N-*ar*-C<sup>2,6</sup>), 120.58 (3C, -CH=CH-*ar*), 111.29 (6C, Bu<sub>2</sub>-N-*ar*-C<sup>3,5</sup>), 50.74 (6C, -N(CH<sub>2</sub>-CH<sub>2</sub>-CH<sub>2</sub>-CH<sub>3</sub>)<sub>2</sub>), 29.42

**3.1.2. 4,4'-[(6-Methyl-1,3,5-triazine-2,4-diyl)di-(1*E*)-2,1-ethenediyl]bis[*N,N*-dibutylbenzenamine] (2B2Trz)**



Reagents	MW [g/mol]	[mg]	[mL]	[mmol]	[eq.]
4-(dibutylamino)benzaldehyde	233.35	855		3.66	2.7
2,4,6-trimethyl-1,3,5-triazine ( <b>8</b> )	123.16	168		1.36	1.0
KOH 20% in MeOH			9		
MeOH			9		

**2B2Trz** was obtained from the reaction mixture from the synthesis of **3B2Trz** by separation via column chromatography (Toluene with 5-30% Et<sub>2</sub>O, 235 g silica gel 60, detection  $\lambda$  = 295 nm). **2B2Trz** eluted after residual 4-(dibutylamino)benzaldehyde from the column using 15% Et<sub>2</sub>O. The pure product was then obtained by removal of the solvents and drying in vacuo at 60°C.

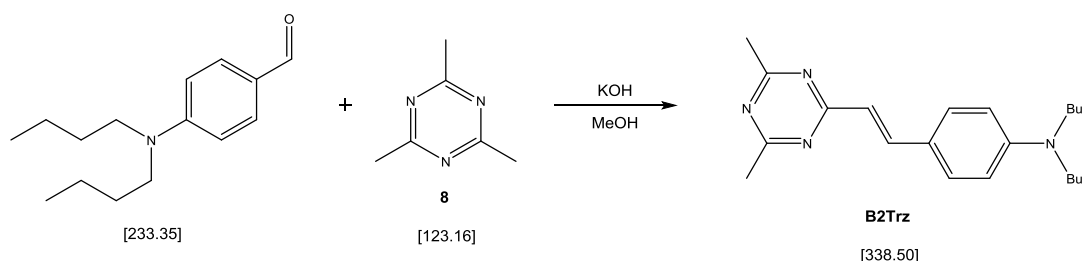
457 mg of dark orange, sticky resin **2B2Trz** (61% of theory)

TLC:  $R_f = 0.57$  (Tol/Et<sub>2</sub>O 5:1)

$^1\text{H}$  NMR (200 MHz,  $\text{CDCl}_3$ )  $\delta$  (ppm) = 8.16 (2H, *d*,  $J=15.80$  Hz,  $-\text{CH}=\text{CH}-\text{ar}$ ), 7.53 (4H, *d*,  $J=8.80$  Hz,  $\text{Bu}_2\text{-N-ar-H}^{2,6}$ ), 6.86 (2H, *d*,  $J=15.65$  Hz,  $-\text{CH}=\text{CH}-\text{ar}$ ), 6.64 (4H, *d*,  $J=9.00$  Hz,  $\text{Bu}_2\text{-N-ar-H}^{3,5}$ ), 3.32 (8H, *t*,  $J=7.50$  Hz,  $-\text{N}(\text{CH}_2\text{-CH}_2\text{-CH}_2\text{-CH}_3)_2$ ), 2.63 (3H, *s*,  $\text{trz-CH}_3$ ), 1.50 - 1.71 (8H, *m*,  $-\text{N}(\text{CH}_2\text{-CH}_2\text{-CH}_2\text{-CH}_3)_2$ ), 1.25 - 1.50 (8H, *m*,  $-\text{CH}_2\text{-CH}_3$ ), 0.98 (12H, *t*,  $J=7.20$  Hz,  $-\text{N}(\text{CH}_2\text{-CH}_2\text{-CH}_2\text{-CH}_3)_2$ )

$^{13}\text{C}$ -NMR (50 MHz,  $\text{CDCl}_3$ )  $\delta$  (ppm) = 175.15 (1C,  $\text{trz-C}^6$ ), 171.43 (2C,  $\text{trz-C}^{2,4}$ ), 149.40 (2C,  $\text{Bu}_2\text{-N-ar-C}^4$ ), 142.02 (2C,  $-\text{CH}=\text{CH}-\text{ar}$ ), 129.99 (2C,  $\text{Bu}_2\text{-N-ar-C}^1$ ), 122.43 (4C,  $\text{Bu}_2\text{-N-ar-C}^{2,6}$ ), 120.08 (2C,  $-\text{CH}=\text{CH}-\text{ar}$ ), 111.28 (4C,  $\text{Bu}_2\text{-N-ar-C}^{3,5}$ ), 50.71 (4C,  $-\text{N}(\text{CH}_2\text{-CH}_2\text{-CH}_2\text{-CH}_3)_2$ ), 29.40 (4C,  $-\text{N}(\text{CH}_2\text{-CH}_2\text{-CH}_2\text{-CH}_3)_2$ ), 25.82 (1C,  $\text{trz-CH}_3$ ), 20.27 (4C,  $-\text{N}(\text{CH}_2\text{-CH}_2\text{-CH}_2\text{-CH}_3)_2$ ), 13.94 (4C,  $-\text{N}(\text{CH}_2\text{-CH}_2\text{-CH}_2\text{-CH}_3)_2$ )

### 3.1.2. 4-[(1*E*)-2-(4,6-Dimethyl-1,3,5-triazin-2-yl)ethenyl]-*N,N*-dibutylbenzenamine (B2Trz)



Reagents	MW [g/mol]	[mg]	[mL]	[mmol]	[eq.]
4-(dibutylamino)benzaldehyde	233.35	855		3.66	2.7
2,4,6-trimethyl-1,3,5-triazine ( <b>8</b> )	123.16	168		1.36	1.0
KOH 20% in MeOH			9		
MeOH			9		

### Procedure

**B2Trz** was obtained from the reaction mixture from the synthesis of **3B2Trz** by separation via column chromatography (Toluene with 5-30%  $\text{Et}_2\text{O}$ , 235 g silica gel 60,

detection  $\lambda = 295$  nm). **B2Trz** eluted after **2B2Trz** from the column using 30% Et<sub>2</sub>O. The pure product was then obtained by removal of the solvents and drying in vacuo at 60°C.

### Yield

31 mg of dark yellow waxy resin **B2Trz** (7% of theory)

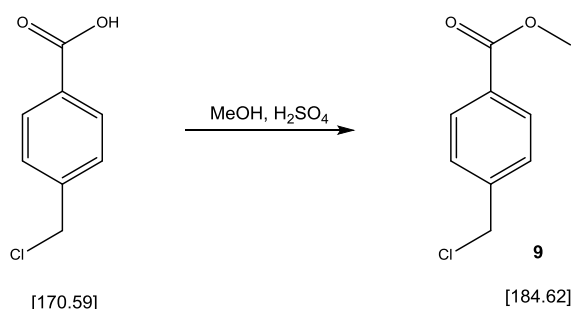
### Analysis

TLC:  $R_f = 0.21$  (Tol/Et<sub>2</sub>O 5:1)

<sup>1</sup>H NMR (200 MHz, CDCl<sub>3</sub>)  $\delta$  (ppm) = 8.13 (1H, *d*,  $J=15.65$  Hz, -CH=CH-*ar*), 7.50 (2H, *d*,  $J=8.80$  Hz, Bu<sub>2</sub>-N-*ar*-H<sup>2,6</sup>), 6.81 (1H, *d*,  $J=15.65$  Hz, -CH=CH-*ar*), 6.63 (2H, *d*,  $J=8.80$  Hz, Bu<sub>2</sub>-N-*ar*-H<sup>3,5</sup>), 3.32 (4H, *t*,  $J=7.80$  Hz, -N(CH<sub>2</sub>-CH<sub>2</sub>-CH<sub>2</sub>-CH<sub>3</sub>)<sub>2</sub>), 2.61 (6H, *s*, trz-CH<sub>3</sub>), 1.51 - 1.69 (4H, *m*, -N(CH<sub>2</sub>-CH<sub>2</sub>-CH<sub>2</sub>-CH<sub>3</sub>)<sub>2</sub>), 1.13 - 1.41 (4H, *m*, -N(CH<sub>2</sub>-CH<sub>2</sub>-CH<sub>2</sub>-CH<sub>3</sub>)<sub>2</sub>), 0.97 (6H, *t*,  $J=7.20$  Hz, -N(CH<sub>2</sub>-CH<sub>2</sub>-CH<sub>2</sub>-CH<sub>3</sub>)<sub>2</sub>)

<sup>13</sup>C-NMR (50 MHz, CDCl<sub>3</sub>)  $\delta$  (ppm) = 175.47 (2C, trz-C<sup>4,6</sup>), 171.71 (1C, trz-C<sup>2</sup>), 149.63 (1C, Bu<sub>2</sub>-N-*ar*-C<sup>4</sup>), 142.97 (1C, -CH=CH-*ar*), 130.15 (1C, Bu<sub>2</sub>-N-*ar*-C<sup>1</sup>), 122.15 (2C, Bu<sub>2</sub>-N-*ar*-C<sup>2,6</sup>), 119.28 (1C, -CH=CH-*ar*), 111.32 (2C, Bu<sub>2</sub>-N-*ar*-C<sup>3,5</sup>), 50.76 (2C, -N(CH<sub>2</sub>-CH<sub>2</sub>-CH<sub>2</sub>-CH<sub>3</sub>)<sub>2</sub>), 29.41 (2C, -N(CH<sub>2</sub>-CH<sub>2</sub>-CH<sub>2</sub>-CH<sub>3</sub>)<sub>2</sub>), 25.67 (2C, trz-CH<sub>3</sub>), 20.29 (2C, -N(CH<sub>2</sub>-CH<sub>2</sub>-CH<sub>2</sub>-CH<sub>3</sub>)<sub>2</sub>), 13.96 (2C, -N(CH<sub>2</sub>-CH<sub>2</sub>-CH<sub>2</sub>-CH<sub>3</sub>)<sub>2</sub>)

#### 4.1.1.1. 4-(Chloromethyl)benzoic acid methyl ester (**9**)<sup>79</sup>



Reagents	MW [g/mol]	[g]	[mL]	[mmol]	[eq.]
4-(chloromethyl)benzoic acid	170.59	10.23		60	1
dry MeOH	32.04		100	2470	41
H <sub>2</sub> SO <sub>4</sub> conc.			0.2		

#### Procedure

4-(Chloromethyl)benzoic acid (10.23 g, 60 mmol, 1 eq.) was dissolved in dry MeOH (100 mL, 2.47 mol, 41 eq.) and H<sub>2</sub>SO<sub>4</sub> conc. (0.2 mL, cat. amount) was added. The mixture was held at reflux with magnetic stirring for 16 h. After cooling down to room temperature the reaction mixture was diluted with Et<sub>2</sub>O (200 mL), extracted with 1M NaOH (100 mL) and the alkaline phase re-extracted with Et<sub>2</sub>O (2 x 100 mL). The unified organic layers were washed with deionized water (100 mL), dried with Na<sub>2</sub>SO<sub>4</sub> and the solvents removed in vacuo. The crude product was recrystallized from PE to afford pure **9** as off-white needles.

#### Yield

8.97 g of off-white needles (81% of theory)

#### Analysis

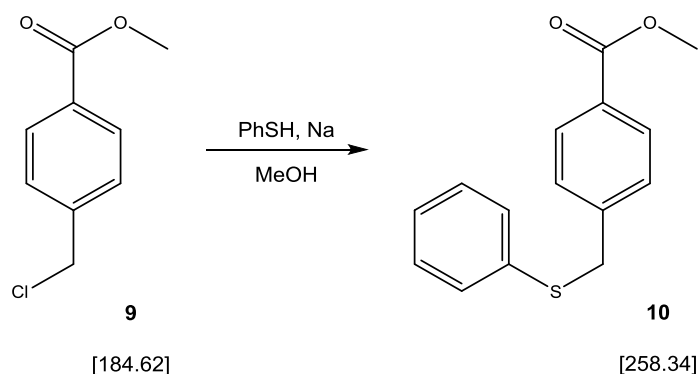
TLC:  $R_f = 0.60$  (DCM)

mp: 38 - 39°C (recryst. from PE)

<sup>1</sup>H NMR (200 MHz, CDCl<sub>3</sub>)  $\delta$  (ppm) = 8.01 (2H, *d*,  $J = 8.2$  Hz, -OOC-ar-H<sup>2,6</sup>), 7.43 (2H, *m*,  $J = 8.2$  Hz, -OOC-ar-H<sup>3,5</sup>), 4.58 (2H, *s*, -ar-CH<sub>2</sub>-Cl), 3.90 (3H, *s*, O=C-O-CH<sub>3</sub>)

$^{13}\text{C}$ -NMR (50 MHz,  $\text{CDCl}_3$ )  $\delta$  (ppm) = 166.5 (1C,  $-\text{O}-\text{C}=\text{O}$ ), 142.2 (1C,  $-\text{ar}-\text{C}^4$ ), 130.1 (1C,  $-\text{ar}-\text{C}^1$ ), 130.0 (2C,  $-\text{ar}-\text{C}^{2,6}$ ), 128.4 (2C,  $-\text{ar}-\text{C}^{3,5}$ ), 52.2 (1C,  $\text{O}=\text{C}-\text{O}-\underline{\text{C}}\text{H}_3$ ), 45.3 (1C,  $\text{ar}-\text{CH}_2-\text{Cl}$ )

#### 4.1.1.2. 4-[(Phenylthio)methyl]benzoic acid methyl ester (**10**)<sup>70</sup>



Reagents	MW [g/mol]	[g]	[mL]	[mmol]	[eq.]
4-(chloromethyl)benzoic acid methyl ester ( <b>9</b> )	184.62	4.62		25	1.0
thiophenol	110.19	2.75		25	1.0
sodium	22.99	0.575		25	1.0
MeOH			60		

#### Procedure

Freshly cut sodium metal scrapings (575 mg, 25 mmol, 1.0 eq.) were introduced into a 100 mL three-neck round-bottom flask equipped with reflux condenser, magnetic stirrer and a rubber septum while maintaining a countercurrent flow of nitrogen. The apparatus was cooled to 0°C and dry MeOH (40 mL) were slowly added through the septum. After dissolution of the sodium was complete, thiophenol (2.75 g, 25 mmol, 1.0 eq.) was added dropwise over a period of 2 min. The solution was stirred for 15 min and then a solution of 4-(chloromethyl)benzoic acid methyl ester (**9**) (4.62 g, 25 mmol, 1.0eq.) in dry MeOH (20 mL) was slowly added during 30 min. The reaction mixture was then heated to reflux for 18 h which lead to formation of a voluminous white precipitate. About half of the solvent was evaporated from the reaction mixture in vacuo; the

precipitate obtained after cooling to  $-20^{\circ}\text{C}$  was washed with cold MeOH and purified by Kugelrohr distillation, affording pure **10** as white crystalline solid.

### Yield

5.49 g of white crystal mass (85% of theory)

### Analysis

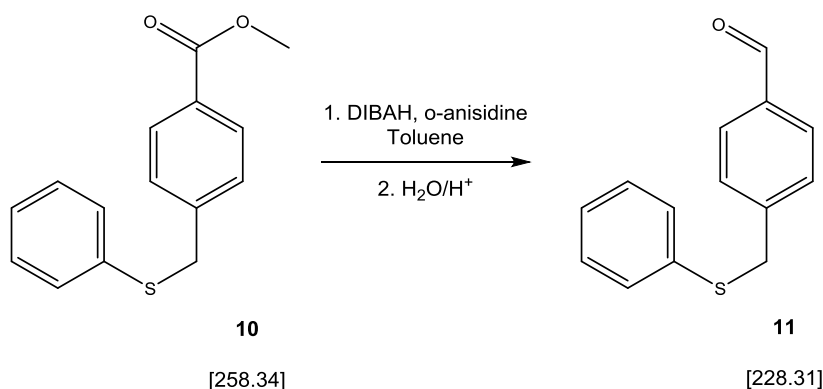
TLC:  $R_f = 0.57$  (DCM)

mp:  $82 - 84^{\circ}\text{C}$

$^1\text{H}$  NMR (200 MHz,  $\text{CDCl}_3$ )  $\delta$  (ppm) = 7.96 (2H, *d*,  $J = 8.2$  Hz,  $-\text{OOC}-\text{ar}-\text{H}^{2,6}$ ), 7.12 – 7.40 (7H, *m*,  $-\text{OOC}-\text{ar}-\text{H}^{3,5}$ ;  $-\text{S}-\text{ph}-\text{H}^{2-6}$ ), 4.12 (2H, *s*,  $-\text{ar}-\text{CH}_2-\text{S}-$ ), 3.90 (3H, *s*,  $\text{O}=\text{C}-\text{O}-\text{CH}_3$ )

$^{13}\text{C}$ -NMR (50 MHz,  $\text{CDCl}_3$ )  $\delta$  (ppm) = 166.8 (1C,  $-\text{O}-\text{C}=\text{O}$ ), 143.0 (1C,  $-\text{ar}-\text{C}^4$ ), 135.4 (1C,  $-\text{S}-\text{ph}-\text{C}^1$ ), 130.5 + 129.8 + 129.0 + 128.9 + 128.8 (9C,  $-\text{ar}-\text{C}^{1,2,3,5,6}$ ,  $-\text{S}-\text{ph}-\text{C}^{2,3,5,6}$ ), 126.8 (1C,  $-\text{S}-\text{ph}-\text{C}^4$ ), 52.1 (1C,  $\text{O}=\text{C}-\text{O}-\text{CH}_3$ ), 39.0 (1C,  $-\text{ar}-\text{CH}_2-\text{S}-$ )

#### 4.1.1.3. 4-[(Phenylthio)methyl]benzaldehyde (**11**)<sup>73</sup>



Reagents	MW [g/mol]	[g]	[mL]	[mmol]	[eq.]
4-[(phenylthio)methyl]benzoic acid methyl ester ( <b>10</b> )	258.34	1.73		6.70	1
o-anisidine	123.15	1.65		13.4	2
DIBALH	1.0 M in heptane		20.1	20.10	3

dry toluene

140

### Procedure

A 250 mL three-neck round-bottom flask equipped with internal thermometer, mechanical stirrer with glass fitting and a rubber septum was charged with 4-[(phenylthio)methyl]benzoic acid methyl ester (**10**) (1.73 g, 6.70 mmol, 1 eq.) and purged with argon. Dry toluene (140 mL) and o-anisidine (1.65 g, 13.4 mmol, 2 eq.) were added through the septum and the solution was cooled to -78°C (acetone / liquid N<sub>2</sub> bath). DIBAH (20.1 mL 1.0M in heptane, 20.1 mmol, 3 eq.) was added dropwise over a period of 30 min and stirring then continued for another 20 min, while keeping the temperature of the reaction mixture at about -80°C at all times. To quench the reaction, 4N HCl (54 mL) were added slowly enough to keep the temperature between -70°C to -60°C, leading to an intense yellow color which suddenly disappears again at about -10°C. The whitish suspension was stirred for 1.5 h at room temperature. The aqueous layer was discarded, the organic layer dried with Na<sub>2</sub>SO<sub>4</sub> and the solvent removed in vacuo leading to a white solid (1.75 g). Purification by column chromatography (PE:EA = 94:6, 123 g silica gel 60) afforded 381 mg pure **11**.

### Yield

381 mg crystalline white mass (25% of theory)

### Analysis

TLC:  $R_f = 0.41$  (PE:EA = 7:1)

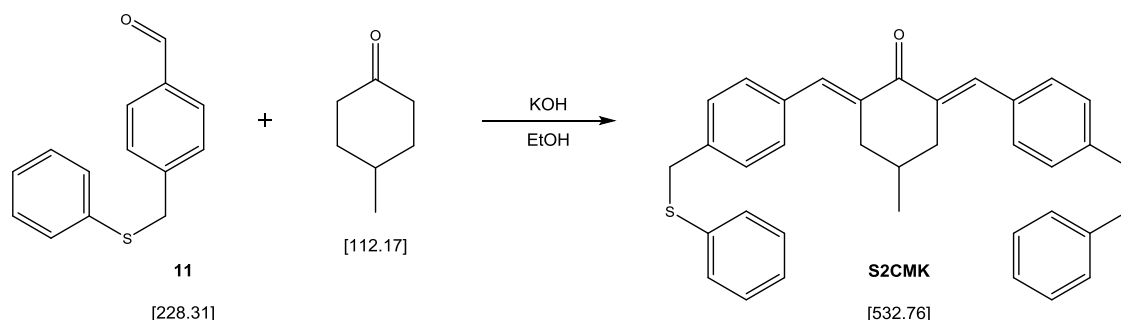
mp: 36 - 37°C

<sup>1</sup>H NMR (200 MHz, CDCl<sub>3</sub>)  $\delta$  (ppm) = 9.98 (1H, s, H-C=O), 7.80 (2H, *d*,  $J = 8.2$  Hz, -O=C-ar-H<sup>2,6</sup>), 7.42 (2H, *d*,  $J = 8.2$  Hz, O=C-ar-H<sup>3,5</sup>), 7.18 - 7.35 (5H, *m*, -S-ph-H<sup>2-6</sup>), 4.15 (2H, s, -ar-CH<sub>2</sub>-S-)

<sup>13</sup>C-NMR (50 MHz, CDCl<sub>3</sub>)  $\delta$  (ppm) = 191.8 (1C, H-C=O), 144.9 (1C, -ar-C<sup>4</sup>), 135.3 + 135.1 (2C, -S-ph-C<sup>1</sup>; -ar-C<sup>1</sup>), 130.6 + 129.9 + 129.4 + 129.0 (8C, -ar-C<sup>2,3,5,6</sup>, -S-ph-C<sup>2,3,5,6</sup>), 127.0 (1C, -S-ph-C<sup>4</sup>), 39.2 (1C, -ar-CH<sub>2</sub>-S-)



#### 4.1.1.4. (2*E*,6*E*)-2,6-Bis[[4-[(phenylthio)methyl]phenyl]methylene]-4-methylcyclohexanone (**S2CMK**)



Reagents	MW [g/mol]	[mg]	[mL]	[μmol]	[eq.]
4-[(phenylthio)methyl]-benzaldehyde ( <b>11</b> )	228.31	200		876	2.0
4-methylcyclohexanone	112.17	49		438	1.0
KOH	56.11	25		445	1.0
EtOH			8		

#### Procedure

All steps were performed in an orange light room. To a solution of aldehyde **11** (200 mg, 876 μmol, 2.0 eq.) and 4-methylcyclohexanone (49 mg, 438 μmol, 1.0 eq.) in EtOH (8 mL) finely powdered KOH (25 mg, 445 μmol, 1.0 eq.) was added and the resulting solution was magnetically stirred at 60°C for 18 h, which lead to precipitation of a yellowish-white solid. After cooling to room temperature this solid was filtered off, washed with EtOH and purified by column chromatography (PE:DCM = 1:2, 123 g silica gel 60) to afford 161 mg pure **S2CMK**.

#### Yield

161 mg of yellowish-white powder (69 % of theory)

#### Analysis

TLC:  $R_f = 0.38$  (PE:DCM = 1:2)

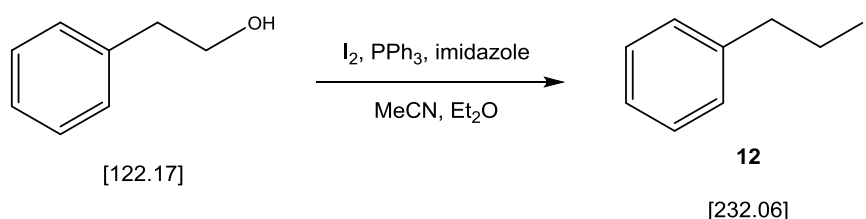
mp: 179 - 181°C

$^1\text{H}$  NMR (200 MHz,  $\text{CDCl}_3$ )  $\delta$  (ppm) = 7.73 - 7.86 (2H, *m*, -C=CH), 7.13 - 7.50 (18H, *m*, -ar-H<sup>2,3,5,6</sup>, -S-ph-H<sup>2-6</sup>), 4.16 (4H, *s*, -S-CH<sub>2</sub>-ph), 3.07 (2H, *dd*, *J* = 3.5 and 15.8 Hz, -CH<sub>2</sub>-C=CH), 2.37 - 2.65 (2H, *m*, -CH<sub>2</sub>-C=CH), 1.77 - 2.02 (1H, *m*, -CH-CH<sub>3</sub>), 1.11 (3H, *d*, *J* = 6.5 Hz, -CH-CH<sub>3</sub>)

$^{13}\text{C}$ -NMR (50 MHz,  $\text{CDCl}_3$ )  $\delta$  (ppm) = 190.0 (1C, -C=O), 138.2 7 (2C, -C=CH-), 136.7 (2C, -C=CH-), 136.0 + 135.3 + 134.9 (6C, -S-ph-C<sup>1</sup>; -ar-C<sup>1,4</sup>), 130.6 + 130.0 + 128.9 + 128.9 + 126.6 (18C, -ar-C<sup>2,3,5,6</sup>, -S-ph-C<sup>2-6</sup>), 38.9 (2C, -S-CH<sub>2</sub>-ph-), 36.5 (2C, -CH<sub>2</sub>-CH-), 29.4 (1C, -CH-CH<sub>3</sub>), 21.7 (1C, -CH-CH<sub>3</sub>)

#### 4.1.2.1.

#### (2-Iodoethyl)benzene (12)<sup>75</sup>



Reagents	MW [g/mol]	[g]	[mL]	[mmol]	[eq.]
2-phenylethanol	122.16	1.83		15	1.0
PPh <sub>3</sub>	262.28	5.10		19.5	1.3
imidazole	68.08	1.46		21.5	1.4
I <sub>2</sub>	253.81	5.30		20.9	1.4
MeCN			12		
Et <sub>2</sub> O			20		

#### Procedure

In a 100 mL round bottom flask 2-phenylethanol (1.83 g, 15 mmol, 1.0 eq.), PPh<sub>3</sub> (5.10 g, 19.5 mmol, 1.3 eq.) and imidazole (1.46 g, 21.5 mmol, 1.4 eq.) were dissolved in MeCN (12 mL) and dry Et<sub>2</sub>O (20 mL). The colorless solution was cooled to 0°C and I<sub>2</sub> (5.30 g, 20.9 mmol, 1.4 eq.) was added in small portions during 30 min, which first lead to formation of a white precipitate and then the reaction mixture turning dark brown after all I<sub>2</sub> had been added. After 1.5 h of magnetic stirring at 0°C, the reaction mixture was

diluted with Et<sub>2</sub>O (200 mL), subsequently extracted with sat. aqueous Na<sub>2</sub>S<sub>2</sub>O<sub>3</sub>, sat. aqueous CuSO<sub>4</sub> and brine. The organic layer was dried with Na<sub>2</sub>SO<sub>4</sub>, the solvent evaporated in vacuo and the solid white residue dissolved in a minimal amount of PE. Purification via flash-chromatography (65 g silica gel 60, pure PE) afforded **12** as a slightly yellowish oil.

### Yield

2.57 g of (74 % of theory)

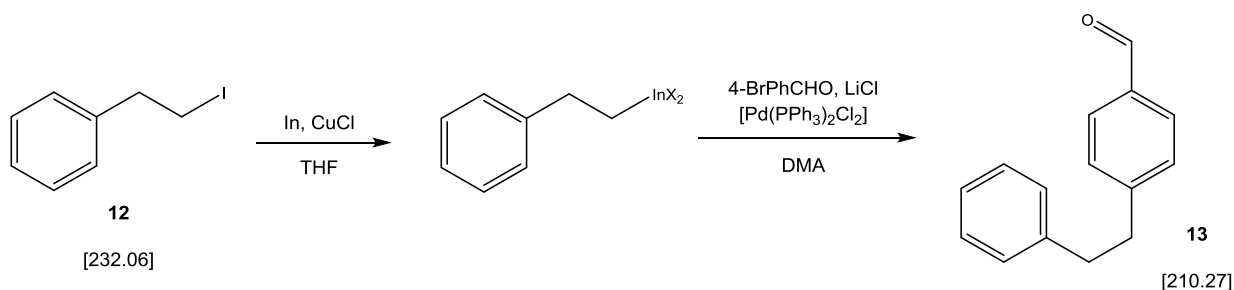
### Analysis

TLC:  $R_f = 0.50$  (PE)

RI: 1.5985 (20°C)

<sup>1</sup>H NMR (200 MHz, CDCl<sub>3</sub>)  $\delta$  (ppm) = 7.12 - 7.36 (5H, *m*, -CH<sub>2</sub>-ph-H<sup>2-6</sup>), 3.24 - 3.39 (2H, *m*, I-CH<sub>2</sub>-CH<sub>2</sub>-ph), 3.08 - 3.22 (2H, *m*, I-CH<sub>2</sub>-CH<sub>2</sub>-ph)

#### 4.1.2.2. 4-(2-Phenylethyl)benzaldehyde (**13**)<sup>74</sup>



Reagents	MW [g/mol]	[mg]	[mL]	[mmol]	[eq.]
(2-iodoethyl)benzene ( <b>12</b> )	232.06	1160		5	1
step 1:					
In	114.82	1150		10	2
CuCl	99.00	990		10	2
THF			15		

step 2:

4-bromobenzaldehyde	185.02	648	3.5	0.7
LiCl	42.39	424	10	2
[Pd(PPh <sub>3</sub> ) <sub>2</sub> Cl <sub>2</sub> ]	701.9	175	0.25	0.05
DMA				15

## Procedure

In a 100 mL round bottom flask was charged with (2-iodoethyl)benzene (**12**) (1.16 g, 5 mmol, 1.0 eq.), powdered indium metal (1.15 g, 10 mmol, 2 eq.) and CuCl (0.99 g, 10 mmol, 2 eq.). Dry THF (15 mL) was added and the resulting suspension was stirred vigorously for 22 h at room temperature, leading to a color change from green to black.

The black solids were allowed to settle, the liquid phase was decanted off and the solids were washed with THF (15 mL). The organic layers were combined, filtered through a 0.22 µm nylon syringe filter and concentrated in vacuo at 40°C, leading to an oily yellowish solution of the indium alkyl intermediate in THF with a mass of 3.64 g.

This residue was dissolved in DMA (15 mL), 4-bromobenzaldehyde (648 mg, 3.5 mmol, 0.7 eq.), LiCl (424 mg, 10 mmol, 2 eq.) and [Pd(PPh<sub>3</sub>)<sub>2</sub>Cl<sub>2</sub>] (175 mg, 0.25 mmol, 0.05 eq.) were added subsequently and the mixture was stirred at 100°C for 24 h. The reaction mixture was diluted with deionized water (200 mL) and extracted with Et<sub>2</sub>O (3 x 150 mL). The combined organic layers were subsequently washed with saturated NH<sub>4</sub>Cl-solution (200 mL) and deionized water (150 mL) and finally dried with anhydrous NaSO<sub>4</sub>. The solvents were evaporated in vacuo, leaving a reddish brown oil (0.9 g) which was purified by Kugelrohr distillation to yield **13** as a colorless oil.

## Yield

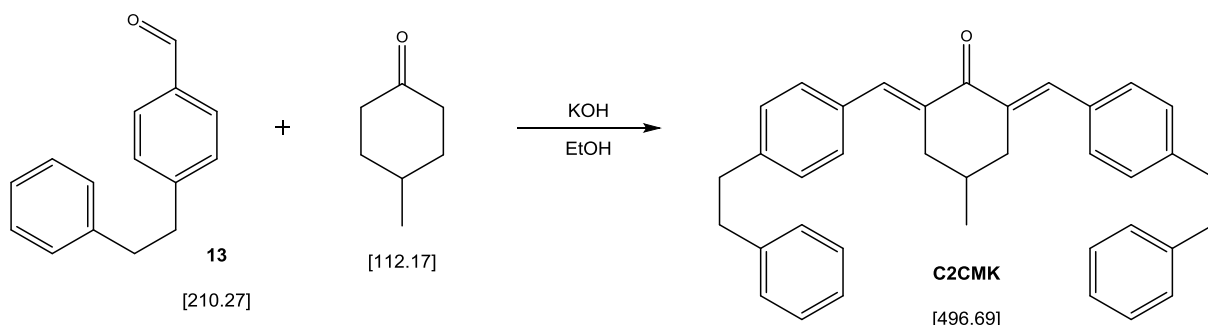
606 mg of colorless oil (82% of theory)

## Analysis

<sup>1</sup>H NMR (200 MHz, CDCl<sub>3</sub>) δ (ppm) = 9.97 (1H, s, H-C=O), 7.71 - 7.86 (2H, *m*, O=C-ar-H<sup>2,6</sup>), 7.10 - 7.39 (7H, *m*, O=C-ar-H<sup>3,5</sup>; -CH<sub>2</sub>-ph-H<sup>2-6</sup>), 2.83 - 3.13 (4H, *m*, -CH<sub>2</sub>-CH<sub>2</sub>-ph)

<sup>13</sup>C-NMR (50 MHz, CDCl<sub>3</sub>) δ (ppm) = 192.0 (1C, H-C=O), 149.1 (1C, -ar-C<sup>4</sup>), 141.0 (1C, -CH<sub>2</sub>-ph-C<sup>1</sup>), 134.6 (1C, -ar-C<sup>1</sup>), 129.9 + 129.2 + 128.5 (8C, -ar-C<sup>2,3,5,6</sup>, -CH<sub>2</sub>-ph-C<sup>2,3,5,6</sup>), 126.2 (1C, -CH<sub>2</sub>-ph-C<sup>4</sup>), 38.1 + 37.4 (2C, ar-CH<sub>2</sub>-CH<sub>2</sub>-ph)

#### 4.1.2.3. (2*E*,6*E*)-2,6-Bis[[4-(2-phenylethyl)phenyl]methylene]-4-methylcyclohexanone (**C2CMK**)



Reagents	MW [g/mol]	[mg]	[mL]	[μmol]	[eq.]
4-(2-phenylethyl)benzaldehyde ( <b>19</b> )	210.27	150		713	2.0
4-methylcyclohexanone	112.17	40		357	1.0
KOH	56.11	20		357	1.0
EtOH			5		

#### Procedure

All steps were performed in an orange light room. To a solution of aldehyde **13** (150 mg, 713 μmol, 2.0 eq.) and 4-methylcyclohexanone (40 mg, 357 μmol, 1.0 eq.) in EtOH (5 mL) finely powdered KOH (20 mg, 357 μmol, 1.0 eq.) was added and the resulting solution was magnetically stirred at 60°C for 24 h, which lead to precipitation of a yellowish-white solid. After cooling to room temperature this solid was filtered off, washed with EtOH and purified by column chromatography (PE with 30-40% DCM, 10 g silica gel 60) to afford 92 mg pure **C2CMK**.

#### Yield

92 mg of yellowish-white powder (52% of theory)

#### Analysis

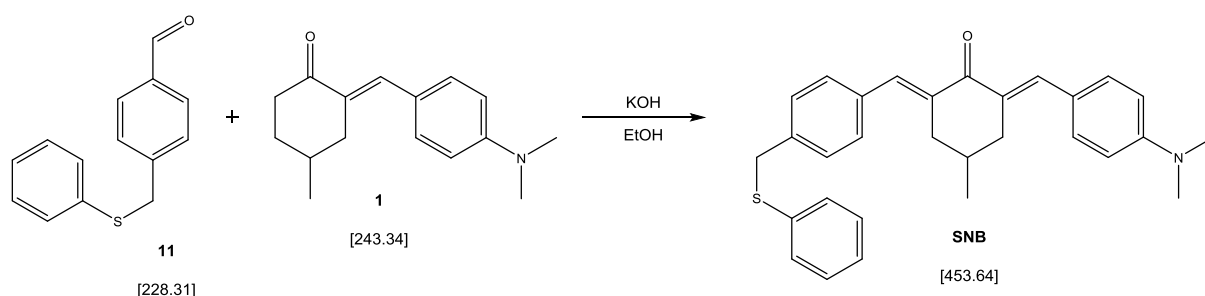
TLC:  $R_f = 0.24$  (PE:DCM = 1:1)

mp: 134 - 136°C

$^1\text{H}$  NMR (200 MHz,  $\text{CDCl}_3$ )  $\delta$  (ppm) = 7.71 (2H, s,  $-\text{C}=\text{CH}$ ), 7.05 - 7.37 (18H, m,  $-\text{ar}-\text{H}^{2,3,5,6}$ ,  $-\text{CH}_2\text{-ph}-\text{H}^{2-6}$ ), 2.99 (2H, dd,  $J = 3.3$  and  $15.7$  Hz,  $-\text{CH}_2\text{-C}=\text{CH}$ ), 2.87 (8H, s,  $\text{ar-CH}_2\text{-CH}_2\text{-ph}$ ), 2.32 - 2.52 (2H, m,  $-\text{CH}_2\text{-C}=\text{CH}$ ), 1.68 - 1.92 (1H, m,  $-\text{CH-CH}_3$ ), 1.00 (3H, d,  $J = 6.5$  Hz,  $-\text{CH-CH}_3$ )

$^{13}\text{C}$ -NMR (50 MHz,  $\text{CDCl}_3$ )  $\delta$  (ppm) = 190.1 (1C,  $-\text{C}=\text{O}$ ), 142.6 (2C,  $-\text{CH}_2\text{-ph}-\text{C}^1$ ), 141.5 (2C,  $-\text{ar-C}^4$ ), 137.0 (2C,  $-\text{C}=\text{CH-}$ ), 134.8 (2C,  $-\text{C}=\text{CH-}$ ), 133.7 (2C,  $-\text{ar-C}^1$ ), 130.6 + 128.6 + 128.5 + 128.4 + 126.0 (18C,  $-\text{ar-C}^{2,3,5,6}$ ,  $-\text{CH}_2\text{-ph}-\text{C}^{2-6}$ ), 37.8 + 37.7 (4C,  $\text{ar-CH}_2\text{-CH}_2\text{-ph}$ ), 36.6 (2C,  $-\text{CH}_2\text{-C}=\text{CH}$ ), 29.4 (1C,  $-\text{CH-CH}_3$ ), 21.7 (1C,  $-\text{CH-CH}_3$ )

#### 4.2.1. (2E,6E)-2-[[4-(Dimethylamino)phenyl]methylene]-6-[[4-[(phenylthio)methyl]phenyl]methylene]-4-methylcyclohexanone (SNB)



Reagents	MW [g/mol]	[mg]	[mL]	[ $\mu\text{mol}$ ]	[eq.]
4-[(phenylthio)methyl]benzaldehyde ( <b>11</b> )	228.31	150		657	1.1
(2E)-2-[[4-(dimethylamino)phenyl]methylene]-4-methylcyclohexanone ( <b>1</b> )	243.34	145		597	1.0
KOH	56.11	33.5		597	1
EtOH			10		

## Procedure

All steps were performed in an orange light room. To a solution of aldehyde **11** (150 mg, 657  $\mu\text{mol}$ , 1.0 eq.) and benzylidene ketone **1** (145 mg, 597  $\mu\text{mol}$ , 1.1 eq.) in EtOH (10 mL) finely powdered KOH (33.5 mg, 597  $\mu\text{mol}$ , 1.0 eq.) was added and the resulting solution was magnetically stirred at 60°C for 24 h, which lead to precipitation of an orange solid. After cooling to room temperature this solid was filtered off, washed with EtOH and purified by column chromatography (DCM, 10 g silica gel 60) to afford 92 mg pure **SNB**.

## Yield

208 mg of (77 % of theory)

## Analysis

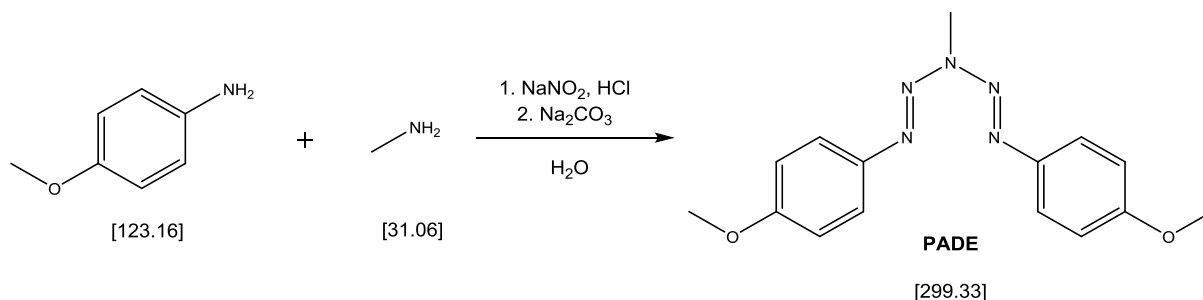
TLC:  $R_f$  = 0.18 (DCM); 0.47 (DCM:MeOH = 99:1)

mp: 159 - 160°C

$^1\text{H}$  NMR (200 MHz,  $\text{CDCl}_3$ )  $\delta$  (ppm) = 7.79 (1H, *br. s.*, -C=CH-), 7.77 (1H, *br. s.*, -C=CH-), 7.14 - 7.52 (11H, *m*,  $(\text{CH}_3)_2\text{N}$ -ar- $\underline{\text{H}}^{3,5}$ ; -S-CH<sub>2</sub>-ar- $\underline{\text{H}}^{2,3,5,6}$ ; -S-ph- $\text{H}^{2,6}$ ), 6.73 (2H, *d*,  $J$  = 8.8 Hz,  $(\text{CH}_3)_2\text{N}$ -ar- $\underline{\text{H}}^{2,6}$ ), 4.13 (2H, *s*, -ar-CH<sub>2</sub>-S-), 2.92 - 3.18 (8H, *m*, -CH<sub>2</sub>-CH-;  $(\text{CH}_3)_2\text{N}$ -ar-), 2.37 - 2.61 (2H, *m*, -CH<sub>2</sub>-CH-), 1.74 - 1.99 (1H, *m*, -CH<sub>2</sub>-CH-), 1.10 (3H, *d*,  $J$  = 6.5 Hz, -CH-CH<sub>3</sub>)

$^{13}\text{C}$ -NMR (50 MHz,  $\text{CDCl}_3$ )  $\delta$  (ppm) = 189.8 (1C, -C=O), 150.5 (1C,  $(\text{CH}_3)_2\text{N}$ -ar- $\underline{\text{C}}^1$ ), 138.4 (1C, -C= $\underline{\text{C}}\text{H}$ -), 137.8 + 135.8 + 135.2 + 131.0 (6C,  $(\text{CH}_3)_2\text{N}$ -ar- $\underline{\text{C}}^4$ ; - $\underline{\text{C}}\text{=CH}$ -; -S-CH<sub>2</sub>-ar- $\underline{\text{C}}^{1,4}$ ; -S-ph- $\text{C}^1$ ), 135.6 (1C, -C= $\underline{\text{C}}\text{H}$ -), 132.7 + 130.5 + 130.0 + 128.9 + 128.8 (10C,  $(\text{CH}_3)_2\text{N}$ -ar- $\underline{\text{C}}^{3,5}$ ; -S-CH<sub>2</sub>-ar- $\underline{\text{C}}^{2,3,5,6}$ ; -S-ph- $\text{C}^{2,3,5,6}$ ), 126.5 (1C, -S-ph- $\text{C}^4$ ), 111.7 (2C,  $(\text{CH}_3)_2\text{N}$ -ar- $\underline{\text{C}}^{2,6}$ ), 40.2 (2C,  $(\text{CH}_3)_2\text{N}$ -ar-), 38.9 (1C, -S-CH<sub>2</sub>-ph-), 37.0 (1C, -CH<sub>2</sub>-CH-), 36.5 (1C, -CH<sub>2</sub>-CH-), 29.4 (1C, -CH-CH<sub>3</sub>), 21.8 (1C, -CH-CH<sub>3</sub>)

### 4.3.1. 1,5-Bis(4-methoxyphenyl)-3-methyl-1,4-pentazadiene (PADE)<sup>78</sup>



Reagents	MW [g/mol]	[g]	[mL]	[mmol]	[eq.]
p-anisidine	123.15	1.85		15	1
NaNO <sub>2</sub>	68.99	1.03		15	1
conc. HCl (~12 N aq. solution)			3.13	37.5	2.5
CH <sub>3</sub> NH <sub>2</sub> (~41% aq. solution)		0.57		7.5	0.5
Na <sub>2</sub> CO <sub>3</sub>				37.5	2.5
deionized water			70		

#### Procedure

All steps were performed in an orange light room. In an open 250 ml three-neck round bottom flask with internal thermometer and magnetic stirring, a solution of p-anisidine (1.85g, 15 mmol, 1 eq.) and conc. HCl (3.13 mL, ~12 N, 37.5 mmol, 2.5 eq.) in deionized water (30 mL) was cooled slightly below 0°C. Under magnetic stirring, a solution of NaNO<sub>2</sub> (1.03 g, 15 mmol, 1 eq.) in deionized water (4 mL) was added dropwise so that the temperature stayed below 2°C, leading to a darkening of the solution. After stirring for about 30 min, a pre-chilled solution of CH<sub>3</sub>NH<sub>2</sub> (568 mg, ~41% aq. solution, 7.5 mmol, 0.5 eq.) and Na<sub>2</sub>CO<sub>3</sub> in deionized water (35 mL) was added slowly (foam builds), with continued stirring afterwards for 1.5 h at about 0 - 5°C. The reaction mixture was then extracted with DCM (3 x 50 mL), the unified organic layers dried over Na<sub>2</sub>SO<sub>4</sub> and the solution applied to pre-conditioned (DCM) silica gel 60 (50 g) to perform a flash column chromatography. After complete elution of the product with DCM, the eluate was carefully stripped of solvent in vacuo on a rotary evaporator. During evaporation, the temperature of the solution was stabilized by a cold water bath



(~15-18°C). The product crystallized forming fine yellow needles as soon as the solution became supersaturated, and was then carefully dried in vacuo.

**Yield**

1.0 g of yellow needles (45% of theory)

**Analysis**

TLC:  $R_f = 0.57$  (DCM)

mp: 106 - 110°C (decomposition, bubble formation)

$^1\text{H}$  NMR (200 MHz,  $\text{CDCl}_3$ )  $\delta$  (ppm) = 7.53 - 7.64 (4H, m,  $\text{CH}_3\text{-O-ar-H}^{3,5}$ ), 6.80 - 6.91 (4H, m,  $\text{CH}_3\text{-O-ar-H}^{2,6}$ ), 3.74 (6H, s,  $\text{CH}_3\text{-O-ar-}$ ), 3.69 (3H, s,  $\text{CH}_3\text{-N-}$ )

$^{13}\text{C}$ -NMR (50 MHz,  $\text{CDCl}_3$ )  $\delta$  (ppm) = 159.9 (2C,  $\text{CH}_3\text{-O-ar-C}^1$ ), 142.6 (2C,  $\text{CH}_3\text{-O-ar-C}^4$ ), 123.4 (4C,  $\text{CH}_3\text{-O-ar-C}^{3,5}$ ), 114.2 (4C,  $\text{CH}_3\text{-O-ar-C}^{2,6}$ ), 55.5 (2C,  $\text{CH}_3\text{-O-ar-}$ ), 28.2 (1C,  $\text{CH}_3\text{-N-}$ )

## Conclusion

The scope of this thesis was to develop novel two-photon initiators (TPIs) for two-photon induced photopolymerization (TPIP) structuring with improved properties regarding the application of stereolithography in the sub-micrometer range. TPIs with large processing windows, i.e. both low polymerization thresholds (optimal fabricated structure quality at low laser powers and high writing speeds) and a robust polymerization at higher energies (no thermal decomposition / fabricated structures keeping high quality at high laser powers and low writing speeds), should be developed.

Two strategies major strategies to improve the efficiency were followed:

- The energy absorption in TPA processes should be optimized by designing systems with molecular features that increase the TPA cross section  $\sigma_{\text{TPA}}$ , like planarized groups as well as branched and higher order polarity systems (octupoles instead of quadrupoles and dipoles).
- The successful formation of radicals from the generated excited states should be increased by the introduction of groups that undergo irreversible cleavage under radical formation, thus avoiding deactivation processes like back electron transfer (BET).

Starting point of the study was the highly efficient and easily prepared TPI **M2CMK** (see **Figure 76**), which had been developed at the Vienna UT in previous work.<sup>52</sup> It was used as a reference compound for photophysical properties (one-photon absorption in the UV/Vis-range and  $\sigma_{\text{TPA}}$ ) as well as for behavior in TPIP, and also as a structural motif for the molecular design of the novel compounds.

By joining 3 units of **M2CMK** together with a shared nitrogen atom to form a tri-branched compound, **Y-M2CMK** was obtained. Because of exceedingly low solubility even in common solvents and especially the acrylate formulation used in polymerization tests, the better soluble **Y-B2CMK** bearing elongated alkyl chains was prepared.

N-benzyl carbazole was used to investigate the effect of planarized electron donor groups in the compound **Cbz2CEK**, and furthermore as a planarized core element for the di-branched substance **B2Cbz**.

**Figure 76** shows a schematic overview of the novel TPIs and the individual steps taken in their design.

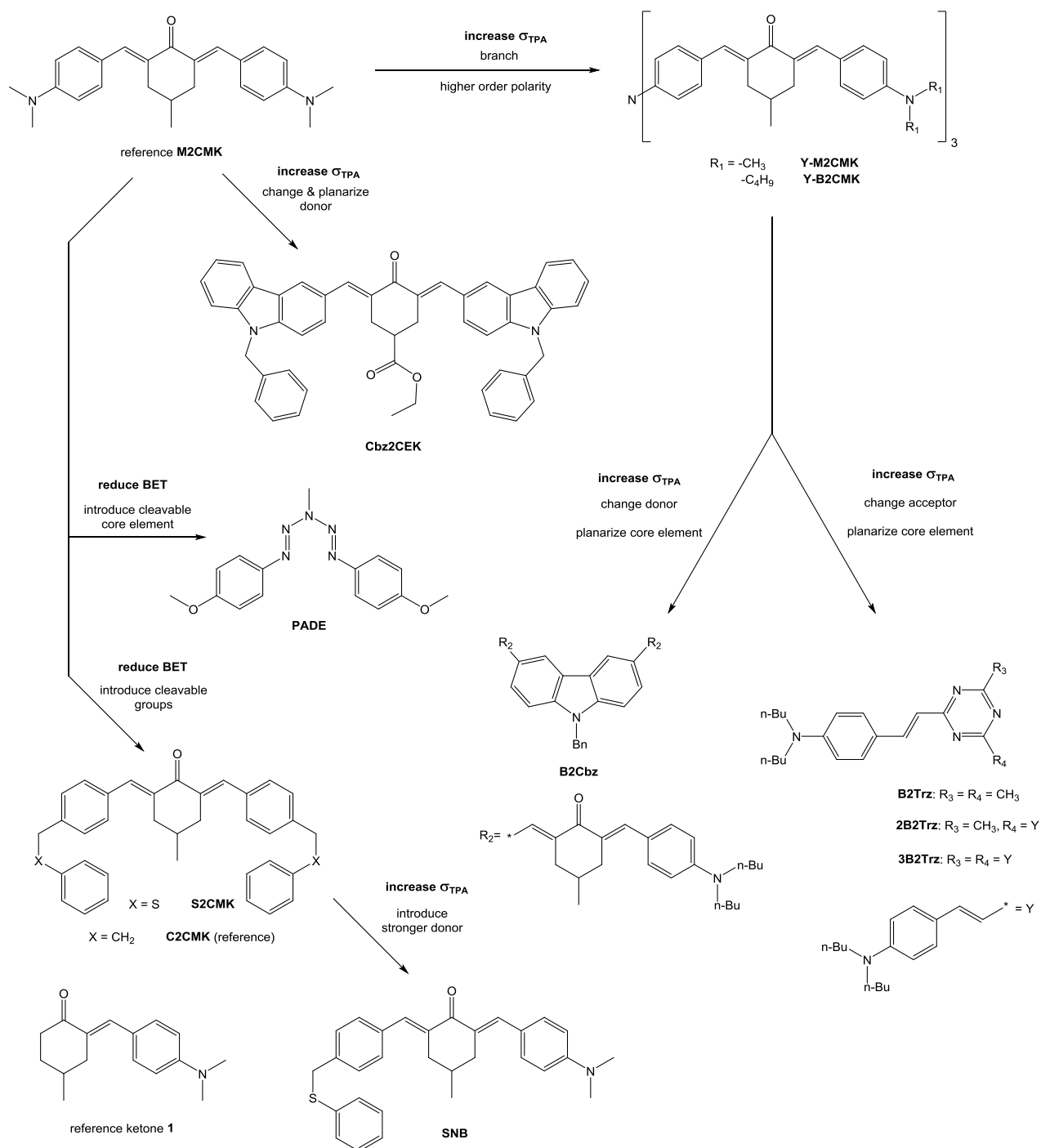


**Figure 76:** Schematic overview of the novel TPIs.

A series of three other compounds **B2Trz**, **2B2Trz** and **3B2Trz** with 1,3,5-triazine as a planarized core element and strong electron acceptor functionality was prepared and tested with the goal to observe the cooperative non-linear increase in  $\sigma_{\text{TPA}}$  by increasing the number of branches.

The second concept of cleavage to avoid BET was tested on the nitrogen releasing compound **PADE**, which is known in literature but has not been used in TPIP before.

A thioether-containing compound **S2CMK** expected to be capable of  $\beta$ -phenylogous cleavage was synthesized along with a non-cleavable analogue **C2CMK** as a reference.

To increase the  $\sigma_{\text{TPA}}$  of **S2CMK**, one of the cleavable groups was replaced with a strong electron donor group to obtain **SNB**. For a better understanding of the effects of a singular donor group only on one side of the acceptor moiety, ketone **1** was compared to **S2CMK** and **SNB**.

For the measurement of  $\sigma_{\text{TPA}}$  open aperture z-scan was performed at 798 nm which is the most intense wavelength emitted by the used fs-pulsed Titanium:Sapphire (Ti:S) laser. To investigate the correlation with the one-photon absorption (OPA) of the TPIs, UV/Vis-spectra measurements were performed as well.

**Table 7** gives an overview of the photophysical properties of all the synthesized TPIs.

**Table 7:** Overview of the photophysical properties of the novel TPIs - one-photon absorption maxima  $\lambda_{\text{abs}}^{\text{OPA}}$ , molar OPA extinction  $\epsilon$  measured at  $\lambda_{\text{abs}}^{\text{OPA}}$ , and TPA cross sections  $\sigma_{\text{TPA}}$ . All measurements performed in THF unless specified otherwise (in brackets), at concentrations of  $10^{-5}$  M for  $\epsilon$  and  $10^{-2}$  M for  $\sigma_{\text{TPA}}$  respectively.

TPI	$\lambda_{\text{abs}}^{\text{OPA}}$ [nm]	$\epsilon$ [ $10^3 \text{ L mol}^{-1} \text{ cm}^{-1}$ ]	$\sigma_{\text{TPA}}$ [GM]
<b>M2CMK</b>	430 (MeCN)	47 (MeCN)	191
<b>Y-M2CMK</b>	451	85	570 (CHCl <sub>3</sub> )
<b>Y-B2CMK</b>	444	120	316
<b>B2Cbz</b>	429	77	109
<b>Cbz2CEK</b>	392	37	83
<b>B2Trz</b>	412 (MeCN)	43 (DCM)	60
<b>2B2Trz</b>	433 (MeCN)	80 (DCM)	244
<b>3B2Trz</b>	439 (MeCN)	120 (DCM)	275
<b>S2CMK</b>	340 (MeCN)	37 (MeCN)	<20
<b>C2CMK</b>	340 (MeCN)	37 (MeCN)	<20
ketone <b>1</b>	372 (MeCN)	32 (MeCN)	N/A
<b>SNB</b>	420 (MeCN)	35 (MeCN)	99
<b>PADE</b>	386	44	85

For the evaluation of TPIP initiation efficiency the TPIs were dissolved in a 1:1 mixture of trimethylolpropane triacrylate (TTA) and ethoxylated-(20/3)-trimethylolpropane triacrylate (ETA). "Woodpile" test structures were written using a fs-pulsed Titanium:Sapphire (Ti:S) with a wavelength of ~796 nm. Laser power was varied between 10 - 130 mW and writing speed between 1 - 151 mm/s. From the resulting grid, a processing window was determined judging structural quality visually from SEM pictures and assigning them a color code (see **Figure 77**).

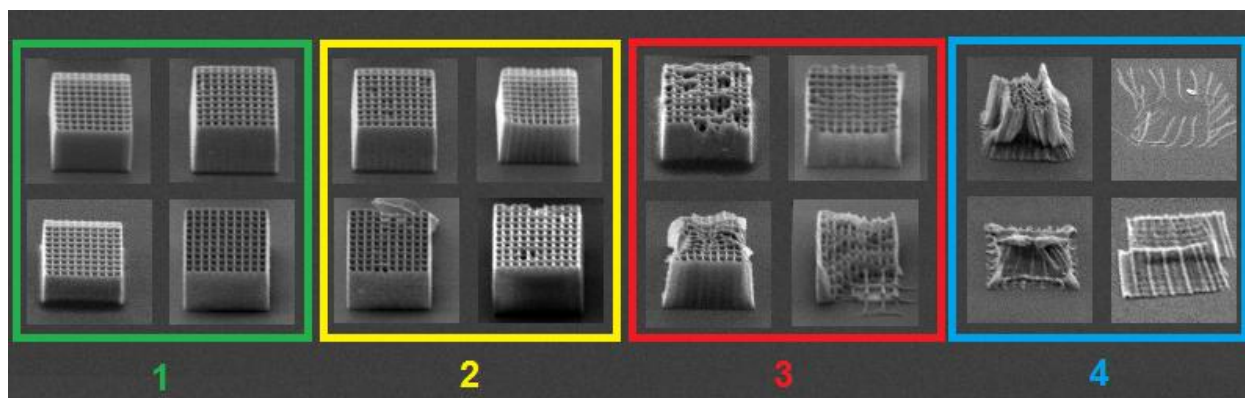


**Figure 77:** Quality classes of woodpile structures 1- 4 with their respective color codes and visual examples.

**Figure 78** show the results of TPIP structuring tests performed at a writing speed of 1 mm/s and different average laser powers. As this was the lowest investigated writing speed there is a maximal power density in this measurement, showing the high energy behavior of the TPIs. **Cbz2CEK** showed significantly worse performance, while **2B2Trz** and **3B2Trz** provide similar results as the reference **M2CMK**. **B2Cbz** shows a slight improvement at 70 mW despite the fact that its  $\sigma_{\text{TPA}}$  of 109 GM is only about half as high as **M2CMK** (191 GM). **Y-B2CMK** shows the best overall performance of all investigated TPIs, still reaching optimal structural quality at 90 mW (60 mW for **M2CMK**). While **B2Trz** has quite a small processing window and doesn't perform well at low power densities (see **Figure 79**), it showed superior performance at high laser powers up to 110 mW.

	M2CMK	Y-B2CMK	B2Cbz	Cbz2CEK	B2Trz	2B2Trz	3B2Trz
mW							
130	3	3	3	N/A	N/A	N/A	N/A
120	3	3	3	N/A	N/A	N/A	N/A
110	3	3	3	N/A	1	3	3
100	3	3	3	3	1	3	3
90	3	1	3	3	1	3	3
80	3	2	3	3	1	3	3
70	2	1	1	3	1	2	2
60	1	1	1	3	1	1	1
50	1	1	1	2	3	1	1
40	1	1	1	1	-	1	1
30	1	1	1	1	-	1	1
20	1	1	1	1	-	1	1
10	4	4	4	4	-	-	4

**Figure 78:** Quality of woodpile structures written at a speed of 1 mm/s using different laser intensities, using the multipolar TPIs with high  $\sigma_{\text{TPI}}$ .

The performance of the novel TPIs at low-medium power densities (medium powers of 30-50 mW and writing speeds up to 151 mm/s) is displayed in **Figure 79**. **B2Trz** is not able to produce any structures of satisfying quality at such low powers, and the results of **Cbz2CEK** are also inferior compared to the reference **M2CMK**. **2B2Trz**, **3B2Trz** and **Y-B2CMK** all show a slight improvement versus **M2CMK**. **B2Cbz** finally showed a significant improvement, performing best of all tested TPIs in the lower power range.

TPI	mW	1	26	51	76	101	126	151	mm/s
<b>M2CMK</b>	50	1	1	1	1	1	1	1	
	40	1	1	1	2	3	3	4	
	30	1	2	4	4	4	4	4	
<b>Y-B2CMK</b>	50	1	1	1	1	1	1	1	
	40	1	1	1	2	3	3	2	
	30	1	1	4	4	4	4	4	

<b>B2Cbz</b>	50	1	1	1	1	1	1	1
	40	1	1	1	1	2	2	2
	30	1	1	4	4	4	4	4
<b>Cbz2CEK</b>	50	2	1	1	1	3	3	4
	40	1	1	4	4	4	4	4
	30	1	4	4	4	4	4	4
<b>B2Trz</b>	50	3	4	4	4	4	4	4
	40	-	-	-	-	-	-	-
	30	-	-	-	-	-	-	-
<b>2B2Trz</b>	50	1	1	1	1	1	1	1
	40	1	1	1	1	2	2	3
	30	1	2	4	4	4	4	4
<b>3B2Trz</b>	50	1	1	1	1	1	1	1
	40	1	1	1	1	2	2	3
	30	1	1	2	3	4	4	4

**Figure 79:** Quality of woodpile structures written at three different laser intensities and several different writing speeds, using the potentially cleavable TPIs and their additional references.

**Figure 80** shows TPIP the cleavable initiators TPIP tests performed at a writing speed of 1 mm/s and different average laser powers. As this was the lowest investigated writing speed there is a maximal power density in this measurement, showing the high energy behavior of the TPIs. They generally were only able at such high powers to give any recognizable results, with the exception of **SNB**.

	<b>M2CMK</b>	<b>S2CMK</b>	<b>C2CMK</b>	<b>SNB</b>	<b>ketone 1</b>	<b>PADE</b>
mW						
130	3	N/A	N/A	N/A	N/A	N/A
120	3	N/A	N/A	N/A	N/A	N/A
110	3	3	4	3	3	3
100	3	3	4	3	3	3
90	3	3	4	3	3	3
80	3	3	4	3	3	3
70	2	3	-	2	3	4
60	1	-	-	1	2	-
50	1	-	-	1	4	-
40	1	-	-	1	-	-
30	1	-	-	1	-	-
20	1	-	-	1	-	-
10	4	-	-	-	-	-

**Figure 80:** Quality of woodpile structures written at a speed of 1 mm/s using different laser intensities, using the potentially cleavable TPIs and their references.

Unfortunately, no performance increase versus **M2CMK** could be achieved in the present work via incorporating cleavable groups into the TPIs. **S2CMK** seems to be cleavable indeed as it shows better results than its non-cleavable analogue **C2CMK**, however both suffer from exceedingly low  $\sigma_{\text{TPA}}$  (below the detection limit) and no satisfying woodpile structures could be obtained. **SNB** showed no improvement over **M2CMK**, but significantly better results than the reference ketone **1**, indicating that its initiation ability is not only due to the introduced singular donor group.



**PADE** was not able to produce any structures that were acceptable, however the visible formation of gaseous nitrogen (see **Figure 81**) was proof for its TPA induced cleavage. The unsatisfying polymerization results obtained in TPIP tests are likely due to the low  $\sigma_{\text{TPA}}$  of 85 GM.

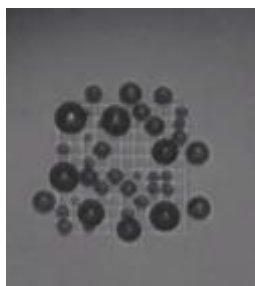


**Figure 81:** N<sub>2</sub>-bubble formation caused by the TPA cleavage of **PADE**.

Finally, high resolution 3D-models (see **Figure 82**) with features in the sub-micrometer range and complex geometries were successfully obtained using the same method as for the woodpile structures.

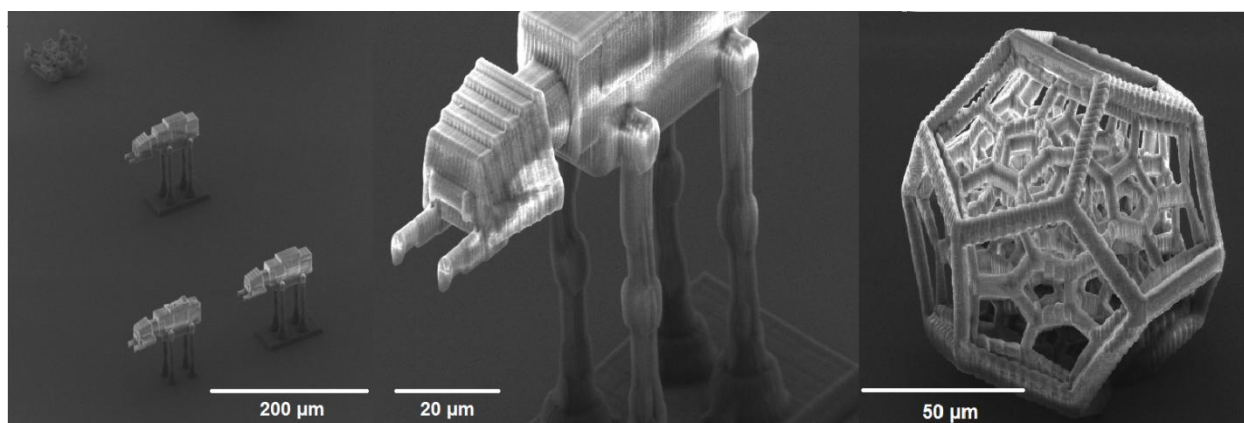


**Figure 82:** Complex 3D models built from ETA:TTA = 1:1 using the TPI **2B2Trz**.

In conclusion, several novel highly efficient TPIs with planarized and branched multipolar structures were synthesized, evaluated and successfully employed in the TPIP of complex 3D-models. The attempt to increase efficiency by introducing cleavable groups that would bypass the possibility of BET did not produce TPIs that offered practical advantages so far. This is most likely due to the exceedingly low  $\sigma_{\text{TPA}}$  that are often associated with structural motifs that are suitable for homolytic photocleavage. Future work will try further to combine the molecular features of cleavable groups with high  $\sigma_{\text{TPA}}$ -multipolar TPIs.

## Technical Equipment & Characterization Methods

### Chemicals

All reagents were purchased from Sigma-Aldrich, Fluka, TCI or ABCR and were used without further purification. The solvents were dried and purified by standard laboratory methods or were dried over  $\text{Al}_2\text{O}_3$  cartridges. Trimethylolpropane triacrylate (**TTA**, Genomer 1330) and ethoxylated-(20/3)-trimethylolpropane triacrylate (**ETA**, Sartomer 415) were received as a gift from Rahn and Sartomer, respectively. Petroleum ether (PE) refers to the fraction boiling in the range 40-60 °C. (Flash) column chromatography was performed by either conventional techniques or preparative MPLC using a Buechi Sepacore Flash System (Buechi pump module C-605, Buechi control unit C-620, Buechi UV-Photometer C-635, Buechi fraction collector C-660). Glass and polyethylene columns were used, packed with Silicagel 60 on VWR silica gel 60 (0.040–0.063 mm particle size). Buechi Sepacore RP C18 Flash Cartridges were used for reversed phase chromatography.

### Mode of practice for photosensitive compounds

The preparation and analysis of the photosensitive compounds and formulations was conducted in an orange light lab. The windows and fluorescent lamps were covered in adhesive foils or coated so that light with a wavelength <520nm was cut off.

### Thin layer chromatography (TLC) analysis

Thin layer chromatography analysis was performed on silica gel 60  $\text{F}_{254}$  aluminium sheets from Merck.

### Melting points (m.p.) analysis

Melting points were measured with the aid of an automated melting point system (SRS OptiMelt).

## Ultrasonic bath

To accelerate dissolution of substances, the ultrasonic bath Sonorex Digitec from the company Bandelin was used.

## Nuclear magnetic resonance (NMR) spectroscopy

$^1\text{H}$ -NMR (200 MHz) and  $^{13}\text{C}$ -NMR (50 MHz) spectra were measured with a BRUKER AC-E 200 FT-NMR-spectrometer. The chemical shift (s = singlet, bs = broad singlet, d = doublet, t = triplet, m = multiplet) is displayed in ppm using the non deuterated solvent as internal standard. Solvents with a grade of deuteration of at least 99.5 % were used and purchased at EURISO-TOP.

## UV/Vis-spectroscopy

Absorption spectra were recorded on a Shimadzu UV-1800 absorption spectrometer at a controlled temperature of 25°C using quartz cuvettes with a beam path length of 1cm. Emission spectra and were obtained on a Cary Eclipse at a controlled temperature of 25°C. Absorption and emission spectra were baseline corrected using the pure solvent. Absorption spectra were obtained on samples with a maximal absorbance of approximately 1, while the maximal absorbance for the emission spectra did not exceed 0.15. The emission spectra were corrected for the wavelength sensitivity of the apparatus using a set of fluorescence standards.<sup>80</sup> Emission quantum yields were obtained using Coumarin 30 in MeCN as a secondary emission standard using the following equation<sup>81</sup>

$$\Phi_s = \frac{\int I_s(\lambda) d\lambda}{\int I_r(\lambda) d\lambda} \frac{1 - 10^{-A_r} n_s^2}{1 - 10^{-A_s} n_r^2} \Phi_r$$

where  $\Phi_x$  is the fluorescence quantum yield of the sample (s) and reference (r),  $I_x(\lambda)$  denotes the corresponding fluorescence spectra.  $A_x$  is the absorbance at the excitation wavelength and  $n_x$  denotes the refractive index of the sample (s) and reference (r) solution.

### Open aperture z-scan devices & tests<sup>82</sup>

A Ti:sapphire laser (Femtopower Compact Pro) was used for the open aperture z-scan measurement to determine MPA. The Laser beam diameter is 15 mm and the shortest pulse width is 25. The central wavelength of the laser beam is 798 nm with the bandwidth of 44 nm and the beam quality factor of 2.2. Some key components for z-scan measurement are shown in **Figure 83**.



**Figure 83:** Scheme of the open aperture z-scan analysis<sup>82</sup>

A large 5 cm diameter beam splitter (2) splits the output laser beam into two parts with fraction of 1/3 and 2/3. The less intense part is directed towards the reference diode (1 cm<sup>2</sup> Si) (1) and the more intense part propagates straightly through the focusing lens (3) (plano-convex lens - Thorlabs, BK7 B-coated,  $f = 175$  mm,  $d = 25.4$  mm) and then through the sample. It should be noticed that the Rayleigh range, which is proportional to the focal length square of the focusing lens, must be larger than the thickness of the sample. For liquid samples like dyes or photoinitiator solutions, a 0.2 mm thick one-time flow cell (170.700 QS from HELMA Company) connected to a syringe pump (NE-300 from SYRINGPUMP) providing a wide range of flow rates was used. The cell was mounted on a translation stage (4) with a stepper motor (DC-Motor model MFA-CC from Newport Company), which allows the movement of the sample up to 25 mm along the beam propagation direction through the beam focus in minimum steps of 50 nm. The motor can be controlled by computer exploiting a Lab VIEW program. A collecting lens (5) with a large diameter and short focal length (50 mm

diameter and 60 mm focal length) was used to ensure the entire energy transmitted through the sample was collected and directed toward the detecting diode (6) to be measured. The signals at the diodes were recorded with a two-channel PC Oscilloscope (model: Picoscope3204 from Picotech). A self-programmed computer software analysed the intensity of individual laser pulses (including averaging over several laser shots) and also handled the movement of the translation stage as well as the entire data acquisition process (LabView).

Rhodamine B in MeOH was used as reference to verify the reliability of the experimental setup. All investigated compounds were prepared as  $1.0 \times 10^{-2}$  M solutions in spectroscopic grade water. The solutions were measured in a 0.2 mm thick flow cell in a non-recycling volumetric flow of 4 mL/h. The excited volume is therefore refreshed approximately every 100 pulses, which approximately corresponds to 10 times for each z-position, which was found to be sufficient. The measurements were carried out at different pulse energies. At higher energies a signal of the pure solvent appears and the solvent will contribute to the effective nonlinear absorption and even thermal effects are more likely to influence the measurement. Care had to be taken to collect the whole transmitted laser energy using a big diameter and short focal length lens. Additionally, a proper Gaussian beam profile in time and space is essential for the analysis.

### TPIP Micro Processing system Mipro<sup>83</sup>

A novel TPIP system based on an old setup from LZH was designed to increase the processing speed (**Figure 84**).

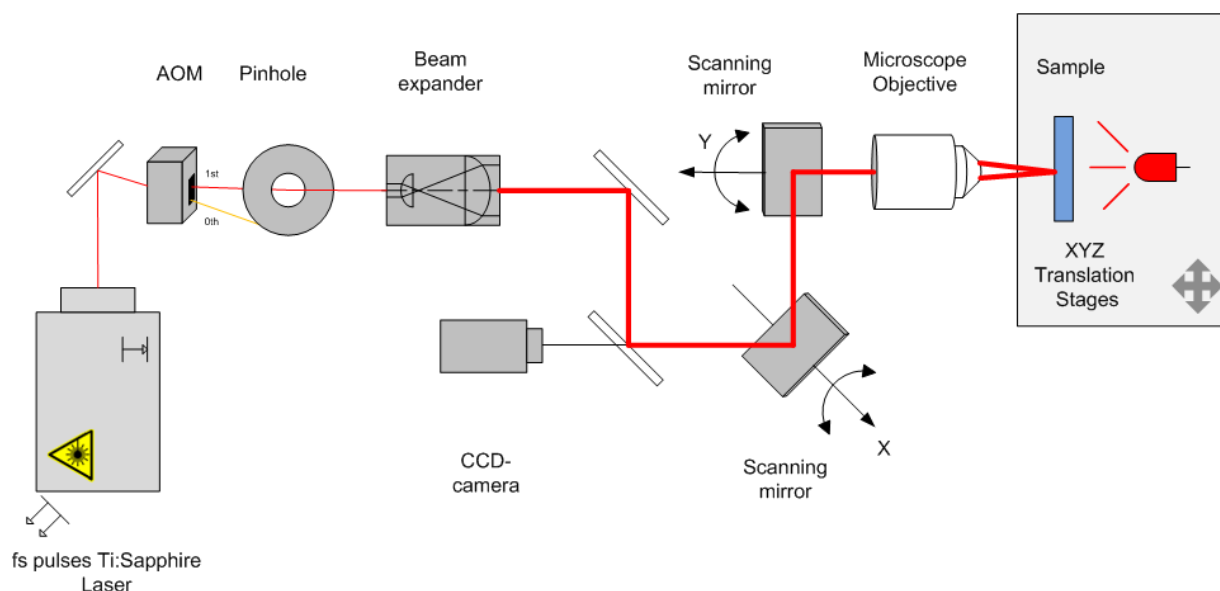


**Figure 84:** Scheme depicting the TPIP Mipro setup.

In the new setup, the laser beam passed through the AOM leaving the first order of diffraction for the structuring. A pinhole blocked the other beam orders from further propagation in the setup. Leaving the pinhole, the beam was expanded six times of its initial 1.8 mm diameter. The galvanoscanner deflected the beam before focusing it with a microscope objective. To create 3D polymeric structures, the rotating mirrors of the galvanoscanner are used to move the focal point inside the formulation. The sample carrying the formulation was mounted to a linear XYZ axes system. For online process observation, a CMOS UI-1240ME-M-GL camera (UEYE) monitored the polymerisation process. The whole setup was mounted on a hard stone frame to reduce vibrations. The laser power was measured after the microscope objective.

More detailed information can be found in Jan Torgersen's PhD thesis.<sup>83</sup>

**TPIP tests**<sup>83</sup>

The samples for 2PP tests were prepared by casting a liquid formulation on a microscope slide as depicted in **Figure 85**.

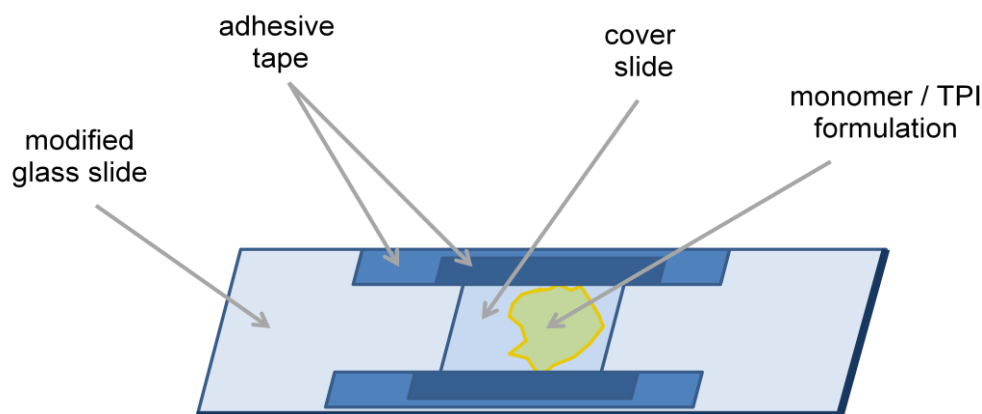


**Figure 85:** Scheme of the glass slides used for TPIP.

To improve adherence of the polymerized structures, the glass substrate was functionalized with methacrylate groups by first cleaning them with a 4:1 mixture of conc.  $\text{H}_2\text{SO}_4$  and  $\text{H}_2\text{O}_2$  (30% in water), then using *3-(trimethoxysilyl)propyl methacrylate* according to literature.<sup>84</sup> A  $18 \times 18 \times 0.17 \text{ mm}^3$  coverslip was placed on a glass slide containing two pieces of parallel adhesive strip with specified thickness of about  $120 \mu\text{m}$ . Then the coverslip was with another two pieces of adhesive strip. About  $30 \mu\text{L}$  of formulation (two-photon initiator (TPI) dissolved in a 1:1 mixture of trimethylolpropane triacrylate (**TTA**, Genomer 1330) and ethoxylated-(20/3)-trimethylolpropane triacrylate (**ETA**, Sartomer 415)) were applied between the modified glass slide and the coverslip, making use of the capillary forces.

The prepared sample was loaded into the designated clamp on the XYZ axes system and exposed to the laser beam. The focus was scanned across the photosensitive material, which leads to an embedded 3D structure inside the material volume. After laser writing, the unexposed material was removed by development of the structures in isopropanol or acetone. The resulting structures, particularly their structural dimensions, integrity and surface quality, were studied by means of SEM (FEI Philips XL 30 or FEI Quanta 200).

## Abbreviations

[PdCl <sub>2</sub> (PPh <sub>3</sub> ) <sub>2</sub> ]	bis(triphenylphosphine)palladium(II) dichloride	MeOH	methanol
μW	microwatt	MHz	megahertz
3D	three-dimensional	mm/s	millimeter/s
A	electron acceptor group	mp	melting point
AcOH	acetic acid	mW	milliwatt
BET	back electron transfer	MW	molecular weight
Bn	benzyl	NIR	near infrared
bp	boiling point	nm	nanometer
Bu	n-butyl	NMR	nuclear magnetic resonance
CDCl <sub>3</sub>	deuterated chloroform	OPI	one-photon initiator
CHCl <sub>3</sub>	chloroform	PE	petrol ether
CW	continuous wave	Ph	phenyl
D	electron donor group	PI	photoinitiator
DCM	dichloromethane	R <sub>f</sub>	retention factor (TLC)
DIBAH	diisobutyl aluminium hydride	SEM	scanning electron microscope
DMA	dimethylacetamide	TEA	triethylamine
DMF	dimethylformamide	THF	tetrahydrofuran
DMSO	dimethyl sulfoxide	Ti:S	Titanium:Sapphire
EA	ethyl acetate	TLC	thin layer chromatography
eq.	equivalent	TPA	two-photon absorption
Et <sub>2</sub> O	diethyl ether	TPEM	two-photon excitation microscopy
ETA	ethoxylated (20/3)-trimethylolpropane triacrylate	TPI	two-photon initiator
EtOH	ethanol	TPIP	two-photon induced photopolymerization
Φ <sup>OPA</sup> <sub>em</sub>	one-photon fluorescence quantum yield	TTA	trimethylolpropane triacrylate
fs	femtosecond	UV/Vis	ultraviolet/visible
GM	Göppert-Mayer (SI unit) 1 GM°= 10 <sup>-50</sup> cm <sup>4</sup> s photon <sup>-1</sup> molecule	voxel	volumetric pixel
ISC	intersystem crossing	δ	chemical shift (NMR)
λ	wavelength	ε <sub>max</sub>	decadic molar extinction coefficient
λ <sup>OPA</sup> <sub>em</sub>	one-photon emission maximum	ν	frequency
λ <sup>OPA</sup> <sub>max</sub>	one-photon absorption maximum	π	π-conjugated core
M	mol L <sup>-1</sup>	σ <sub>TPA</sub>	two-photon absorption cross section
MeCN	acetonitrile		



### Novel TPIs

<b>2B2Trz</b>	4,4'-[(6-methyl-1,3,5-triazine-2,4-diyl)di-(1 <i>E</i> )-2,1-ethenediyl]bis[ <i>N,N</i> -dibutylbenzenamine]
<b>3B2Trz</b>	4,4',4''-[1,3,5-triazine-2,4,6-triyltri-(1 <i>E</i> )-2,1-ethenediyl]tris[ <i>N,N</i> -dibutylbenzenamine]
<b>B2Cbz</b>	(2 <i>E</i> ,6 <i>E</i> ,6' <i>E</i> )-6,6'-[[9-(phenylmethyl)-9 <i>H</i> -carbazole-3,6-diyl]dimethylidyne]bis[2-[[4-(dibutylamino)phenyl]methylene]]-4-methylcyclohexanone
<b>B2Trz</b>	4-[(1 <i>E</i> )-2-(4,6-dimethyl-1,3,5-triazin-2-yl)ethenyl]- <i>N,N</i> -dibutylbenzenamine
<b>C2CMK</b>	(2 <i>E</i> ,6 <i>E</i> )-2,6-bis[[4-(2-phenylethyl)phenyl]methylene]-4-methylcyclohexanone
<b>Cbz2CEK</b>	(3 <i>E</i> ,5 <i>E</i> )-4-Oxo-3,5-bis[[9-(phenylmethyl)-9 <i>H</i> -carbazol-3-yl]methylene]-cyclohexane-carboxylic acid ethyl ester
<b>PADE</b>	1,5-bis(4-methoxyphenyl)-3-methyl-1,4-pentazadiene
<b>S2CMK</b>	(2 <i>E</i> ,6 <i>E</i> )-2,6-bis[[4-[(phenylthio)methyl]phenyl]methylene]-4-methylcyclohexanone
<b>SNB</b>	(2 <i>E</i> ,6 <i>E</i> )-2-[[4-(dimethylamino)phenyl]methylene]-6-[[4-[(phenylthio)methyl]phenyl]methylene]-4-methylcyclohexanone
<b>Y-B2CMK</b>	2,2',2''-[nitrilotris(4,1-phenylenemethylidyne)]tris[6-[4-(dibutylamino)phenyl]-methylene]-4-methylcyclohexanone
<b>Y-M2CMK</b>	2,2',2''-[nitrilotris(4,1-phenylenemethylidyne)]tris[6-[4-(dimethylamino)phenyl]-methylene]-4-methylcyclohexanone

## References

- (1) Stodolna, A. S., Rouzée, A., Lépine, F., Cohen, S., Robicheaux, F., Gijsbertsen, A., Jungmann, J. H., Bordas, C. and Vrakking, M. J. J., *Hydrogen Atoms under Magnification: Direct Observation of the Nodal Structure of Stark States*. Physical Review Letters, 2013. **110**(21): p. 213001.
- (2) Baeumer, W., *Selection criteria for photoinitiators*. Kontakte (Darmstadt), 1989(3): p. 42-9.
- (3) Kirchmayr, R., Berner, G. and Rist, G., *Photoinitiators for UV curing of paints*. Farbe Lack, 1980. **86**(3): p. 224-30.
- (4) Kirchmayr, R., Berner, G., Huesler, R. and Rist, G., *Nonyellowing photoinitiators*. Farbe Lack, 1982. **88**(11): p. 910-16.
- (5) Davis, M. J., Doherty, J., Godfrey, A. A., Green, P. N., Young, J. R. A. and Parrish, M. A., *The UV-curing behavior of some photoinitiators and photoactivators*. J. Oil Colour Chem. Assoc., 1978. **61**(7): p. 256-63.
- (6) Pappas, S. P., *Photochemical aspects of uv curing*. Prog. Org. Coat., 1974. **2**(4): p. 333-47.
- (7) Osborn, C. L., *Photoinitiation systems and their role in UV-curable coatings and inks*. J. Radiat. Curing, 1976. **3**(3): p. 2-3, 5-11.
- (8) Davidson, R. S. and Orton, S. P., *Photo-induced electron-transfer reactions. Fragmentation of 2-aminoethanols*. J. Chem. Soc., Chem. Commun., 1974(6): p. 209-10.
- (9) Oster, G. and Yang, N.-L., *Photopolymerization of vinyl monomers*. Chem. Rev., 1968. **68**(2): p. 125-51.
- (10) Oldring, P. K. T., Dowling, J. P. and Dietliker, K. K., *Chemistry & Technology of UV & EB Formulation for Coatings, Inks & Paints: Formulation*. 1991: SITA Technology.
- (11) Valeur, B., *Characteristics of Fluorescence Emission*, in *Molecular Fluorescence*. 2001, Wiley-VCH Verlag GmbH. p. 34-71.
- (12) Fouassier, J. P., *Radiation Curing in Polymer Science and Technology*. 1993: Springer.
- (13) Green, W. A., *Industrial Photoinitiators: A Technical Guide*. 2010: CRC PressINC.
- (14) Goppert-Mayer, M., *Elementary processes with two quantum jumps*. Ann. Phys. (Berlin, Ger.), 1931. **9**: p. 273-94.
- (15) Kaiser, W. and Garrett, C. G. B., *Two-photon excitation in CaF<sub>2</sub>:Eu<sup>++</sup>*. Phys. Rev. Lett., 1961. **7**: p. 229-31.
- (16) He, G. S., Tan, L.-S., Zheng, Q. and Prasad, P. N., *Multiphoton absorbing materials: molecular designs, characterizations, and applications*. Chemical reviews, 2008. **108**(4): p. 1245-1330.
- (17) Lee, K.-S., Kim, R. H., Yang, D.-Y. and Park, S. H., *Advances in 3D nano/microfabrication using two-photon initiated polymerization*. Progress in Polymer Science, 2008. **33**(6): p. 631-681.
- (18) Rumi, M., Barlow, S., Wang, J., Perry, J. W. and Marder, S. R., *Two-photon absorbing materials and two-photon-induced chemistry*, in *Advances in Polymer Science, Photoresponsive Polymers I* 2008, Springer. p. 1-95.
- (19) Reinhardt, B. A., *Two-photon technology. New materials and evolving applications*. Photonics Sci. News, 1999. **4**(2): p. 21-34.
- (20) Rumi, M. and Perry, J. W., *Two-photon absorption: an overview of measurements and principles*. Advances in Optics and Photonics, 2010. **2**(4): p. 451-518.

- (21) Terenziani, F., Painelli, A., Katan, C., Charlot, M. and Blanchard-Desce, M., *Charge Instability in Quadrupolar Chromophores: Symmetry Breaking and Solvatochromism*. Journal of the American Chemical Society, 2006. **128**(49): p. 15742-15755.
- (22) Pawlicki, M., Collins, H. A., Denning, R. G. and Anderson, H. L., *Two-photon absorption and the design of two-photon dyes*. Angew. Chem., Int. Ed., 2009. **48**(18): p. 3244-3266.
- (23) Ajami, A., Husinsky, W., Liska, R. and Pucher, N., *Two-photon absorption cross section measurements of various two-photon initiators for ultrashort laser radiation applying the Z-scan technique*. JOSA B, 2010. **27**(11): p. 2290-2297.
- (24) Makarov, N. S., Drobizhev, M. and Rebane, A., *Two-photon absorption standards in the 550-1600 nm excitation wavelength range*. Optics Express, 2008. **16**(6): p. 4029-4047.
- (25) Andrade, C. D., Yanez, C. O., Rodriguez, L. and Belfield, K. D., *A Series of Fluorene-Based Two-Photon Absorbing Molecules: Synthesis, Linear and Nonlinear Characterization, and Bioimaging*. The Journal of Organic Chemistry, 2010. **75**(12): p. 3975-3982.
- (26) Sun, H.-B. and Kawata, S., *Two-photon photopolymerization and 3D lithographic microfabrication*, in *NMR• 3D Analysis• Photopolymerization*. 2004, Springer. p. 169-273.
- (27) Maruo, S., Nakamura, O. and Kawata, S., *Three-dimensional microfabrication with two-photon-absorbed photopolymerization*. Optics letters, 1997. **22**(2): p. 132-134.
- (28) Serbin, J. and Gu, M., *Experimental Evidence for Superprism Effects in Three-Dimensional Polymer Photonic Crystals*. Advanced materials, 2006. **18**(2): p. 221-224.
- (29) Xu, B.-B., Zhang, Y.-L., Xia, H., Dong, W.-F., Ding, H. and Sun, H.-B., *Fabrication and multifunction integration of microfluidic chips by femtosecond laser direct writing*. Lab Chip, 2013. **13**(9): p. 1677-1690.
- (30) Cumpston, B. H., Ananthavel, S. P., Barlow, S., Dyer, D. L., Ehrlich, J. E., Erskine, L. L., Heikal, A. A., Kuebler, S. M., Lee, I. Y. S., McCord-Maughon, D., Qin, J., Rockel, H., Rumi, M., Wu, X.-L., Marder, S. R. and Perry, J. W., *Two-photon polymerization initiators for three-dimensional optical data storage and microfabrication*. Nature, 1999. **398**(6722): p. 51-54.
- (31) Krivec, S., Matsko, N., Satzinger, V., Pucher, N., Galler, N., Koch, T., Schmidt, V., Grogger, W., Liska, R. and Lichtenegger, H. C., *Silica-Based, Organically Modified Host Material for Waveguide Structuring by Two-Photon-Induced Photopolymerization*. Advanced Functional Materials, 2010. **20**(5): p. 811-819.
- (32) Jhaveri, S. J., McMullen, J. D., Sijbesma, R., Tan, L.-S., Zipfel, W. and Ober, C. K., *Direct three-dimensional microfabrication of hydrogels via two-photon lithography in aqueous solution*. Chemistry of Materials, 2009. **21**(10): p. 2003-2006.
- (33) LaFratta, C. N., Fourkas, J. T., Baldacchini, T. and Farrer, R. A., *Multiphoton fabrication*. Angewandte Chemie International Edition, 2007. **46**(33): p. 6238-6258.
- (34) Schafer, K. J., Hales, J. M., Balu, M., Belfield, K. D., Van Stryland, E. W. and Hagan, D. J., *Two-photon absorption cross-sections of common photoinitiators*. Journal of Photochemistry and Photobiology A: Chemistry, 2004. **162**(2-3): p. 497-502.
- (35) Belfield, K. D., Ren, X., Van Stryland, E. W., Hagan, D. J., Dubikovsky, V. and Miesak, E. J., *Near-IR two-photon photoinitiated polymerization using a fluorone/amine initiating system*. Journal of the American Chemical Society, 2000. **122**(6): p. 1217-1218.
- (36) Belfield, K. D., Schafer, K. J., Liu, Y. U., Liu, J., Ren, X. B. and Van Stryland, E. W., *Multiphoton-absorbing organic materials for microfabrication, emerging optical applications and non-destructive three-dimensional imaging*. Journal of Physical Organic Chemistry, 2000. **13**(12): p. 837-849.

- (37) Mongin, O., Porrès, L., Charlot, M., Katan, C. and Blanchard-Desce, M., *Synthesis, Fluorescence, and Two-Photon Absorption of a Series of Elongated Rodlike and Banana-Shaped Quadrupolar Fluorophores: A Comprehensive Study of Structure–Property Relationships*. Chemistry-a European Journal, 2007. **13**(5): p. 1481-1498.
- (38) Belfield, K. D., Hagan, D. J., Van Stryland, E. W., Schafer, K. J. and Negres, R. A., *New two-photon absorbing fluorene derivatives: Synthesis and nonlinear optical characterization*. Organic Letters, 1999. **1**(10): p. 1575-1578.
- (39) Cumpston, B. H., Ananthavel, S. P., Barlow, S., Dyer, D. L., Ehrlich, J. E., Erskine, L. L., Heikal, A. A., Kuebler, S. M., Lee, I.-Y. S. and McCord-Maughon, D., *Two-photon polymerization initiators for three-dimensional optical data storage and microfabrication*. Nature, 1999. **398**(6722): p. 51-54.
- (40) Xing, J.-F., Chen, W.-Q., Gu, J., Dong, X.-Z., Takeyasu, N., Tanaka, T., Duan, X.-M. and Kawata, S., *Design of high efficiency for two-photon polymerization initiator: combination of radical stabilization and large two-photon cross-section achieved by N-benzyl 3, 6-bis (phenylethynyl) carbazole derivatives*. Journal of Materials Chemistry, 2007. **17**(14): p. 1433-1438.
- (41) Zhou, H.-P., Li, D.-M., Zhang, J.-Z., Zhu, Y.-M., Wu, J.-Y., Hu, Z.-J., Yang, J.-X., Xu, G.-B., Tian, Y.-P., Xie, Y., Tao, X.-T., Jiang, M.-H., Tao, L.-M., Guo, Y.-H. and Wang, C.-K., *Crystal structures, optical properties and theoretical calculation of novel two-photon polymerization initiators*. Chem. Phys., 2006. **322**(3): p. 459-470.
- (42) Lemercier, G., Martineau, C., Mulatier, J.-C., Wang, I., Stéphan, O., Baldeck, P. and Andraud, C., *Analogues of Michler's ketone for two-photon absorption initiation of polymerization in the near infrared: synthesis and photophysical properties*. New journal of chemistry, 2006. **30**(11): p. 1606-1613.
- (43) Wang, T., Zhao, Y. X., Shi, M. Q. and Wu, F. P., *The synthesis of novel coumarin dyes and the study of their photoreaction properties*. Dyes and Pigments, 2007. **75**(1): p. 104-110.
- (44) Wu, J., Zhao, Y. X., Li, X., Shi, M. Q., Wu, F. P. and Fang, X. Y., *Multibranched benzylidene cyclopentanone dyes with large two-photon absorption cross-sections*. New Journal of Chemistry, 2006. **30**(7): p. 1098-1103.
- (45) Xue, J. Q., Zhao, Y. X., Wu, F. P. and Fang, D. C., *Effect of Bridging Position on the Two-Photon Polymerization Initiating Efficiencies of Novel Coumarin/Benzylidene Cyclopentanone Dyes*. Journal of Physical Chemistry A, 2010. **114**(15): p. 5171-5179.
- (46) Xue, J. Q., Zhao, Y. X., Wu, H. and Wu, F. P., *Novel benzylidene cyclopentanone dyes for two-photon photopolymerization*. Journal of Photochemistry and Photobiology a-Chemistry, 2008. **195**(2-3): p. 261-266.
- (47) Li, Z., Pucher, N., Cicha, K., Torgersen, J., Ligon, S. C., Ajami, A., Husinsky, W., Rosspeintner, A., Vauthey, E., Naumov, S., Scherzer, T., Stampfl, J. and Liska, R., *A Straightforward Synthesis and Structure–Activity Relationship of Highly Efficient Initiators for Two-Photon Polymerization*. Macromolecules, 2013. **46**(2): p. 352-361.
- (48) Kannan, R., He, G. S., Yuan, L., Xu, F., Prasad, P. N., Dombroskie, A. G., Reinhardt, B. A., Baur, J. W., Vaia, R. A. and Tan, L.-S., *Diphenylaminofluorene-based two-photon-absorbing chromophores with various  $\pi$ -electron acceptors*. Chemistry of materials, 2001. **13**(5): p. 1896-1904.
- (49) Xing, J.-F., Chen, W.-Q., Dong, X.-Z., Tanaka, T., Fang, X.-Y., Duan, X.-M. and Kawata, S., *Synthesis, optical and initiating properties of new two-photon polymerization initiators: 2,7-Bis(styryl)anthraquinone derivatives*. Journal of Photochemistry and Photobiology A: Chemistry, 2007. **189**(2–3): p. 398-404.
- (50) Lin, T.-C., Chung, S.-J., Kim, K.-S., Wang, X., He, G. S., Swiatkiewicz, J., Pudavar, H. E. and Prasad, P. N., *Organics and polymers with high two-photon activities and their*

- applications, in *Advances in Polymer Science, Polymers for Photonics Applications II*. 2003, Springer. p. 157-193.
- (51) Tian, Y., Zhang, M., Yu, X., Xu, G., Ren, Y., Yang, J., Wu, J., Zhang, X., Tao, X. and Zhang, S., *Two novel two-photon polymerization initiators with extensive application prospects*. Chemical physics letters, 2004. **388**(4): p. 325-329.
- (52) Zhiquan, L., *Novel Organic Materials for Multi-photon Photopolymerization and Photografting: Powerful Tools for Precise Microfabraccation and Functionalization in 3D*. PhD Thesis, 2013.
- (53) Lu, Y., Hasegawa, F., Kawazu, Y., Totani, K., Yamashita, T. and Toshiyuki, W., *Investigation of mechanism of photo induced polymerization excited by two-photon absorption*. Sen'i Gakkaishi, 2004. **60**(6): p. 165-172.
- (54) Tehfe, M.-A., Dumur, F., Graff, B., Clément, J.-L., Gigmes, D., Morlet-Savary, F., Fouassier, J.-P. and Lalevée, J., *New Cleavable Photoinitiator Architecture with Huge Molar Extinction Coefficients for Polymerization in the 340–450 nm Range*. Macromolecules, 2013. **46**(3): p. 736-746.
- (55) Li, Z., Pucher, N., Cicha, K., Torgersen, J., Ligon, S. C., Ajami, A., Husinsky, W., Rosspeintner, A., Vauthey, E., Naumov, S., Scherzer, T., Stampfl, J. and Liska, R., *Straightforward Synthesis and Structure-Activity Relationship of Highly Efficient Initiators for Two-Photon Polymerization*. Macromolecules (Washington, DC, U. S.). **46**(2): p. 352-361.
- (56) Wu, J., Zhao, Y., Li, X., Shi, M., Wu, F. and Fang, X., *Multibranched benzylidene cyclopentanone dyes with large two-photon absorption cross-sections*. New J. Chem., 2006. **30**(7): p. 1098-1103.
- (57) Smith, P. J., Dimmock, J. R. and Turner, W. A., *Mass spectrometry of some substituted 2-benzylidenecyclohexanones and 2,6-bis(benzylidene)cyclohexanones*. Can. J. Chem., 1973. **51**(9): p. 1458-70.
- (58) Mallegol, T., Gmouh, S., Meziane, M. A. A., Blanchard-Desce, M. and Mongin, O., *Practical and efficient synthesis of tris(4-formylphenyl)amine, a key building block in materials chemistry*. Synthesis, 2005(11): p. 1771-1774.
- (59) Li, L., Wu, Y., Zhou, Q. and He, C., *Experimental and theoretical studies on the one-photon and two-photon properties of a series of carbazole derivatives containing styrene*. J. Phys. Org. Chem. **25**(5): p. 362-372.
- (60) Kreher, U. P., Rosamilia, A. E., Raston, C. L., Scott, J. L. and Strauss, C. R., *Direct Preparation of Monoarylidene Derivatives of Aldehydes and Enolizable Ketones with DIMCARB*. Organic Letters, 2003. **5**(17): p. 3107-3110.
- (61) Xing, J.-F., Chen, W.-Q., Gu, J., Dong, X.-Z., Takeyasu, N., Tanaka, T., Duan, X.-M. and Kawata, S., *Design of high efficiency for two-photon polymerization initiator: combination of radical stabilization and large two-photon cross-section achieved by N-benzyl 3,6-bis(phenylethynyl)carbazole derivatives*. Journal of Materials Chemistry, 2007. **17**(14): p. 1433-1438.
- (62) Qiu, F., Tu, C., Chen, Y., Shi, Y., Song, L., Wang, R., Zhu, X., Zhu, B., Yan, D. and Han, T., *Control of the Optical Properties of a Star Copolymer with a Hyperbranched Conjugated Polymer Core and Poly(ethylene glycol) Arms by Self-Assembly*. Chem. - Eur. J. **16**(42): p. 12710-12717, S12710/1-S12710/6.
- (63) Cui, Y.-z., Fang, Q., Huang, Z.-l., Xue, G., Xu, G.-b. and Yu, W.-t., *Frequency up-conversion of s-triazine derivatives via two photon absorption and second-harmonic generation*. Journal of Materials Chemistry, 2004. **14**(15): p. 2443-2449.
- (64) Meier, H., Holst, Hans C. and Oehlhof, A., *Star-Shaped Compounds Having 1,3,5-Triazine Cores*. European Journal of Organic Chemistry, 2003. **2003**(21): p. 4173-4180.

- (65) Cui, Y.-Z., Fang, Q., Xue, G., Xu, G.-B., Yin, L. and Yu, W.-T., *Cooperative Enhancement of Two-photon Absorption of Multibranched Compounds with Vinylenes Attaching to the s-Triazine Core*. Chemistry Letters, 2005. **34**(5): p. 644-645.
- (66) Schaefer, F. C. and Peters, G. A., *Synthesis of the s-Triazine System. III.1 Trimerization of Imidates*. The Journal of Organic Chemistry, 1961. **26**(8): p. 2778-2784.
- (67) Herrera, A., Martínez-Alvarez, R., Ramiro, P., Chioua, M. and Chioua, R., *A Practical and Easy Synthesis of 2,4,6-Trisubstituted-s-triazines*. Synthesis, 2004. **2004**(EFirst): p. 503-505.
- (68) Bonham, J. A., *Chromophore substituted vinyl-halomethyl-s-triazines*. 1976.
- (69) Yamaji, M., Inomata, S., Nakajima, S., Akiyama, K., Tobita, S. and Marciniak, B., *Photoinduced  $\omega$ -Bond Dissociation in the Higher Excited Singlet ( $S_2$ ) and Lowest Triplet ( $T_1$ ) States of a Benzophenone Derivative in Solution*. J. Phys. Chem. A, 2005. **109**(17): p. 3843-3848.
- (70) Greeves, N. and Torode, J. S., *Synthesis of Phenylthiomethyl Substitution Furans by Lewis Acid Catalysed Substitution*. Synthesis, 1993. **1993**(11): p. 1109-1112.
- (71) Zakharkin, L. I. and Khorlina, I. M., *Reduction of esters of carboxylic acids to aldehydes with diisobutylaluminum hydride*. Tetrahedron Lett., 1962: p. 619-20.
- (72) Carey, F. A., Sundberg, R. J. and Schäfer, H. J., *Organische Chemie: Ein weiterführendes Lehrbuch*. 1995: Wiley-VCH Verlag GmbH.
- (73) Kim, S. H., Kim, J. H. and Yoon, N. M., *An improved synthesis of aldehydes from carboxylic acid esters with diisobutylaluminum hydride in the presence of o-anisidine*. Bull. Korean Chem. Soc., 1989. **10**(1): p. 117-18.
- (74) Shen, Z.-L., Goh, K. K. K., Yang, Y.-S., Lai, Y.-C., Wong, C. H. A., Cheong, H.-L. and Loh, T.-P., *Direct Synthesis of Water-Tolerant Alkyl Indium Reagents and Their Application in Palladium-Catalyzed Couplings with Aryl Halides*. Angewandte Chemie International Edition, 2011. **50**(2): p. 511-514.
- (75) Tian, Y., Chen, N., Wang, H., Pan, X.-F., Hao, X.-J. and Chen, C.-X., *An Expeditious Synthetic Route to Carnosic Acid Type Diterpenes*. Synthetic Communications, 1997. **27**(9): p. 1577-1582.
- (76) Goldschmidt and Badl, *Chemische Berichte*, 1889. **22**: p. 934.
- (77) Novikova, O. O., Syromyatnikov, V. G., Avramenko, L. F., Kondratenko, N. P., Kolisnichenko, T. M. and Abadie, M. J. M., *Photoinitiation ability of some pentaaza-1,4-dienes*. Mater. Sci., 2002. **20**(4): p. 19-28.
- (78) Baidl, A., Lang, A. and Nuyken, O., *High and low molar mass 3-alkyl-1,4-pentazadienes. Synthesis and photolysis*. Macromolecular Chemistry and Physics, 1996. **197**(12): p. 4155-4171.
- (79) El-Hegazy, F. E.-Z. M., El-Bardan, A. A. and Hamed, E. A., *Alkaline C-S bond cleavage of some (arylthio)methylbenzoates*. Phosphorus, Sulfur Silicon Relat. Elem., 1994. **88**(1-4): p. 113-22.
- (80) Gardecki, J. and Maroncelli, M., *Set of secondary emission standards for calibration of the spectral responsivity in emission spectroscopy*. Applied Spectroscopy, 1998. **52**(9): p. 1179-1189.
- (81) Valeur, B., *Molecular fluorescence: principles and applications*. 2013: John Wiley & Sons.
- (82) Ajami, A., *Two-photon Modification of materials with ultrashort laser radiation: Z-scan measurements and 3D-modification of selected materials*. PhD Thesis, 2012.
- (83) Torgersen, J., *Novel biocompatible materials for in situ two-photon polymerisation*. PhD Thesis, 2013.
- (84) Garoff, H. and Ansorge, W., *Improvements of DNA sequencing gels*. Analytical Biochemistry, 1981. **115**(2): p. 450-457.